The University Of Sheffield.

Establishment and validation of organ-on-chip models for Inflammatory Bowel Disease modelling *in vitro*

Kinga Kosim

A thesis submitted for the degree of Doctor of Philosophy

Supervisor Dr. Kai Erdmann

The University of Sheffield

Faculty of Science

Department of Biomedical Science

February 2021

Contents

Declaration

I hereby declare that my thesis entitled "*Establishment and validation of organ-on-chip models for Inflammatory Bowel Disease modelling in vitro*" has been entirely composed by myself and is the sole result of my work, unless otherwise stated by reference or acknowledgement. I confirm that this work has not been submitted, in whole or in parts, in any previous application for a degree.

Acknowledgements

I would like to thank Dr Kai Erdmann and Dr Dorota Kurek for their mentorship and scientiffic guidance over the course of my PhD training. I wish to thank the industrial partners of the MIMIC consortium Mimetas BV and Galapagos BV. I would also like to acknowledge my previous mentor Dr Christophe Lancrin who largely inspired me to pursue the scientific career and reinforced my confidence. In addition, I would like to thank my family, especially my mother and father for continuous support and love. Lastly, I send a big thanks to my dear friends without whom I would not have been able to complete this challenging journey.

“We can never go back to the place and find it exactly where we left it.

Something, somewhere will always have changed, most of all, ourselves. People.”

- ***Taiye Selasi***

Abstract

Inflammatory Bowel Disease is a chronic disorder resulting in inflammation and ulceration of the intestinal mucosa. It is a multifactorial disease caused by the interplay between genetics of an individual, microbiota and environment. A number of genes have been reported as susceptibility factors, including *NOD2* that plays a role in the recognition of bacterial cell wall components and activation of pro-inflammatory pathways. The main aspects of the disease are disruption of the intestinal barrier and upregulation in the expression of pro-inflammatory cytokines. Standard 2D models of the intestine fail to mimic physiological complexity of the intestinal tissue inclusive of presence of various cell types, extracelular matrix and incorporation of the fluid flow. There is a need for novel *in vitro* models that would mimic human biology more closely while being suitable for including in the drug development pipeline.

In this thesis we present the development of multiple gut on a chip models that capture boundary aspect of the intestinal tissue. We investagated epithelial immune response to the pro-inflammatory triggers characteristic to IBD in mono- and co-culture with hematopoietic cells. We decribe generation of the models established with commonly used Caco-2 adenocarcinoma cell line, iPSC-derived as well as human stem cells derived intestinal organoids. Our results show that organ on a chip technology could be successfully used to model human intestine. OrganoPlate® platform used in the development of the models suited for high throughput screening allowed for generation of physiologically relevant models with pump-free perfusion. Obtained epithelial barriers exhibited rapid cell polarization, expression of major intestinal markers and barrier integrity. We show a proof of concept study in which iPSC-derived intestinal organoids cultured in a tubular form were triggered with pro-inflammatory cytokines. The inflamed phenotype was efficiently reverted with the addition of an anti-inflammatory compound proving suitability of the model for IBD-related drug discovery research. These findings provide the basis for further research towards generation of novel *in vitro* models. Combining organoid cultures with organ on chip technology advances the current state of the art in tissue and disease modelling giving a promise for significant developments in the drug discovery field.

List of Figures

List of Tables

Abbreviations

3Rs	The Three Rs (guiding principles for more ethical use of animals in testing)
ABCB1	ATP Binding Cassette Subfamily B Member 1 (also known as MDR1 or PGP)
Ac-tub	Acetylated alpha tubulin
ARHGEF2	Rho/Rac Guanine Nucleotide Exchange Factor 2
ARHGEF7	Rho/Rac Guanine Nucleotide Exchange Factor 7
ATG16L1	Autophagy Related 16 Like 1 protein
ATP	Adenosine triphosphate
BCRP	Breast Cancer Resistance Protein
BL21 *E. coli*	Chemically competent *Escherichia coli*
BMP	Bone Morphogenic Protein
BSA	Bovine serum albumin
βtub	Beta-tubulin
Caco-2	Human colorectal adenocarcinoma cell line
CARD	Caspase recruitment domain
CARD15	Caspase recruitment domain-containing protein 15
Cas9	CRISPR associated protein 9
CCL-20	C-C Motif Chemokine Ligand 20
CD45	Lymphocyte common antigen
CD68	Cluster of Differentiation 68
cDNA	Complementary DNA
CDX2	Claudal Type Homeobox Transcription Factor 2
CES2	Carboxylesterase 2
CHGA	Chromogranin A
Chir99021	Aminopyrimidine derivative, WNT pathway activator (glycogen kinase 3 inhibitor)
CIITA	Class II Major Histocompatibility Complex Transactivator
Colo205	Human colon adenocarcinoma cell line
CRISPR	Clustered Regularly Interspaced Short Palindromic Repeats
CTR	Control

CYP3A4	Cytochrome P450 3A4
DLD-1	Human Colorectal Adenocarcinoma cell line
DMEM	Dulbecco's Modified Eagle Media
DMSO	Dimethyl sulfoxide
DNA	Deoxyribonucleic acid
dNTP	Deoxynucleoside triphosphate
ECM	Extracellular matrix
EDTA	Ethylenediaminetetraacetic acid
EGF	Epidermal Growth Factor
ELISA	Enzyme-linked Immunosorbent Assay
FACS	Fluorescence-activated Cell Sorting
FBS	Fetal Bovine Serum
FITC-dextran	Fluorescein isothiocyanate-dextran
FOXA2	Forkhead Box A2
FRMPD2	FERM And PDZ Domain-Containing Protein 2
gDNA	Genomic DNA
GFP	Green Fluorescent Protein
Glut-2	Glucose Transporter 2
GWAS	Genome-wide association study
HBSS	Hanks' Balanced Salt Solution
HBV	Hepatitis B virus
HCT116	Human colorectal carcinoma cell line
HDR	Homology Directed Repair
HEK hNOD2	Human NOD2-expressing HEK293 cells
HEK293	Human Embryonic Kidney cells
HEPES	4-(2-Hydroxyethyl)piperazine-1-ethanesulfonic acid
HSP90	Heat Shock Protein 90
HT-29	Human colorectal adenocarcinoma cell line
IBD	Inflammatory Bowel Disease
IBD1	Inflammatory Bowel Disease Protein 1 (also known as NOD2)
ICAM-1	Intracellular Adhesion Molecule 1

iE-DAP	γ-D-glutamyl-meso-diaminopimelic acid (dipeptide, NOD1 agonist)
IFNγ	Interferon gamma
IκB	Inhibitor of nuclear factor kappa B
IL-1β	Interleukin 1 Beta
IL10	Interleukin 10/Cytokine Synthesis Inhibitory Factor
IL-12	Interleukin 12
IL-16	Interleukin 16/Lymphocyte Chemoattractant Factor
IL-18	Interleukin 18/Interferon-Gamma-Inducing Factor)
IL-2	Interleukin 2/T Cell Growth Facto
IL-23	Interleukin 23
IL23R	Interleukin 23 Receptor
IL-8	Interleukin 8/Neutrophil Chemotactic Factor
IPSC	Induced Pluripotent Stem Cell
IRGM	Immunity Related GTPase M/Interferon-inducible protein 1
KO	Knock-out
LB medium	Lysogeny Broth medium
LGR5	Leucine-rich repeat-containing G-protein coupled receptor 5
LRR domain	Leucine-rich repeat domain
LS174	Human colorectal adenocarcinoma cell line
LSL	L WNT-3A Mouse fibroblast cell line
LYZ	Lysozyme
M cell	Microfold cell
MAPK	mitogen-activated protein kinase
MDP	Muramyl Dipeptide
MHC	major histocompatibility complex
M-MLV RT	Moloney Murine Leukemia Virus Reverse Transcriptase
mRNA	Messenger RNA
MUC-2	Mucin 2
MUTZ-3	Human acute myelomonocytic leukemia cell line
NANOG	Nanog Homeobox
NBD	Nucleotide Binding Domain

NEMO	NF-kappa-B essential modulator/ inhibitor of nuclear factor kappa-B kinase subunit gamma
NFκB	nuclear factor kappa-light-chain-enhancer of activated B cells
NHEJ	Non-homologous end joining
NLR	Nod-like receptor
NLRC5	NOD-Like Receptor C5
NLRP2	NLR Family Pyrin Domain Containing 2
NLRP4	NLR Family Pyrin Domain Containing 2
NMD	non-sense mediated decay
NOD1	Nucleotide Binding Oligomerization Domain Containing 1
NOD2	Nucleotide Binding Oligomerization Domain Containing 2
OATP2B1	Organic Anion Transporting Polypeptide 2B1
OCT4	Octamer-binding Transcription Factor 4
OOC	Organ on chip
OptiMEM	Reduced serum media
PAM	Protospacer Adjacent Motif
PBS	Phosphate-buffered Saline
PBST	Phosphate-buffered Saline with low-concentration detergent solution
PCR	Polymerase chain reaction
PDMS	Polydimethylsiloxane
PEPT1	Peptide Transporter 1
PGP	P-glycoprotein 1 (also known as MDR1/ABCB1)
PMA	Phorbol 12-myristate 13-acetate
PRRs	Pattern Recognition Receptors
PTPN2	Protein Tyrosine Phosphatase Non-Receptor Type 2
qPCR	Quantitative polymerase chain reaction
RAC1	Rac Family Small GTPase 1
RAJI-B	Human Burkitt's lymphocyte cell line
RIP2	Receptor-interacting serine/threonine-protein kinase 2
RLU	Relative Light Units
RNA	Ribonucleic acid

RT	Room temperature
SDCCAG3	Serologically defined colon cancer antigen 3
SDS	Sodium dodecyl sulfate
SDS-PAGE	Sodium dodecyl (lauryl) sulfate-polyacrylamide gel electrophoresis
sgRNA	Single guide RNA
siRNA	Small interfering RNA
SLC15A4	Solute Carrier Family 25A4
SNP	Single nucleotide polymorphism
SOX17	SRY-Box Transcription Factor 17
SpiB	Spi-B Transcription Factor
Subsp.	Subspecies
SW48	Human colorectal adenocarcinoma cell line
SW480	Human colorectal adenocarcinoma cell line
SW620	Human colorectal adenocarcinoma cell line
T4 PNK	T4 Polynucleotide Kinase
T84	Human colorectal carcinoma cell line
TAE	Tris acetate EDTA
TCF/LEF	Transcription factor family involved in WNT signaling pathway
TEER	Transepithelial Electrical Resistance
TGFβ	Transforming growth factor beta
Th1	T helper type 1 lymphocyte
Th-17	T helper type 17 lymphocyte
THP-1	Human monocyte cell line
TLR	Tool-like receptor
TNFα	Tumor Necrosis Factor alpha
TPCA-1	Selective inhibitor of IκB kinase
TRAF6	Tumor Necrosis Factor Receptor-associated factor 6
TRIM27	Tripartite Motif Containing 27
Tris	Tris(Hydroxymethyl)aminomethane
TRITC-dextran	Tetramethylrhodamine
UGT	Uridine 5'-diphospho-glucuronosyltransferase

VIL1	Villin 1
WT	Wild type
XBP1	X-box binding protein 1
ZO-1	Zonula occludens-1

1. Introduction

1.1. Inflammatory Bowel Disease

1.1.1. Occurrence, symptoms and available treatment options

Inflammatory Bowel Disease is a chronic condition characterized by inflammation and ulceration of gut mucosa. In the western population 1 in 1000 individuals suffers from IBD (Molodecky *et al.*, 2012). The highest incidence is observed in northern Europe, United Kingdom and North America (Cosnes *et al.*, 2011). Two major variations of the disease are Crohn's disease and ulcerative colitis. Both forms are similar in many aspects. The common symptoms are abdominal pain, diarrhoea, bloody stools as well as weight loss. Additional manifestations on the skin, joints and eyes have been reported as well (Vavricka *et al.*, 2015). The disease affects men and women equally and it most often develops in teenagers and young adults. Ulcerative colitis is limited to the colon while Crohn's disease can cause lesions throughout the whole gastrointestinal tract. Inflammation observed in ulcerative colitis is continuous and in Crohn's inflamed areas can be scattered through the body. Ulcerative colitis causes the destruction of the innermost part of the gut as opposed to Crohn's that involves all the layers of the gastrointestinal wall (mucosa, submucosa, muscularis, serosa).

Medical treatment of IBD patients is costly and up to 50% of patients require surgical resection of parts of the intestine within 10 years after the diagnosis (Frolkis *et al.*, 2013). Current therapeutics include classic anti-inflammatory drugs (e.g. corticosteroids, aminosalicylates), immunosuppressors (e.g. azathioprine, methotrexate, ciclosporin-A), blockers of pro-inflammatory cytokines signalling (e.g. Janus kinase inhibitors, TNFα blockers) (Plichta *et al.*, 2019). Emerging therapeutics currently being tested in the clinical trials involve integrin blockers to prevent lymphocyte homing to the inflamed intestinal tissue, targeting fibrosis and tissue remodelling factors, new blockers of pro-inflammatory cytokines and cytokine signalling, blockers of transcription factors controlling cytokine gene transcription, strengthening barrier function and activation of anti-inflammatory pathways as well as stem

cells for Crohn's disease fistulas (Neurath, 2017). Matching patient with a proper treatment option remains a challenge as up to 40% of patients fail to respond to the first choice treatment. Moreover, a proportion of patients that respond to the initial treatment lose the response within a year (Roda *et al.*, 2016). There is a clear need for advancement in IBD therapy which includes better understanding of disease pathogenesis across patients with different genetic background as well as improved classification systems for prognosis and individual-suited treatment.

1.1.2. Susceptibility genes and etiological factors

The exact aetiology of IBD remains unknown but certain factors like genetic susceptibility of an individual, intestinal microbiota, immune system and environment contribute to the development of the disease. It is not a genetic disease but some level of heredity is involved. Our understanding of the contribution of genetic component comes mostly from genome-wide association studies (GWAS) that allow for the identification of new single nucleotide polymorphisms (SNPs). Population-based studies and especially the ones on twins provide information on genetic predisposition to IBD. The first and most reported susceptibility gene for Crohn's disease is nucleotide-binding oligomerization domain containing 2 (NOD2) (Hugot *et al.*, 2001) (Ogura *et al.*, 2001). Its role in the pathogenesis of IBD has been described in **Section 1.2** of this introduction. Throughout the years other loci involved in the intestinal immune system have been identified. Autophagy-related genes (*IRGM* and *ATG16L1*) were reported, confirming the importance of autophagy in IBD. Some genes associated with autoimmune responses, like *IL23R* and *PTPN2* were also correlated with IBD. IBD can be classified as a group of polygenic disorders which means that a high number of susceptibility genes altogether elevate the risk of the disease. Increasing numbers of reports on the genetic component of the disease suggest that those play an important role in pathogenesis.

IBD is caused by the interaction of an individual with the environment. Genome, immune system and microbiota can be significantly altered by certain exogenous factors like diet, drugs, breastfeeding. Smoking and high dietary intake of fats are known risk factors of

Crohn's disease (Ho and Khalil, 2015). DNA methylation, RNA interference and histone modifications are predominant epigenetic mechanisms that shape the environment-genome interplay. In particular, DNA methylation is a known cause of some human diseases and could act as a potential factor in a complex disorder like IBD (Loddo and Romano, 2015).

Another regulator of gene expression, miRNA has been shown to be involved in IBD pathogenesis. Its role lies within the development, regulation and differentiation of the immune system (Kalla *et al.*, 2015). Additionally, they contribute to the regulation of intestinal tissue homeostasis, cell differentiation and barrier function (Iborra *et al.*, 2012). It has been shown that IBD patients display unique miRNA expression profiles that were linked to canonical pathways of pathogenesis (Chapman and Pekow, 2015). Further investigation in this field is required for a better understanding of the role or miRNA in IBD. It holds a promise to be an important diagnostics tool and eventually a candidate for the development of novel therapies.

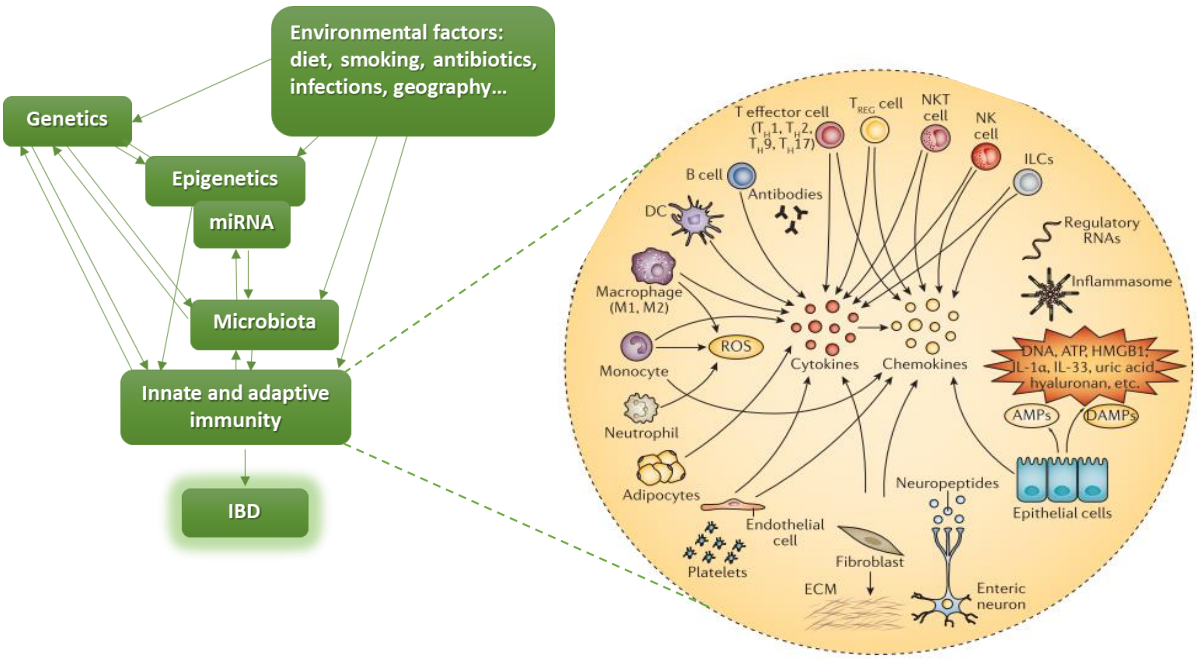

Figure 1. Complex pathogenesis of Inflammatory Bowel Disease.

Multiple factors play a role in IBD pathogenesis, including dysregulated immune response affected by immune and non-immune cells and their products (e.g. cytokines, chemokines). Additionally, other regulatory and mediator elements (RNAs, inflammasome), exogenous stimuli (diet, bacteria, xenobiotics) can stimulate immune system that leads to chronic inflammation (De Souza and Fiocchi, 2016).

1.1.3. Disease mechanism

The disease mechanism of IBD can be described from three different angles: epithelial barrier function, mucosal immune response and repair of damaged tissue. The epithelial barrier is a crucial line of defence that prevents from an invasion of bacteria. The monolayer is composed mostly of enterocytes and the barrier is strengthened by the excreted mucins produced by goblet cells. Other cell types are incorporated in the monolayer and have various functions. $LGR5^{+}$ stem cells reside at the bottom of the intestinal crypts and give rise to all the other cell types. Newly differentiated cells move up towards the luminal surface and are shed every 5 days. Paneth cells (found mostly in the small intestine) are the only cell type that do not migrate but stay at the bottom of the crypt to create a stem cell niche by excreting WNT3, NOTCH ligands and pro-EGF (Sato *et al.*, 2013). They produce various antimicrobial agents (lysozyme, defensins) thus have a crucial antimicrobial role. Changes in functionality of these cells are said to increase the risk of Crohn's disease as they express autophagy-related genes like *ATG16L1* and *IRGM* (Adolph *et al.*, 2013) (Vandussen *et al.*, 2015) (Liu *et al.*, 2013). M cells reside at the site of gut-associated lymphoid tissues and allow for the transfer of antigens from the lumen to lymphoid cells. Finally, enteroendocrine cells act as signal transducers by producing various hormones and signalling molecules (Sternini, Anselmi and Rozengurt, 2008).

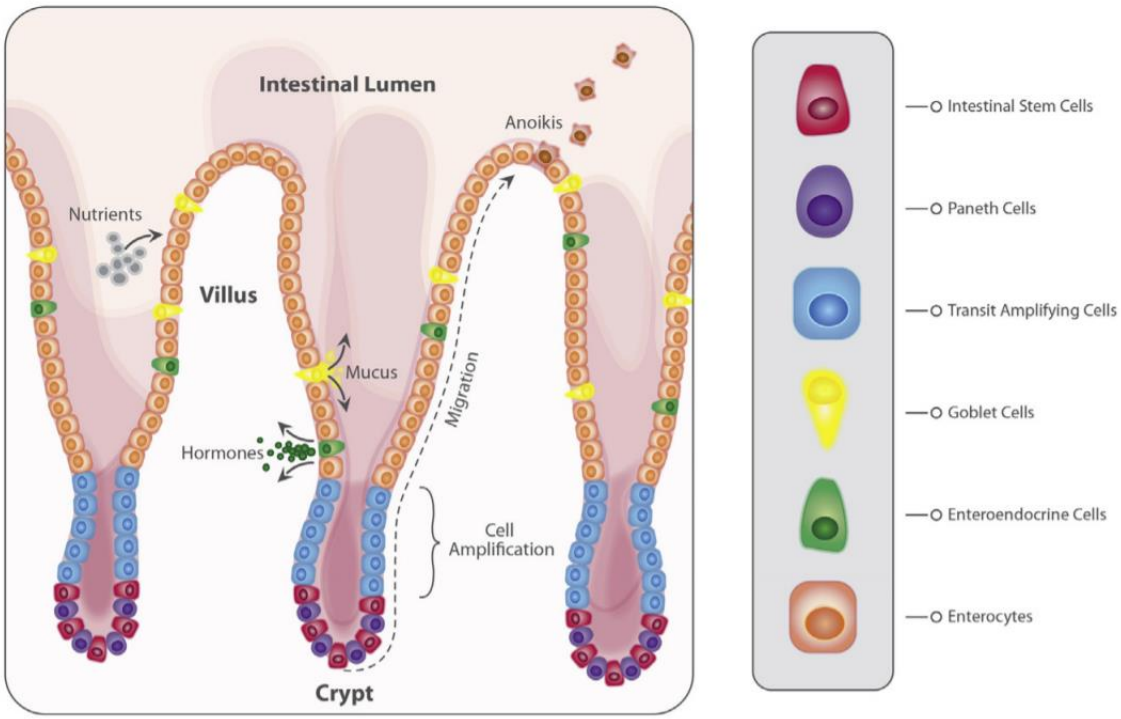

Figure 2. Intestinal epithelium (Dey and Bradbury, 2018).

The cells are connected by epithelial junctions formed by various protein classes, including claudins and occludins. The functional status of the junctions is influenced by cytokines secreted when inflammation occurs. Disruption of the junctions allows for the infiltration by microbiota and in turn, may lead to an increased inflammation state. Epithelium apart from being a physical barrier is recognized as a component of the mucosal immune response. By expressing various Toll-like receptors, it contributes to innate immunity. Recognition of the ligands facilitates monitoring of luminal microbiota and initiates relevant cytokines expression at the basolateral side that act on activation of the immune cells. Any disruption at this stage may lead to inadequate immune response and persistent inflammation. Alterations in the expression of the pattern recognition receptors and associated epithelial response to bacterial products are linked with IBD. The molecular mechanism associated with NOD2 signalling pathway has been described in **Section 1.2** of the **Introduction**.

1.1.3.1. Role of immune component in IBD pathogenesis

Mucosal immune response is a central part of IBD pathogenesis. The gut-associated lymphoid tissue is a major immune component in the gut but many types of immune cells are scattered throughout the tissue. T cells mostly stay in the epithelium layer and lamina propria is filled with all the various types of adaptive and innate immune cells (Mowat and Agace, 2014). It is apparent that IBD-affected sites of the intestine are infiltrated by a large number of immune cells. It remains controversial if the observed phenomenon is the primary cause of the disease or a secondary effect of elevated activation resulting from epithelial barrier defects or overstimulation by the luminal microbiome. Insights into immune system and its homeostatic imbalance come from extensive research on animal models of colitis as well as clinical data involving patients. Immune system is present in multicellular organisms and evolved to provide defence mechanism against pathogens (Janeway *et al.*, 2001). In a healthy individual a balance between protective and disruptive response of the immune system is maintained. In turn, in IBD patients the homeostasis is perturbed and results in aggravated immune response. Based on the type of response to the infection, human immune system can be divided into innate and adaptive. There is broad evidence for the involvement of both types of immune responses in IBD pathogenesis.

Innate immune response is rapid, not very specific and mediated by pattern recognition receptors (PPR). GWAS studies on IBD patients pointed a number of susceptibility genes involved in innate mucosal response (NOD2, CARD9, REL, SLC1A) and antigen presentation (ERAP2, LNPEP) (Dave *et al.*, 2015). It has been suggested that impairment of detection and responsiveness to pathogenic microbiota by innate immune and epithelial cells leads to chronic inflammation in the intestinal tissue. Therapies targeted against inflammatory cytokines released by innate immune cells have shown promise in proportion of the affected patients, providing evidence for the role of innate immune response in IBD pathogenesis. High concentration of TNFα and IL-12, the cytokines attracting effector T cells, are released by activated macrophages and are known targets in IBD therapy (TARGAN *et al.*, 1997; Mannon *et al.*, 2004; Moss and Farrell, 2006; Balzola *et al.*, 2012). Defective inflammatory response to injury and bacterial infiltration has been marked as characteristic of Crohn's patients and can be observed with decreased neutrophils infiltration, deficiency in

release of pro-inflammatory cytokines and reduction in vascular flow (Marks *et al.*, 2006). Defective response is followed by ineffective clearing of microbes and debris which is associated with autophagy. As reported in literature, many autophagy-associated genes have been suggested as susceptibility factors for Crohn's disease (Hampe *et al.*, 2007; Cadwell *et al.*, 2008).

Adaptive immune response is highly specific and comes as a second line of defence in case of pathogen invasion. T cells, and specifically activated CD4+ T cells are believed to be central to IBD pathogenesis (Powrie *et al.*, 1994; Fuss *et al.*, 2004). It has been reported that Th17 cells presence is increased in inflamed areas of intestine in IBD patients (Hovhannisyan *et al.*, 2011; Pariente *et al.*, 2011). Mutation in IL-23 receptor leads to impairment of IL-23 induced Th17 effector function and is considered to be a protective variant against Crohn's disease (Di Meglio *et al.*, 2011). Many therapies are designed to either target activated effector T cells or block pro-inflammatory signalling initiated by T-cells (Danese, 2012). IBD patients produce antibodies targeting microbial antigens which suggests that adaptive immune response can act in a pathogenic way by targeting intestinal microbiota (Lodes *et al.*, 2004).

Many aspects of the role of mucosal immunity in IBD pathogenesis are still unknown. Clinical representation of the disease can be similar between patients but the underlying cause and disfunction of immune response may be very different. It is a dynamic disease and in a single patient the pathophysiology can change over time. In order to decipher the pathogenesis of IBD new technologies to enable studying complexity and dynamics of cellular interactions need to be exploited.

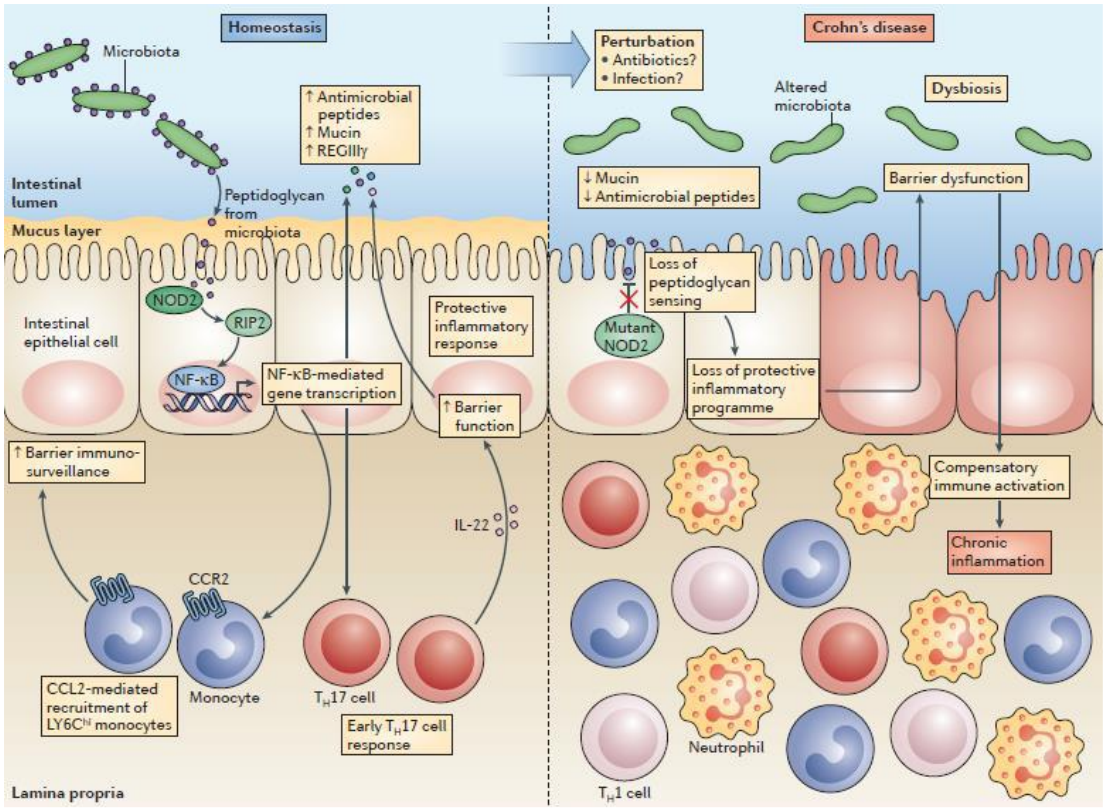

Figure 3. Cellular interactions in response to microbial dysbiosis (Philpott et al., 2014).

NOD2 has a central role in maintaining intestinal homeostasis by detecting microbial components and driving physiological immune response leading to NFκB activation. In healthy response, antimicrobial peptides and mucins are released by Paneth and Goblet cells which help in maintaining physical distance between microbiota and epithelial barrier. Activation of T helper 17 cells induces production of IL-22 that enhances protection of the barrier. Additionally, regenerating islet-derived protein IIIγ (REGIIIγ) and CCL2 mediate recruitment of monocytes that enhances barrier surveillance. In Crohn's disease, in patients with NOD2 mutation, altered protective inflammatory programme leads to disruption of the epithelial barrier and microbial dysbiosis. Since NOD2 signalling pathway is not active, compensatory immune activation occurs and drives chronic inflammation.

1.1.3.1.1. Role of macrophages in intestinal inflammation

Macrophages aid in maintaining homeostasis by identifying potential pathogens and tolerating commensal agents. Tolerance to the non-harmful microbiota occurs via stimulation of regulatory T cells by releasing IL-10 (Mowat, 2018). Blood-derived monocytes differentiate upon entrance into the lamina propria and are attracted to the intestinal tissue by chemoattractants, chemokines and microbial products (Dave *et al.*, 2015). It was believed that macrophages exist in two distinctive states: inflammatory M1 and wound-healing M2. This view has been changed recently as it is highly probable that these cells acquire distinct phenotypes depending on the environmental stimulants (Steinbach and Plevy, 2014). Non-activated macrophages show limited responsiveness to TLR ligands and lack the ability to stimulate the components of the adaptive immune system. In that state, their function is restricted to phagocytosis and intracellular killing (Smith, Ochsenbauer-Jambor and Smythies, 2005). In an inflamed state, macrophages initiate the expression of receptors including TLR and NOD, proceed with phagocytosis and intracellular killing. Macrophages release inflammatory cytokines that signal further to T cells, hence constitute a tie between innate and adaptive immunity (Bamias *et al.*, 2012). Among others, TGFβ release by macrophages acts as an attractant for a higher number of macrophages and neutrophils to the inflamed site (Wahl *et al.*, 1987).

In IBD patients, regulation of immune responses is dysfunctional and results in reoccurring inflammation. The correlation between defects in the regulation of immune response and dysfunction in the differentiation of monocytes into macrophages is manifested in IBD patients (Na *et al.*, 2019). An elevated number of monocytes migrate to the intestinal tissue, which results in the accumulation of pro-inflammatory macrophages. It has been reported that monocytes of Crohn's patients show upregulation in IL-23 and TNFα secretion (Kamada *et al.*, 2008). Other characteristics observed are aberrant maturation, differential marker expression and increase in the capability of Th17 activation (Ogino *et al.*, 2013; Dige *et al.*, 2016). As studies show, the IL-23 signalling to Th17 cells is an important pathogenesis factor in IBD (Duerr *et al.*, 2006; Neurath, 2007). Genome-wide association studies implicate that many IBD susceptibility genes are associated with macrophage differentiation and activation which supports the concept of a genetic deficiency that limits the transition from

inflammatory monocytes to pro-resolving macrophages in chronic inflammation (Na *et al.*, 2019). There is a need for the development of novel *in vitro* models that would allow for further investigation of the macrophage role in IBD and serve as a tool for target discovery research aimed at molecular pathways involved in the specification of the intestinal macrophages.

1.2. NOD2 as a potential key player in IBD

1.2.1. NOD-like receptors

Nucleotide-binding oligomerization domain-like receptors are part of pattern recognition receptors and play key roles in the regulation of innate immune response. They are highly conserved, and their homologs are found in many different animal and plant species. The NLR families belong to the signal-transduction ATPases with numerous domains. In the centre of the protein is a nucleotide-binding domain which is usually followed by a C-terminal leucine-reach domain (LRR) - in each phylum, there is diversity in the N terminus of these domains (Maekawa, Kufer and Schulze-Lefert, 2011). **Figure 4** depicts the main differences in structure in plant and animal NLRs. The central nucleotide-binding domain is participating in dNTPase activity and oligomerization, the C-terminal LRR domain binds the ligand or is involved in activator sensing, N-terminal domain interacts with other proteins (Kim, Shin and Nahm, 2016).

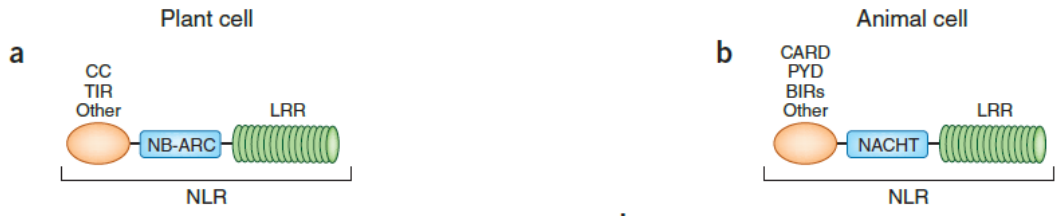

Figure 4. Structure of plant (a) and animal (b) NLRs (Maekawa, Kufer and Schulze-Lefert, 2011).

The function of NLRs is to recognize the ligands from various sources: microorganisms (like peptidoglycan, flagellin, fungal hyphae, viral RNA), host cells (cholesterol crystals, ATPs, uric acid…), and environment (asbestos, silica, UV radiation, skin irritants…). Most NLRs act as pattern recognition receptors that recognize ligands and initiate inflammatory responses. Nevertheless, some NLRs instead of acting like PRRs respond to cytokines like interferons. The mode of action of activated NLRs can be grouped into four broad categories in respect of their function: inflammasome formation, signaling transduction, transcription activation and autophagy (Kim, Shin and Nahm, 2016). The functions of NLRs have been shown in **Figure 5**.

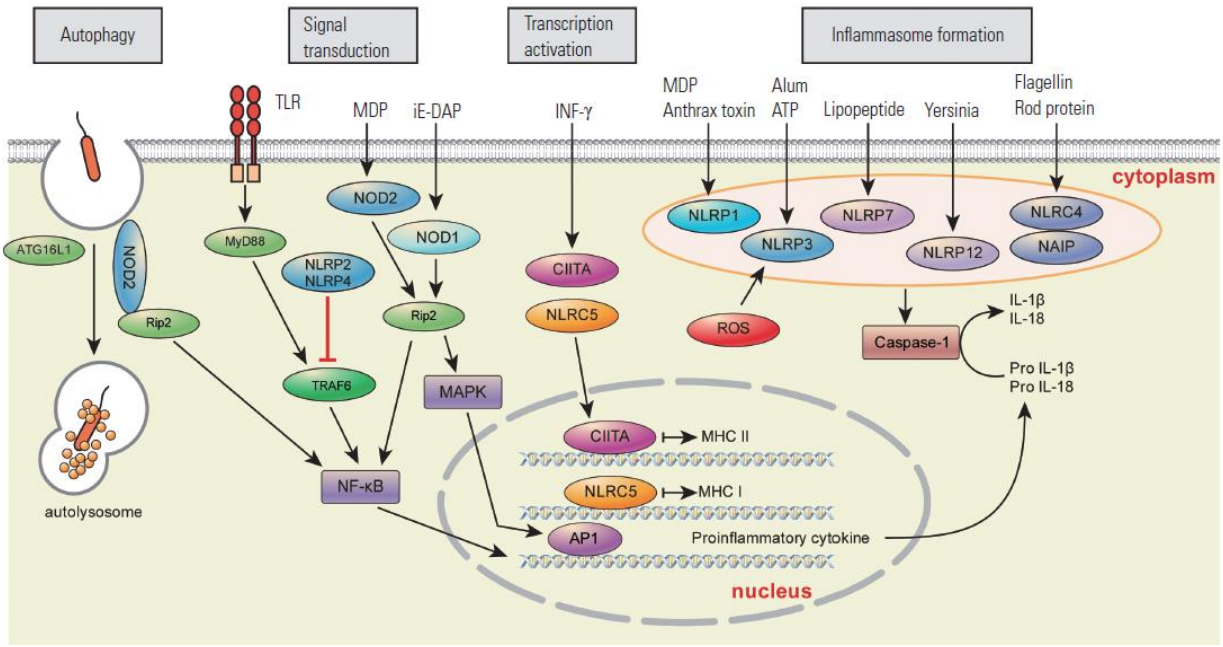

Figure 5. Functions of NLR receptors (Kim, Shin and Nahm, 2016).

The NLRs can be grouped into four broad categories according to their activity; autophagy, signal transduction, transcription activation, and inflammasome formation. NOD2 induces autophagy in order to remove pathogens by recruiting ATG16L1 to the plasma membrane at the bacterial entry site (Travassos *et al.*, 2010). NOD1 recognizes γ-D-glutamyl-meso-diaminopimelic acid (iE-DAP) (Girardin, Boneca, Carneiro, *et al.*, 2003) and NOD2 muramyl dipeptide (MDP) (Grimes *et al.*, 2012); consequently, they activate the nuclear factor kappa B (NFκB) and mitogen-activated protein kinase (MAPK) signalling pathways. NLRP2 and NLRP4 act as negative regulators of NFκB pathway by modifying tumor necrosis factor receptor-associated factor 6 (TRAF6) (Cui *et al.*, 2012). CIITA and NLRC5 are transactivators of major histocompatibility complexes (MHC) (Steidl *et al.*, 2011). Inflammasome-forming NLRs (orange circle) convert pro-cytokines to active IL-1β and IL-18 .

Additionally, NLRs have other functions that are not related to pathogen recognition, like apoptosis and playing a role in early development (Kufer and Sansonetti, 2011). For that reason, abnormalities in their functions are linked to various diseases such as infections, inflammation, and cancer. Indicating their engagement in the pathogenesis of particular diseases may help us develop new approaches in the treatment of those diseases. Genome-wide association studies (GWAS) have reported a significant association of polymorphisms of genes encoding different NLRs with numerous diseases, such as hereditary periodic fever syndromes, Crohn's disease and Blau's syndrome, allergic rhinitis, multiple sclerosis, inflammatory bowel disease, asthma, multi-bacillary leprosy, vitiligo, early-onset menopause, and bone density loss in elderly women (Zhong, Kinio and Saleh, 2013).

1.2.2. NOD2 structure and expression

NOD2, also known as caspase recruitment domain-containing protein 15 (CARD15) or inflammatory bowel disease protein 1 (IBD1), is a protein in human encoded by the NOD2 gene located on chromosome 16p21. It is a member of the NLR family that regulates innate and adaptive immune responses. NOD2 is a cytosolic protein that consists of 1040 aa (110kDa) (Sidiq *et al.*, 2016). It has two caspase recruitment domains (CARD) at N-terminus, central nucleotide-binding domain and C-terminus leucine-rich domains (LRR). CARD domains interact with the CARD of receptor-interacting protein 2 (RIP2), nucleotide-binding domain binds ATP and mediates NOD oligomerization, and LRRs are important for ligand sensing.

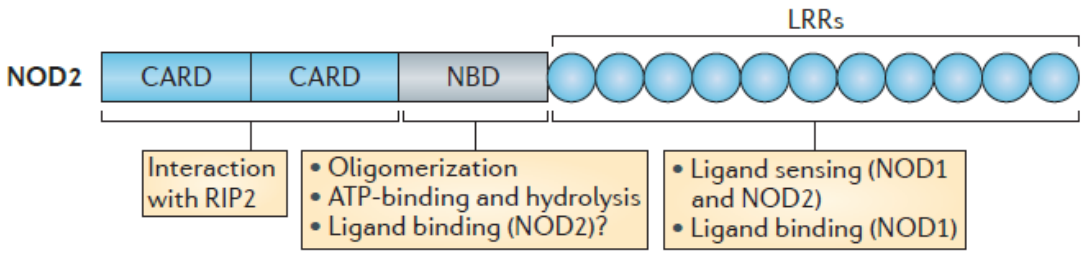

Figure 6. Structure of NOD2 protein (Philpott et al., 2014).

NOD2 is mostly expressed in the hematopoietic compartment in cells of both myeloid and lymphoid origin (Philpott *et al.*, 2014). High expression of NOD2 is found in myeloid cells (dendritic cells and macrophages) and the expression is low in T cells (Ikeuchi *et al.*, 2013). NOD2 expression has been documented in intestinal epithelial cells (Barnich *et al.*, 2005), likewise in Paneth cells (Ogura *et al.*, 2003), and can be modulated by diverse stimuli. It is induced by bacterial cell wall components, short-chain fatty acids, hormonal vitamin D, and pro-inflammatory cytokines (Girardin, Boneca, Viala, *et al.*, 2003) (Ikeuchi *et al.*, 2013) (Rosenstiel *et al.*, 2003) (Leung *et al.*, 2009). The degradation of NOD2 is strongly regulated. When the macrophages are stimulated with MDP, the proteasome-dependent degradation of NOD2 and RIP2 is triggered. This leads to hyperresponsiveness to re-stimulation with MDP. Dissociation from the heat shock protein 90 (HSP90) chaperone and TRIM27 dependent Lys48 ubiquitylation have been involved in promoting NOD2 degradation (Lee *et al.*, 2012).

1.2.3. Cellular localization

In the cell, NOD2 is maintained in an inactive, autoinhibited conformation thanks to interactions between the NBD and LRR domains as well as with cellular chaperones (Boyle, Parkhouse and Monie, 2014). NOD2 is a cytoplasmic protein that lacks transmembrane domains. Nevertheless, various studies have shown that NOD2 is recruited to the plasma membrane where it recognizes microbial invasion at the point of entry (Philpott and Girardin, 2010). In agreement with this observation, NOD2 together with NOD1 is recruited to the site of *S. flexneri* invasion, recruiting autophagy-related protein 16 like 1 (ATG16L1) to stimulate targeting of this pathogen to autophagosomes (Travassos *et al.*, 2010). Also scaffolding FERM and PDZ domain-containing protein 2 (FRMPD2) has been reported to bring an essential link between NOD2 and ERBB2-interacting protein ERBIN (membrane-associated protein) (Lipinski *et al.*, 2012). This study is in line with previous reports that determined NOD2 and ERBIN complex (McDonald *et al.*, 2005) (Kufer *et al.*, 2006). NOD2 and FRMPD2 co-immunoprecipitate and co-localize at the membrane which is explained by their interaction through the NOD2 LRR domain and PDZ domains of FRMPD2. When FRMPD2 is knocked down, NOD2 is less present at the membrane and NFκB response is reduced (Lipinski *et al.*, 2012).

Localization of NOD2 to the membrane corresponds to the capability to trigger NFκB activation. The truncated version of NOD2 protein (frameshift mutation in LRR domain associated with Crohn's disease) has been shown to be unable to target the plasma membrane (Barnich *et al.*, 2005) (Travassos *et al.*, 2010). Certainly, NOD2 localization at the plasma membrane is essential in some contexts, though the response of NOD2 to endocytosis of intracellular peptidoglycan fragments indicates that signalling can also take place in other regions. It is not evident how the NOD-mediated ligand recognition occurs in infections with bacteria that reside in endosomes (like *Salmonella enterica* subsp. *enterica* serovar Typhimurium) in spite of several reports stating NODs are important for the immune response to this bacterium (Geddes *et al.*, 2010)(Le Bourhis *et al.*, 2009). Although the proximity of the NOD2 signalling complex to the membrane might be essential it should be studied in more detail to fully understand the process. What is intriguing, SDCCAG3 (colon cancer antigen-3) has been recently identified as one of the new NOD2 interacting proteins (Thiébaut *et al.*, 2016). It is an endosomal protein that is mainly found at early and recycling endosomes and interacts with proteins from the retromer complex essential for membrane receptor sorting (Hagemann *et al.*, 2013)(McGough *et al.*, 2014).

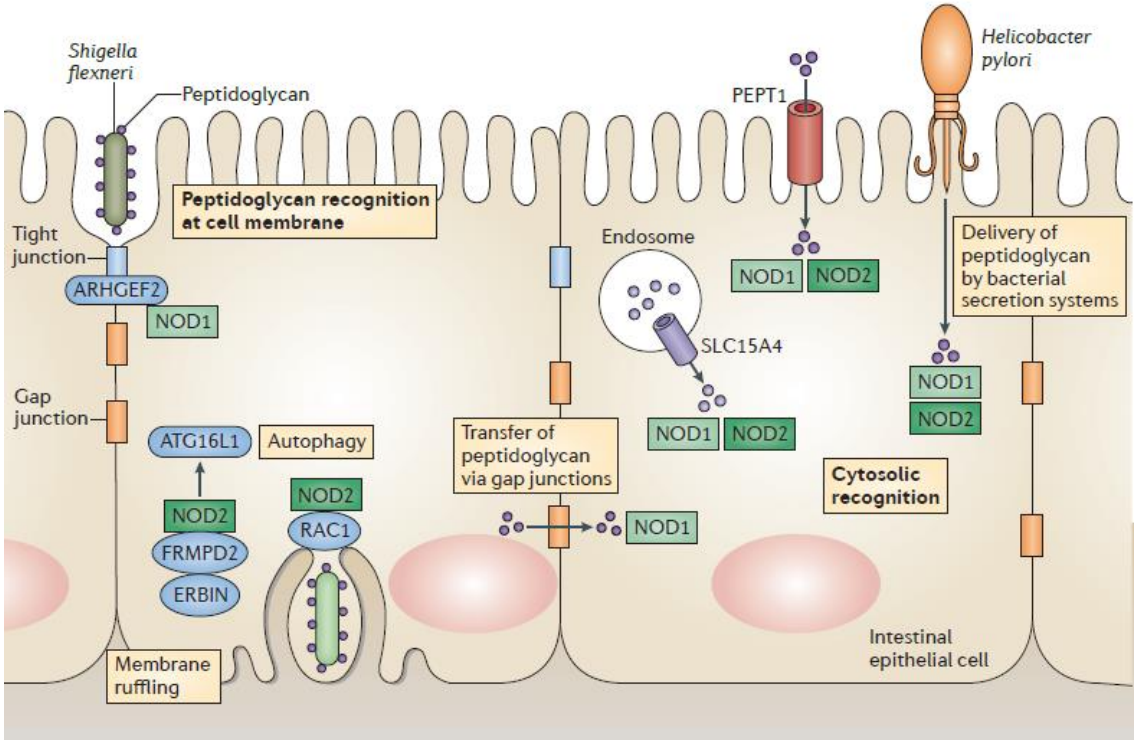

Figure 7. NOD1 and NOD2 localization during infection and ligand recognition (Philpott et al., 2014).

NOD1 and NOD2 can be recruited to the plasma membrane. NOD1 interacts with the tight junction-associated protein RHO guanine nucleotide exchange factor 2 (ARHGEF2), which assists the recognition of microorganism that utilize tight junctions for entry. NOD2 interacts with a complex of ARHGEF7 and ERBIN, as well as RAC1, which together mediate localization to the plasma membrane and membrane ruffling. NOD1 and NOD2 are capable of recognition of cytosolic fragments of peptidoglycan. Peptidoglycan fragments can be endocytosed and transported to the cytosol by solute carrier family 15 member 4 (SLC15A4). Alternatively, gap junctions can help in the movement of peptidoglycan fragments from infected cells to adjacent uninfected cells to drive NOD1 activation. Peptidoglycan delivery to the cytosol can be also mediated by the bacterial secretion systems. Finally, extracellular peptidoglycan can be transported into the cytosol by pH-sensing regulatory factor of peptide transporter 1 (PEPT1).

1.2.4. NOD2 signalling pathway

NOD2 is the cytoplasmic protein that serves as the receptor for muramyl dipeptide (MDP), the cell wall component of bacteria (Girardin, Boneca, Viala, *et al.*, 2003). It interacts with the ligand as shown in **Figure 8**. It has been demonstrated by (Grimes *et al.*, 2012) and (Mo *et al.*, 2012) that MDP interacts directly with NOD2. It is commonly considered that the interaction with the ligand occurs through LRR domains (Boyle, Parkhouse and Monie, 2014),

(Grimes *et al.*, 2012) but the essential role of the NBD domain has been suggested (Mo *et al.*, 2012) which could be due to the necessity for correct LRR folding in the cell.

The best-known interaction partner of NOD2 is receptor-interacting serine/threonine-protein kinase 2 (RIPK2) which is essential for the NFκB activation and MAPK pathway (Magalhaes *et al.*, 2011). NOD2 binds to RIPK2 through CARD domains. It has been shown that overexpression of two NOD2 CARD domains is enough to trigger NFκB response, yet this is not possible with either individual CARD domain (Ogura *et al.*, 2001). Point mutations in CARD domains abolish RIPK2 binding which in consequence hamper NFκB signalling (Tanabe *et al.*, 2004). Subsequently, activation of IκB complex (inhibitor of κB) occurs through NEMO (a key component of the NFκB signalling complex) (Abbott *et al.*, 2004), which leads to the degradation of IκB. After that, NFκB (nuclear factor kappa B - transcription factor) is activated and migrates into the nucleus and turns on the transcription of proinflammatory target genes (e.g., IL-8 and IL-1β) (Li *et al.*, 2004) and antimicrobial effectors (Voss *et al.*, 2006).

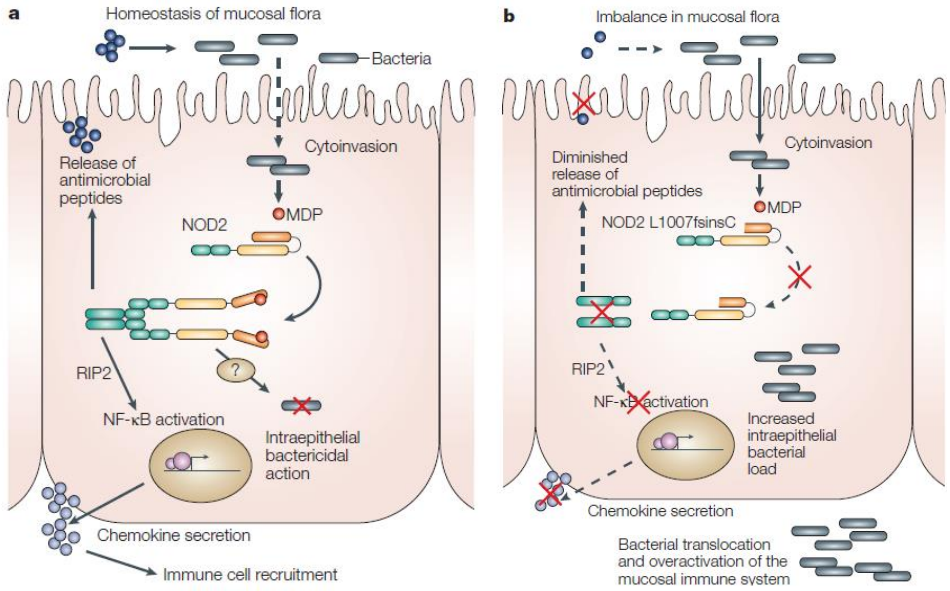

Figure 8. NOD2 signalling and the intestinal epithelial barrier (Schreiber et al., 2005).

(a) Detection of MDP by LRR domain of NOD2 leads to self-oligomerization and NFκB activation. Chemokine and defensin secretion is regulated what contributes to mucosal homeostasis; (b) Truncated version of NOD2 is unable to initiate NFκB activation what leads to the increased exposure to the mucosal bacterial flora.

1.2.5. NOD2 and Crohn's disease

The healthy human intestine is lined with an epithelial layer that together with the mucus layer serves as a barrier against microorganisms. In Inflammatory Bowel Disease patients, this barrier is not functioning properly (due to genetic, environmental, microbial and immunological factors) what results in relapsing inflammation of the intestine wall (Podolsky, 2002).

There are 163 susceptibility loci reported for IBD, of which 30 are specific to Crohn's disease (Jostins *et al.*, 2012). NOD2 was the first gene reported to be the risk factor for Crohn's disease (Hugot *et al.*, 2001) (Ogura *et al.*, 2001). NOD2 is highly expressed in Paneth cells (cells mostly found in terminal ileum) (Ogura *et al.*, 2003). These cells are essential in the innate regulation of microflora in the gut because they synthesize and secrete antimicrobial molecules. Consequent to NOD2 stimulation with MDP, Paneth cells start to secrete molecules like lysozyme in the intestinal lumen (Wehkamp *et al.*, 2005). When NOD2 is mutated, and MDP fails to stimulate it, host-microbe interaction is dysregulated, which leads to the increase in sensitivity to ileal inflammation. However, Crohn's disease etiology is still not very well understood and many other factors lead to the development of this disease.

A study by Economou reported that in *NOD2* homozygotes as well as in compound heterozygotes the risk for developing Crohn's disease was elevated to 17.1-fold and 2.4-fold in *NOD2* heterozygotes (Economou *et al.*, 2004). Three main *NOD2* variants are highly associated with Crohn's disease: a frameshift mutation at position 1007, a glycine to arginine conversion at aa residue 908, arginine to tryptophan conversion at aa residue 702 (Ogura *et al.*, 2001) (Hugot *et al.*, 2001) (Lesage *et al.*, 2002). All of the mentioned mutations occur in the LRR domain that is responsible for the recognition of MDP. There have also been many studies reporting the increased risk of complications in patients with mutated versions of *NOD2*. *L1007fsinC* mutation is reported to be the strongest disease predictive factor. Patients homozygous for this mutation were much younger when they were diagnosed with Crohn's. Also, the majority of them had to undergo surgery (Seiderer *et al.*, 2006). Many studies stating the association of *NOD2* mutations with Crohn's disease are conducted on European and Ashkenazi Jewish populations. This association is not found in patients of Asian origin (Pugazhendhi *et al.*, 2013) (Yamazaki *et al.*, 2002). Altogether, a mutation in the *NOD2* gene

and the probability of having Crohn's disease are strongly connected due to interaction between intestinal bacteria and mucosal immunity.

1.3. Modelling the intestinal biology in health and disease

Inflammatory bowel disease is a complex idiopathic disorder and many models have been developed to study the causes of the disease as well as to test novel therapies. Those include *in vivo* animal models, *ex vivo* patient explants and *in vitro* tissue culture models. Although in recent years many novel approaches to disease modelling have been developed, most advances in our understanding of IBD pathophysiology comes from animal studies. The first animal model of colitis was described in 1961 (Joseph B.Kirsner, 1961) and since then over 60 others have been developed, one of the most significant ones being the cytokines knock-out animals (Kühn *et al.*, 1993; Sadlack *et al.*, 1993). The most important findings reported from animal research are: (1) inflammation is not observed in germ-free animals; (2) genetic composition of an individual has an impact on inflammatory response; (3) T cells are the main immune component involved in IBD pathophysiology; (4) dendritic cells interact with T cells to initiate the inflammatory response. Developed models have been divided into five groups: (1) antigen-specific and bacterial models; (2) inducible models (chemical/immunological/physical); (3) genetic models; (4) adoptive transfer models and (5) spontaneous models (Hoffmann *et al.*, 2003). In vivo models are complex organisms which in combination with a multifactorial nature of IBD make it difficult to study certain aspects of the disease individually. Moreover, current guidelines encourage adhering to the 3Rs principles which assure the humane treatment of animals in research (WMS and RL, 1959). The rules aim for a reduction of animals used, refinement of the methods to ensure minimum stress on the subjects and replacement of the animals with alternative models.

In *in vitro* studies, the cell types and culture conditions are pre-defined and easier to control. In order to investigate specific aspects of the disease like barrier function and certain cell type activation, simpler models have been developed and will be discussed in more detail in the following sections. A more in-depth review of the current challenges in intestinal *in vitro* modelling has been described by Costa et al. (Costa and Ahluwalia, 2019). *In vitro* models

can be used to delineate potential factors in the pathophysiology of the disease for further investigations. A good example of such an approach is the study on the anti-inflammatory effect of IL-10 and the pro-inflammatory effect of TNFα, consequently being the current targets in IBD treatments (McKay, Philpott and Perdue, 1997). The *in vitro* cell models are of interest in IBD research as the variety of cells localized in the mucosa excrete factors potentially affecting the epithelium. During the inflammation, additional immune cells infiltrate lamina propria leading to the elevated complexity of the environment. Studies performed on *in vitro* models aid in understanding what are the key cells and effectors that act directly on the epithelium (McKay and Perdure, 1993). In contrary to the old belief that the epithelium is only a 'bystander in the inflammatory response' it is currently believed that the epithelium poses the activated cell phenotype (Gribar *et al.*, 2008). Epithelial cells release cytokines to regulate the inflammatory response, signal the recruitment of phagocytes and excrete factors that stimulate self-repair (McKay, Philpott and Perdue, 1997).

The pharmaceutical industry largely advances the development of new *in vitro* models. Since oral administration of the drugs is the preferred method, intestinal models are widely used and there is a need for more advanced and physiologically relevant models. A good model that could be used in the drug discovery process ought to fulfil certain requirements that have been listed in the **Table 1** (Fowler *et al.*, 2020).

Table 1. Requirements for in vitro model to be used in the drug discovery process.

Feature	Detailed requirements
Proper barrier function of the cell monolayer	Reflective of in vivo data: TEER 50-100Ω.cm2
Sufficient cell viability and architecture	Maintained up to a week of culture
Easy sampling	Access to both apical and basolateral side
Verified asymmetric distribution of key transporters	Comparable to in vivo
Expression of key drug transporters	Peptide transporter 1 (PEPT1), organic- anion-transporting polypeptide 2B1 (OATP2B1), and efflux transporters (PGP and BCRP)
Drug metabolizing activity	Functional expression enzymes i.e. CYP3A4, CES2, UGT
Mimicking of a dynamic nature of intestinal lumen	Introduction of the fluid flow

Additionally, pharmaceutical companies are in need of novel intestinal models to study the epithelium in homeostasis and a number of diseases, including IBD. The ideal *in vitro* model of IBD should mimic most of the key aspects of the disease including changes in barrier function and cytokines release. It should include various components i.e. epithelium, stromal cells, ECM, immune cells, microbiota. Such a model needs to be suitable for high throughput screenings and the assays to capture changes in phenotype should be readily available. The cost of the model is also of huge importance as the drug development process requires enormous investment and is bound to high risk.

1.3.1. *In vitro* models

1.3.1.1. Immortalized cell lines

The intestinal epithelium is composed of various cell types and has the ability to self-renew thanks to the presence of stem cells localized in the crypts. Depending on the research question, simplified models can be used to recapitulate only certain aspects of intestinal

biology. Simplification of the model allows for better control over the experimental conditions. Very often in drug discovery research, a simple monoculture model is used as it allows for an easy scale-up and does not elevate the costs of the initial screens. If the focus of the research is on the function of enterocytes that are the most predominant cell type in the gut, studies of absorption and transport can be done on a simple colorectal cell line model like Caco-2. However, when the interaction between various cell types is of interest or the interest lies in a specific protein not expressed by the basic models the more advanced *in vitro* models come into play. The experimental design should always depend on the research question and follow the great statement of Albert Einstein on how to conduct science:

> *"It can scarcely be denied that the supreme goal of all theory is to make the irreducible basic elements as simple and as few as possible without having to surrender the adequate representation of a single datum of experience."*

Over the years, Caco-2 carcinoma cell line was widely used to model intestinal epithelium, based on its ability to differentiate after reaching confluence (Fogh, Wright and Loveless, 1977). For over 30 years this line has been the accepted standard in drug permeability studies (Hidalgo, Raub and Borchardt, 1989). Standard culture protocol lasts 21 days, after which cells form a confluent polarized monolayer expressing several receptors, enzymes and transporters (Antunes *et al.*, 2013). To facilitate polarization and improve differentiation of the cells, they are cultured on permeable filter inserts (Corning, Costar etc) that enable access to the media from both apical and basolateral side (Hidalgo, Raub and Borchardt, 1989). It has been shown that the data obtained from Caco-2 cultured in this way correlate with drug absorption studies in humans (Artursson and Karlsson, 1991; Cheng, Li and Uss, 2008). Nevertheless, the long and labour-intensive protocol of culturing these cells is the limiting factor in using the model in high throughput screens. This has become a motivating factor to further advance and develop new culture protocols. It has been observed that the application of the fluid flow improves Caco-2 differentiation and barrier formation (Kim and Ingber, 2013) (Giusti *et al.*, 2014). Addition of cyclic strains to mimic peristaltic motions pronounces these effects (Kim *et al.*, 2012).

Despite being such a widely used model Caco-2 monoculture lacks important features like a mucus layer and a stromal component (Li *et al.*, 2013). More advanced multi-cellular models have been developed to add complexity to the system. Addition of HT-29 cell line,

that has the ability to produce mucus, provides more faithful results of drug transport due to the important role of mucus in the process (Pontier *et al.*, 2001; Gretchen J., Shulerb L. and Glahnc P., 2009). A few authors managed to differentiate Caco-2 cells into M-like cells by co-culturing them with Raji-B cells (Araujo et al., 2015; Gullberg et al., 2000; Kernéis et al., 1997). Others incorporated this approach in co-culture with HT-29 and in addition to M-cell phenotype observed increase in insulin transport (Antunes *et al.*, 2013; Araujo *et al.*, 2015).

Since the epithelium is thought to have an important role in the inflammatory response, a number of intestinal models have been used to study IBD. Kämpfer et al. established a Transwell® model with Caco-2 and human monocyte cell line THP-1 co-culture with both normal and inflamed phenotype (Kämpfer *et al.*, 2017). Their inflamed cultures exhibited epithelial barrier disruption, pro-inflammatory cytokines release, NO generation and cell death. This model shows potential for use in anti-inflammatory compounds research as the co-culture proved to be stable in the homeostatic condition, being a good control. Another group developed a similar Transwell® co-culture model, except that the immune component was embedded in the gel thus in close interaction with the epithelial layer (Leonard, Collnot and Lehr, 2010). More scalable model, an OrganoPlate® was used to model IBD by stimulating Caco-2 cells with pro-inflammatory cytokines and the effect on barrier integrity and cellular activation was measured (Beaurivage *et al.*, 2019). A more complex co-culture version of this model was developed and contained Caco-2, HT-29 as an epithelial layer and THP-1 together with MUTZ-3 as immune component mimicking dendritic cells (Gijzen *et al.*, 2020). Here as well the cultures were exposed to the cytokine trigger and the changes in barrier function were measured. Additionally, the proof of concept experiment with the use of TPCA-1 was performed exhibiting the anti-inflammatory role of the compound. Dosh et al. showed an alternative way of culturing Caco-2 and HT-29 in the 3D environment by embedding the cells in hydrogel (Dosh *et al.*, 2019). These cultures could be maintained over a long time and the IBD phenotype was observed after stimulation with the factors leading to inflammation.

1.3.1.2. Primary material

To fully recapitulate gut biology, all cell types need to be incorporated in the model. It is difficult to achieve that by using immortalized cell lines. Hence, researchers attempted to culture primary intestinal epithelial cells *in vitro*. Despite being very relevant, such cultures are short-lived and require complex media compositions. Aldhous et al. developed duodenal cultures on collagen membranes together with lamina propria cells and B-lymphocytes (Aldhous *et al.*, 2001). Another group successfully cultured intestinal epithelial cells with myofibroblasts (Lahar *et al.*, 2011). Notably, the biggest advantage of such cultures is the possibility to generate patient-derived models. With IBD being such a complex disease personalized medicine approach allows for the investigation of individual traits and amelioration of the drug failure probability. One study reported the isolation of 65 primary intestinal epithelial cell lines to investigate the interaction with microbiota that aimed at developing novel assays (Van Dussen *et al.*, 2015). Another group discovered the correlation in the expression of Oncostatin M with the severity of IBD and responsiveness to anti-TNFα therapy (West *et al.*, 2017). Even though some successful cultures have been reported, the reproducibility and maintenance of the primary cells over a long time remain challenging.

1.3.1.3. Organoids

In order to maintain the primary cells culture for a long time and with all the various cell types present, stem cell population needs to be sustained. When isolated from intestinal crypts, LGR5 positive stem cells are able to form 3D structures *in vitro* and can be cultured over many passages (Sato *et al.*, 2009, 2011). Those structures called organoids closely mimic the biology of the original tissue. They contain most of the cell types and recapitulate the folding of the intestine by recreating crypt-villi architecture. Organoids grow in a cystic form with a hollow centre, the protruding structures resemble crypts and contain stem cells with accompanying Paneth cells (Sato *et al.*, 2013). As the stem cells proliferate, they move up the crypt-like structure towards the central part of the organoid and differentiate into various cell types. The whole process is orchestrated by the gradients of growth factor including high WNT

and low BMP concentration in the stem cell niche (Qi *et al.*, 2017). Thus organoids can be described as self-organizing, self-renewing structures composed of various cell types. Aforementioned primary material derived stem cells are not the sole cell type capable of generating such structures. Human intestinal organoids can be generated from pluripotent stem cells and are composed of epithelial and mesenchymal cells (Spence *et al.*, 2011). Induced pluripotent cells are an attractive alternative to the primary material as they are self-renewing, subject to genome editing and increasingly available.

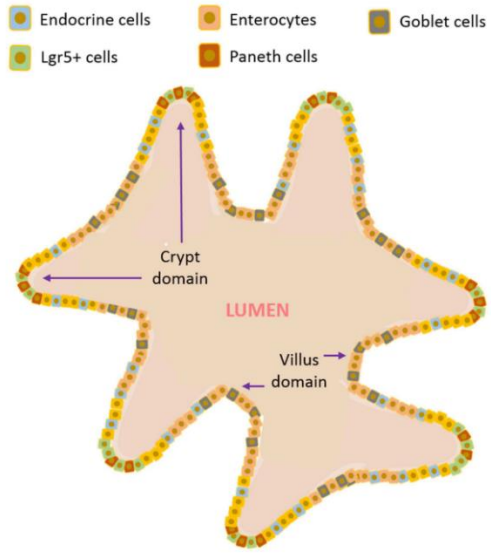

Figure 9. Schematics of an organoid structure (Costa and Ahluwalia, 2019).

Despite being a physiologically relevant model organoids have their disadvantages. The most crucial one being the enclosed structure. Access to the apical side of the organoid is restrained which poses a huge complication for studying transport and drug absorption (Fatehullah, Tan and Barker, 2016). Another important missing feature is the lack of exposure to the mechanical forces that the cells experience in vivo. In order to ameliorate such deficiencies new ways of culturing organoids have been developed, including simplified monolayer cultures on the collagen-coated surfaces to allow the access from the apical side (Ettayebi *et al.*, 2016; Braverman and Yilmaz, 2018) and more advanced organ-on-chip devices

that incorporate fluid flow and peristaltic movements (Kasendra *et al.*, 2020) as well as physiologically relevant architecture (Nikolaev *et al.*, 2020). Kasendra et al. published a more physiologically relevant version of their first PDMS-based organ-on-chip device with organoid-derived cells. The clear advantage over the Caco-2 model presented in this research was pronounced CYP3A4 expression which makes the model useful in pharmacokinetics studies. Nikolaev et al. generated perfusable intestinal model containing crypt-villi architecture and reported the presence of rare epithelial cells populations scarcely found in conventionally cultured organoids. Their model was stable in long culture and maintained self-renewal capacity.

Concerning disease modelling organoids similarly to the primary cell lines enable research towards designing patient-tailored treatments. The pathogenesis of IBD is yet to be fully understood and establishment of the treatment successful in a large patient cohort remains challenging. As an example, popular anti-TNFα antibody treatment (Infliximab) has beneficial effects in 60-87% of patients, of which 23-46% become insensitive to the treatment within 5 years (Ding, Hart and Cruz, 2015). Therefore developments in personalized medicine approach are of a great need and emerging models utilizing organoid technology are building the foundation for that. Noel et al. integrated intestinal epithelium and a component of the mucosal immune system, namely macrophages to study the host response to the infection (Noel *et al.*, 2017). Barrier function, cytokines release and protein expression were compared between normal and post-infection conditions. The results showed coordinated action of both epithelium and macrophages in response to the bacterial infection. An important cell type of the intestinal epithelium are M cells as they play a role in endocytosis of luminal antigens and further transfer to immune cells (Mabbott *et al.*, 2013). It has been shown that organoids can be enriched with M cells upon treatment with RANKL (NFκB ligand) which would increase the relevance of the model and allow for more in-depth study of the antigen presentation by epithelium (Rouch *et al.*, 2016). One of the pathologies of the IBD involves fibrosis that occurs as the reaction of the tissue to the damage induced by chronic inflammation (Rieder and Fiocchi, 2009). As the iPSC-derived intestinal organoids are the only ones containing mesenchymal cells being the main effector in fibrosis, Rodansky et al. used this model as a tool in a drug screening for anti-fibrotic drugs (Rodansky *et al.*, 2018). Currently, more research is done towards the development of the protocols of culturing

organoids and increasing number of disease models are being generated. The field is still evolving and the combination of organoids with the organ-on-chip technology holds a great promise for future developments.

Table 2. Tissue sources for *in vitro* organ models.

Cell source	Advantages	Disadvantages
Immortalized cell lines	Readily available Established culture protocols Mature phenotype	Derived from cancerous cells Not always representative of normal metabolism
Primary cells	Patient specific Derived from adult	Difficult to maintain in culture long term Inaccessibility of some tissues
Adult stem cell-derived organoids	Derived from adult Mature phenotype	Not readily available Labour intensive culture
iPSC-derived organoids	Commercially available Patient specific	Foetal phenotype

1.3.1.4. Adding the dimension

The organ-on-chip is one of the emerging technologies of the 21st century and it can be described as a biomimetic device designed on a basis of a microfluidic chip that represents the physiological features of the living organ. By combining cell biology, engineering and biomaterial technology the devices can mimic the microenvironment of the body by tissue interfaces and mechanical stimulation. These complex models emulate structural and functional features of the organs which in turn provides more reliable prediction for the drug response. In human body, cells are arranged in a complex 3D manner allowing for a functional contact between various cell types and consecutively different organs. Microfluidics enables

cell patterning, therefore such complex co-cultures can be established. Hydrogels are often used to define the geometrical distribution of individual components (Tibbe *et al.*, 2018). Scaffolds can also be used to mimic the architecture of the organ. In gut modelling, two approaches can be taken, either recapitulating villi/crypt (Jong et al., 2011; Yi et al., 2017; Yu et al., 2012) or the tubular structure of the intestine (Chen *et al.*, 2015).

Microfluidics permits the perfusion of the cells much like in in vivo conditions. Cells in the human body experience constant fluid flow through the transmission of blood and other bodily fluids which cannot be reflected in static 2D tissue cultures. Fluid flow produces sheer stress and it has been shown to induce cell polarization (Theobald *et al.*, 2018). In endothelial cells, such physical stress is functionally indispensable as it activates surface markers and initiates signalling pathways (Davies, 1995). Incorporation of the fluid flow in OOC devices is usually achieved by placing it on the rocker (oftentimes bidirectional flow, gravity-driven) or by connecting it to the pumping systems (Ronaldson-Bouchard and Vunjak-Novakovic, 2018). One of the first reports describing a gut on a chip system with perfusion featured long-term Caco-2 culture showing the application in toxicity and drug screening (Kimura *et al.*, 2008). Imura et al. used a model with a microsyringe pump and showed suitability for absorption studies (Imura *et al.*, 2009). Later, they used the same system in conjunction with hepatic model and used it to mimic intestinal absorption, liver metabolism and compounds bioactivity (Imura, Sato and Yoshimura, 2010).

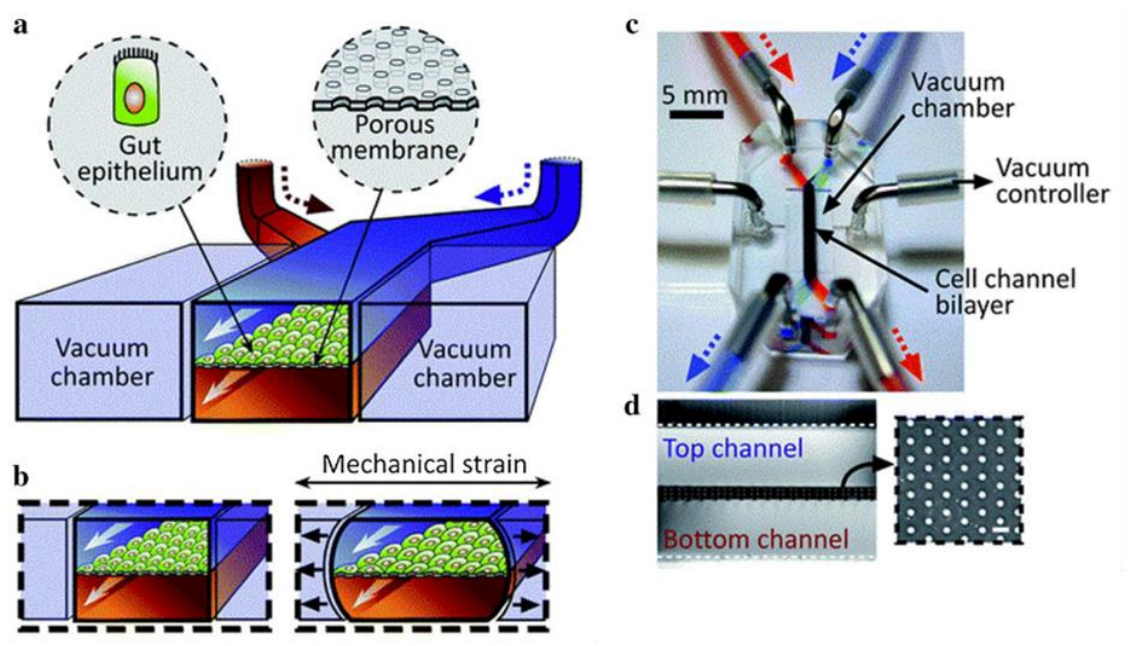

Figure 10. Illustration of PDMS-based gut-on-chip model (Kim et al., 2012).

(a) schematic of the device; (b) cross-section schematic of the device showing application of mechanical stretching of the PDMS membrane; (c) device connected to the perfusion system; (d) cross-section view of the device with magnified top view of the membrane.

Motility is yet another mechanical feature that plays a role in the tissue function. It has been described that the application of cyclic stretches can promote proliferation and influence spatial organization of the cells. The intestine is subject to the peristalsis movement resulting from the recurrent shortening of the villi. Caco-2 cells when cultured on an elastic membrane with applied stretching increase their proliferation rate and upregulate brush border enzyme expression (Basson and Di, 1996). It has been shown that cyclic stretch influences the integrity of the cell-cell junctions resulting in increased paracellular permeability (Samak *et al.*, 2014). Kim et al. established a more advanced model that combines fluid flow and cyclic stretching and led to the formation of villi-like folds by Caco-2 cells (Kim and Ingber, 2013). Later, the same device was used with small intestinal organoids (Kasendra *et al.*, 2020). With advances in OOC technology the new models more closely resemble human physiology and hopefully in the future will allow for acceleration in the drug discovery process. This thesis describes the development of a novel gut on a chip model for IBD modelling that could be used in high throughput drug screening.

1.4. Hypothesis

The objective of this thesis was to generate a physiologically relevant gut-on-a-chip model that would mimic pathophysiology of Inflammatory Bowel Disease and would be suitable for high throughput screening in drug development process. We based our initial model on the hypothesis that deficiency in *NOD2* signalling would allow for recapitulating the disease phenotype *in vitro,* as *NOD2* signalling is thought to be critical for the maintenance of immune homeostasis. We chose to focus on the epithelial component of the intestinal tissue and subsequently added immune cells to study the interaction upon stimulation with pro-inflammatory trigger (MDP, the ligand of NOD2). As an alternative approach to model IBD *in vitro* we set to recreate inflamed gut-on-a-chip by introducing exogenous cytokines to the system. Over the course of the project we tested a number of different cell sources for recreating epithelial component of IBD-on-a-chip to match physiological relevance and responsiveness to pro-inflammatory trigger.

2. Materials and Methods

2.1.Cell culture

2.1.1. Cell culture conditions

Caco-2 cells (86010202, Sigma) and HEK293 cells (85120602, ECACC) were maintained in high glucose DMEM glutaMAX (31966047, Thermo Fisher Scientific) supplemented with 10% FBS (16140-071, Gibco) and 1% Penicillin/Steptomycin (P4333, Sigma). DLD-1 cells (90102540, ECACC), THP-1 cells (TIB-202, ATCC) and Raji Burkitt's Lymphoma cells (CCL-86, ATCC) were maintained in RPMI-1640 (R8758, Sigma) supplemented with 10% FBS (16140-071, Gibco) and 1% Penicillin/Steptomycin (P433, Sigma). iPSC-derived intestinal organoids (Defi-INT, DefiniGEN) were maintained in Def-INTESTINAL Thawing, Recovery and Maintenance Medium (IRMM, DefiniGEN) supplemented with Def-INTESTINAL Supplement Additive A (IRMM-A, DefiniGEN) and additionally Rock inhibitor (Y-27632) (688000-1MG, Merck) until the first medium change after thawing/splitting. Primary-derived organoids (Hubrecht Institute, Netherlands) were embedded in Matrigel GFR (Corning, 356231) and cultured in 24-well plates in 1× CNM media containing 50% Wnt3a CM, Advanced Dulbecco's modified Eagle medium/F12 (ThermoFisher 12634028) supplemented with penicillin/streptomycin, 10 mmol/L HEPES, 1× Glutamax, 1× B27 supplement, 1.25 mM N-acetyl-cysteine (Sigma A9165), 10 mM Nicotinamide (Sigma, N0636), 5 nM Gastrin (Sigma, G9145), 100 ng/mL Noggin (Peprotech 120-10C), 250 ng/mL Rspondin-3 (Tocris, 3500), 50 ng/mL EGF (Peprotech, AF-100-15), 500 nM A83.01 (Tocris 2939), 10 µM SB2020190 (Sigma, S7076) and 50 µg/mL Primocin (Invivogen ANT-PM-2). Culture was passaged every 7 days and Y-27632 dihydrochloride (Torcis 1254) was added to the media for the initial 48 h. All cell lines were cultured in the incubator at 37°C, 5% CO2 and 96% relative humidity.

To improve attachment of the cells to the cell culture plates (in case of culture of HEK293 cells and Caco-2 cells), wells were coated with poly-L-lysine (3438-100-01, Culturex).

iPSC-derived organoids were cultured in growth factors reduced Matrigel droplets (356231, Corning) in 24-well cell culture plates.

2.1.2. Passaging cells

Adherent cells (Caco-2, DLD-1, HEK293 cell lines) were normally cultured in T75 flasks and passaged before they reached 80% confluency. Cells were washed with 5ml 1xPBS (70013065, Gibco), 2ml 0.25% trypsin (15090-46, Gibco) and incubated at 37°C for couple of minutes. As soon as cells detached from the cell culture plate surface, 5ml of culture medium was added and the cell suspension was transferred to a falcon tube. Cells were centrifuged for 5 min at 200 g. After that medium was aspirated and cells were resuspended in an appropriate volume of the fresh culture medium. Cells were passaged in a ratio 1:2 to 1:8 (Caco-2), 1:2 to 1:10 (DLD-1), 1:5 to 1:30 (HEK293). Culture medium was refreshed every 2-3 days.

Suspension cells (THP-1 and Raji Burkitt's Lymphoma cell lines) were normally cultured in T25 flasks and passaged before they reached concentration of $1x10^6$ cells/mL. Cells suspension was transferred into falcon tube and centrifuged for 5min at 300 g. After that medium was aspirated and cells were resuspended in an appropriate volume of the fresh culture medium. $0.5x10^6$ cells were seeded in a new T25 cell culture flask. Culture medium was refreshed every 5 days.

2.1.3. Freezing and thawing of cells

Cells were harvested as described in **Section 2.1.2** and resuspended in freezing medium (respective culture medium with 10% DMSO). Cells were frozen in concentration 1-$3x10^6$ cells/mL. Vials were immediately stored at -80°C in a CoolCell® freezing containers and transferred to liquid nitrogen the next day.

When thawing, the content of a vial was pipetted into 9 mL of warm culture medium and mixed gently. Cells were centrifuged for 5 min at 200 g to remove the residual DMSO. After centrifugation cells were resuspended in a culture medium and transferred into culture flask.

2.2. Generation of knock out cell lines by using CRISPR technology

In brief, cells are transfected with a plasmid containing Cas9 coding sequence, a specific sgRNA sequence and GFP or antibiotic resistance gene (puromycin) to allow for selection. Cas9 is an RNA-guided nuclease able to introduce sequence-specific double strand breaks in DNA. The break is repaired in the cells by nonhomologous end joining or homologous directed repair. As the repair system is not perfect, often the mutations are introduced. To select for the desired mutations, cells are sorted by FACS or treated with puromycin. Single clones are tested for the presence of mutations by PCR and sequencing. Chosen clones are then propagated and stable cell lines are banked.

2.2.1. Molecular cloning – vector generation

Vectors SpCas9(BB)-2A-GFP (PX459) (Plasmid#48138, Addgene) and pSpCas9(BB)-2A-Puro (PX459) (Plasmid#62988, Addgene), both deposited by Zhang lab. sgRNA sequences were designed in CRISPOR (Haeussler *et al.*, 2016) and crispr.mit.edu (Zhang lab, no longer available).

2.2.1.1. Phosphorylation and annealing of the sgRNA oligos

Designed oligos (designed sgRNA sequence) were synthesized by Sigma (listed in **Table 12**) and resuspended to a final concentration of 100 µM. Following mixture (**Table 3**) was

prepared and incubated for 30 min at 37°C and for 5 min in 95°C. Tubes were left at RT to cool down completely.

Table 3. sgRNA phosphorylation and annealing.

sgRNA top	1 µL
sgRNA bottom	1 µL
10x T4 ligation buffer (B69, Thermo Fisher)	1 µL
T4 PNK (EK0031, Thermo Fisher)	1 µL
dd H_2O	6 µL
TOTAL	10 µL

2.2.1.2. Digestion of the vector

The digestion reaction was set up as in table 3 and incubated at 37°C for 1h.

Table 4. Digestion of the vector.

Vector (pX458 or pX459)	1 µg
BbsI enzyme (R0539S, NEB)	1 µL
Cut smart buffer (B7204S, NEB)	5 µL
dd H_2O	X
TOTAL	**50 µL**

After digestion, the reaction mix was subject to gel electrophoresis and gel extraction in order to purify the digested vector. Electrophoresis was performed in 1% agarose gel in 1x TAE buffer (40 mM Tris, 20 mM acetic acid, 1 mM EDTA). SYBR® Safe DNA Gel Stain (S33102, Invitrogen) was used to visualize the product in UV light (Gel Doc™ System, Bio-Rad). Correct band was cut out of the gel and taken for purification with NucleoSpin® Gel and PCR Clean-up kit (740609.50, Marcherey-Nagel). Procedures were performed as stated in the manual of the kit. The concentration of obtained DNA was measured by NanoDrop.

2.2.1.3. Ligation

Ligation of the vector and sgRNA sequence was performed at RT for 1 h.

Table 5. Ligation.

digested vector	100 ng
annealed oligos (diluted 1:200 in dd H_2O)	1 µL
10x T4 ligation buffer (B69, Thermo Fisher)	1 µL
T4 ligase (EL0014, Thermo Fisher)	0.5 µL
dd H_2O	X
TOTAL	**10 µL**

2.2.1.4. Bacterial Transformation

BL21 competent *E.coli* cells were used for the transformation. Prior to transformation, cells were thawed on ice and 5 µL of the ligation was added. Cells were incubated on ice for 20 min, at 42°C for 1 min and back on ice for 2 min. LB medium (250 µL) was added and cells were incubated for 45 min at 37°C with shaking (220 rpm). Afterwards, the cells were plated on LB agar plates with ampicillin (100 µg/mL) and incubated overnight at 37°C.

2.2.1.5. Plasmid DNA isolation and purification

Following day, couple of bacterial colonies were picked from LB agar plate and dissolved in 5ml of LB medium containing ampicillin (100 µg/mL). Cultures were incubated overnight at 37°C with shaking (220 rpm). The day after bacterial cultures were pelleted and plasmid DNA was isolated with GeneJET Plasmid Miniprep kit (K0502) according to the manufacturer protocol. Isolated DNA was sent for sequencing at University Genomic Facility. If correct insert sequence was confirmed, 100ml cultures were established from transformant bacterial culture and subject to Midiprep purification with Nucleo Bond® Xtra Midi kit (740410.50, Macherey-Nagel). Purified plasmids were used for further transfections.

2.2.2. Transfection

Cells were seeded 1 day before transfection at a density of $0.25x10^6$ cells/well in 6 well plate and $0.02x10^6$ cells/well in 96 well plate. Lipofectamine 2000 (11668027, Thermo Fisher Scientific) was used as the transfection agent. Transfection mix was prepared in OptiMEM medium (11058-021, Gibco). Briefly, DNA/RNA mix was prepared in one Eppendorf tube and Lipofectamine mix in another Eppendorf tube. Mixes were incubated at RT for 5 min. After that DNA/RNA mix was added to Lipofectamine mix and incubated for additional 20min at RT. Culture medium was changed on the cells (culture medium without Penicillin/Streptomycin) before transfection. Transfection mix was added in droplets on top of the cells. Culture medium was refreshed the next day and transfection efficiency was assessed within 48 h. Respective transfection conditions are gathered in **Table 6**.

Table 6. Transfection conditions.

Cell line	Cell culture plate format	Lipofectamine amount/well	Nucleic Acid amount/well	OptiMEM amount/well
Caco-2, DLD-1, HEK293	6 well	5 µL	2.5 µg DNA	150 µ + 150 µL
Caco-2, DLD-1, HEK293	96 well	0.5 µL	0.2 µg DNA	50 µl + 50 µL

2.2.3. FACS sorting

Cells were detached from the culture plates with trypsin 48 h after transfection and resuspended in OptiMEM. Single cell suspension was used for FACS sorting performed on FACS Aria (BD Biosciences). Cells were single cell sorted based on GFP expression into 96 well plates coated with collagen and filled with culture medium. Additionally, part of the sorting was performed as bulk sort into tubes for DNA isolation and T7 assay (assessment of efficiency of introduction of mutations). In that case, GFP positive cells were sorted as well as GFP negative cells and samples were taken for DNA extraction. Immediately after the sorting, plates were transferred to the incubator and checked regularly for the growth of colonies. As soon as ready to be split, the cells were propagated, and some cell pellets were saved for DNA

extraction. Sequencing was performed to detect incorporated mutations (primers list in **Table 12).**

2.2.4. DNA extraction

Cells were pelleted, washed once with 1x PBS and resuspended in lysis buffer. DNeasy Blood & Tissue kit (69504, Qiagen) or phenol:chlorophorm extraction protocol were used to isolate DNA.

Phenol:chlorophorm protocol:

Lysis buffer:

20 mM EDTA

10 mM Tris pH 8

200 mM NaCl

0.2 % Triton X-100

100 µg/mL Proteinase K (added just before the lysis)

1. Lyse the cells in 0.5 mL lysis buffer and incubate the sample for 1 h at 37°C.
2. Heat inactivate proteinase K at 95°C for 5 min.
3. Centrifuge for 5 min at 13000 rcf.
4. Transfer supernatant to a new tube.
5. Add equal volume of phenol:chloroform:isoamyl alcohol pH 8.8 (lower phase in the original bottle).
6. Centrifuge at the maximum speed for 2 min.
7. Remove the top phase (DNA dissolved in aqueous phase) to a new tube.
8. Repeat steps 5-7.
9. Add 1:10 volume of 3 M Sodium Acetate (pH 5.2) and equal to the sample volume of the Isopropanol to precipitate the DNA.

10. Incubate 1-2 h at -80°C.
11. Centrifuge at 13000 rcf, 4°C for 30 min.
12. Discard the supernatant.
13. Wash with 1 ml 70% ethanol.
14. Centrifuge at the maximum speed for 5 min.
15. Discard supernatant and dry the pellet.
16. Resuspend in 20 µL of nuclease free water and measure the concentration on NanoDrop.

2.2.5. PCR amplification

Polymerase chain reaction was used for amplification of the target region. Routinely, 100 ng of gDNA was taken for reaction. List of primers is contained in **Table 12**.

Table 7. PCR set up.

GoTaq® Hot Start Polymerase (M500A, Promega)	0.1 µL
5x Green GoTaq® Flexi Buffer (M891A, Promega)	4 µL
dNTPs (10 mM; R0191, Thermo Fisher)	0.4 µL
Forward primer (20 µM)	0.5 µL
Reverse primer (20 µM)	0.5 µL
H_2O	X
TOTAL	20 µL

Proportion of the PCR product was subject to electrophoresis in 1% agarose gel and if the correct size of the band was detected, following PCR purification was performed with QIAquick PCR purification kit (28104, Qiagen) according to the manufacturer's protocol.

2.2.6. T7 assay

T7 assay was used to determine genome targeting efficiency. T7 Endonuclease I is an enzyme that recognizes non-perfectly matched DNA sequences and cleaved detected regions. PCR products are subject to annealing and then treated with T7 Endonuclease I. Fragments are analyzed on 2.5% agarose gel to determine the efficiency of introducing mutations. Briefly, PCR was performed as described in previous section on all the sorted samples (GFP positive, GFP negative and non-transfected control) and the reaction was performed as stated in **Table 8** and **Table 9**.

Table 8. T7 assay reaction set up.

Purified PCR product	200 ng
10x NEBuffer 2 (B7002S, Promega)	2 µL
H_2O	X
TOTAL	**19 µL**

Table 9. Reaction conditions (hybridization).

STEP	**TEMPERATURE**	**RAMP RATE**	**TIME**
Initial denaturation	95°C		5 min
Annealing	95-85°C	-2°C/second	
	85-25°C	-0.1°C/second	

After hybridization, T7 Endonuclease I (M0302, Promega) was added to the annealed PCR products and incubated for 15 min at 37°C. The reaction was stopped by addition of 0.25 M EDTA (1.5 µL per sample). The samples were subject to electrophoresis in 2.5% agarose gel in 1xTEA buffer.

2.3. Generation of NOD2 overexpression plasmids

NOD2 overexpression plasmids were used in validation of the anti-NOD2 antibodies. NOD2 sequence was amplified from pHAGE C-TAP (HSCD00462562, Harvard Plasmid ID) and inserted into pCDNA3.1GFP and pCDNA3.1myc. List of used primers is included in **Table 12**. pCDNA plasmids and amplified NOD2 insert were digested with NotI-HF (R3189, NEB) and KpnI-HF (R3142S) enzymes in CutSmart® buffer (B7204S) for 1h at 37°C. Calf Intestinal Alkaline Phosphatease (CIP; M0290S, NEB) was added after the digestion of vectors to allow for dephosphorylation of 3' and 5' ends. Digested vectors were subject to gel electrophoresis and purification prior to ligation (see **Section 2.2.1**).

Ligation of the vectors and insert (ratios 1:1 and 1:3) was performed at RT for 3 h. See **Table 5** for the details of reagents used. Subsequently, transformation of *E.coli* and plasmid isolation was performed (see **Section 2.2.1.4** and **2.2.1.5**). Obtained samples were checked for the presence of the insert by digestion of the vector and comparison of sizes with a control empty plasmid. Final confirmation was sequencing of the vector (primers shown in **Table 12**).

2.4. Western blot

Buffers:

1x PBS:

137 mM NaCl, 2.7 mM KCl, 10 mM Na_2PO_4, 1.8 mM KH_2PO_4

Lysis buffer:

50 mM HEPES pH 7.5, 150 mM NaCl, 1.5 mM $MgCl_2$, 1 mM EDTA, 10% glycerol, 1% Triton X-100, protease cocktail inhibitor

4x Laemmli sample buffer:

250 mM Tris-HCl pH 6.8, 40% glycerol, 20% β-metcaptoethanol, 8% SDS, 1% bromophenol blue

10x Running buffer:

0.192 M glycine, 0.025 M Tris, 0.1% SDS

10x Transfer buffer:

0.192 M glycine, 0.025 M Tris, 20% ethanol

Ponceau S:

30% trichloroacetic acid, 2% Ponceau S

PBST:

0.05% Tween 20 in 1xPBS

TBST:

50 mM Tris, 150 mM NaCl, 0.1% Tween 20, pH 7.6

2.4.1. Cell lysis

Confluent cells were subject to lysis (routinely 6 well culture dishes were used for this purpose). Plates were kept on ice, washed twice with 1xPBS and incubated with ice cold lysis buffer (250 µL per well) for couple of minutes. Cells were harvested with cell scrapers and transferred to cold tubes. Samples were incubated on ice for up to 60 min and vortexed every 15 min. Cell lysates were centrifuged at 15000 rpm, 4°C for 20 min. Supernatants were collected in new tubes and protein concentration was determined by DC Protein Assay.

2.4.2. Determination of protein concentration

DC Protein Assay (5000111, Bio-Rad) is a colorimetric assay that allows for determination of protein concentration. Assay is basing on the reaction of protein with an alkaline copper tartrate and folin. As the result, blue product with maximum absorbance at 750 nm can be detected in absorbance reader. Procedures stated in the manufacturer's

protocol were followed. Standard curve was prepared with serial dilutions of albumin (2 mg/mL) in lysis buffer. All samples were adjusted to the same protein concentration for further analysis on the Western Blot.

2.4.3. SDS-PAGE gel electrophoresis and protein transfer

SDS-PAGE electrophoresis was used to separate proteins in the samples according to their molecular weight. Bio-Rad Mini-PROTEAN® Tetra Cell device was used. Prior to electrophoresis samples were mixed with Laemmli buffer and boiled at 95°C for 5 min and cooled down to RT. PageRuller™ Prestained Protein Ladder (26616, Thermo Fisher) was used as the size indication. Samples were run in the 1x running buffer at 50 V for initial time of 30 min (concentration of the samples) and 120 V for the rest of the run. Subsequently, proteins were transferred onto the nitrocellulose membrane in Mini Transfer-Blot® Electrophoretic for 90 min at a constant current 250 mA. Membranes were subsequently stained with Ponceau S.

2.4.4. Antibody staining of the membranes

Ponceau S stain was removed from the membranes with 1x PBST. Membranes were incubated with 5% non-fat dry skimmed milk solution in 1x PBST or 1xTBST for 1 h at RT with agitation (blocking). After that, primary antibody dilutions were prepared in blocking buffer and membranes were incubated at 4°C overnight. Membranes were washed three times with 1x PBST and incubated with secondary antibody diluted in a blocking buffer (1 h at RT with agitation and covered from the light). Subsequently the membranes were washed three times in 1x PBST and taken for protein detection with Odyssey Sa® Infrared Imaging System (LI-COR). The analysis was performed in Image Studio™ Life Software.

2.5. RNA extraction

Total RNA was extracted with RNeasy Mini kit (74104, Qiagen) following the manufacturer's protocol. Cells were harvested, washed with 1x PBS and centrifuged at 200 g for 5 min. The cell pellets were resuspended in RLT buffer with or without the addition of β-mercaptoethanol and processed immediately or stored at -80°C.

2.6. cDNA synthesis

First strand cDNA was synthesized using SuperScript™ IV First-Strand Synthesis System (18091050, Thermo Fisher) or M-MLV Reverse Transcriptase (28025013, Thermo Fisher) and random primers (48190011, Invitrogen) according to manufacturer's protocols. Negative control in these experiments was non-reverse transcriptase control, where instead of the enzyme nuclease-free water was added. Synthesized cDNA was used to determine the expression levels of the genes of interest in qPCR.

2.7. qPCR

Quantitative PCR was performed in order to determine the expression levels of NOD2 and other genes of interest in used cell lines. FastStart Essential DNA Green Master (06402712001, Roche) and primers listed in **Table 12** were used. Firstly, the efficiency of designed primers was checked by performing qPCR on serially diluted cDNA sample (or NOD2 overexpression vector). Dilutions x4 to x1024 were taken for the experiment. The primer pairs were chosen based on their efficiency (close to 2 and similar to one another).

Table 10. qPCR reaction set up.

2x Fast Start DNA Green	5 µL
Primer mix (50 µM each)	0.1 µL
H_2O	1.9 µL
cDNA (diluted x10)	3 µL
TOTAL	**10 µL**

Table 11. qPCR reaction conditions.

Preincubation	1 cycle	95°C for 600 sec
3 Step Amplification	45 cycles	TD 95°C, 0 cycles -> 95(1°C)
		TD 61°C, 0 cycles -> 51(-0°C)
		72°C 15 sec (single)
Melting	1 cycle	95°C 10 sec
		65°C 60 sec
		97°C 1 sec (continuous)
Cooling	1 cycle	37°C 30 sec

All samples were prepared in triplicates and -RT control was included for each sample. Plates were kept on ice at all times and centrifuged at 2000 rpm for 2 min to collect all the reaction mix at the bottom of the tube. LightCycler® 480 Real-Time PCR machine (Roche) was used to perform the assay and accompanying software (LightCycler® 96, Roche) for the data analysis. Relative quantification was performed in all the analysis.

2.8. Luciferase Assay

Dual Luciferase Assay (E1910, Promega) was used to determine the activity of NFκB. Cells were transfected in triplicate with NFKβ Luciferase reporter plasmid mix, containing NFκB dependent *Firefly* Luciferase plasmid (pNFkB_Luc) and normalization *Renilla* luciferase plasmid (pRLK_Luc). Luciferase activity was measured 48 h after transfection. Cells were stimulated or not with MDP (10 µg/mL) for 6 hours. NFκB activity is shown as Relative

Luciferase Unit (RLU) corresponding to the NFκB dependent *Firefly* Luciferase signal normalized against *Renilla* signal.

2.9. PDMS-based organ-on-chip

An organ-on-chip device is a 3D microfluidic cell culture chip that allows for mimicking more closely the microenvironment of the cells in a body. One of the methods used to manufacture such devices is PDMS technology. PDMS (polydimethylsiloxane) is an easily accessible silicone based, transparent, non-toxic organic polymer that comes in a liquid form. As soon as mixed with a curing agent it starts to solidify. Parts of the chip can be manufactured in the aluminum molds (University of Cambridge workshop). The below protocol shows in detail the steps performed in order to manufacture 2 channel PDMS-based chips with a polystyrene membrane in between. The protocol is based on the method developed at Wyss Institute (Benam *et al.*, 2016). Manufacture of the devices was performed at Prof. Pietro Cicuta lab with an invaluable help of Nicola Pellicciotta (Department of Physics, The Cavendish Laboratory, The University of Cambridge).

2.9.1. Manufacture of the device

1. 100 g of PDMS was added to the plastic container and curing agent (ration 15:1) was added. The mixture was vigorously mixed with a spatula.
2. Obtained mixture was degassed for 30 min in desiccator.

3. Bubble-free mixture was poured into the previously cleaned moulds (1x 100% acetone, 1x 70% ethanol, air dry). Two moulds were used – one containing top channel feature and second one with bottom channel feature (see **Figure 11**).

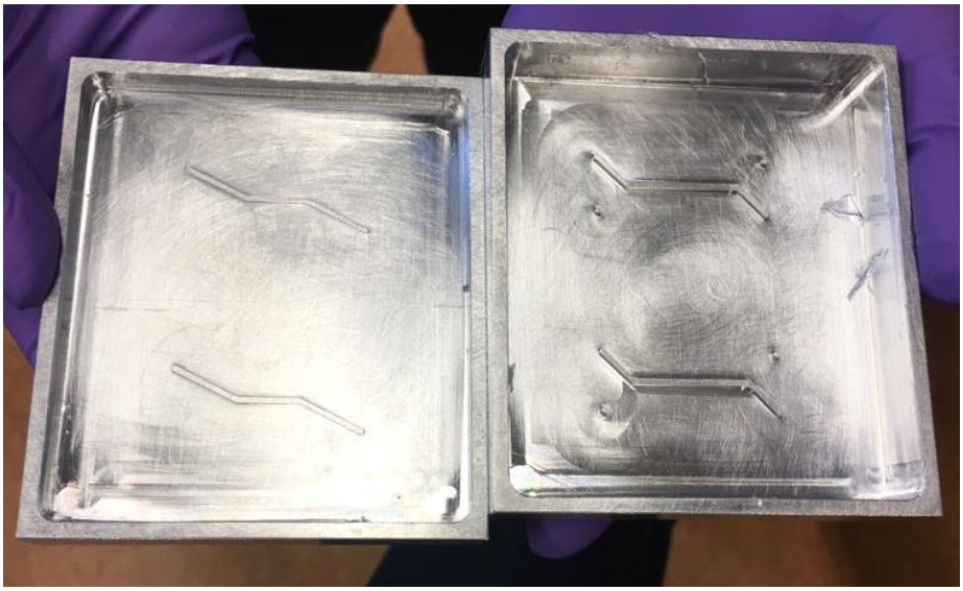

Figure 11. Moulds used to manufacture PDMS-based organ-on-chip.

Bottom part containing 200 nm high channel for medium perfusion (left side in the picture) and top part containing 1 mm high channel for culturing cells (right side in the picture).

4. Moulds were incubated at 60°C for 2 h to allow for solidification.
5. In the meantime the tubing (microbore tubing, 0.020" x 0.060" OD, 100ft/roll cole parmer; WZ-06419-01, Tygon) and pins (90 degree bend, 22 gauge stainless dispensing steel tips; FIS5601171, Intertronics) were prepared. Those were needed to be able to initiate the fluid flow inside the device. All the items were sterilized with 70% ethanol. Each device required 4 tubes (at least 5 cm) and 4 pins to connect the tubes.
6. Solidified PDMS slabs were removed from the moulds with the help of steel scalpel and forceps. Holes for the pins were punched in at the inlet and outlets of each channel. All the impurities that could prevent proper assembly were removed with the sticky tape.
7. Pre-cut fragments of polyester membrane (Transwell® permeable supports (6 well plate); Corning, CLS3450) together with both PDMS slabs was plasma treated prior to assembly.

8. Within 15 min after the treatment all the components of the device were aligned and assembled. The device was incubated at 60°C for 1 h to improve the binding.
9. Afterwards another plasma treatment was required in order to bind glass slide underneath the device. This allows for improved imaging and prevents bending of the chip which could result in folding of the membrane inside the device. After proper alignment the whole device was incubated at 60°C for 1 h to improve the binding.
10. The pins with connected tubing were inserted into the inlets and outlets of each channel. Fully assembled device is shown in **Figure 12**.

Figure 12. PDMS-based organ-on-chip 2 channel device with tubing.

11. The device was sterilized in the UV-oven ozone cleaner for 40 min.
12. Prior to cell seeding the channels were coated with collagen solution (0.3 mg/mL) for 1.5 h at 37°C. Collagen was washed away with culture medium and the device was kept with the medium in both channel for at least 2 h.

2.9.2. Cell culture in the PDMS-based organ-on-chip device

Cells were harvested and resuspended in a concentration $5x10^6$ cells/mL. Cell suspension was injected into the top channel with the syringe. The tubes were clipped and the device was incubated for 2 h at 37°C to allow for the cells attachment. The device was

flushed with culture medium to remove all the cells that did not attach to the membrane. The tubing was connected to the syringe pump and the cells were cultured in the incubator at 37°C.

2.9.3. Immunostaining in the PDMS-based organ-on-chip device

Cells were washed with 1xPBS, fixed with 4% paraformaldehyde for 15 min and washed again. If the staining was not performed immediately afterwards, the device was incubated at 4°C with 1xPBS in both channels. Cells were permeabilized with 0.2% Triton X-100 (T8787, Sigma) in PBS for 2 h. Cells were blocked with 1% BSA (A2153, Sigma), 5% FBS (16140-071, Gibco) for 30 min. Primary antibody diluted in blocking buffer was added to the channels and the device was incubated at 4°C overnight. Cells were washed trice with 1xPBS. Secondary antibody diluted in blocking buffer was added to the channels and the device was incubated at RT for 45 min. Cells were washed trice with 1xPBS. Imaging was performed using spinning disc confocal (Perkin Elmer Ultraview Vox) at Light Microscopy Facility at University of Sheffield.

2.10. OrganoPlate®

2.10.1. Seeding cells in a 3-lane OrganoPlate®

3-lane OrganoPlate® (4003-400-B, Mimetas) was used to culture cells in a 3D manner under the gravity driven fluid flow. Tubular structures of epithelial cells were established by growing the cells against the ECM gel. The OrganoPlate® is a microfluidic device based on a titre plate format. 3-lane version can accommodate up to 40 separate cultures on one plate. It contains three channels: two perfusion channels (13 mm long) separated by a gel channel (9 mm long). The membrane free culture is possible thanks to the presence of PhaseGuides™,

small ridges (100 µm x 55 µm) at the borders of a gel channel (Vulto *et al.*, 2011). The below protocol was developed by Mimetas and is freely available to the OrganoPlate® users.

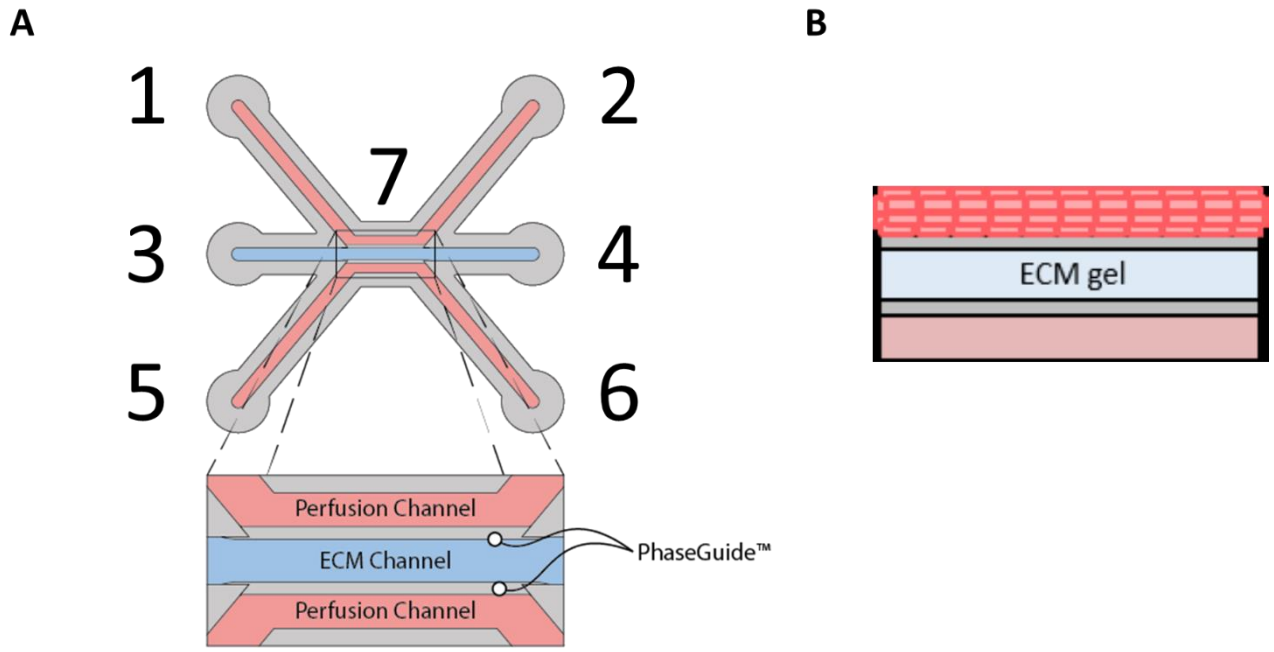

Figure 13. Schematic representation of an OrganoPlate® 3-lane chip.

(A) Organization of the channels in the chip: top medium inlet (1), top medium outlet (2), gel inlet (3), gel outlet (4), bottom medium inlet (5), bottom medium outlet (6), observation window (7); (B) Schematic representation of the tube formation against the ECM gel.

2.10.1.1. Gel filling

Firstly, all the observation windows were filled with 50 µL HBSS (55037C, Sigma) to maintain humidity in the plate and to allow for better visualization of the channels under the microscope. Prior to cells seeding gel channels need to be filled with ECM. For most of the experiments 5 mg/mL Collagen I from rat tail (3447-020-01, AMSbio Culturex) was used. Collagen stock was mixed with 100 mM HEPES (15630-122, Life Technologies) and 3.7 mg/mL $NaHCO_3$ (S5761, Sigma) in 8:1:1 ratio. Final concentration of collagen was 4 mg/mL. The tubes were kept on ice. All the components were mixed vigorously and the tube was briefly centrifuged to remove any bubbles. Each gel channel was filled with 1.7 µL of the gel. Plate was incubated at 37°C for 15 min and 50 µL of HBSS was added to all gel inlets. The plate was incubated further at 37°C until cell seeding.

2.10.1.2. Cell seeding

2.10.1.2.1. Epithelial cells – seeding against ECM

After the gel had polymerized, cells were seeded in the channels. In brief, cells were harvested and resuspended at a concentration of $10x10^6$ cells/mL. Top perfusion channel was filled with 2 µL of cell suspension and 50 µL of culture medium was added to the top medium inlet. The plate was incubated on the side for up to 3 h at the 75° angle to allow for the cells' sedimentation on attachment to the ECM. After that, the medium was added to the top medium outlet and bottom medium inlet and outlet. Plate was transferred to the incubator and placed on a perfusion rocker (Mimetas). Most of the cultures were maintained at 7° inclination and an interval of 8 min. Culture medium was refreshed every 2-3 days

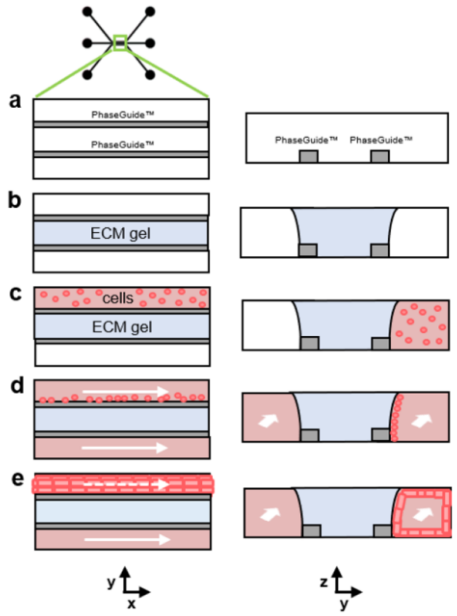

Figure 14. Schematic representation of cell seeding against ECM gel in the 3-lane OrganoPlate®.

(a) Single chip with featured PhaseGuides™; (b) ECM gel in the gel channel; (c) single cell suspension in the perfusion channel; (d) cells' attachment to the ECM interphase; (e) formation of the tube against the ECM.

2.10.1.2.2. Monocytes differentiation and wet channel seeding

In some experiments THP-1 monocyte cell line was co-cultured with Caco-2 tubes. Prior to seeding THP-1 cells needed to be differentiated into macrophage-like cells. On day 0, $0.8x10^6$ cells were seeded in 6 well culture plate and 5 ng/ml Phorbol 12-myristate 13-acetate (PMA; P1585-1MG, Sigma-Aldrich) was added. After 48 h of culture the medium was refreshed, and the cells were cultured for additional 24 h. Cells were harvested with TrypLE Select (12563029, Thermo Fisher), counted, centrifuged at 300 g for 5 min and resuspended in required volume of the culture medium. An OrganoPlate® with day 5 Caco-2 tubes was taken for the experiment. Leak tightness of the tubes was checked by TEER measurement prior to addition of THP-1 cells. Medium from all the channels in the OrganoPlate® was aspirated. THP-1 cells we seeded in the bottom channel (2 µl per chip) and the plate was incubated at 75° angle for 30 min to allow for better attachment of the cells. Subsequently medium was added to all in- and outlets. Caco-2 culture medium was added on the top, THP-1 culture medium was added on the bottom and gel channel. The trigger was added only to the bottom channel: L-18 MDP (tlrl-lmdp, Invivogen) at 10 ng/mL or 1 ng/mL; cytokines cocktail rh TNFα (11343015, ImmunoTools), rh IFNγ (11343536, ImmunoTools), rh IL-1β (11340015, ImmunoTools) each at 100 ng/mL. Afterwards, the plate was placed back on the rocking platform.

2.10.1.2.3. Lymphoid cells – in gel seeding

In some experiments Raji Burkitt's Lymphoma cells were co-cultured with Caco-2 tubes. Raji cells were seeded in gel first (1500 cells per chip). Cells were harvested from the flask, counted, centrifuged and resuspended in the required volume of the gel (rat tail Collagen I or GFR Matrigel). The gel channels were filled with 1.7 µL of the cell mix. Afterwards, the same steps as in **2.10.1.1** were followed.

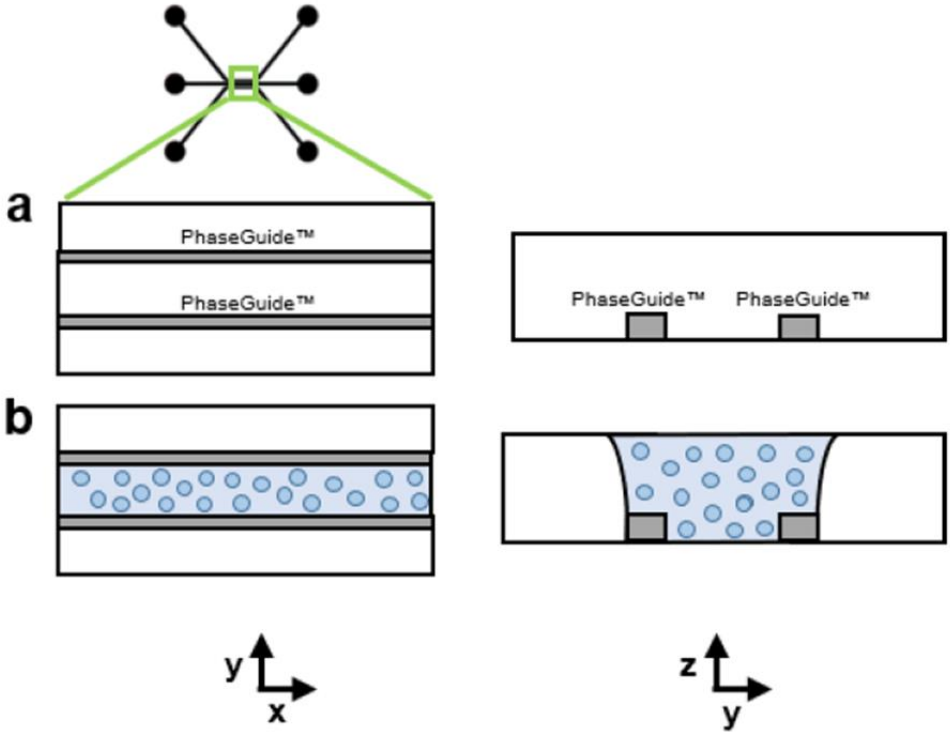

Figure 15. Schematic representation of cell in gel seeding in the 3-lane OrganoPlate®.

(a) Single chip with featured PhaseGuides™; (b) cell suspension in ECM gel in the gel channel.

2.10.1.2.4. Seeding of iPSC-derived intestinal organoids in the OrganoPlate®

Organoids were harvested from 24 well plates by adding Cell Recovery Solution (Corning Cat. No. 354253). After 30 min incubation at 4°C the cells were collected with a pipette and washed in basal media. TrypLE with the addition of Rock-inhibitor was used to disassociate the cells, cells were counted and resuspended at 10x106 cells/mL. Cells were seeded according to the protocol described in Section 2.10.1.2.1. Additionally, the top channel of the chip was coated with 1:100 Matrigel GFR diluted in PBS for at least 1 h prior to cell seeding. Organoids were cultured in the expansion media, similarly to the 24 well culture.

2.10.1.2.5. Seeding of primary intestinal organoids in the OrganoPlate®

Organoids were harvested from 24 well plates by flushing with cold Advanced DMEM media supplemented with HEPES and Pen/Strep. All the tips and pipettes were pre-wetted with DMEM media containing BSA to prevent sticking of the organoids to the plastic. Organoids were washed twice with cold Advanced DMEM media to remove Matrigel. Cells were trypsinized (TrypLE with the addition of Rcok-inhibitor) for 5 min at 37°C, counted and resuspended at 10x106 cells/mL. The remaining steps were as mentioned in Section 2.10.1.2.1. Organoids in the OrganoPlate® were maintained in the expansion media, similarly to the 24 well culture.

2.10.2. Live staining

Calcein-AM (C3099, Life Technologies) and NucRed™ Live 647 ReadyProbes™ Reagent (R37106, Thermo Fisher) were used to stain the live cells. Hoechst 33342 (H3570, Thermo Fisher) was used to stain the nuclei. Dilution of each stain was prepared in a culture medium: Calcein-AM 1:2000 (0.5 µg/mL), NucRed™ 2 drops/mL, Hoechst 1:2000. The mix was added to each chip as shown in figure 3 and kept in standard culturing conditions for 1 h. Afterwards the medium was replaced, and the plate was imaged on ImageExpress® Micro Confocal High-Content Imaging System (Molecular Devices). Z stacks were acquired, and maximum projection was analysed.

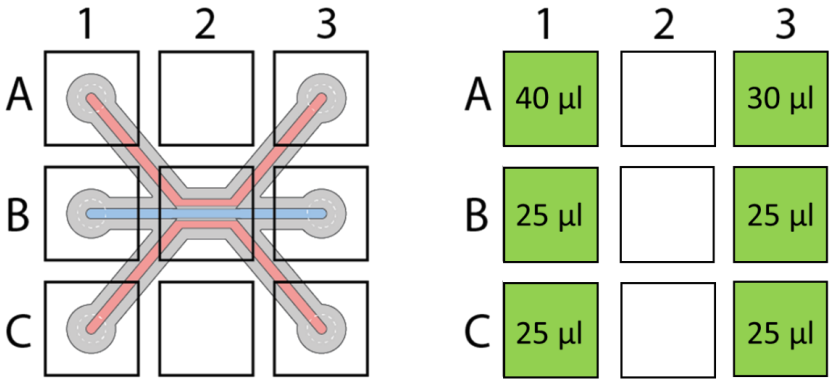

Figure 16. Pipetting scheme – live stain in the 3-lane OrganoPlate®.

Different volumes of the staining mix were added to top, gel and bottom channel to force the fluid flow through the gel and facilitate the staining of in-gel cultures.

2.10.3. Barrier Integrity Assay

Barrier Integrity Assay is performed to assess the leak tightness of the tubes cultured in the OrganoPlate®. Epithelial cells were grown as tubes in a 3-lane OrganoPlate® and the barrier integrity was typically checked at day 4 of culture. Leakage of the fluorescent compound from the top channel into the adjacent ECM is monitored. The lesser the leakage is, the tighter barrier is formed. Various sizes of fluorescently labelled dextran can be used to assess the level of the leak tightness of the tubes. Culture medium in the top channel was replaced for the medium containing 0.5 mg/mL 150 kDa FITC-dextran and 0.5 mg/mL 4.4 kDa TRITC-dextran (see **Figure 17** for the pipetting scheme). Plate was imaged in ImageXpress® Micro (Molecular Devices) in a time laps manner with pictures taken every 3 min for 15 min.

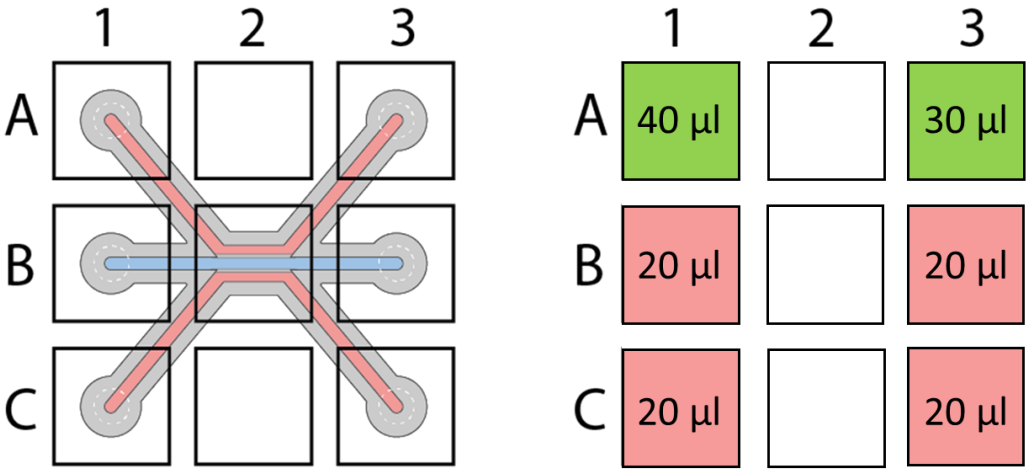

Figure 17. Pipetting scheme – Barrier Integrity Assay.

Culture medium with fluorescently labelled dextran was added only to the top channel (A). Culture medium was added to the gel and bottom channel. Volume difference between the top in- and outlet facilitates the flow in static conditions.

2.10.4. TEER measurement

TEER measurement was performed in the 3-lane OrganoPlate® with the OrganoTEER® (Mimetas). Barrier integrity was typically assessed on day 5 of culture before addition of the trigger (MDP or cytokines) and after 72 h of the treatment. To measure the TEER culture medium needed to be added to all the in- and outlets. Plate was incubated at RT for at least 30 min before the measurement. After that the plate was placed in the holder and measurement top with an electrode board was fitted on top of the plate. The electrode boards were disinfected with 70% ethanol and air dried before each use. The measurement was performed with the following settings: Min f 1000 [Hz], Max f 1000000 [Hz], 51 steps, Amplitude 100 [mV], Precision 0.0, Averaging 1. The results are represented as $\Omega.cm^2$.

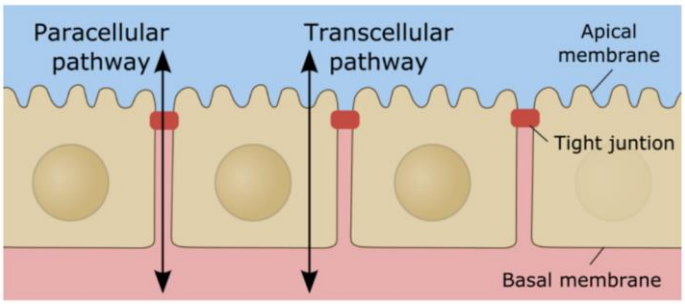

Figure 18. Epithelial monolayer (Yashunsky et al., 2012).

2.10.5. Immunostaining

Cells were fixed with 3.7% formaldehyde (252549, Sigma) in HBSS (55037C, Sigma) for 15 min and washed trice with 1x PBS (70013065, Gibco). If the staining was performed later in time, the plates were stored at 4°C. Cells were washed once with wash buffer (4% FBS in PBS) and permeabilized with 0.3% Triton X-100 in PBS for 10 min. After that cells were washed again with wash buffer. To prevent unspecific antibody binding, cells were incubated with blocking solution (2% FBS, 2% BSA, 0.1% Tween-20 in PBS) for 40 min. The primary antibodies solution was prepared in blocking buffer and added to top (25 µL in- and outlet) and bottom channel (15 µl in- and outlet) and incubated overnight at 4°C. The list of antibodies can be found in **Table 15**. Afterwards, the cells were washed trice with wash buffer and secondary antibodies solution was added. Plate was incubated for 30 min at RT. Cells were washed with 1x PBS. The plate was imaged on ImageExpress® Micro Confocal High-Content Imaging System (Molecular Devices). Z stacks were acquired, and maximum projection was analysed.

2.10.6. RNA extraction

Total RNA was extracted with RNeasy Mini kit (74104, Qiagen) following the manufacturer's protocol. Cell lysis was performed directly in the OrganoPlate®. Couple of chips were pooled together to obtain higher yield of RNA (typically 3-5 chips). RLT buffer with or without the addition of β-mercaptoethanol was added to the channel and after 2 min cell

lysate was collected into the Eppendorf tube. The lysates were processed immediately or stored at -80°C.

2.10.7. IL-8 ELISA

Concentration of IL-8 released to the culture medium was measured by ELISA Human IL-8 Duoset kit (DY208-05, R&D Systems). Medium was typically collected after 72 h of induction and stored at -80°C. Samples were diluted in RD buffer such that they were in the standard detection range (31.25 pg/mL – 2000 pg/mL). All samples were measured in triplicates. The assay was performed following the manufacturer's protocol and the absorbance was read at 450 nm.

Table 12. List of primers.

	Gene	Primer name	Sequence (5' - 3')	Application
1	NOD2	Forward	GCTGGTACCGGGGAAGAGGGTGGTTCAG	cloning into pcDNA3 (KpnI on 5')
2	NOD2	Reverse	CTGCGGCCGCTCAAAGCAAGAGTCTGGTGTCC	cloning into pcDNA3 (NotI on 5')
3	NOD2	NOD2_T7_F	ACAGATCCAGGCTCACCAGT	T7 assay, sequencing primer
4	NOD2	NOD2_T7_R	CAGAAAACAGCCCAGAAACAG	
5	NOD2	NOD2_1	CATCGCGGCTGCCCAAGAAG	sequencing of pcDNA3 construct
6	NOD2	NOD2_2	GAAGTATATGGCCAAGCTGAGGACC	sequencing of pcDNA3 construct
7	NOD2	NOD2_3	AGCTGCAGTGCATGGCCAAA	sequencing of pcDNA3 construct
8	NOD2	NOD2_4	GCTGTACCTGAGGAAGCGCC	sequencing of pcDNA3 construct
9	NOD2	NOD2_5	AGCTCCAGGCAGCACAGGTC	sequencing of pcDNA3 construct
10	NOD2	NOD2_6	CTGGGGCCTGCTGGCTGAG	sequencing of pcDNA3 construct
11	NOD2	NOD2_7	GGGTGACATTGGCGTGGAGC	sequencing of pcDNA3 construct
12	NOD2	NOD2_8	CCTGGCTGAAGCCTTGGGTG	sequencing of pcDNA3 construct
13	vector	CMV_forward	CGCAAATGGGCGGTAGGCGTG	sequencing pcDNA from CMV
14	sgRNA targeting NOD2	sgRNA1NOD2_top	CACCGTCTTTCCTCCTCATCGTGAG	generation of sgRNA1 plasmid
15	sgRNA targeting NOD2	sgRNA1NOD_bottom	AAACCTCACGATGAGGAGGAAAGAC	
16	sgRNA targeting NOD2	sgRNA2NOD2_top	CACCGTGGTTCAGCCTCTCACGATG	generation of sgRNA2 plasmid
17	sgRNA targeting NOD2	sgRNA2NOD2_bottom	AAACCATCGTGAGAGAGGCTGAACCAC	
18	sgRNA targeting NOD2	sgRNA3top_NOD2	CACCGAGACCAGCAGCTCGACCAGC	generation of sgRNA3 plasmid
19	sgRNA targeting NOD2	sgRNA3bottom_NOD2	AAACGCTGGTCGAGCTGCTGGTCTC	
20	sgRNA targeting NOD2	sgRNA4top_NOD2	CACCGACACTCTCGAAGCCTTCCA	generation of sgRNA4 plasmid
21	sgRNA targeting NOD2	sgRNA4bottom_NOD2	AAACTGGAAGGCTTCGAGAGAGTGTC	
22	NOD2	T7F_sg3_NOD2	TCTGAGGCTAGAACCATGGC	amplification for T7 assay, editing with sgRNA3
23	NOD2	T7R_sg3_NOD2	GACAGGCCCAAGTACCCTTA	
24	NOD2	NOD_F_cDNA	GGACATTCTCCGGGTTGTGA	amplification of cDNA
25	NOD2	NOD2_qPCRF1	AGCCATTGTCAGGAGGCTC	qPCR primer pair 1
26	NOD2	NOD2_qPCRR1	CGTCTCTGCTCCATCATAGG	
27	NOD2	NOD2_qPCRF2	CAACACCTCCTTGCAGTTCC	qPCR primer pair 2

28	NOD2	NOD2_qPCRR2	ACACTGCCAATGTTGTTCCC	
29	GAPDH	GAPDH F	CTCCTGCACCACCAACTGCT	qPCR primer pair GAPDH
30	GAPDH	GAPDH R	GGGCCATCCACAGTCTTCTG	
31	ACTB	hACTB_973_fw	CTCTTCCAGCCTTCCTTCCT	qPCR primer pair ACTB
32	ACTB	hACTB_1088_rev	AGCACTGTGTTGGCGTACAG	
33	IL-8	h_CXCL8_104_fw	CAAGAGCCAGGAAGAAACCA	qPCR primer pair IL-8
34	IL-8	h_CXCL8_237_rev	ACTCCTTGGCAAAACTGCAC	
35	CDX2	Hs01078080_m1	n/a	qPCR primer Taqman (FAM)
36	CHGA	Hs00900375_m1	n/a	qPCR primer Taqman (FAM)
37	ABCB1	Hs00184491_m1	n/a	qPCR primer Taqman (FAM)
38	VIL1	Hs01031722_g1	n/a	qPCR primer Taqman (FAM)
39	LYZ	Hs00426232_m1	n/a	qPCR primer Taqman (FAM)
40	LGR5	Hs00969422_m1	n/a	qPCR primer Taqman (FAM)
41	MUC2	Hs00159374_m1	n/a	qPCR primer Taqman (FAM)
42	ACTB	Hs01060665_g1	n/a	qPCR primer Taqman (VIC)

Table 13. List of siRNAs.

Name	Target sequence	Sense strand	Antisense strand	Additional information
siRNA1_NOD2	5'-CAACATGGCCGTGAACTTTAT-3'	5'-ACAUGGCCGUGAACUUUAUTT-3'	5'-AUAAAGUUCACGGCCAUGUTG-3'	Targeting exon 12 (Cooney *et al.*, 2010)
siRNA2_NOD2	5'-AACGGTGAAAGCGAATGGATT-3'	5'-CGGUGAAAGCGAAUGGAUUTT-3'	5'-AAUCCAUUCGCUUUCACCGTT-3'	Targeting exon 3 (Sabbah *et al.*, 2009)

Table 14. List of antibodies.

Target protein	Catalogue number	Manufacturer	Host species	Dilution
NOD2	NB100-524, lot D-2	Novus Bio	mouse	IF: 1:50/1:500 WB: 1:2000/1:1000/1:500
	PRS2513, lot 25130204	Sigma	rabbit	IF: 1:50/1:500
	2098-1-AP lot 00016262	Proteintech	rabbit	WB: 1:500
	2098-1-AP lot 00018178	Proteintech	rabbit	WB: 1:500
	NOD-15 (lot 625801)	Biolegend	mouse	WBL: 1 ug/mL and 3 ug/mL
	HPA041985 lot R38439	ATLAS	rabbit	WB: 1:250
GFP	-	Gift from Andrew Peden	rabbit	WB: 1:2000
B-tubulin	T4026	Sigma-Aldrich	mouse	WB: 1:500
ZO-1	617300	Life Technologies	rabbit	IF: 1:50
Ezrin	610603	BD Transduction Laboratories	mouse	IF: 1:125
E-cadherin	610181	BD Biosciences	mouse	IF: 1:100
Villin	Sc-58897	Santa Cruz Biotechnology	mouse	IF: 1:200
PGP	13342	Cell Signaling	rabbit	IF: 1:800
Glut-2	9117	Santa Cruz Biotechnology	rabbit	IF: 1:20

Lysozyme	MA182873	Thermo Fisher	mouse	IF: 1:100
	A0099	Agilent Technologies	rabbit	IF: 1:200
Muc-2	7314	Santa Cruz Biotechnology	rabbit	IF: 1:100
	MA512345	Thermo Fisher	mouse	IF: 1:100
Ac-tubulin	T6793	Sigma	mouse	IF: 1:2000
Occludin	711500	Life Technologies	rabbit	IF: 1:100
Chromogranin	13090	Santa Cruz Biotechnology	rabbit	IF: 1:50
ICAM-1	BBA3	Bio Techne	mouse	IF: 1:100

3. Results

3.1. Chapter I: Modelling gut epithelium *in vitro* with colon derived cell lines – 2D vs 3D culture systems.

3.1.1. Introduction

In the current state of the art, the 2D biological culture systems are well established and widely used. Very often carcinoma cell lines, originally derived from patients are used as a representation of human tissue from a particular organ. The examples of commonly used intestinal cell lines include Caco-2, HT-29, HCT116 and SW48 (Berg *et al.*, 2017). These *in vitro* models serve the purpose in understanding the basic biology of the specific organ. They represent the main features of the tissue, like morphology and protein expression profile. However, since they are derived from a cancer tissue their genome contains mutations that can show a phenotype not present in healthy cells. In our study, we focused on the gut and the following results will show the generation of a reliable model of this organ that is suitable for high throughput drug screening. A satisfactory gut model would be composed of a stable cell monolayer with a good barrier function. The proper epithelial barrier allows for the separation of the apical and basolateral environment and therefore enables investigation of absorption and transport. Disruption of the barrier is an important characteristic of IBD and will be studied in the generated *in vitro* disease model. Establishment of a healthy model with a functional barrier is the first building block in that process. Scalability of the model is important for future implementation in the high throughput screening. The addition of fluid flow to mimic the physiological environment would be desirable. Since the final aim of this project is to model inflammatory bowel disease *in vitro* additional features as reactivity to the pro-inflammatory triggers would need to be included.

In the first step, we decided to use Caco-2, which is a human epithelial colorectal adenocarcinoma line established by Jorgen Fogh at the Sloan-Kettering Cancer Research Institute (Fogh, Wright and Loveless, 1977). As the intestine is composed of several different

cell types, it was crucial to use a cell line that would represent at least some of the most important characteristics of the epithelium. Caco-2 is distinctive in this regard because it differentiates upon reaching confluence. Confluent cells mostly resemble small intestinal enterocytes. They form tight junctions and grow in a monolayer that has high transepithelial electrical resistance. Polarization of the cells leads to the formation of a brush border on the apical side. Cells express some of the main digestive enzymes present in the small intestine, like sucrose isomaltase. Importantly, the cells have high expression of transporters crucial for the function of the intestine, like PGP efflux pump (Verhoeckx *et al.*, 2015). The cells are easy to handle and are typically grown on permeable supports (Transwell®, Corning). Full differentiation of the monolayer in such system lasts 21 days, which is quite a limitation for routine experiments.

Another human colorectal adenocarcinoma cell line, DLD-1 was used in the experiments included in this thesis. This cell line polarizes when grown to confluence and forms a brush border (Baas *et al.*, 2004). However, in comparison to Caco-2 to a lesser degree. In contrary to Caco-2 that is a polyploid cell line with 96 chromosomes, this cell line is diploid which is of huge importance when subject to genome engineering (following step in the project, described in **Appendix**). Literature research shows that this cell line was mostly used in studies related to colorectal cancer. Although, some studies in our area of interest have been published. Diegelmann et al. used this cell line to investigate findings from expression analysis of IBD patient-derived tissue (Diegelmann *et al.*, 2013). It has also been used in the study on NOD interaction partners (Krieg *et al.*, 2009). Importantly, it has already been successfully modified with CRISPR/Cas9 technology (Fujiwara *et al.*, 2015) suggesting that it is a suitable model for our project.

In this chapter, I will introduce the initially chosen epithelial cell lines and draw a comparison between 2D and 3D culture of those cells. At first, the 2D culture of the gut epithelial cells will be discussed, as it has been a gold standard in biomedical research of the last century. The introduction of more advanced culture systems (polydimethylsiloxane-based organ on a chip device and OrganoPlate®) will follow with the aim to transition towards organ on chip technology, according to the current trends in research.

***Aim 1*: Characterization of Caco-2 and DLD-1 cell lines in relation to barrier formation in 2D culture (tissue culture plate and Transwell® device)**

***Aim 2*: Establishment of advanced gut on chip models (PDMS-based device and OrganoPlate®)**

3.1.2. Characterization of intestinal carcinoma cell lines Caco-2 and DLD-1 cultured in conventional monolayers and Transwell® permeable support systems

In standard tissue culture approach, cells are cultured in plastic flasks and plates of various dimensions. In such vessels, the cells grow on a flat surface and have access to the medium from the apical side. They are kept in humidified incubators at 37°C and 5% CO_2. A variation of the standard 2D culture are permeable support systems. These filters contain a membrane, the surface on which cells' monolayer is formed. The permeable supports are inserted into the wells of a standard tissue culture plate in such a way that the cells have access to the culture medium from both apical and basolateral side. In this setup, the formation of a properly differentiated monolayer is facilitated, and its barrier integrity can be assessed by Transepithelial Electrical Resistance (TEER) measurement. In the following experiments, both epithelial cell lines (Caco-2 and DLD-1) were cultured in standard tissue culture plates and in Transwell® Permeable Support system (Corning). **Figure 19** shows junction formation in Caco-2 monolayers. In both conditions, cells form cell junctions (ZO-1 in green). Monolayers grown on Transwell® system are more homogenous with the cells equally distributed. In **Figure 20**, DLD-1 monolayers cultured on Transwell® permeable supports and stained for junction protein. This cell line forms proper junctions and seems to be differentiating in a faster manner than Caco-2.

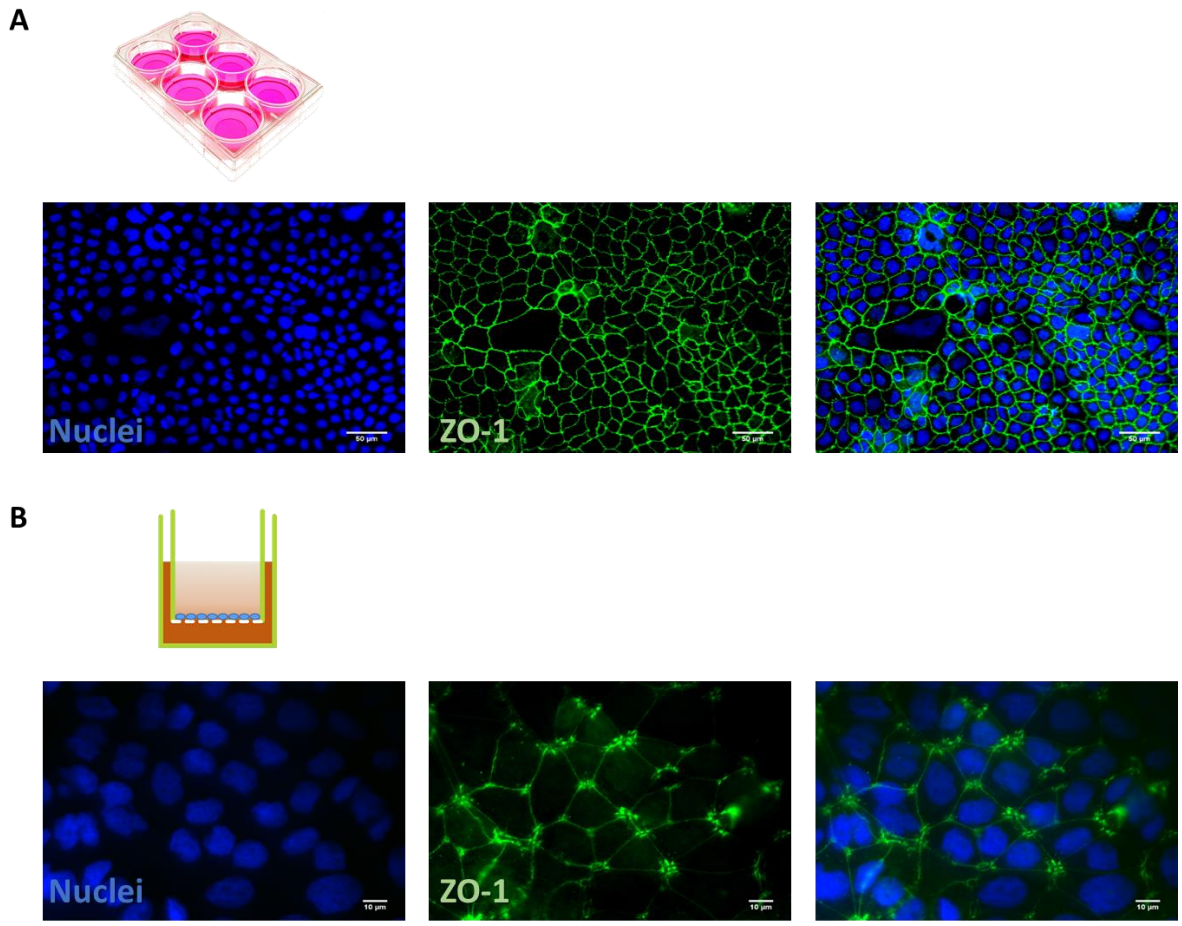

Figure 19. Caco-2 cells cultured in 2D, formation of cell junctions.

(A) Cells grown on the coverslip in a standard 12-well tissue culture plate; (B) Cells grown on the Transwell® permeable support (fully differentiated monolayer at day 22). Cell junctions marker (ZO-1) in green, nuclei in blue. Scale bars in top panel 50 µm, bottom panel 10 µm.

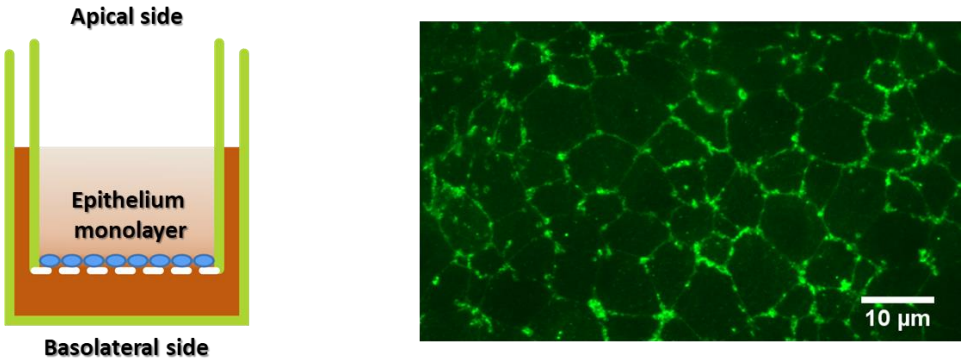

Figure 20. DLD-1 cells cultured in 2D, formation of tight junctions.

Cells grown on Transwell® permeable support (day 13). Tight junctions marker (ZO-1) in green, nuclei in blue. Scale bars in top panel 50 µm, magnified are in the bottom panel 10 µm.

To assess the formation of a continuous monolayer Transepithelial Electrical Resistance (TEER) needs to be measured. TEER is a very sensitive and reliable method. It relies on the measurement of the impedance spectrum (electrical conductivity of the tissue to alternating current for a given frequency). The measurements reflect the permeability of the monolayer considering both, paracellular and transcellular transport. The higher the resistance is, the more leak-tight the barrier. **Figure 21** shows the measurements of the barrier integrity over time. It is advised that the Caco-2 require approximately 21 days to form a fully differentiated monolayer in this system. As the data show, Caco-2 barrier reaches high resistance on day 7 of the culture with its maximum around day 20 and persists for approximately a week after that. This gives a reasonable window for experiments. On the contrary, DLD-1 monolayers reach the maximal resistance on day 9 and sustain it until day 30. However, the values are significantly lower when compared to Caco-2. It can be concluded that DLD-1 form a barrier on the Transwell® device, which is also supported by the detection of properly developed cell junctions (shown in **Figure 20**).

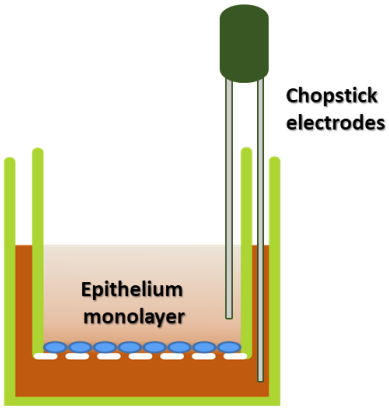

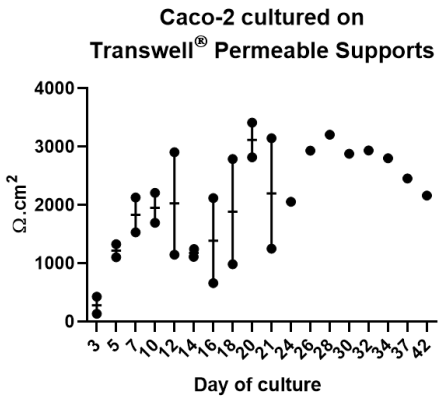

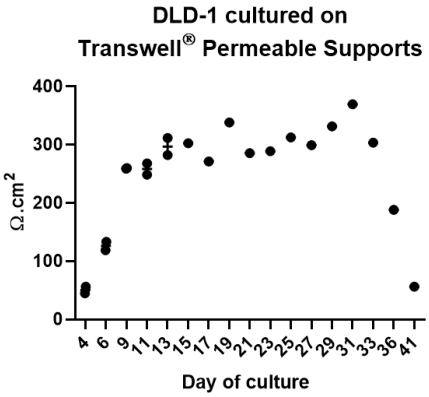

$$TEER = (TEER_{monolayer} - TEERblank)\ x\ 1.12cm^2$$

Figure 21. Measurement of Transepithelial Electrical Resistance (TEER) of Caco-2 and DLD-1 monolayers cultured on Transwell® permeable supports over time.

Chopstick electrodes were used to measure the resistance of the barriers over 40 days of culture. Equation explains how the resistance per well was calculated, the resistance of the no-cell control was subtracted from the measured value and adjusted for the surface area of the insert suited for 12-well tissue culture plate. Data represent measurements of two membranes until day 21 (Caco-2) and 13 (DLD-1), after that one of each membranes was fixed and stained for the tight junctions and the measurements were continued until day 42 (Caco-2) and 41 (DLD-1).

Described results indicate that both epithelial cell lines can be used to model simplified colon epithelium in a 2D setup. The cells form monolayers with a functional barrier when cultured to confluency on Transwell® permeable supports.

3.1.3. Generation of gut-on-chip models – Caco-2 and DLD-1 cell lines

3.1.3.1. Intestinal epithelium culture in a PDMS-based organ-on-chip device with continuous perfusion

As shown above, a simple *in vitro* model can be used to study gut epithelial barrier integrity. However, it comes with certain disadvantages. Firstly, the generation of a fully differentiated barrier of Caco-2 cells on Transwell® permeable support system requires 21 days. Secondly, in such a system there is no fluid flow or mechanical forces naturally occurring in gut tissue. It has been shown that the application of those results in further differentiation of the epithelium and leads to the formation of a more physiologically relevant model (Kim and Ingber, 2013). Acknowledging the limitations of previously shown culture systems, we planned to use a platform that would enable the establishment of a more physiologically relevant gut model while simultaneously being easy to use. To begin with, we attempted to build a model based on PDMS technology – a conventional organ on a chip platform developed at Wyss Institute (Benam *et al.*, 2016). In **Figure 22**, the schematic explains the design of the chip. It contains two channels separated by a polyester membrane. The device can be connected to a syringe pump that would provide a pulsatile fluid flow that mimics physiological conditions. Details on the manufacture procedure of the device were described in section **2.9 PDMS-based organ-on-chip** of **Materials and Methods**. It has been shown that addition of such mechanical cues allows for differentiation of Caco-2 cells into more complete intestinal epithelium (polarized columnar cells with basal nuclei with higher TEER values) (Kim and Ingber, 2013).

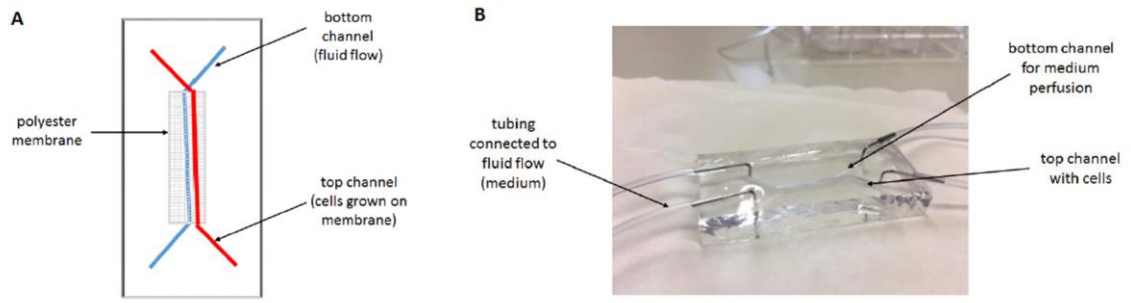

Figure 22. PDMS-based organ-on-chip device.

(A) Schematics of the device; (B) picture of a fabricated device connected to the tubing.

To generate gut on a chip model with applied fluid flow, we seeded Caco-2 cells into manufactured PDMS-based device. **Figure 23** shows microscopy pictures of a successful culture. The applied fluid rate was 120 µL/h. The cells formed homogenous monolayer and developed proper cell junctions as assessed by immunofluorescence imaging.

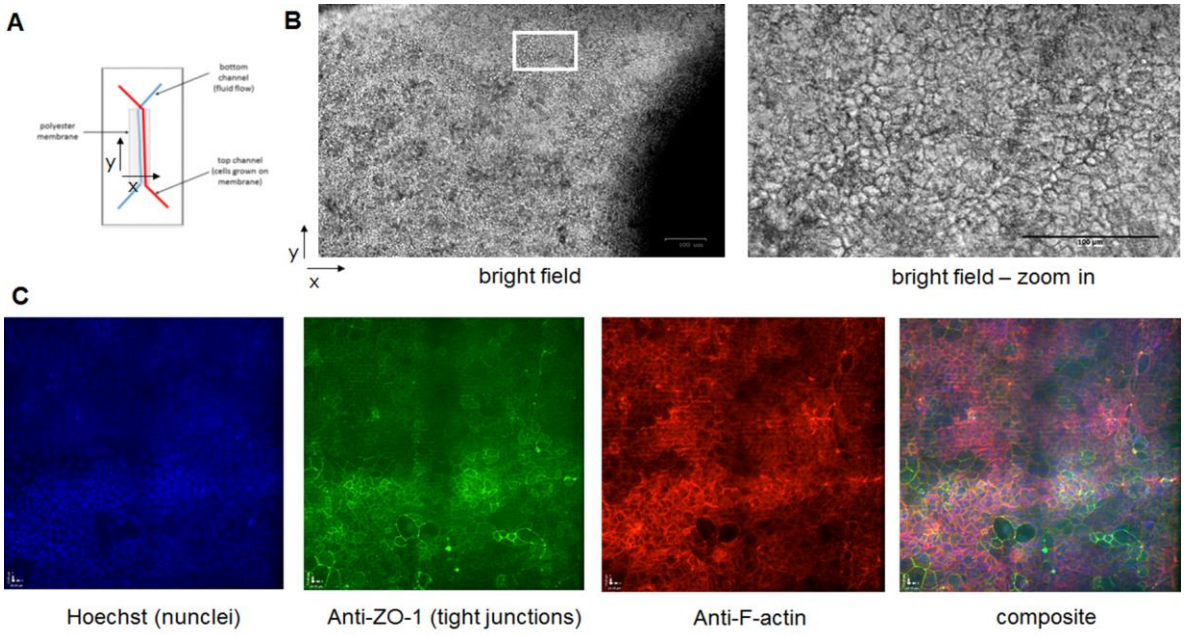

Figure 23. Representative microscopy images of Caco-2 cells cultured in PDMS-based organ-on-chip with applied fluid flow.

(A) schematic of organ-on-chip device; (B) bright field image, on the right side magnification of the area marked by white rectangle (scale bars 100 µm); (C) immunofluorescent staining depicting nuclei (DAPI in blue), tight junctions (ZO-1 in green), cytoskeleton (fluorescent phalloidin in red); scale bar 18 µm.

3.1.3.2. Intestinal epithelium culture in the OrganoPlate® - a microfluidic high throughput platform

The described PDMS-based organ on a chip device, despite being a step forward in modelling gut tissue, proved to be challenging to use. The unarguable advantage of the system was the implementation of a unidirectional flow. However, the addition of the pump to the system had a negative impact on the throughput of the experiments. Having such set up in the lab requires additional space and conducting multiple experiments at the same time is virtually impossible. Likewise, manufacturing of PDMS devices itself requires special equipment and dedicated lab space. Such a model could not be used in high throughput experiments. As the aim of this project was to generate a model that could potentially be used in the drug development process, we decided to turn to a more suitable alternative. We chose to work with a high throughput system that allows for a perfused culture without any additional equipment. OrganoPlate® developed by Mimetas is a microfluidic tissue culture plate. The microfluidic systems are built into the glass bottom that facilitates the imaging. Top of the plate constitutes of a 384-well titter plate that is compatible with all the lab equipment. The bidirectional fluid flow is initiated in the device when placed on a rocking platform. **Figure 24** shows the 3-lane version of the device in which 40 single chips are incorporated. Each chip consists of three channels, the middle one allows for the formation of ECM scaffold required for the 3D patterning inside the microfluidics. Cells can be seeded in the top and/or bottom channel. Addition of the cells to the ECM is also possible. In the following model, only the top channel will be used for cell culture and the bottom channel serves as basolateral media access (see **Figure 25** for cell seeding method). Variations of the model that rely on the incorporation of the multiple cell types into the system will be discussed in further chapters.

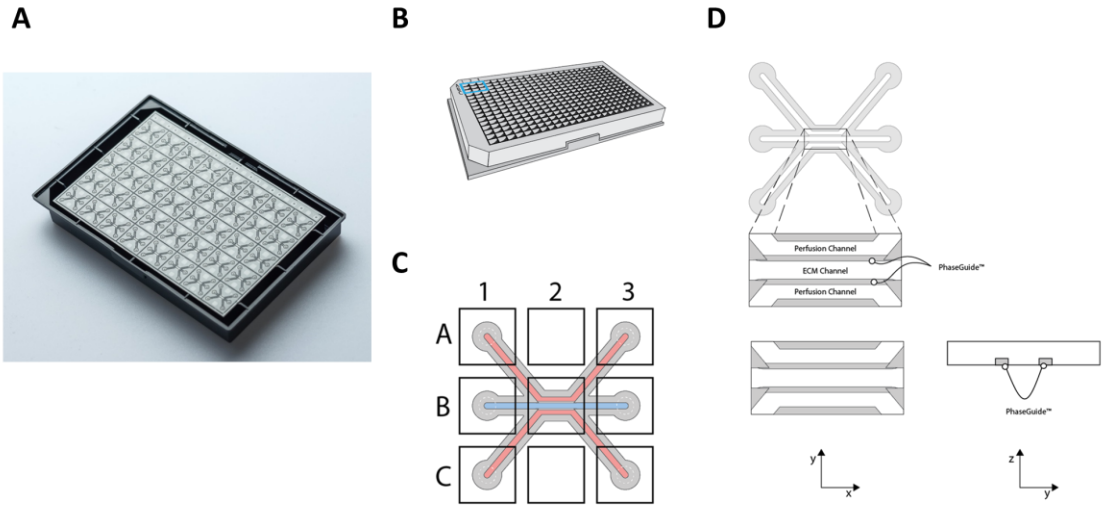

Figure 24. The OrganoPlate® - a microfluidic 3D culture plate.

3-lane design accommodates 40 tissue models on a single plate. (A) bottom view showing glass bottom plate and the distribution of microfluidic chips across the plate; (B) top side of the OrganoPlate® based on a standard 384-well plastic plate; (C) a single chip showing top channel inlet (A1) and outlet (A3), gel inlet (B1) and outlet (B3), bottom channel inlet (C1) and outlet (C3) and observation window (B2); (D) Schematics of a single chip of 3-lane OrganoPlate®. A single chip consists of three microfluidic channels: top and bottom perfusion channels and middle gel channel. Phaseguides™ (marked with white circles) allow for the membrane-free definition of the culture matrices. Internal volumes: top and bottom perfusion channels: 1.1 µL, gel channel: 0.87 µL. Microfluidic lane height: 220µm. Microfluidic channels widths: top and bottom 320µm, gel 360µm. Phaseguide dimensions: 100 x 55 µm (w x h).

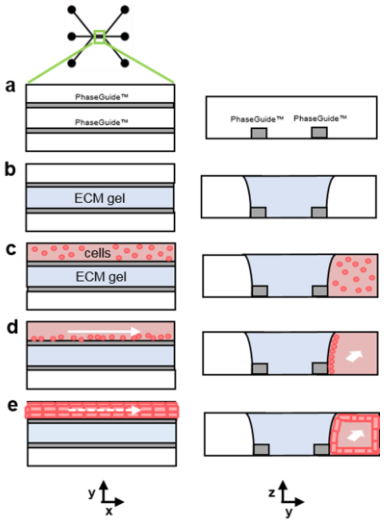

Figure 25. Schematic representation of cell seeding against ECM gel in the 3-lane OrganoPlate®.

Single chip with featured PhaseGuides™ (a), polymerization of ECM gel in the gel channel (b), addition of single cell suspension in the perfusion channel (c), cells' attachment to the ECM interphase (d), formation of the tube against the ECM (e).

3.1.3.2.1. Characterization of Caco-2 tubes in the OrganoPlate®

Tubular Caco-2 Intestinal model suited for high-throughput screening has been previously developed by Mimetas (Trietsch et al., 2017) and the results below are based on the established protocol. As shown in the prior section, Caco-2 require 21 days to develop fully differentiated monolayer in the Transwell® system. In the OrganoPlate®, fully formed and leak-tight tubes are generated within only 4 days. One of the methods to check for the permeability of the tubes in the plate is fluorescence-based barrier integrity assay. Two differently labelled dextrans of various sizes were added into the tubes (top channel) and the plates were imaged in the fluorescent microscope. Incorporation of dextrans with distinct molecular sizes allows for better assessment of the barrier permeability, smaller size molecules pass through potential breaches in the barrier more easily increasing the sensitivity of the assay. No fluorescence was detected in the bottom channel indicating that the tubes were leak-tight for 150 kDa and 4 kDa dextrans (**Figure 26**).

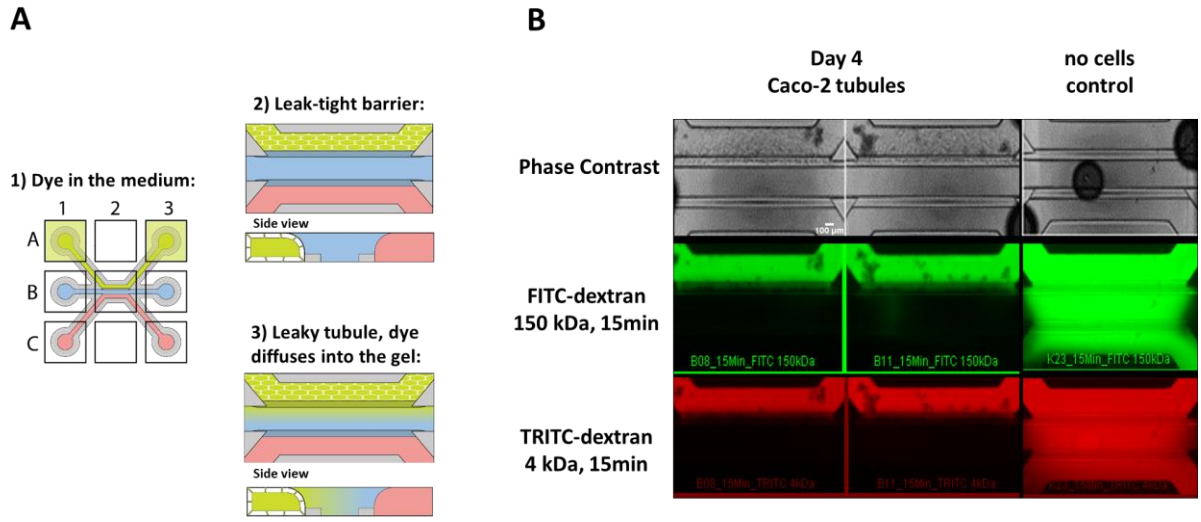

Figure 26. Caco-2 form leak-tight tubules in the OrganoPlate®.

A: Barrier Integrity Assay - principle. Schematic representation of an assay. (1) Dye is introduced to the lumen; (2) In case of leak tight barrier the dye is retained inside; (3) when barrier is disrupted the dye leaks to the adjacent channel. B: Barrier Integrity Assay on day 4 Caco-2 tubes, on the right hand side cell-free control, N=2. Top panel shows phase contrast images. In green, permeability for 150 kDa FITC-dextran. In red, permeability for 4 kDa TRITC-dextran.

Another method to assess barrier formation is TEER measurement. It is a much more sensitive method as it monitors the flow of electric current through the barrier. It is possible to measure the resistance of all 40 chips on one OrganoPlate® simultaneously with the use of the OrganoTEER®. The device consists of a plate holder, an electrode board and a measuring top (**Figure 27**). Caco-2 were cultured in OrganoPlate® and subject to measurements on day 4 and day 7 of culture. As shown in **Figure 27**, the majority of the tubes are leak-tight by day 4 of culture and they remain stable for at least three additional days.

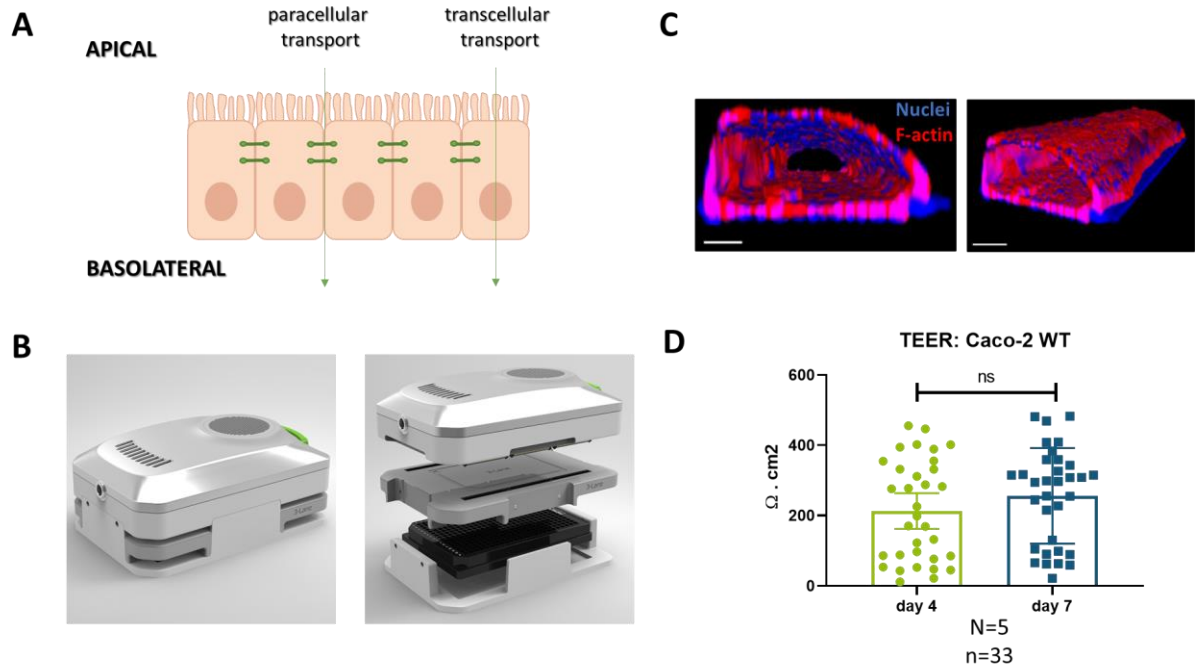

Figure 27. Measurement of epithelial monolayer permeability.

(A) Epithelial monolayer. TEER measurement reflects permeability of the cells monolayer with regard to paracellular and trancellular transport; (B) OrganoTEER®; (C) Immunofluorescent staining, 3D reconstruction of a confocal z-stack showing tubular structure formed in the OrganoPlate®. Nuclei (DAPI stain in blue) and actin filaments (fluorescent phalloidin in red). Scale bar 50µm; (D) TEER of Caco-2 tubes in the OrganoPlate®, N=5, n=33 (N: biological replicate, n: technical replicate). Mean with 95% CI, t-test, p=0,1355.

To characterize the model with regard to polarization, absorption and transport, the tubes were stained for several markers of a junction protein (ZO-1) and brush border (villin and ezrin). It was confirmed that they form tight junctions (**Figure 28**). As stated previously, Caco-2 cells upon differentiation form a brush border. It is an essential feature of gut enterocytes because it increases the absorption surface. We confirmed that Caco-2 express brush border markers when cultured in the OrganoPlate® (**Figure 28**). The transport proteins like P-glycoprotein (P-gp), breast cancer resistance protein (BCRP) and multidrug resistance protein 2 (MRP2) allow for transcellular transport of the molecules. They play a role in defence mechanism against xenobiotics and can limit bioavailability of orally administered drugs (Misaka, Müller and Fromm, 2013). Here we confirmed the expression of PGP (ABCB1) , the transporter present at the brush border of enterocytes which functions as an efflux pump. We showed that expression of this efflux pump concentrates near the ECM side (bottom side of the tube) as shown in **Figure 29**. Similarly, glucose receptor Glut-2 is expressed in the tubes. This receptor is mainly found in the basolateral side of enterocytes and translocates to the apical side upon glucose sensing.

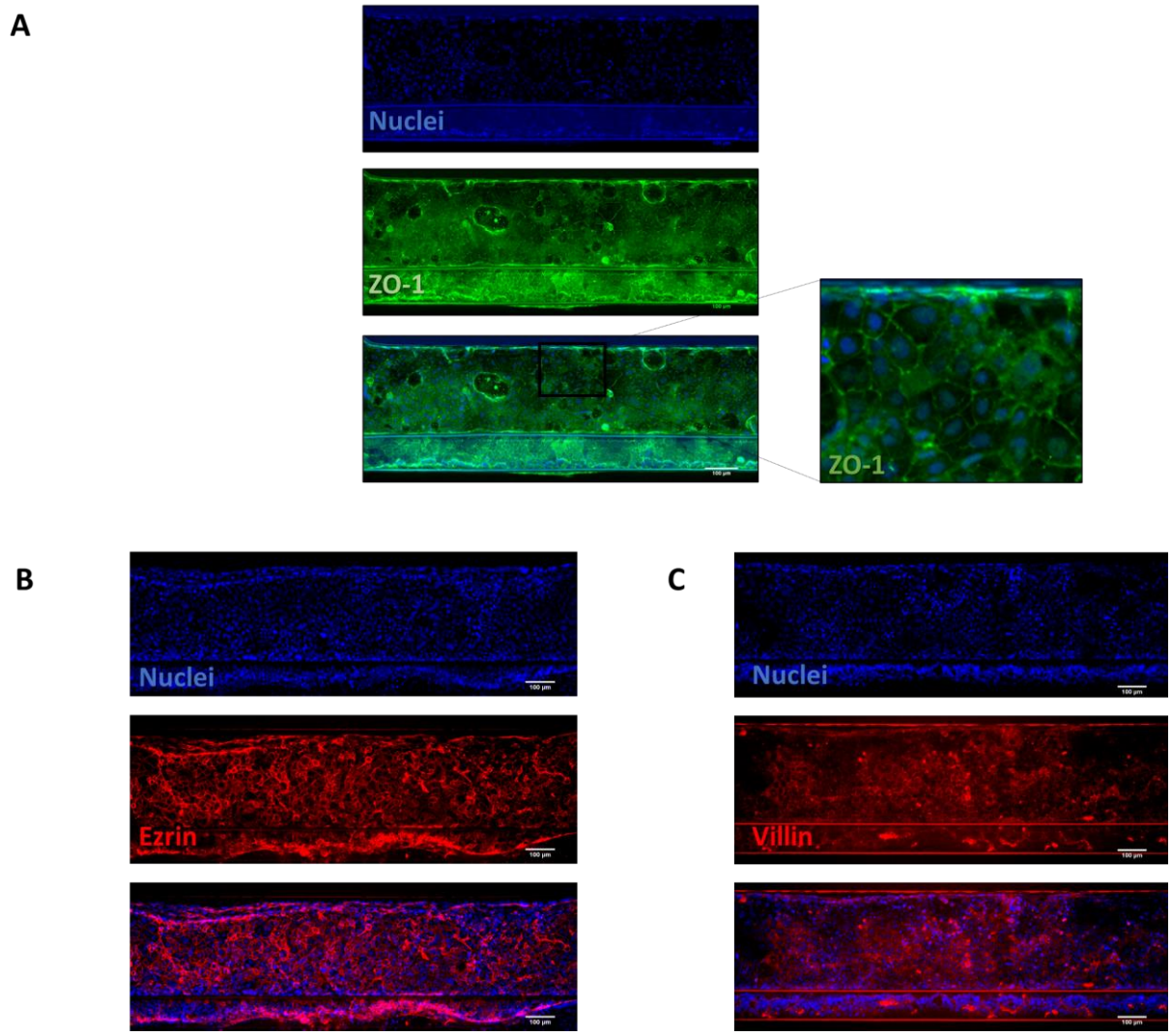

Figure 28. Caco-2 cultured in the OrganoPlate® form tight junctions and express brush border markers.

Characterization of the tubules by immunofluorescent staining. Max projections of the tubular structures depicting nuclei (DAPI staining in blue), tight junction marker (ZO-1 in green), ezrin (B) and villin (C) (red). Images represent top view of the top channel of the OrganoPlate®. Note: PhaseGuide seen as a horizontal band at the bottom of each panel. Scale bars 100 µm.

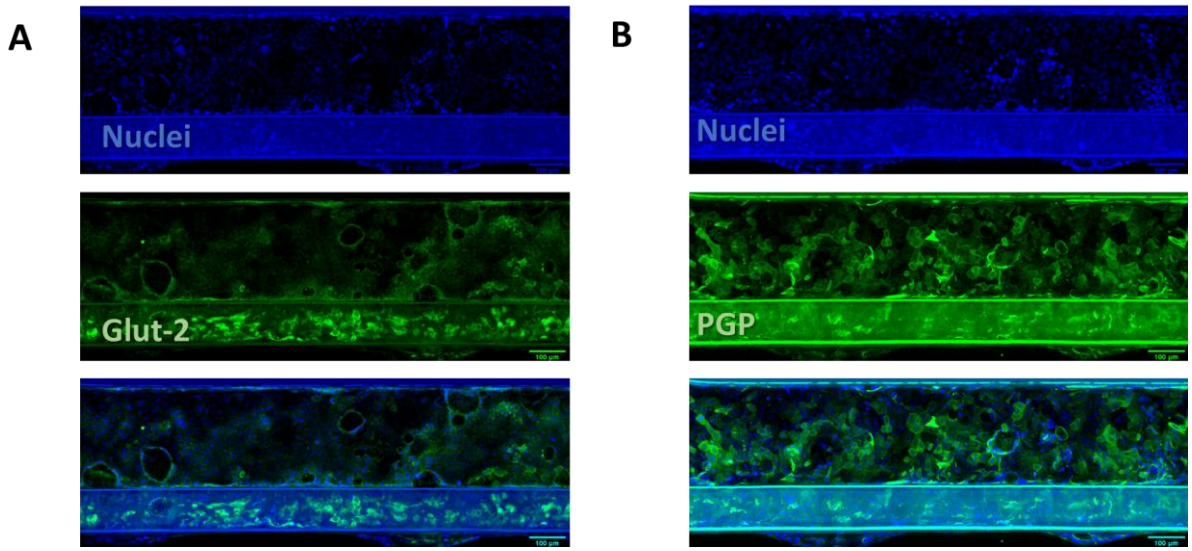

Figure 29. Caco-2 tubes express important transporters.

Characterization of the tubules by immunofluorescent staining depicting (A) nuclei (DAPI in blue), glucose receptor (Glut-2 in green); (B) nuclei (DAPI in blue), efflux pump (PGP in green). Images represent top view of the top channel of the OrganoPlate®. PhaseGuide seen as a horizontal band at the bottom of each panel. Maximum projections, scale bars 100 µm.

3.1.3.2.2. Characterization of DLD-1 tubes in the OrganoPlate®

DLD-1 model was established in the 3-lane OrganoPlate® according to the previously described Caco-2 protocol (Trietsch *et al.*, 2017). Similarly to the other epithelial cell line, those cells formed leak-tight tubes within four days of culture and remained stable until at least day 14 (**Figure 30**). The cells express tight junction protein ZO-1 and ezrin (brush border component) (**Figure 31**). Expression of the transporters is less apparent than in Caco-2 (**Figure 32**).

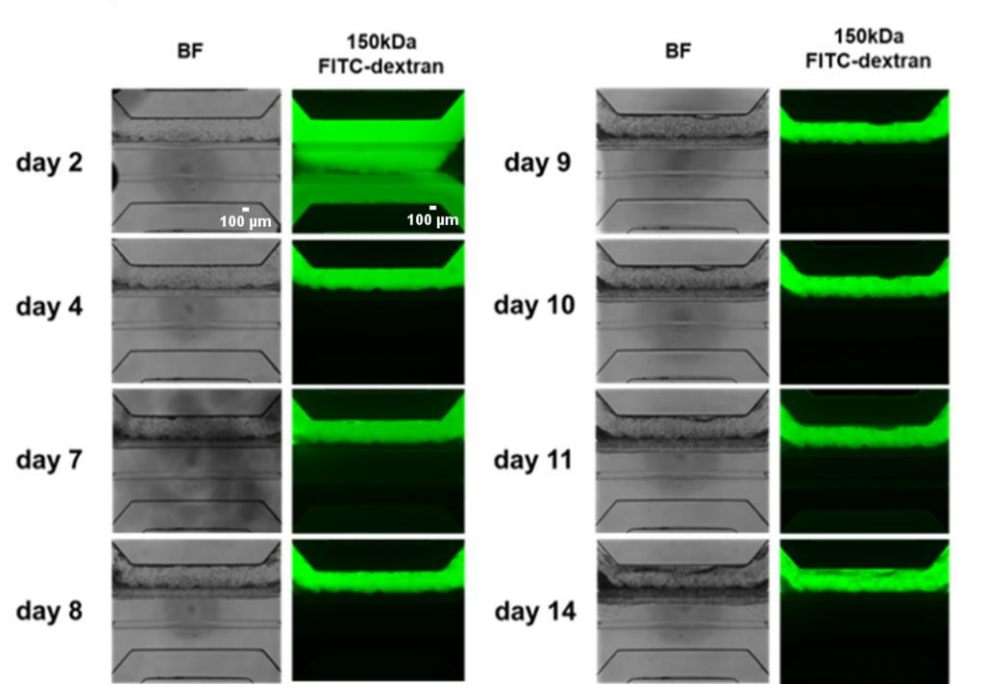

Figure 30. DLD-1 form leak-tight tubules in the OrganoPlate®.

Bright field pictures in the left panel, barrier integrity assay in the right panel N=1. Scale bar 100 µm.

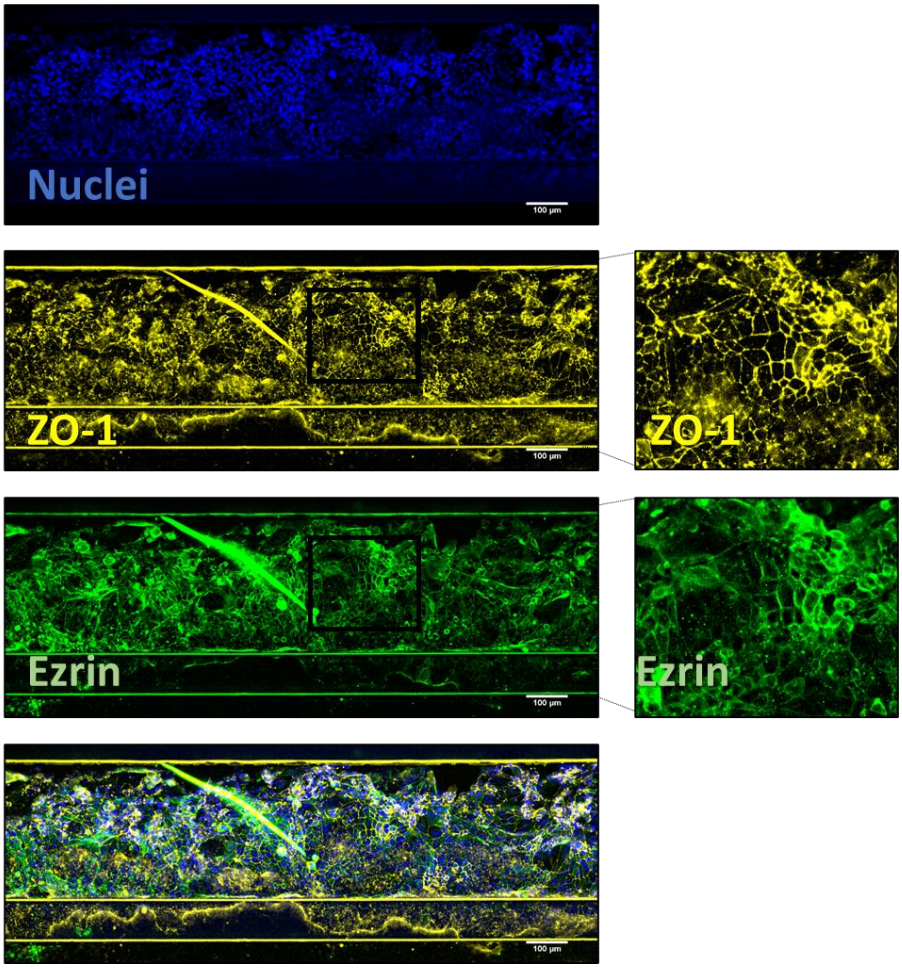

Figure 31. DLD-1 tubes form tight junctions and express brush border marker.

Characterization of the tubules by immunofluorescent staining depicting nuclei (DAPI in blue), tight junctions (ZO-1 in yellow), brush border (ezrin in green). Images represent top view of the top channel of the OrganoPlate®. PhaseGuide seen as a horizontal band at the bottom of each panel. Maximum projections, scale bars 100 µm.

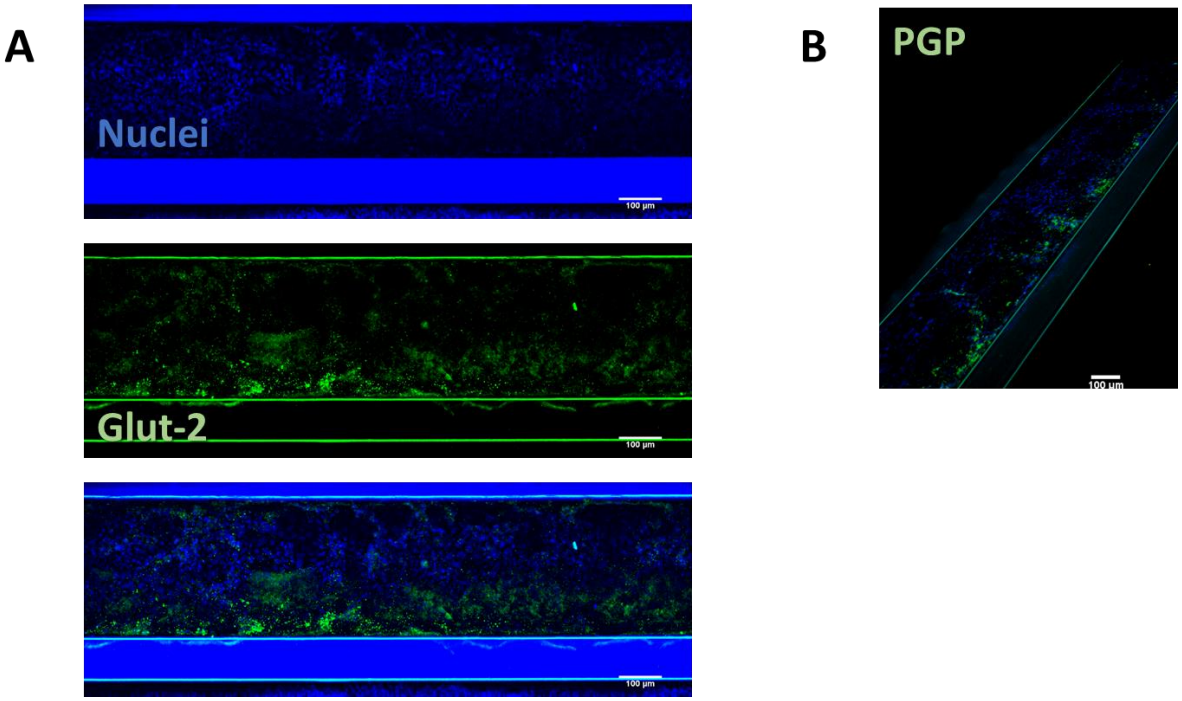

Figure 32. DLD-1 tubes express important transporters.

Characterization of the tubules by immunofluorescent staining showing (A) nuclei (DAPI in blue), glucose receptor (Glut-2 in green); (B) nuclei (DAPI in blue), efflux pump (PGP in green). Images represent top view of the top channel of the OrganoPlate®. PhaseGuide seen as a horizontal band at the bottom of each panel. Maximum projections, scale bars 100 µm.

As shown above, both cell lines formed tubular structures in the OrganoPlate®. Stable barrier function was observed, and the expression of key markers was confirmed (junction protein, brush border, PGP transporter, Glut2 receptor). All the above indicate that a satisfactory gut model with a proper barrier function and the presence of key markers can be generated with this technology. Further chapters will capitalise on this model but also further and more sophisticated developments of the gut on a chip will be presented, including exploiting the model to mimic IBD conditions.

3.1.4. Discussion

3.1.4.1. Advantages of the 3D tissue culture methods over standard approaches

The intestine is a complex organ that plays a crucial role in the human body. Not only composed of various cell types with specific roles but also colonized by hundreds of microbial species (Rajili and Vos, 2014). To study the biology of this particular organ, a number of *in vitro* models have been developed. Traditionally, monolayers of intestinal cells were grown in tissue culture dishes. Nowadays more advanced culturing methods have been developed to better reflect the conditions cells experience in their natural environment. Addition of mechanical cues like perfusion or cyclic stretching improves the differentiation of cells thus providing physiologically relevant models. Presented in this chapter, Transwell® permeable supports are the most popular alternative to the standard tissue culture dishes. As shown in the results section, enterocyte-like cells develop tight junctions and form homogenous leak-tight barriers on those filters. Transwell® systems allow for the differentiation of epithelial monolayer but they pose certain disadvantages. It is nearly impossible to assess the morphology of the monolayer by only looking at phase-contrast images. As the membrane is suspended inside of the tissue culture plate, the significant focal length does not allow for the proper focusing on the sample. Additionally, the presence of the membrane itself disturbs the image as its porous surface overlays with the monolayer of cells. Immunostaining is possible but it is also challenging. The membranes with attached cells need to be cut out of the plastic support skeleton and mounted onto the glass slide. Consequently, the presence of said membrane obstructs the confocal images. In our experiments, both tested cell lines formed monolayers that were suitable for further experiments. Caco-2 cells remain the first choice cell line as it forms more leak-tight barriers, which is essential when modelling intestine. It is especially important, in the experiments related to drug transport, to work with fully formed monolayers and if those experiments were to be performed, the cells would need to be cultured for a substantial amount of time beforehand. In addition to that, the volumes of culture medium in this system are quite high and it can be problematic when using expensive compounds. Overall, the Transwell® system is easy to use and provides a good platform to

model an intestinal barrier. However, it is not an ideal solution due to the presence of an artificial membrane that apart from being not a physiological feature also obstructs imaging and influences permeability.

The second approach described in this chapter was a PDMS-based organ on a chip device. Cells were grown on the membrane with access to the medium from both apical and basolateral side just like in a Transwell® system. While the system adds obvious value, namely the incorporation of the fluid flow, it is technically challenging to work with. Manufacture of the chips is time-consuming and even though relatively easy, requires access to specialized equipment usually not present in biological labs. Addition of the fluid flow is important in modelling tissue that is subject to a constant exchange of the fluids (Kim and Ingber, 2013). In this system, multiple tubes need to be connected to the device and this significantly complicates the culture. Due to the limited access to the pumping systems, only a single chip could have been cultured at once. The advantage of this system is that the fluid flow rate and consecutively sheer stress inflicted on the cells can be adjusted by simply changing the pump settings. Importantly, the fluid flow in this system is unidirectional. There is also a possibility of adding mechanical stretching of the membrane on which cells are cultured but this requires access to costly equipment. Even though the system poses certain advantages, we decided not to continue with this approach in our lab. To work with such devices on a regular basis, major improvements to the lab environment would need to be introduced.

After our experience with the Transwell® system and PDMS-based device, we focused our efforts on the system that would be more physiologically relevant than 2D culture but also relatively simple to use. OrganoPlate® appeared to be a good alternative as it does not contain any artificial membranes, allows for the application of the fluid flow and is a device in a form of a 384 well plate. It is the only tested device that is well suited for imaging. The bottom glass plate of the device allows for microscopy at any time point of the culture thus giving a possibility to apply a wide range of microscopy-based assays. Its main advantage is scalability. We were aiming at generating a gut model that would be suitable for drug screening. Here, high throughput is of major importance, as thousands of compounds need to be tested within a short time. Performing the assays on this platform is also relatively easy due to the compatibility of the plate with the standard lab equipment like multichannel pipettes and aspiration systems, absorbance/fluorescence/luminescence readers and high

throughput microscopes. Additionally, the OrganoTEER device was used to measure barriers' electrical resistance. However, this model possesses certain disadvantages. First of all, the fluid flow applied to the tissue, although it can be controlled by adjusting the angle of the rocking platform, remains bidirectional. This does not fully reflect the environment in the gut. Another important feature, the ECM support present in the middle channel of the chip is considerably thick (the same width as the tube grown in the top channel). Even though, no artificial membrane is separating the tissue from the environment on the basolateral side, it still creates some kind of a barrier which interferes with the free movement of the medium and secreted factors. In our experiments, we accounted for that by extending the time of exposures up to 24-72 h.

One of methods used for the assessment of the barrier integrity was measurement of Transepithelial Electrical Resistance. The TEER values obtained for Caco-2 cultured in the OrganoPlate® for 7 days were 256.4 $\Omega.cm^2$ ± 135.9. Interestingly, values reported for Caco-2 monolayers cultured in one of the PDMS-based systems were considerably higher and in line with the values obtained for similar cultures in Transwell® permeable supports measured alongside (736 $\Omega.cm^2$ ± 120) (van der Helm *et al.*, 2019). In another study, TEER for Caco-2 monolayers cultured in Transwell® was oscillating around 1000 $\Omega.cm^2$ and dynamic organ-on-chip culture showed 3-4 fold higher values (Kim *et al.*, 2012). It should be noted that in our Transwell® culture the values obtained with the epithelial voltammeter ranged around 2000 $\Omega.cm^2$. As reported by van der Helm et al., the TEER values measured with different devices can only be compared when normalized to electrical stimulation. Therefore, direct comparison of the results between studies is not always possible. TEER values reported for in vivo intestine range from 40 $\Omega.cm^2$ in human small intestine (Takenaka *et al.*, 2014) to 40 – 100 $\Omega.cm^2$ in mouse models (Linnankoski *et al.*, 2010; Srinivasan *et al.*, 2015a).

We acknowledge that each of the presented platforms has it shortcomings and choices have to be made according to the aim of the research. Simple absorption and toxicity studies could be performed on Transwell® systems if the extended time of the culture prior to the exposure is not considered as a serious downside. The research on host-microbiota interactions could be performed on PDMS-based devices as the fluid flow can be easily adjusted in that setup and the microbial cultures need to be subject to the constant fluid flow to prevent overgrowth of intestinal cultures. Additionally, application of the mechanical

forces to induce stretching of the membrane, thus mimicking peristalsis, is very much possible in those devices (Kim *et al.*, 2012; Kim and Ingber, 2013). OrganoPlate® would be the first choice for high throughput experiments. In addition, due to the availability of three channels (with the possibility of adjustments in the design allowing for further compartmentalization) generation of more complex models containing a number of various cell types is possible.

3.2. Chapter II: Modelling Inflammatory Bowel Disease *in vitro*.

3.2.1. Introduction

Inflammatory Bowel Disease is a group of chronic inflammatory conditions and can be caused by many different factors, as described in the general introduction. There is a huge need for reliable models that would help in the understanding of the disease mechanism and serve as tools to test new treatments. Various approaches could be taken to model such a complex disorder and there are already many *in vitro* and animal models available that reflect some of the features of the disease. 2D culture systems poorly resemble human biology as the cells lack spatial arrangement and are not subject to fluid motion, mechanical forces and chemical gradients. Animal models on the other hand, even though complex systems, fail to accurately predict human responses to treatments due to species differences. The problem we are facing is an oversimplification of the cellular environment and biology mismatch. In drug development research, the models we work with should be relatively uncomplicated. It simplifies the readouts, decreases overall time and costs of the research. Presented in a previous chapter organ on chip technology seems to be a perfect choice, balancing between simplification of the model and physiological relevance. A gut on a chip model that would recapitulate pathophysiology of IBD could be used to further the understanding of the disease mechanism, screen for the potential drug targets and eventually perform pre-clinical trials. High throughput of the developed model is of key importance to the pharma industry, as many targets and compounds need to be tested to proceed with the development of successful treatments.

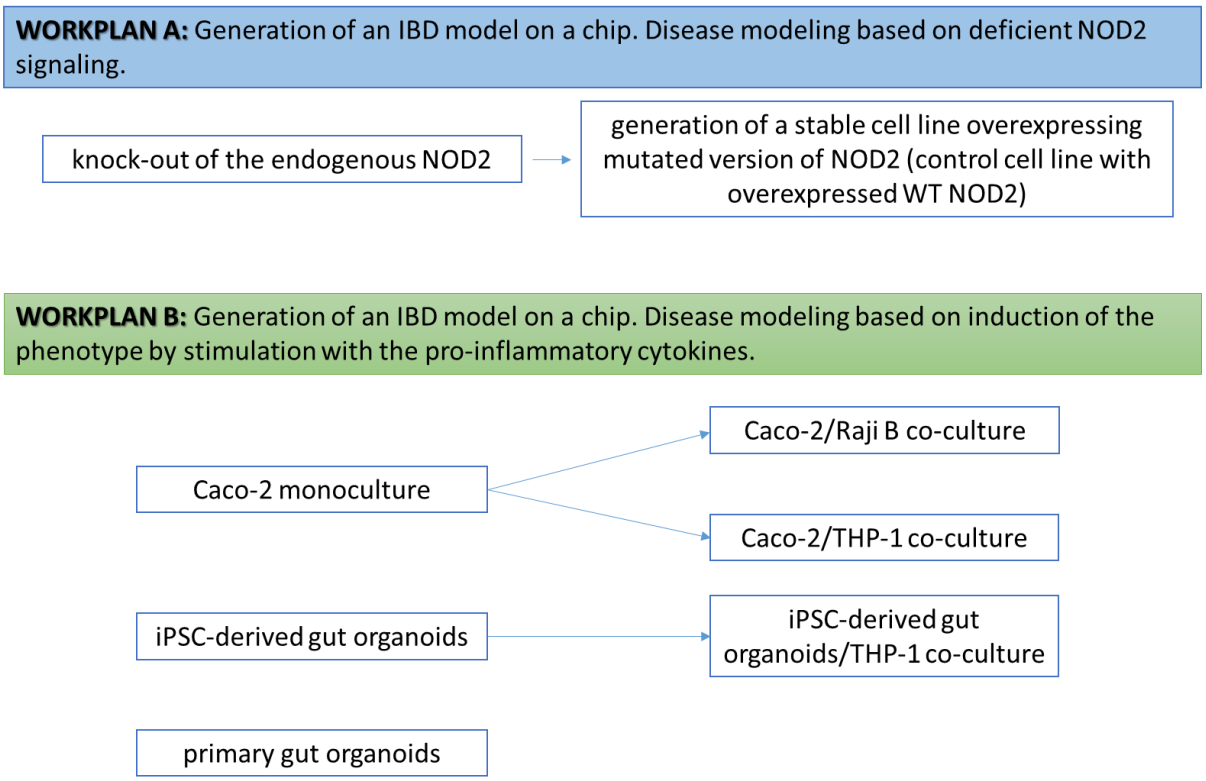

Figure 33. Experimental outline.

In this study, we originally intended to model Crohn's disease (one of the forms of IBD) by focusing on the NOD2 gene that has been reported as one of the potential players in Crohn's disease due to its genomic localization and the role in recognition of bacterial cell wall components (Ogura *et al.*, 2001). NOD2 is an intracellular receptor for muramyl-dipeptide (MDP) and is essential to initiate an immune response against bacterial pathogens (Schreiber *et al.*, 2005). Its signalling pathway leads to regulation of NFκB activation, which has been reported to be disrupted in Crohn's patients. Several mutations in CARD15 gene coding for NOD2 protein have been found (Hugot *et al.*, 2001) (Ogura *et al.*, 2001) (Chamaillard *et al.*, 2003). In our approach, we chose to work with previously described human adenocarcinoma cell lines, which we genetically modified such that they would fail to express a functional NOD2 protein. Those cell lines were implemented in the OrganoPlate® and tested with respect to the activation of immune responses. Data covering this part of the research was described in the **Appendix**.

An alternative way to model IBD on a chip that we decided to follow is the recapitulation of an inflamed phenotype by direct introduction of pro-inflammatory

cytokines. In a normal environment, those cytokines would be released by immune cells present in gut-associated lymphoid tissue. As IBD patients experience symptoms related to the defects in barrier function, we are recreating that environment in our gut on a chip model. In the gut, epithelial cells act as sensors for bacteria and release factors like IL-8 upon bacterial entry (Eckmann, Kagnoff and Fierer, 1993). In a body, this results in the recruitment of immune cells and enhances the protective inflammatory response. In our model, we focused on the assessment of barrier integrity and release of pro-inflammatory cytokines.

The results presented in the following chapter outline those two approaches to IBD modelling. Firstly, the NOD2 activation in epithelial cell lines will be investigated. Generation of NOD2KO cell lines and establishment of the IBD model based on NOD2 signalling has been described in the **Appendix** in sections **3.5.2. Modelling IBD on a chip based on deficiency in NOD2 signalling: incorporation of NOD2KO cell lines into the microfluidic device**; **3.5.3. Modelling IBD on a chip based on deficiency in NOD2 signalling: introduction of the pro-inflammatory trigger and its effect on barrier integrity and release of IL-8**. Since the NOD2 signalling was not readily detected in our model the alternative approach will be presented where the induction of the inflamed phenotype was achieved by stimulation with cytokines cocktail. Eventually, the possibilities of introduction of co-cultures with immune component and the impact on the pro-inflammatory response will be explored.

***Aim 1*: Generation of an in vitro model for IBD based on disrupted NOD2 signalling.**

***Aim 2*: Generation of an in vitro model for IBD by recreating inflamed phenotype with the addition of exogenous pro-inflammatory cytokines.**

3.2.2. Modelling Inflammatory Bowel Disease based on NOD2 signalling

3.2.2.1. Characterization of the cell lines in relation to NOD2 signalling

3.2.2.1.1. Detection of NOD2

An essential step at the beginning of this project was to establish a method to detect NOD2 expression in epithelial cell lines. A standard technique to detect protein expression is Western-Blotting. Several commercially available anti-NOD2 antibodies were tested and **Figure 34** shows immunoblotting with the most successful antibodies. Initial attempts were promising as the bands of appropriate size (110 kDa) were detected across different cell lines.

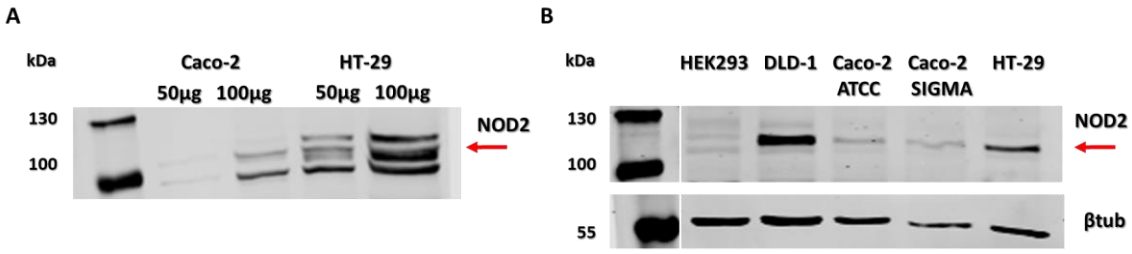

Figure 34. Detection of endogenous NOD2 across different cell lines.

Various commercially available anti-NOD2 were tested and β-tubulin was used as a loading control. Red arrows indicate bands of expected size. (A) detection with Sigma antibody PRS2513, lot 25130204 (B) detection with Proteintech 2098-1-AP lot 00018178.

Further validation of the antibodies was necessary to determine if the detected band is specific to NOD2. In order to do that, siRNA experiments were performed. Firstly, HEK293 cells were transfected with NOD2 overexpression plasmid and subsequently, the NOD2 expression was silenced with specific siRNAs. As a control, non-targeting siRNA was used (**Figure 35**). Overexpression plasmid was used to better assess the specificity of siRNAs. The results showed that siRNA2 is more efficient in silencing NOD2 expression. No change in the intensity of endogenous NOD2 was observed. This might be due to the low specificity of the

tested antibodies, the band of 110 kDa might be the result of the unspecific binding to another protein.

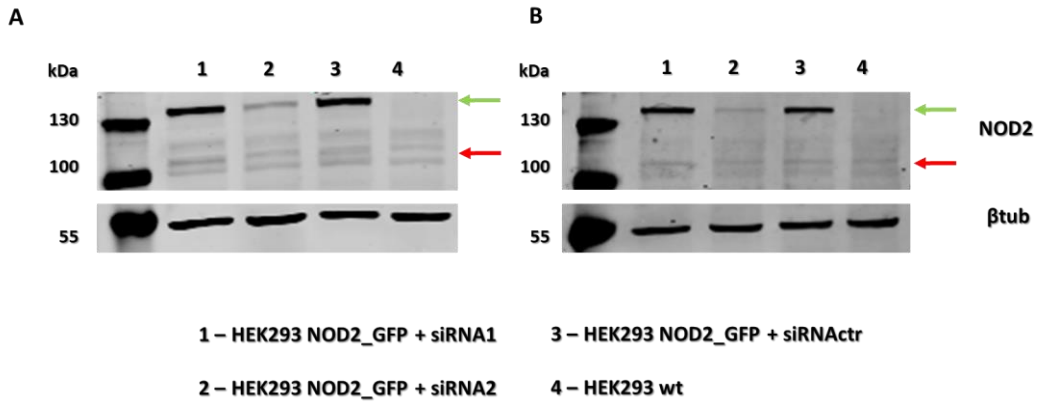

Figure 35. Validation of anti-NOD2 antibodies.

NOD2 overexpression and siRNA experiment in HEK293 cell line. Green arrow indicates the bands of GFP-tagged NOD2, red arrow endogenous NOD2. (A) detection with Proteintech 2098-1-AP lot 00018178; (B) detection with ATLAS HPA041985 lot R38439.

The subsequent step was to validate the antibodies on protein extracts of Caco-2 and DLD-1, the cell lines chosen for the project. Those are gut epithelial cell lines and were expected to have higher NOD2 expression than HEK293. Cells were transfected with siRNAs and lysates were subject to electrophoresis and immunoblotting (**Figure 36**). Bands of the expected size were detected and only a couple of unspecific bands of a bigger size were observed in DLD-1 cell line lysate. However, previously validated NOD2 siRNAs did not show any silencing in either cell line. Again, the reason might be that the antibodies bind unspecifically and the band of 110 kDa is not NOD2. However, the expression levels of endogenous NOD2 could be very low in the first place and this prevented from observing any significant changes upon siRNA transfection.

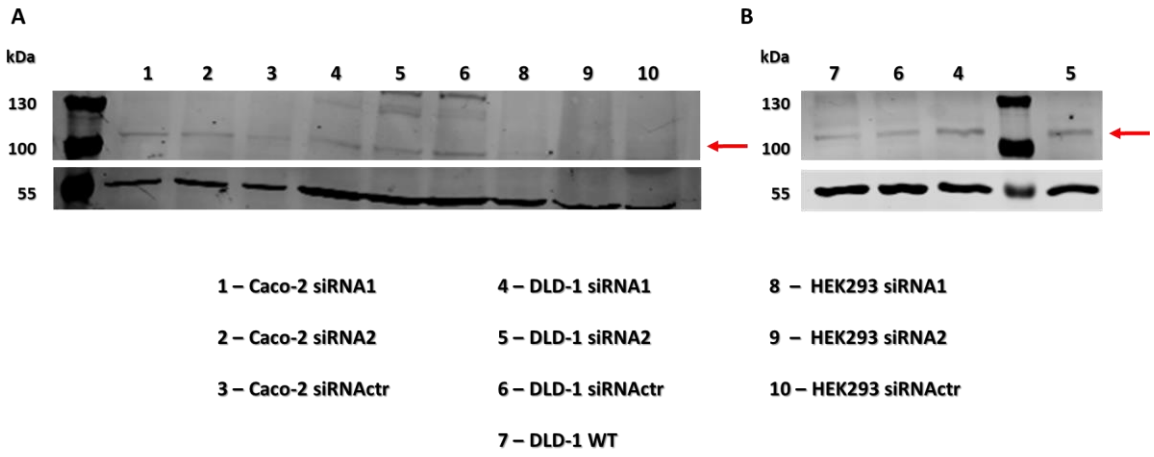

Figure 36. Validation of anti-NOD2 antibodies.

siRNA targeting endogenous NOD2 across different cell lines. Red arrows indicate the bands of expected size for endogenous NOD2 (110 kDa). (A) detection with ATLAS HPA041985 lot R38439; (B) detection with Proteintech 2098-1-AP lot 00018178.

As it was difficult to validate commercially available antibodies, we attempted to measure the NOD2 expression on mRNA level. We included two cell lines with known high expression of NOD2, hNOD2 HEK overexpression cell line (Invivogen) and THP-1 monocyte cell line (ATCC). For comparison, also iPSC-derived gut organoids were included. Those are meant to represent more physiological condition and were expected to show some NOD2 expression. As the results in **Figure 37** show, very low expression of NOD2 was detected in both Caco-2 and gut organoids (Cq for those cell lines ¬30 cycles, for comparison THP-1 ¬24). The primers were previously validated, and the efficiency was checked on both NOD2 overexpression plasmid and RNA extracted from THP-1 cell line. To conclude, NOD2 expression in epithelial cells appears to be very low.

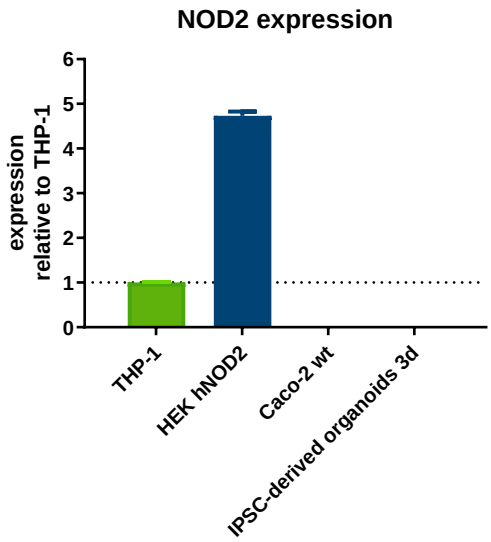

Figure 37. NOD2 expression across different cell lines.

NOD2 expression was measured by qPCR. Data normalized to expression of GAPDH and represented as relative to the expression in THP-1 cell line, N=2.

3.2.2.1.2. Functional analysis of NOD2 signalling

NOD2 protein is an intracellular receptor that is specifically activated by MDP. When activation occurs, NOD2 signals further through RIPK2 and in result leads to the release of NFκB transcription factor and its translocation to the nucleus. NFκB turns on the transcription of pro-inflammatory genes like IL-8 and CCL-20 (**Figure 38**). Since detection of NOD2 was challenging we decided to focus on NOD2 signalling and check if by activating the pathway we would observe initiation of pro-inflammatory signalling. NFκB activation was measured with Dual Luciferase assay (**Figure 39**). Cells were transfected with plasmids containing Firefly luciferase with NFκB reporter for detection of activation and *Renilla* luciferase for correction for transfection efficiency. After the transfection, cells were stimulated with MDP. For the initial establishment of the assay, HEK293 were used as it is the most suitable transfection host. Working with an easy to transfect cell line would allow for easy detection of the signal produced by luciferase and therefore establishment of the trigger conditions. Triggering with MDP resulted in 6 fold induction as compared to the non-treated control. In DLD-1 cell line, the MDP treatment did not result in a significantly elevated response. Similarly, the Caco-2

cell line did not respond to MDP treatment. Optimization steps with varying times of induction and various concentrations of the trigger were not successful. Gut epithelial cell lines remained to be insensitive to MDP treatment. Surprisingly, HEK293 cell line reacted to the treatment even though it previously showed low NOD2 expression levels in immunoblotting supporting the hypothesis of the low sensitivity of anti-NOD2 antibodies.

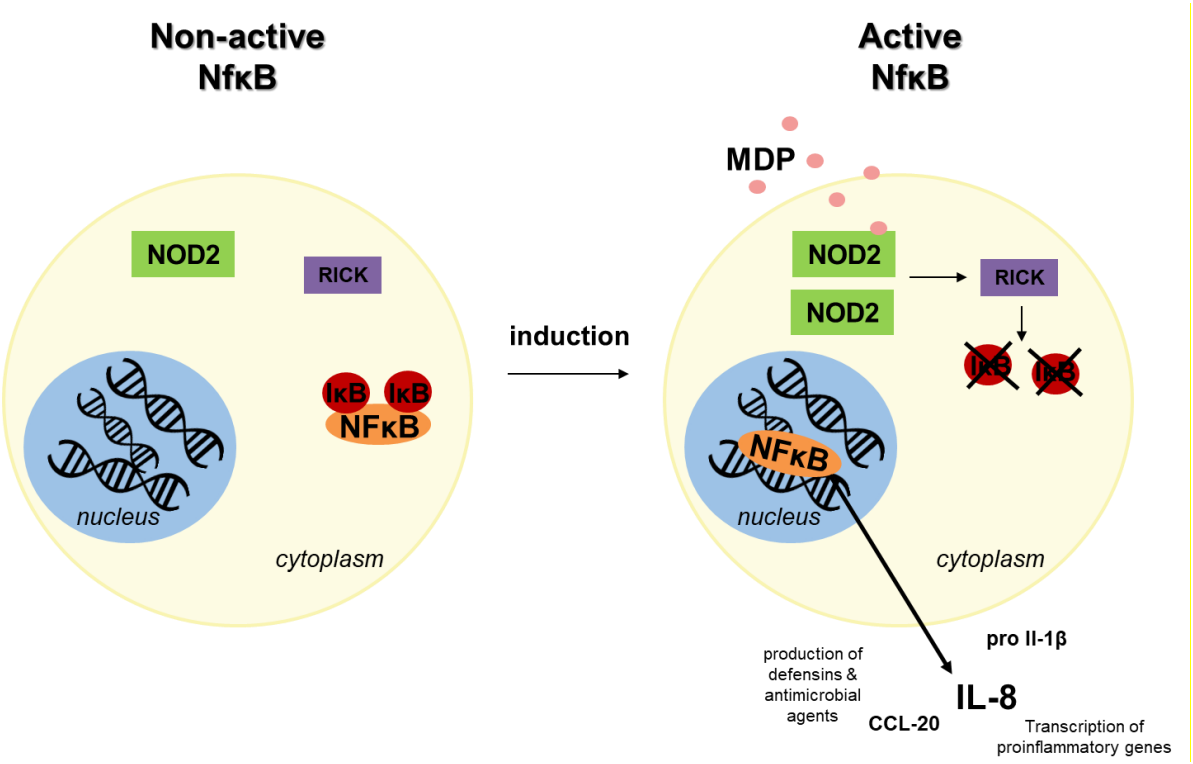

Figure 38. Activation of NOD2 signalling pathway leads to NFkB translocation and activation of pro-inflammatory response.

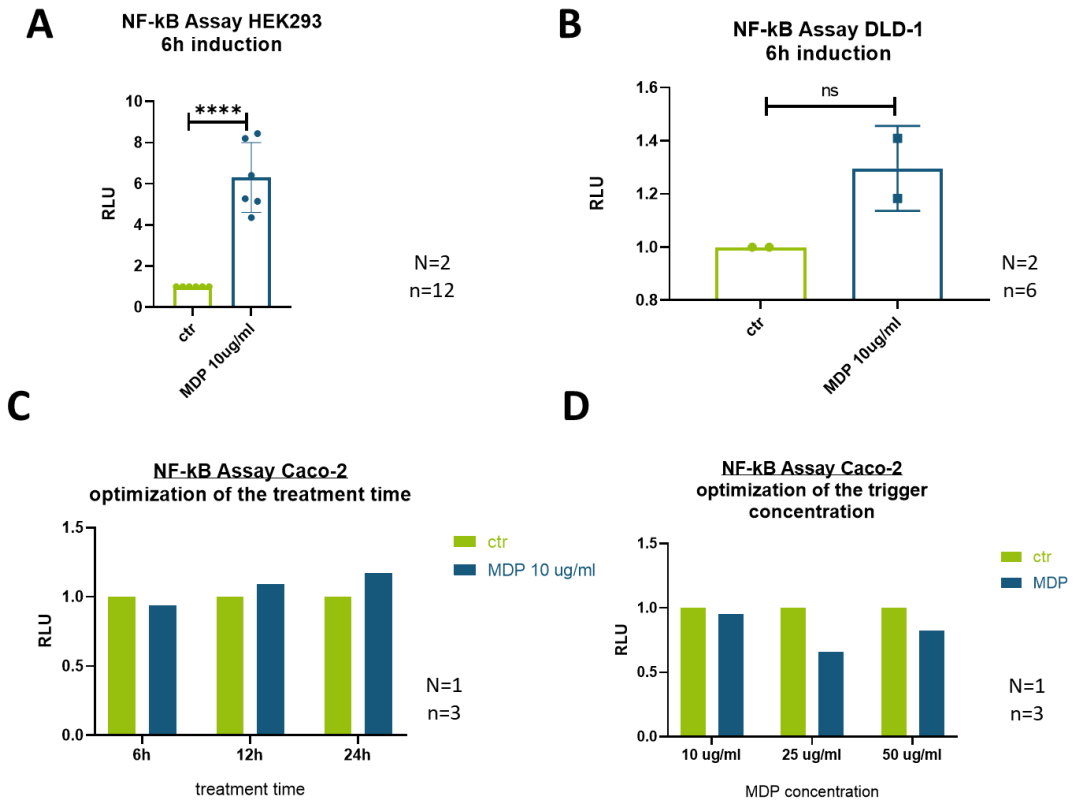

Figure 39. NFkB activation across cell lines – as assessed by dual luciferase assay.

(A) NFkB activation in HEK293 cells in response to MDP. Significant difference between conditions, t-test, p value <0.0001; (B) NFkB activation in DLD-1 cells in response to MDP. Non-significant difference between conditions, t-test, p value 0.1202; (C) NFkB activation in Caco-2 cells in response to MDP, optimization of the treatment time; (D) NFkB activation in Caco-2 cells in response to MDP, optimization of the trigger concentration. Data presented as relative luminescence unit and relative to untreated control. The data is expressed as fold change in relative light unites (RLU) as compared to the unstimulated control. N: biological replicate, n: technical replicate.

To gather more supportive evidence for the presence of functional NOD2 in the chosen cell lines, other means to assess the activation of the NFκB pathway were undertaken. One of them being immunostaining of NFκB transcription factor and tracking of its translocation to the nucleus upon addition of the trigger. In its inactive state, NFκB is sequestered in the cytoplasm by inhibitory proteins IκB. Activation of NOD2 signalling leads to phosphorylation of IκBs and results in the release of NFκB and its translocation to the nucleus. In this experiment, a cytokine cocktail containing TNFα, IFNγ and IL-1β was used as a positive control. Cytokines activate NFκB pathway regardless of NOD2. MDP specifically

activates NOD2 and was used as a test condition. In **Figure 40** it is visible that cytokines activate NFκB translocation to the nucleus within only 30 min. After 24 h the translocation is reverted. Triggering with MDP did not result in activation of NFκB and only cytoplasmic staining could be detected. This supports further our conclusion that NOD2 signalling is not active in Caco-2 cells.

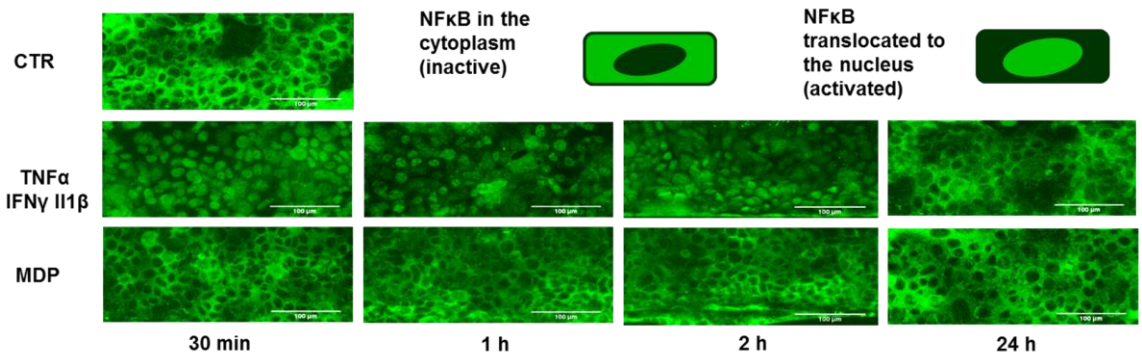

Figure 40. NFkB activation in Caco-2 cell line – as assessed by nuclear translocation.

Caco-2 were cultured as tubes in the OrganoPlate®, treated with cytokines cocktail or MDP for 30 min, 1 h, 2 h and 24 h. Cells were fixed with 3.7% PFA and stained with anti-P65 NFkB antibody. Untreated control on the top, cytokines treated cells in the middle panel and MDP treated cells in the bottom panel. Scale bars 100 µm.

Final data set to confirm the lack of NOD2 activation with MDP in Caco-2 cells is the assessment of barrier integrity of the tubes cultured in the OrganoPlate® and the release of pro-inflammatory cytokine IL-8. Cells were cultured according to previously described protocol until they became fully leak-tight. Cytokines or MDP were added to the chips and the assays were performed after 72 h (**Figure 41**). TEER measurement shows increased permeability of the tubes induced with cytokines. No difference between MDP treated and control tubes was observed. This suggests that MDP did not activate NOD2 signalling and the barriers remained fully intact. At the same time, IL-8 release was measured. THP-1 is a monocyte cell line that can be differentiated with PMA into macrophage-like cells. Macrophages are a crucial component of intestinal tissue and have a role in maintaining homeostasis by hampering inflammatory response directed at harmless microbiota (Na *et al.*, 2019). As shown in **Figure 37**, these cells highly express NOD2 and thus, when activated with MDP they should produce a significant amount of IL-8. Therefore these cells were used as a positive control for MDP stimulation in this experiment. As expected, THP-1 were efficiently

activated by cytokines and MDP treatment. Caco-2 cells responded to cytokines treatment with upregulation of IL-8 release but MDP treatment did not result in elevated IL-8 release. As indicated by the above results, NOD2 signalling could not be activated by stimulation with MDP in Caco-2 cell line and therefore generated model could not be used to model NOD2-related IBD phenotype.

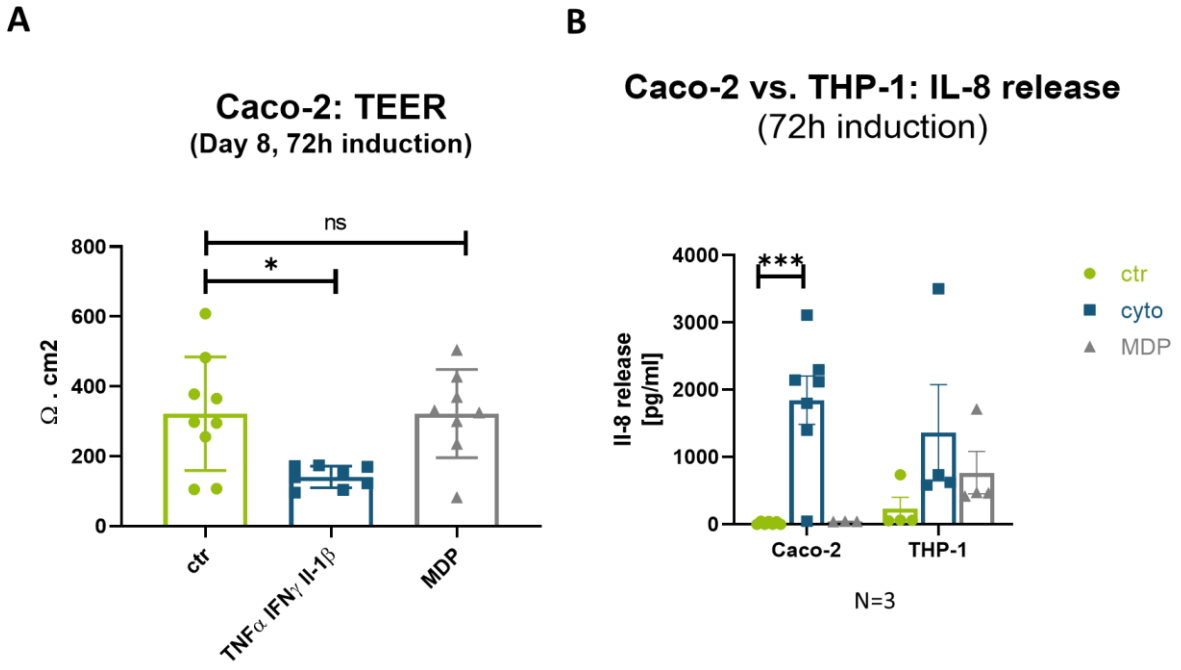

Figure 41. NFkB activation in Caco-2 cell line – as assessed by barrier integrity and Il-8 release.

(A) Barrier integrity upon 72 h treatment. Mean with 95% CI, One-way ANOVA *, p<0,05; (B) Il-8 concentration in the culture medium upon 72 h treatment measured by Il-8 ELISA. Mean with 95% CI, Two-way ANOVA ***, p=0,0003.

3.2.2.1.3. Co-culture with Raji B cell line as the way of promoting Caco-2 differentiation

Caco-2 is the epithelial cell line that represents the enterocytes population of the intestine. As shown in the previous experiments, this cell line is insensitive to MDP treatment. Since we were interested in modelling IBD in relation to NOD2 signalling, we needed to have a population of cells that would have that pathway active. In the intestine, the cells that play

an active role in anti-bacterial defence are the M cells. It is a population of epithelial cells that is associated with a lymphoid tissue and is responsible for the transport of antigens, in this way connecting the lumen of the gut with immune component adjacent to the tissue (Mabbott *et al.*, 2013). Having this in mind, we attempted to promote the differentiation of Caco-2 into M-like cells. Although NOD2 expression has not been confirmed in M cells (Ferrand *et al.*, 2019), we hypothesized that differentiation of Caco-2 cells might lead to increased sensitivity to MDP treatment. As described previously, co-culture with Raji B cells (B lymphocyte cell line) can promote such differentiation (Kernéis *et al.*, 1997). When successful, the following physiological changes should be observed: disorganization of brush border (precisely cytosolic redistribution of villin), downregulation of sucrase-isomaltase expression, increase in translocation of inert particles as well as redistribution of ICAM (intracellular adhesion molecule) to the apical side.

To begin with, co-culture of the above-mentioned cell lines in the 3-lane OrganoPlate® was established. In the original article (Kernéis *et al.*, 1997), Caco-2 were seeded on top of the membrane in the Transwell® system and Raji B cells were added beneath, into the well of the tissue culture plate. In such way, the cells did not have a direct contact but the Caco-2 monolayer had access to the effectors released by B cells (from the basolateral side). In our system, Raji B cells were embedded in the gel in the middle channel. Directly after gel seeding, Caco-2 cells suspension was added to the top channel. As a result, within four days of culture fully formed Caco-2 tubes were in very close proximity to Raji B cells present in the gel. The co-culture had no artificial membrane. We were expecting that such set up would reproduce the results from the original paper. We were able to co-culture the cells in such system and both cell types were viable for at least eight days (**Figure 42**). Viability was performed with calcein green staining which marks living cells.

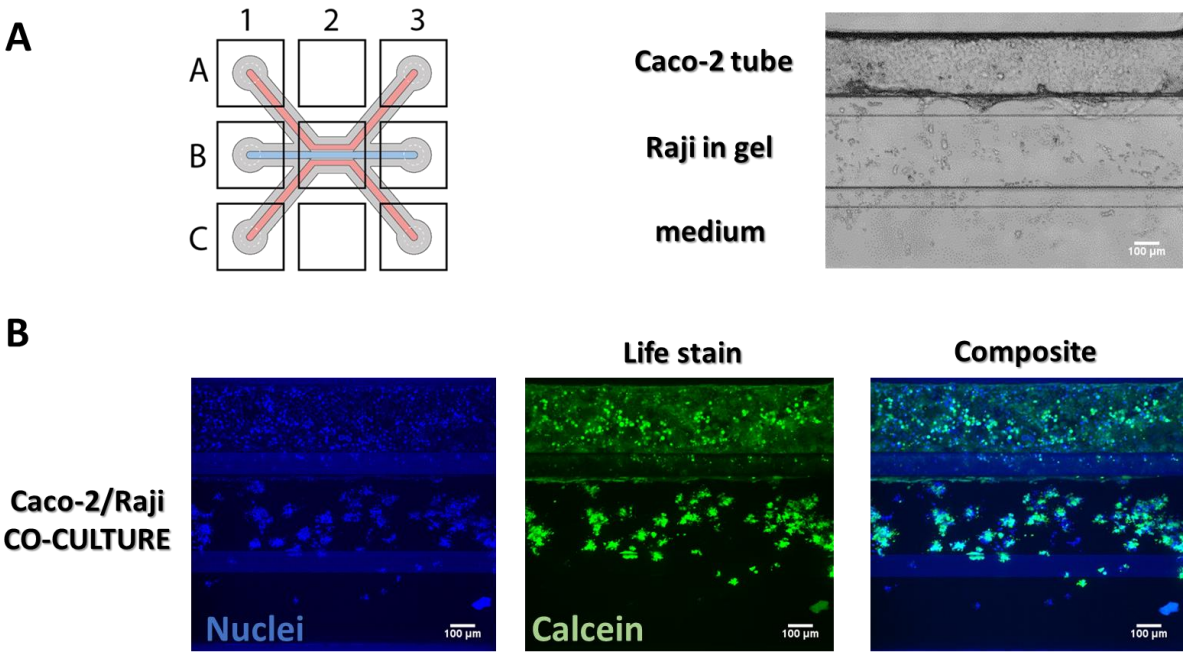

Figure 42. Caco-2/Raji B co-culture system.

Overview of the Caco-2/Raji B co-culture in the OrganoPlate®: (A) Phase contrast image of the co-culture; (B) viability of the culture: nuclei (DAPI in blue), life cells (calcein in green). Images represent top view of the chip. PhaseGuides seen as a horizontal bands. Scale bar 100 µm.

As we were specifically interested whether the M-cell line population would be enriched in this system, we checked if any physiological changes could be noticed (**Figure 43**). Brush border staining did not reveal any differences between mono- and co-culture. In both cases, Caco-2 tubes showed similar staining pattern, with ezrin as well as villin. TEER of Caco-2 tubes was measured and if the differentiation was successful, the drop in co-culture was expected. M cells have flattened shape and they form more loose cell junctions which should lead to decreased barrier resistance. Importantly, according to our hypothesis the enrichment in M-cells should result in responsiveness to MDP treatment. In this experiment cells were subject to the stimulation with cytokines or MDP and compared to the untreated control. As expected, cytokines treated tubes showed decrease in TEER in both culture configurations. MDP treatment did not influence the electrical resistance of the tubes. Interestingly, Caco-2 tubes cultured together with Raji B cells had slightly lower TEER values and those values remained stable in control condition. This could suggest that indeed differentiation could have occurred to some degree. However, due to the low N number of this experiment such

conclusion could not be drawn. The most vital experiment that would confirm if co-culture system led to differentiation and increased sensitivity of Caco-2 tube to MDP treatment was detection of IL-8 cytokine in the culture medium. It was shown that Raji B alone do not release IL-8, therefore they would not contribute to the overall cytokine concentration. Cytokines treatment served as a positive control and in both culture set ups Caco-2 reacted to that treatment with high concentration of IL-8 released into the medium. Unfortunately, no difference between the different culture systems was observed with regard to MDP stimulation.

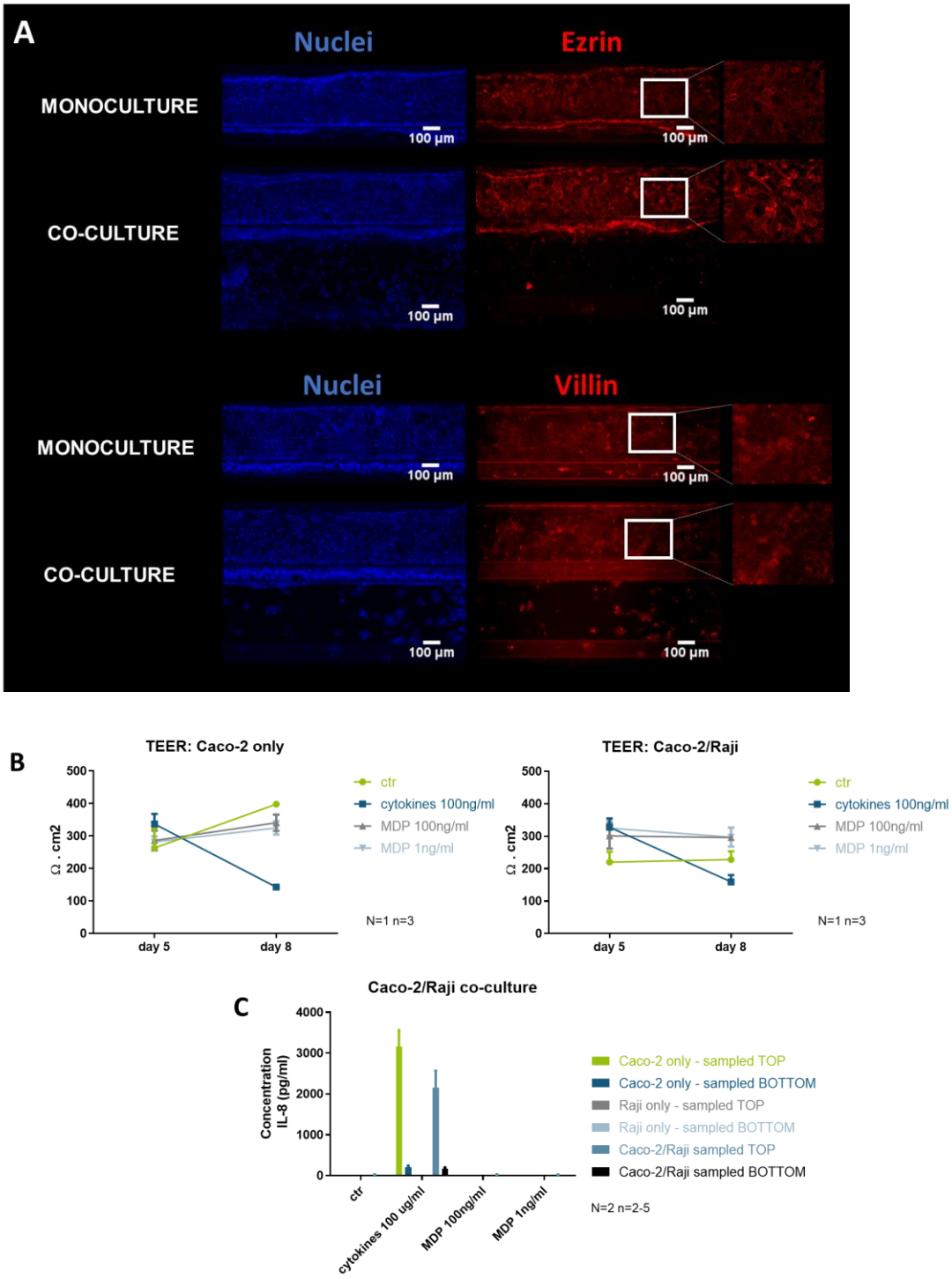

Figure 43. Promoting Caco-2 differentiation into M-cells like phenotype.

Investigation of the Caco-2 differentiation in the co-culture condition (A) Characterization of the brush border formation in mono- and co-culture system. Immunofluorescent staining depicting nuclei (DAPI in blue), brush border (ezrin and villin in red). Images represent top view of the top channel of the OrganoPlate®. PhaseGuide seen as a horizontal band at the bottom of each panel; (B) barrier formation by Caco-2 in mono and co-culture set up characterized by trans epithelial electrical resistance (TEER); (C) Il-8 release upon pro-inflammatory trigger measured with ELISA. N: biological replicate, n: technical replicate.

In conclusion, co-culture of Caco-2 cells with Raji B did not contribute to the increase of sensitivity to MDP. We could not confirm if the differentiation into M-cells occurred as apart from TEER data, no other assay gave such indication. It should be noted that physiologically, M-cells constitute only about 10% of the cells population in the gut (Ude *et al.*, 2019). Even if the differentiation in the plate was successful, we cannot be sure if the difference in response to the trigger would be noticeable.

3.2.2.2. Discussion

3.2.2.2.1. Detection of NOD2 on expression and functional level

As presented in the results section, detection of NOD2 in the intestinal epithelial cell lines proved to be difficult. Our findings showed very low level of expression on RNA level and Western Blot results suggested lack of detectable amounts of NOD2 protein. The results published in literature show contradictory claims which implies that there might be clonal differences between carcinoma cell lines cultured in different labs. Caco-2 cell line is known to be heterogenous, the main contributing factors being the different culture conditions, including varying media composition and passage number used in the experiments (Verhoeckx *et al.*, 2015). Hisamatsu et al. tested number of intestinal epithelial cell lines and only some of them showed detectable NOD2 expression, including SW480, SW620, T84, colo205 and LS174. NOD2 expression has not been confirmed in either Caco-2 and HT29 cell line (Hisamatsu *et al.*, 2003). In the same study, primary material from human intestine was tested and it has been shown that epithelial cells in vivo express this gene at considerably high levels. Possible contamination of the biopsies with lymphoid cells was prevented by FACS sorting of the $CD45^+$ and $CD68^+$ (lymphocyte and monocyte markers). Similarly, as published in Journal of Cell Biology, only low levels of NOD2 protein were detected by Western Blot and the functional analysis with luciferase assay exhibited lack of sensitivity to MDP stimulation in Caco-2 cells (Barnich *et al.*, 2005). Here HT-29 cell line showed higher NOD2 expression and was effectively triggered by MDP. On the contrary, in the study of Farin et al. Caco-2 and HT-29, used as a positive control for activation of immune response to microbial stimuli

demonstrated upregulation of IL-8 expression when treated with MDP (Farin *et al.*, 2014). Since MDP is a ligand specific to NOD2 it can be assumed that NOD2 signalling pathway was active in the cells used in the study. Another group showed functional activity of NOD2 in Caco-2 cells confirming NFκB activation after triggering the cells with MDP (Tan, Zeng and Zhi, 2015). Despite extensive investigation of NOD2 expression in our model, we were unable to confirm the presence of functional NOD2. We looked at the expression on both RNA and protein level, and tested activation of NOD2 signalling pathway in a functional assay. Appropriate controls were incorporated in the experiments, including (1) siRNA targeting NOD2 and (2) GFP-NOD2 overexpression plasmids to confirm specificity of the antibodies; (3) NOD2 overexpressing HEK293 cell line and (4) THP-1 monocyte cell line known to express NOD2 at high levels.

In the following step we attempted to differentiate Caco-2 cells into M-cells as described in the published reports (Kerneis *et al.*, 1997; Beloqui *et al.*, 2017). Enrichment of the cell monolayer with cells specialized in anti-microbial defence might aid in elevating the responsiveness of the system to the stimulation with a bacterial cell wall component. However, we could not confirm if the differentiation of Caco-2 cells was successful in our co-culture system. In contrast to the Caco-2 monoculture which showed increase in barrier function between day 5 and 8, TEER values of co-culture with Raji B cells remained stable, indicating that indeed M-like cell population could be present in our model. Such strong conclusion cannot be drawn from this experiment because of the low replicate number. No additional evidence was gathered to support this claim. More in-depth investigation of Caco-2 tubes should be performed in order to draw conclusions. As the percentage of differentiated cells in the tube could be very low, detailed microscopy analysis should be performed in order to be able to observe those cells. SpiB transcription factor is specifically expressed in this cell type and could be used as a marker (de Lau *et al.*, 2012). Alternatively, gene expression analysis including this marker could be performed.

3.2.3. Modelling IBD based on recreating inflamed phenotype by adding exogenous cytokines to the system

As the previous experiments with Caco-2 showed, those cells were only reactive to the cytokine trigger. Treatment with MDP was unsuccessful in all the performed experiments and due to that the change of the research direction had to be implemented. The epithelium of the intestine forms a barrier that separates the lumen lined with microbiome from the underlying environment, most importantly the immune component. In IBD patients that barrier is very often disturbed which causes constant inflammation of the tissue. It is not fully understood whether impaired barrier function is the causation of the disease or the effect. A breach in the barrier leads to infiltration of the intestinal tissue with bacterial material which in turn initiates inflammation (Chelakkot, Ghim and Ryu, 2018). With our approach, we aimed at recreating tissue inflammation and investigated the phenotypic changes in the epithelium.

***Aim 1*: Recreate the inflamed phenotype of the epithelium with the aim to test anti-inflammatory drugs.**

3.2.3.1. Introduction of immune component to mimic IBD on a chip: co-culture of intestinal epithelial cells with THP-1 monocyte cell line

It has already been shown that THP-1 cell line could be efficiently activated by cytokines and MDP. Monocytes differentiate into macrophages upon the migration from blood stream into the tissue. The main functions of these cells in vivo are phagocytosis, antigen presentation and release of cytokines. This differentiation process can be mimicked *in vitro* by stimulation of the THP-1 cells with PMA. As we aimed for generation of IBD model *in vitro* we induced the inflamed phenotype by co-culturing intestinal epithelial cells with macrophage-like cells. In the following experiments, we established a co-culture system with Caco-2 tubes and differentiated THP-1 cells. **Figure 44** shows the set up in the 3-lane

OrganoPlate® in which epithelial tube formed in the top channel is cultured adjacent to monocytes seeded in the bottom channel. There are no artificial membranes in between; the middle channel is filled with ECM.

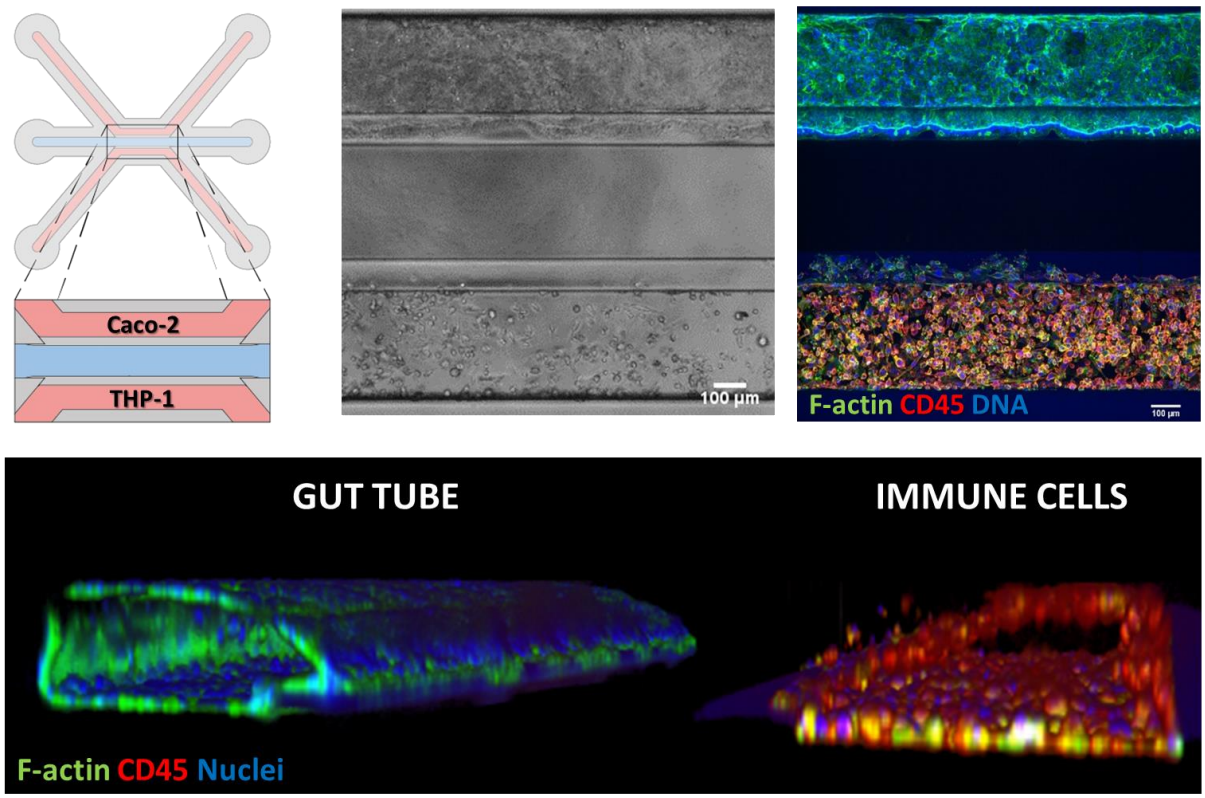

Figure 44. Caco-2/THP-1 co-culture system.

Overview of the co-culture system. Caco-2 tube formed in the top channel of 3-lane OrganoPlate® with THP-1 cells seeded in the bottom channel. ECM in the middle channel. Immunofluorescent staining depicting nuclei (DAPI in blue), actin filaments (fluorescent phalloidin in green), hematopoietic marker (CD45 in red). Top panel: images represent top view of the chip, PhaseGuides seen as horizontal bands. Bottom panel: 3D reconstruction of the confocal images, side view. Scale bars 100 µm.

In this design, we added the trigger only to the THP-1 cells seeded in the bottom channel and hypothesized that the activated monocytes would release cytokines (secondary trigger) which would migrate through the gel and would induce a pro-inflammatory response in Caco-2 cells upon stimulation of the basolateral side of the tube. Here again we used the cytokines trigger as well as MDP to stimulate THP-1 cells. It should be noted that THP-1 were differentiated with PMA for 48 h prior to seeding in the OrganoPlate® and those cells alone

showed substantial basal IL-8 release. THP-1 are suspension cells and upon differentiation into macrophages they become adherent to the surface of tissue culture plate. Before harvesting the cells the surface was rinsed to ensure collection of only the differentiated proportion of the cells. Caco-2 tubes were already fully leak tight on the day of adding monocytes with the trigger. The experiment was terminated after 72 h stimulation and the medium was harvested separately from the top and bottom channel. Data from this experiment is presented in **Figure 45** and monoculture was added as a control condition.

Graph on the bottom presents concentration of IL-8 in the medium harvested from the bottom channel (the release by THP-1 cells). It is clear that there is a significant difference between mono- and co-culture systems. Caco-2 tubes alone release IL-8 only upon cytokines stimulation and the concentrations are much lower than the ones released by THP-1. As mentioned beforehand, non-treated THP-1 release significant amount of IL-8. However, when triggered with cytokines or MDP we could clearly observe an upregulation in IL-8 release. Cytokines trigger was more potent than MDP.

Knowing that the THP-1 were efficiently stimulated by both of the triggers we were hoping to see Caco-2 reaction to the secondary trigger as measured in the medium collected from the top channel. Data depicted in the graph "Caco-2/THP-1 co-cultured sampled from the top channel" show the highest peak in the condition stimulated with cytokines. It is logical as the cytokines were more potent in activating THP-1 and that condition showed highest Il-8 release in the bottom channel. However, the difference between mono- and co-culture was not significant as shown in the graph with media sampled from the bottom channel. Other conditions showed some IL-8 release but the values were close to detection limit. All that indicates that there is no real benefit of co-culture system as the addition of THP-1 cells did not result in responsiveness of Caco-2 to MDP trigger. In conclusion, Caco-2 cells appear not to be sensitive enough to efficiently respond to the triggers.

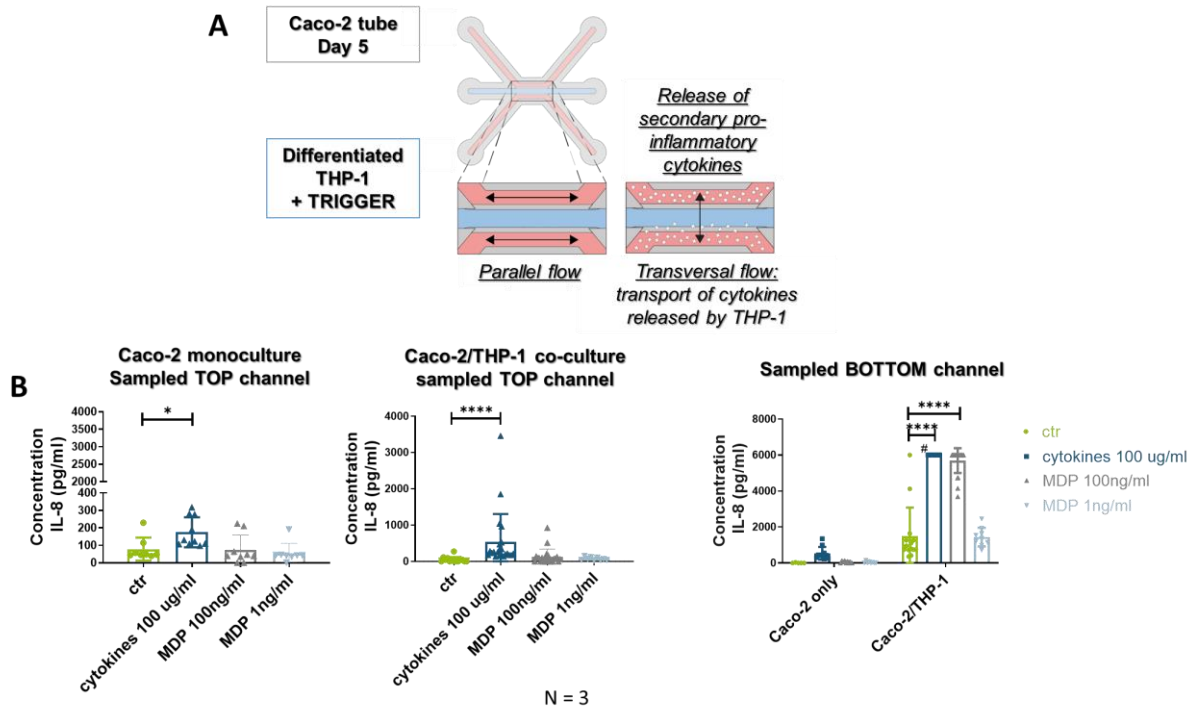

Figure 45. Caco-2/THP-1 co-culture: triggering immune response.

(A) Caco-2 cells were seeded in the top channel of the 3-lane OrganoPlate® and THP-1 cells together with the trigger were added to the bottom channel on day 5 of culture. Parallel flow is forced by gravitation when the plate is placed on the rocking platform. It is expected that cytokines released by activated THP-1 cells will migrate to the basolateral side of Caco-2 tube thanks to the transversal flow; (B) Il-8 released into the culture medium in mono- and co-culture system. Samples from top (apical release of Caco-2 tubes) and bottom (THP-1 and/or basolateral release of Caco-2 tubes) were analysed separately. Some values were above the read out range (#). Mean with 95% CI, Caco-2 monoculture One-way ANOVA *, p=0,0294. Caco-2/THP-1 co-culture One-way ANOVA ****, p<0,0001.

3.2.3.1.1. Cell phase synchronization: starvation of Caco-2 cells prior to introduction of the pro-inflammatory trigger

As Caco-2 did not show a strong response, we wanted to sensitize them to the trigger before starting the exposure. Therefore, the tubes were starved (withdrawal of FBS from the culture medium) for 24 h prior to the addition of THP-1 and the trigger. Removal of the FBS from the media should lead to cell phase synchronization making the cell response unified across the tubule (Kues *et al.*, 2000). The data are gathered in **Figure 46**. Caco-2/THP-1 co-

culture was triggered with either cytokines or MDP. Caco-2 monoculture was included in the experiment as a control condition. All the culture conditions responded to the cytokines trigger and that response was more profound when the cells were subject to starvation. In general, starved Caco-2 showed slightly higher IL-8 release than control tubes but the differences were not significant. Importantly, that upregulation was also observed in non-treated tubes which indicates that the starvation alone leads to activation of low level immune response. Since the difference between conditions were not significant, starvation of Caco-2 tubes prior to experiment had no added value.

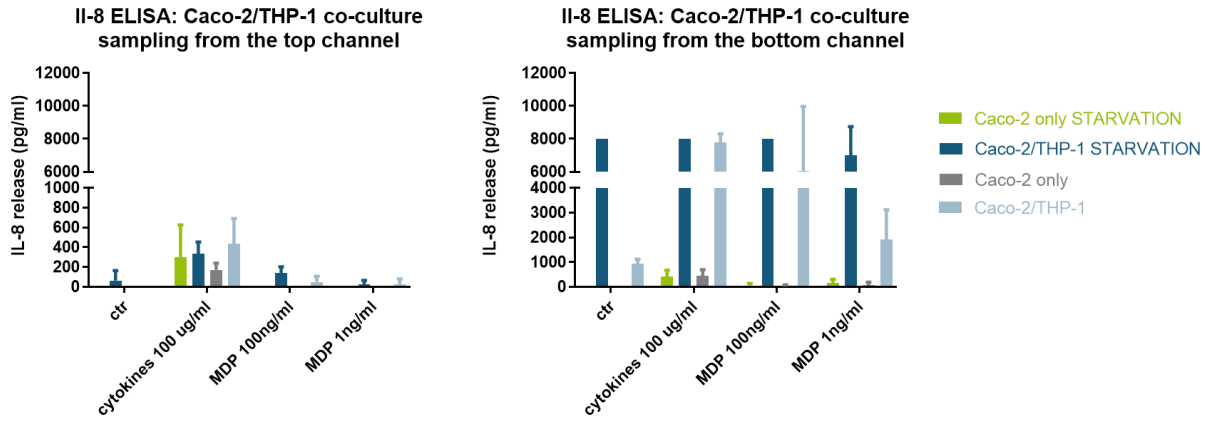

Figure 46. Starvation of Caco-2 as a way to sensitization to the trigger.

Caco-2 tubes were cultured in no FBS medium for 24 h prior to the addition of THP-1 and the trigger. Il-8 concentration in the medium was measured by ELISA. Medium from top and bottom channel was analysed separately, N=1.

3.2.3.1.2. THP-1 conditioned medium as a more potent trigger to stimulate inflamed condition in Caco-2 tubules

Since THP-1 could be efficiently triggered by cytokines and MDP, we thought that THP-1 conditioned medium could be used as a trigger itself and that such trigger would be more potent (**Figure 47**). We examined the effect of such stimulation on Caco-2 tubes. Firstly, we established the concentration of IL-8 in the THP-1 conditioned medium. As expected, differentiated THP-1 alone released significant amount of IL-8. Concentration of this pro-

inflammatory cytokine was much higher in cytokines triggered condition and stimulation with 100 ng/mL MDP resulted in double the amount of Il-8 than in the control condition. This conditioned medium was added into the top channel (apical side of Caco-2 tubes) and Caco-2 response was measured by ELISA. Difference between trigger conditions was observed, however we probably mostly measured the IL-8 already present in THP-1 conditioned medium. No difference between control (differentiated THP-1 medium) and MDP-treated differentiated THP-1 medium was observed. Those observations were in line with the previous experiments, as the cytokines trigger proved to be more efficient than MDP. Even though significant amount of Il-8 was measured in the top channel, we cannot say if Caco-2 contributed to that or we measured only Il-8 that remained stable in the THP-1 conditioned medium. IL-8 is not the only pro-inflammatory cytokine released by THP-1 cells and the composition of the secondary trigger was not investigated further. Clearly, there was a difference between potency of cytokines and MDP trigger and therefore it can be concluded that the composition of the secondary trigger released in response to each of them differed. With this experiment we conclude that Caco-2 cells are not sensitive enough and some other epithelial material should be used to model IBD on a chip.

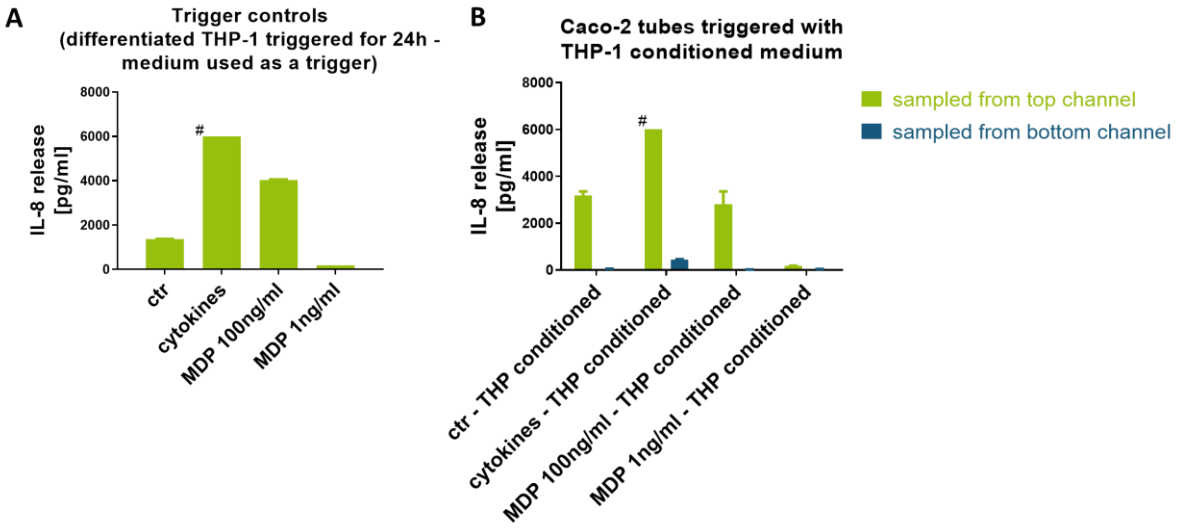

Figure 47. Triggering immune response with THP-1-conditioned medium.

(A) Il-8 concentration in THP-1-conditioned medium that was used as a trigger on Caco-2 cells. Control refers to medium collected from differentiated THP-1 cells. Other medium samples are taken from differentiated THP-1 cells stimulated for 24 h with cytokines or MDP; (B) Caco-2 tubes triggered with THP-1-conditioned medium. Stars indicates that the values were above the read out range, N=1.

3.2.3.2. Discussion

3.2.3.2.1. Suitability of Caco-2 cell line for IBD modelling *in vitro*

In our study we used Caco-2 cell line to model IBD on a chip. Initial approach in modelling the disease based on NOD2 signalling deficiency was not very successful, therefore we focused on recreating the intestinal inflammation with exogenous cytokines released by the immune component added to the system. Since our interest initially lied in NOD2-related immune response, we included MDP as one of the THP-1 triggers. We observed substantial IL-8 release by THP-1 stimulated with both cytokines cocktail and 100 ng/mL MDP. Caco-2 reacted to the secondary trigger released by the macrophage-like cell line but the amount of IL-8 detected in the top channel of the chip was not striking. We observed significant difference only between control and cytokines-triggered condition. This suggests that the composition of the secondary trigger released by THP-1 in response to the stimulants differed. It is important to note that we only measured IL-8 release in Caco-2 cells. It would be worthwhile to examine the release of other inflammatory cytokines to better understand the regulation of signalling pathways in the system. We concluded that the addition of the immune component did not have an added value, as Caco-2 remained insensitive to the stimulation with MDP-induced inflammation. However, the general inflammatory condition could be observed in cytokines-induced chips which is in line with the previously published reports (Watanabe *et al.*, 2004; Satsu *et al.*, 2006; Kämpfer *et al.*, 2017). Withdrawal of FBS prior the addition of the trigger resulted in slightly higher Il-8 production but the change was not significant. The response to MDP-triggered THP-1 was slightly more pronounced in the starved condition but remained within the range of the unstimulated condition. We reckon that the change of the media from starvation to the one containing FBS at the moment of the addition of the trigger might have resulted in the change of Caco-2 cells behaviour. It would be suggested to maintain starved condition throughout the entire experiment.

Caco-2 alone can be used to model IBD, as presented by Beaurivage *et al.* (2019). As shown in this thesis as well as in the literature, Caco-2 tubules stimulated with the cytokines trigger show release of pro-inflammatory cytokines and decreased barrier function. Here we

present the data for IL-8 release only but Beaurivage et al. examined expression of IP-10 and CCL-20, showing upregulation in release of those cytokines. Additionally, it has been shown that the effects of cytokine-induced inflammation could be effectively reversed by the addition of a known anti-inflammatory compound TPCA-1. This simplified IBD model could serve a purpose in anti-inflammatory drug screen. Possibility of including immune cells in the system broadens the application of the model.

3.2.3.2.2. Importance of the immune component in IBD modelling *in vitro*

A challenge in co-culturing immune cells with epithelium is the maintenance of stability of the system in the untriggered condition. Both Watanabe et al. and Satsu et al. described reduction of Caco-2 barrier integrity upon addition of unstimulated THP-1 cells to their systems. Only Kämpfer et al. managed to sustain the equilibrium in the system and the presence of THP-1 cells did not negatively influence epithelial barrier integrity. In our experiments we did not measured barrier integrity but the low levels of IL-8 release in the control condition suggest that the co-culture was stable. Interestingly, the number of THP-1 cells per chip in our system was considerable and yet did not negatively influence Caco-2 morphology. Viability assay should be included in order to properly assess the impact of THP-1 on Caco-2 cell. Advantage of our model is the lack of artificial barrier between the cell compartments. However, closer proximity of both cell types could be achieved by seeding THP-1 cells in the gel channel.

As presented in the **Figure 47**, THP-1- conditioned media was a potent pro-inflammatory trigger with high IL-8 content. We used this trigger to stimulate Caco-2 tubules from the apical side and measured their response with IL-8 release. Presence of other inflammatory cytokines should have been examined in order to exclude the interference of the IL-8 signal from the trigger media. Similarly, to isolate the response of epithelial cells, the activation of NFκB signalling could be checked by staining of this transcription factor. Nuclear localization would prove activation of the inflammatory response. Additionally, the composition of THP-1 conditioned media should be investigate further. As the results showed,

there was a clear difference between the response to the THP-1 induced with different triggers. In conclusion, Caco-2 cells proved to be insensitive to MDP-induced inflammation and other cell source was suggested to be included in further experiments. Our data showed that it is possible to model cytokines-induced inflammation with Caco-2 and THP-1 cells which is in line with the published data. The added value of our model is the development of a high throughput system that allows for shortening of the time required to obtain a stable culture, reduction of the amount of the compounds used and increase in physiological relevance of the model thanks to the lack of artificial barrier between the compartments.

A study based on the similar to the presented here co-culture concept in the OrganoPlate® platform was published and contained Caco-2/HT-29 tubule with the immune component consisting of MUTZ-3 and THP-1 added to the bottom channel (Gijzen *et al.*, 2020). Similarly to our results, they saw reduction of the barrier integrity and upregulation of IL-8 release. Concentrations of IL-8 reported in this study were higher than what was shown in our experiments. These differences could be explained by the slightly different composition of the trigger and the impacted stability of the cytokines. Additionally, in our system Caco-2 and THP-1 were cultured alone and the experiments in the published paper were performed on the tetra-culture.

Immune component plays a role in maintaining intestinal homeostasis, thus malfunction in the innate immune response is central to the IBD pathogenesis. Susceptibility genes have been bound to the innate immune cell functions (Cho and Brant, 2011) and more efforts are devoted to elucidate the mode of action of macrophages and dendritic cells in individuals with IBD. More in-depth understanding would allow for the development of new, more efficient therapies. Indispensable in this process is generation of physiologically relevant *in vitro* models that combine epithelial and immune components.

3.3. Chapter III: Establishment of a physiologically relevant model: generating gut tubules from iPSC- and primary-derived intestinal organoids

3.3.1. Introduction

In **Chapter II** of this thesis, the efforts to establish a reliable IBD model have been described. As the results show, modelling the disease with the use of adenocarcinoma epithelial cell lines and based on NOD2 signalling proved to be challenging. Modelling IBD based on recreating inflamed phenotype with the addition on exogenous proinflammatory cytokines successfully mimicked disease phenotype. Combining epithelial cell line with THP-1 cells as the more complex gut on a chip model showed some promise, but Caco-2 cells failed to robustly respond to the pro-inflammatory triggers. In a search for a more suitable cell source to model a gut on a chip we turned to organoids. Those enclosed structures constitute of a folded monolayer of various cell types typically found in the intestine. They represent biology of the intestinal wall by generating crypt-villi architecture with stem cell niche present at the tip of protruding structures and differentiating cells moving towards the inside of the organoid. Organoids can be established from either adult-derived stem cells acquired during biopsy or from differentiating induced pluripotent stem cells. Such material is more physiologically relevant than the immortalized cell lines, and *in vitro* models can be established for a particular patient. In this project both types of organoids were used to generate *in vitro* gut-on-a-chip model. We worked with already established organoid cultures and derivation of the lines was performed by other researchers. iPSC-derived organoids were purchased from DefiniGEN (UK) and primary-derived organoids were obtained from Hubrecht Institute (The Netherlands). In the following chapter, characterization of the novel gut-on-chip models will be presented. In addition, we tested suitability of those models for the future drug screening of anti-inflammatory compounds. There is a huge potential in the emerging field of disease modelling with the use of organoids and combining that with an organ on chip technology gives promise to generate truly relevant tissue models for drug testing.

***Aim 1*: Generation of physiologically relevant gut on a chip model by using organoid technology.**

3.3.2. iPSC-derived gut organoids: accessible source of physiologically relevant material

iPSC cells were first established from mouse cells (Takahashi and Yamanaka, 2006) but the technology developed quickly and is currently widely used in research. It has a huge potential, as these cells are very similar to the embryonic stem cells and can be expanded indefinitely. Most importantly, there is no ethical concern in using them because they can be obtained by reprogramming any somatic cells taken from the patient. There are many existing protocols for differentiating them into almost any cell types desired, one of them being differentiation into gut cells and further growing into 3D organoid structures (JL *et al.*, 2016). The principle of differentiation iPSCs into intestinal organoids has been presented in **Figure 48**. There are many potential applications of this technology and the possibility to use it in personalized medicine is very exciting. In this thesis, we present the proof of concept experiments on how genetically defined human iPSC-based disease models could be used in drug screening.

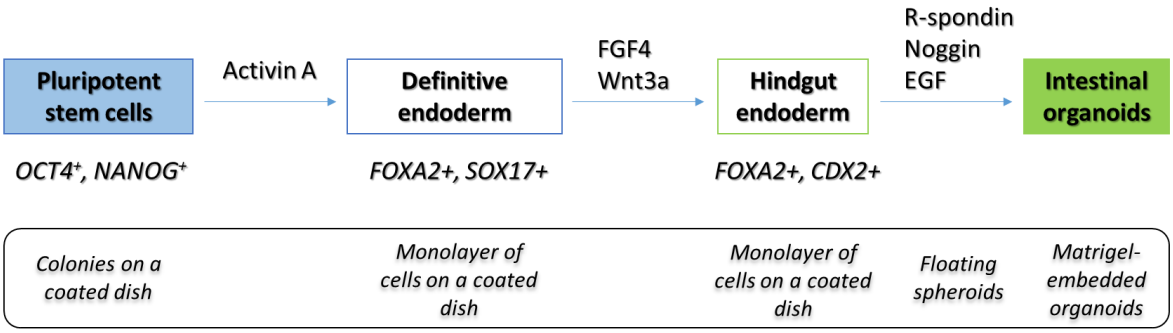

Figure 48. Generation of iPSC-derived intestinal organoids adapted from Sato and Clevers, 2015.

3.3.2.1. Changing organoids' architecture: establishment of tubular structures in the microfluidic device

Normally the organoids are grown in Matrigel® droplets. Matrigel represents a protein mixture that resembles extracellular environment found in living tissues. It is mainly composed of structural proteins, like collagen that serves as a scaffold, and growth factors. Important feature of this matrix is that it remains in liquid form at 4°C and solidifies at 37°C. Initially we cultured the organoids as 3D structures embedded in such droplets. As they proliferated and vast amount of organoids was available, we dissolved the matrix and prepared single cells suspension that was seeded into the top channel of 3-lane OrganoPlate® (**Figure 49**). Similarly to previous protocols, we aimed to generate tubules adjacent to the ECM in the middle channel.

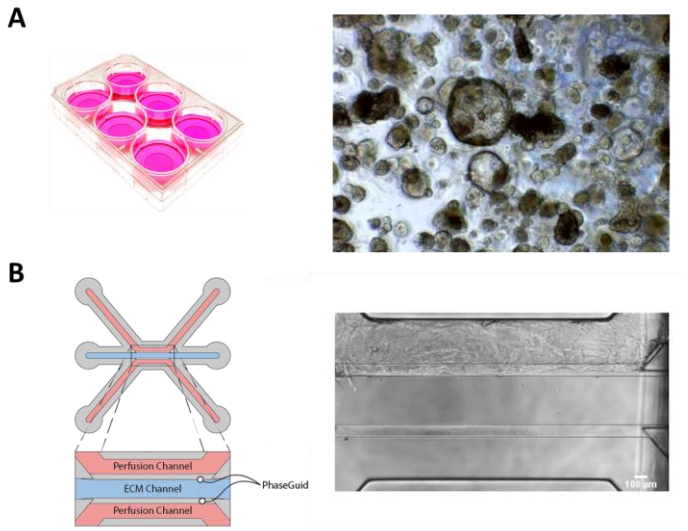

Figure 49. iPSC-derived organoids culture.

(A) iPSC-derived organoids cultured as 3D structures in Matrigel® droplets; (B) iPSC-derived gut organoids form tubules in the top channel of the OrganoPlate®, with an access from both, apical and basolateral side. Scale bar 100µm.

3.3.2.2. Characterization of iPSC organoids-derived gut-on-chip model

Optimization of the protocol was necessary, which included adjustments in cell number seeded per chip as well as coating of the top channel. With the final protocol, approximately 50% of the tubes were able to form leak tight barriers at day 5 (**Figure 50**). Those tubes maintained the barrier for at least five more days.

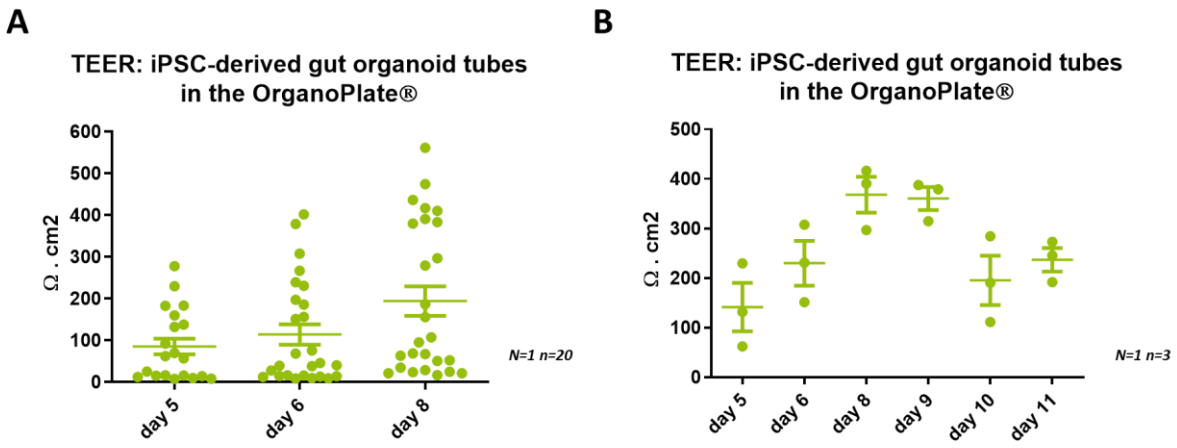

Figure 50. iPSC-derived gut organoids form leak tight tubes in the OrganoPlate®.

(A) Efficiency of barrier formation across a single OrganoPlate®; (B) Barrier stability of fully formed tubules. N: biological replicate, n: technical replicate.

Apart from formation of the tubules, it was important to know what characteristic markers were expressed by those organoids and how the expression would compare to the primary organoids and extensively tested Caco-2 cells. Primary organoids served as a gold standard in this experiment as the marker expression should be as close to human tissue as possible. We tested expression in both, iPSC-derived organoids cultured in matrigel droplets (3D) and in tubular structures in the OrganoPlate® (OP) with qPCR. The main reason to switch to organoids in this project was to exchange Caco-2 epithelium with a more physiologically relevant material, thus all the expression levels were compared to that adenocarcinoma cell line. HEK293 cells were included as a negative control, representation of cells from a different organ. However, since it is a cell line of embryonic origin it can give some misleading results. It appeared that primary organoids had higher expression of *LGR5* suggesting that they are

more stem cell-like than iPSC-derived organoids (**Figure 51**). Both organoid types expressed high levels of lysozyme which is the marker for Paneth cells, indicating that those cells are present. Enteroendocrine cells were not detected in primary organoids but they were present in iPSC-derived ones. Similarly, enterocytes markers were upregulated in iPSC-derived organoids. None of the organoids expressed PGP transporter. It should be noted that qPCR analysis was performed only a single time and should be repeated to confirm the findings. The results suggest that iPSC-derived organoids could be used as a gut model because in addition to formation of the barrier, they seem to express multiple intestinal markers and the expression is considerably higher than previously used Caco-2 cells. No expression of efflux pump was detected which poses a disadvantage to this system. However, it has not been confirmed on the functional level and expression of other transporters was not checked. The presence of transporters is essential in modelling gut *in vitro* and is relevant in absorption studies. The lack of expression could be explained by the fact that iPSC cells, due to their origin have more embryonic phenotype but further investigation would be necessary.

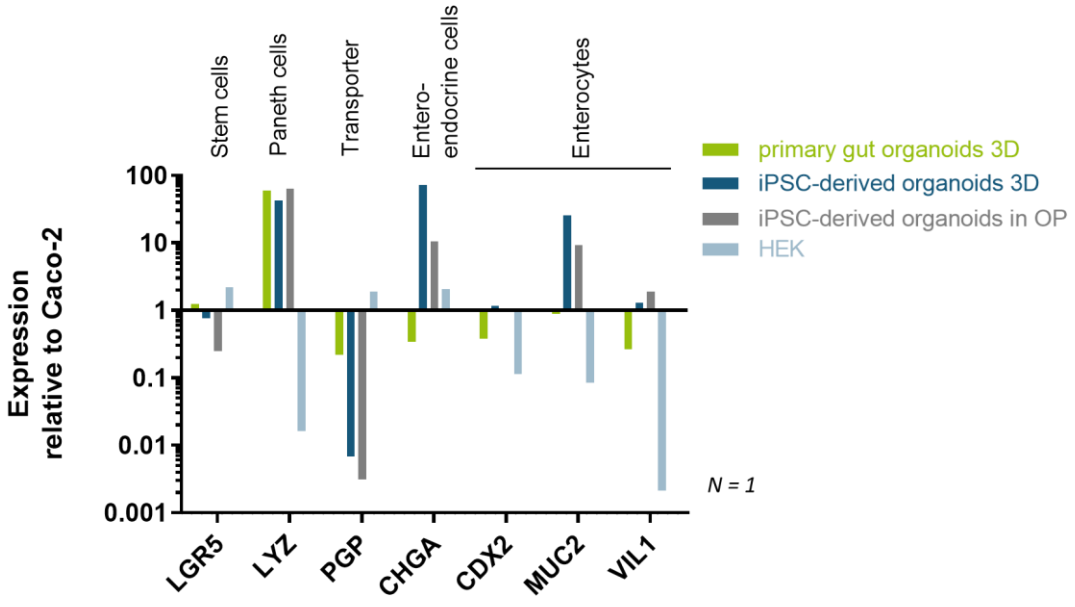

Figure 51. Expression analysis of intestinal markers.

Expression normalized to GAPDH, presented as relative to the expression in Caco-2 cells. Primary gut organoids 3D cultured in Matrigel droplets, iPSC-derived gut organoids cultured in Matrigel droplets (3D) and in the OrganoPlate® (OP). Expression of *LGR5* (biomarker of adult stem cells), lysozyme (Paneth cells marker, enzyme that plays a role in bacterial clearance), *PGP* (P-glycoprotein, efflux pump), *CHGA* (chromogranin A, marker for enteroendocrine cells), enterocytes markers: *CDX2* (transcription factor, essential in intestinal homeostasis), *MUC2* (mucin, responsible for mucus formation), *VIL1* (villin, formation of brush border).

Expression of key intestinal markers was confirmed by immunostaining and again 3D organoids were compared to the tubules cultured in the OrganoPlate®. Staining of Matrigel-embedded structures are shown in **Figure 52**, while **Figure 53** and **Figure 54** represent organoids grown in form of tubules. No major differences were observed between the growth conditions. Organoids formed proper brush border, as shown by ezrin and villin staining. Mucus producing cells were found in both structures, but it is important to mention that distribution of those cells was very scattered and not all the samples contained positive cells. It can be easily explained, as organoids need to be differentiated to some extent to contain goblet-like cells. Possibly, if cultured in a medium facilitating differentiation, more positive cells would have been present. Clearly, a good number of Paneth-like cells were present in both cultures as seen with lysozyme staining. *PGP* transporter was not detected, confirming lack of expression found by qPCR. Staining for chromogranin and *LGR5* was not confirmed due to the quality of commercially available antibodies. In conclusion, immunofluorescence experiments confirmed expression of the intestinal markers detected at mRNA level, proving that iPSC-derived gut organoids could be used to model intestine on a chip.

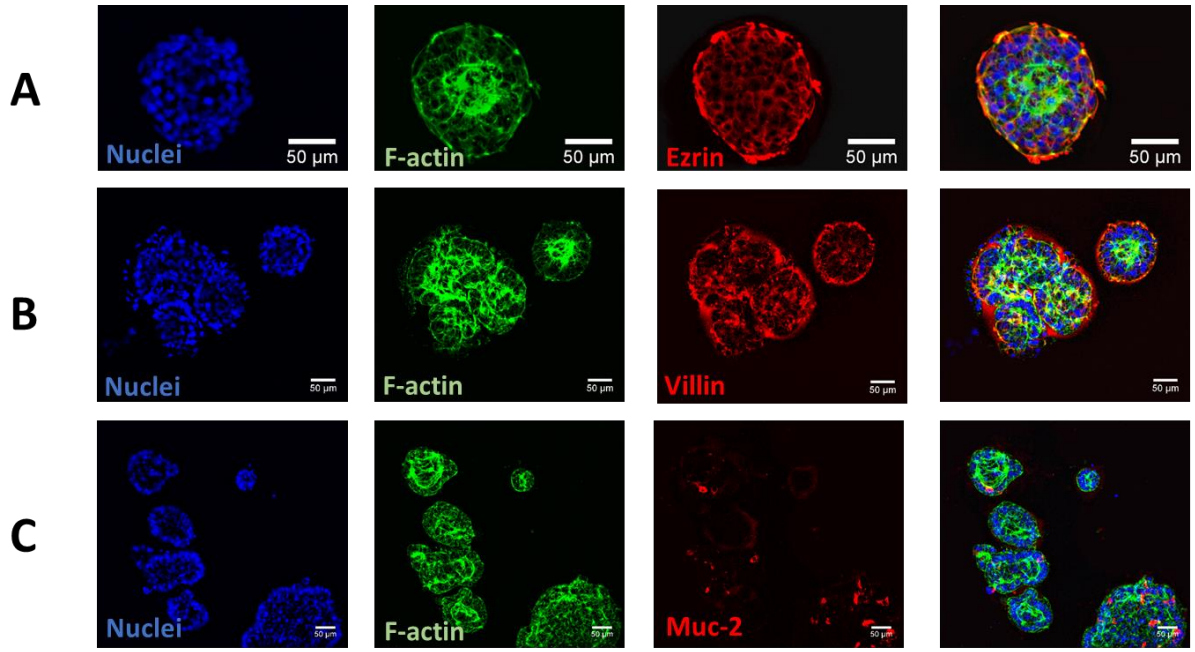

Figure 52. Expression of intestinal markers in iPSC-derived gut organoids cultured in Matrigel.

Cells were cultured in form of 3D structures embedded in Matrigel and subject to immunostaining. Nuclei (DAPI in blue), actin (fluorescent phalloidin in green), intestinal markers: brush border (ezrin and villin in red) and mucin (muc2 in red). Scale bars 50 µm.

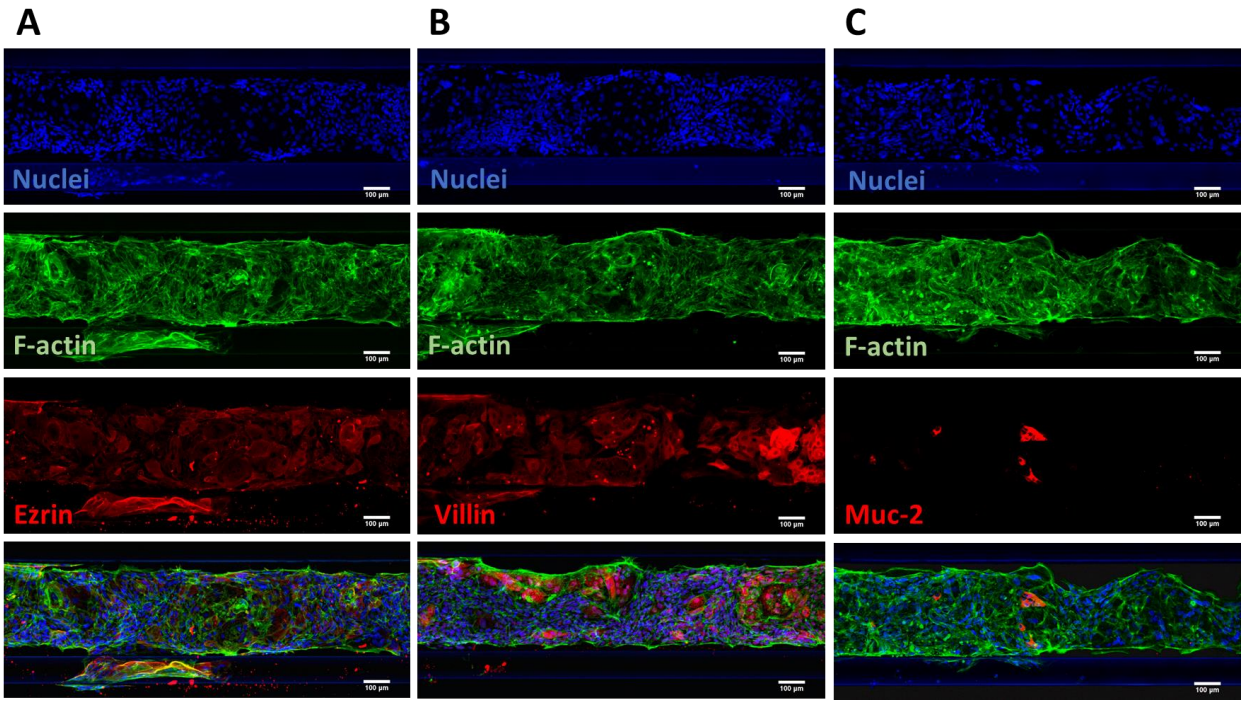

Figure 53. Expression of intestinal markers in iPSC-derived gut organoids cultured as tubules in the OrganoPlate®.

Cells were cultured in form of tubules in a 3-lane OrganoPlate® and subject to immunostaining. Nuclei (DAPI in blue), actin (fluorescent phalloidin in green), intestinal markers: brush border (ezrin and villin in red) and mucin (muc2 in red). Images represent top view of the top channel of the OrganoPlate®. PhaseGuide seen as a horizontal band at the bottom of each panel. Scale bars 100 µm.

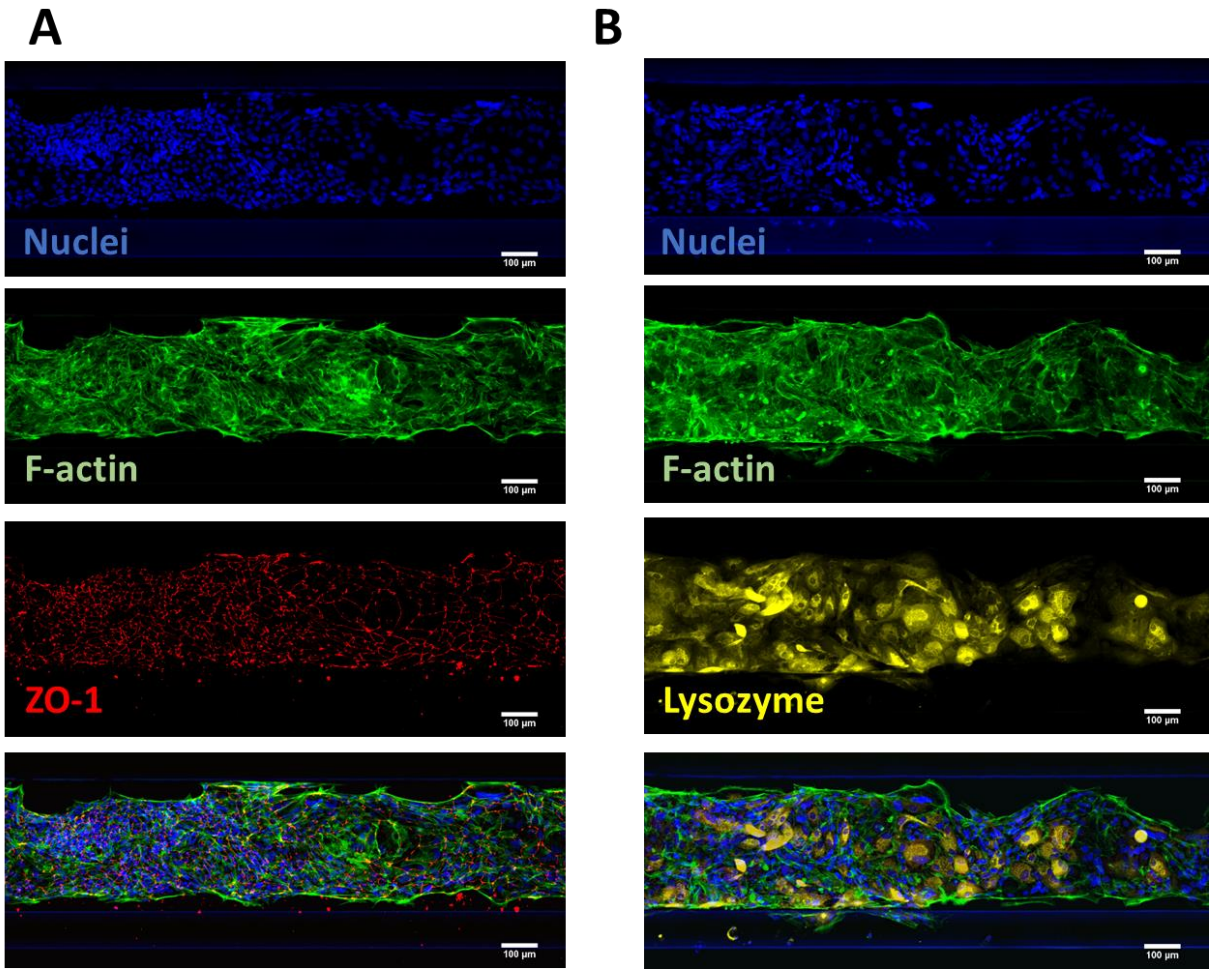

Figure 54. Expression of intestinal markers in iPSC-derived gut organoids cultured as tubules in the OrganoPlate®.

Cells were cultured in form of tubules in a 3-lane OrganoPlate® and subject to immunostaining. Nuclei (DAPI in blue), actin (fluorescent phalloidin in green), intestinal markers: tight junctions (ZO-1 in red) and Paneth cells (lysozyme in yellow). Images represent top view of the top channel of the OrganoPlate®. PhaseGuide seen as a horizontal band at the bottom of each panel. Scale bars 100 µm.

3.3.2.3. Modelling IBD on a chip: inflamed phenotype of IPSC organoids-derived tubules

3.3.2.3.1. Inflamed phenotype is efficiently reverted with the addition of an anti-inflammatory compound: suitability of the generated model for drug screening

After successful establishment of the model in the OrganoPlate®, we tested if it could be used to model IBD on a chip. Previous attempts with Caco-2 tubes proved to be inefficient due to the low sensitivity of those cells to the pro-inflammatory stimuli. After optimization of the trigger conditions, we decided to treat the cells for 24 h with 50 ng/mL TNFα, as exposure to higher concentration or the cytokines cocktail used previously resulted in high cell death (data not shown). This already proved that iPSC-derived gut organoid model is more sensitive than Caco-2. Treatment with pro-inflammatory cytokine led to increased release of IL-8, confirmed both by ELISA and qPCR. Since the model was efficiently stimulated, we wanted to prove that it could be used in a drug screen. In a simple proof of concept experiment, we added the well-known anti-inflammatory drug (TPCA-1) and observed significant downregulation of Il-8 expression. TPCA-1 is an inhibitor of IκB kinases which are the activators of NFκB pathway. By blocking the translocation of NFκB to the nucleus we can prevent the initiation of transcription of pro-inflammatory cytokines like IL-8. This experiment showed that established model could be successfully used in a drug screen based on the pro-inflammatory response (**Figure 55**).

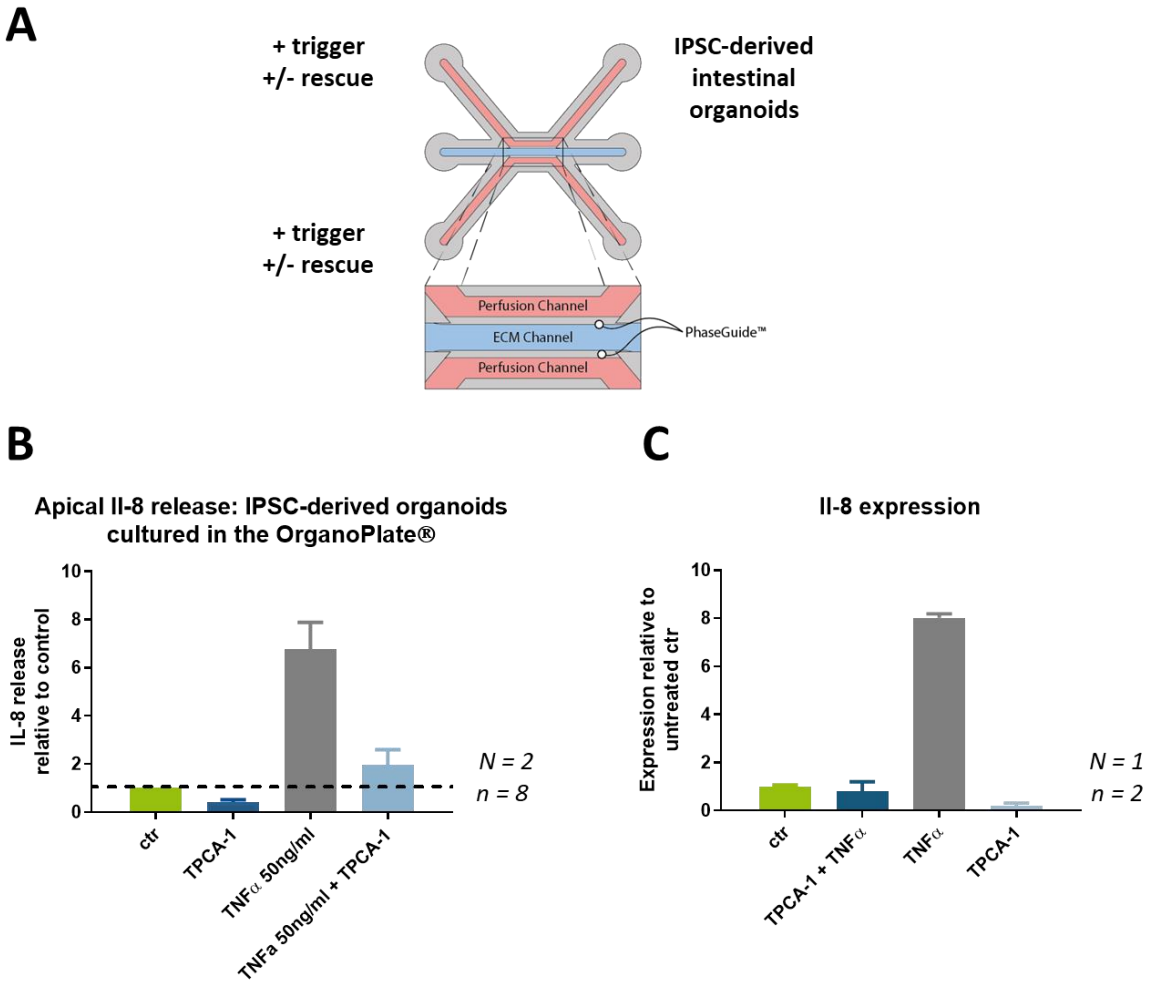

Figure 55. Modelling IBD in vitro. Proof of concept drug screening experiment.

iPSC-derived gut organoids cultured in the OrganoPlate® were subject to pro-inflammatory trigger (50 ng/ml TNFα) to induce anti-inflammatory response measured by Il-8 release. IBD phenotype was rescued by addition of an anti-inflammatory drug (TPCA-1). (A) experimental set-up; (B) Il-8 release after 24 h of treatment; (C) Il-8 expression normalized to actin expression and represented as relative to untreated control. N: biological replicate, n: technical replicate.

3.3.2.3.2. Towards a co-culture model: introduction of the immune component

To more closely mimic inflamed intestine, we attempted to add immune cells to the established model. Immune cells play an essential role in maintaining homeostasis in the gut and generation of such co-culture system would greatly improve the model. We cultured the

iPSC-derived gut organoids as previously and at day eight of the culture, we added differentiated THP-1 cells together with pro-inflammatory stimuli. Already after 48 h of stimulation, we noticed clear morphological changes in the gut tubes. Intestinal cells started to invade the ECM and appeared to form tighter barrier in that region. After 72 h, we ended the experiment and collected the medium separately from top (gut response) and bottom channel (immune response) for IL-8 detection by ELISA. In **Figure 56C**, we present the results obtained in control condition, where only organoid tube was present in the system. As shown previously, stimulation with cytokines led to upregulation of IL-8 release. MDP treatment did not induce production of IL-8. **Figure 56D** represents the results from co-culture system. As shown previously, THP-1 have considerably high basal IL-8 release thus IL-8 was detected in high amounts in the bottom channels in all conditions. Similarly, as in the experiment with Caco-2 cells (**Figure 45**), we wanted to see if co-culture with THP-1 would allow for modelling IBD in a NOD2 dependent manner. We stimulated THP-1 cells with MDP and as in the previous experiment, the co-culture did not bring any benefit to NOD2-related IBD modelling. Organoids do not show upregulated IL-8 release when co-cultured with MDP-stimulated THP-1.

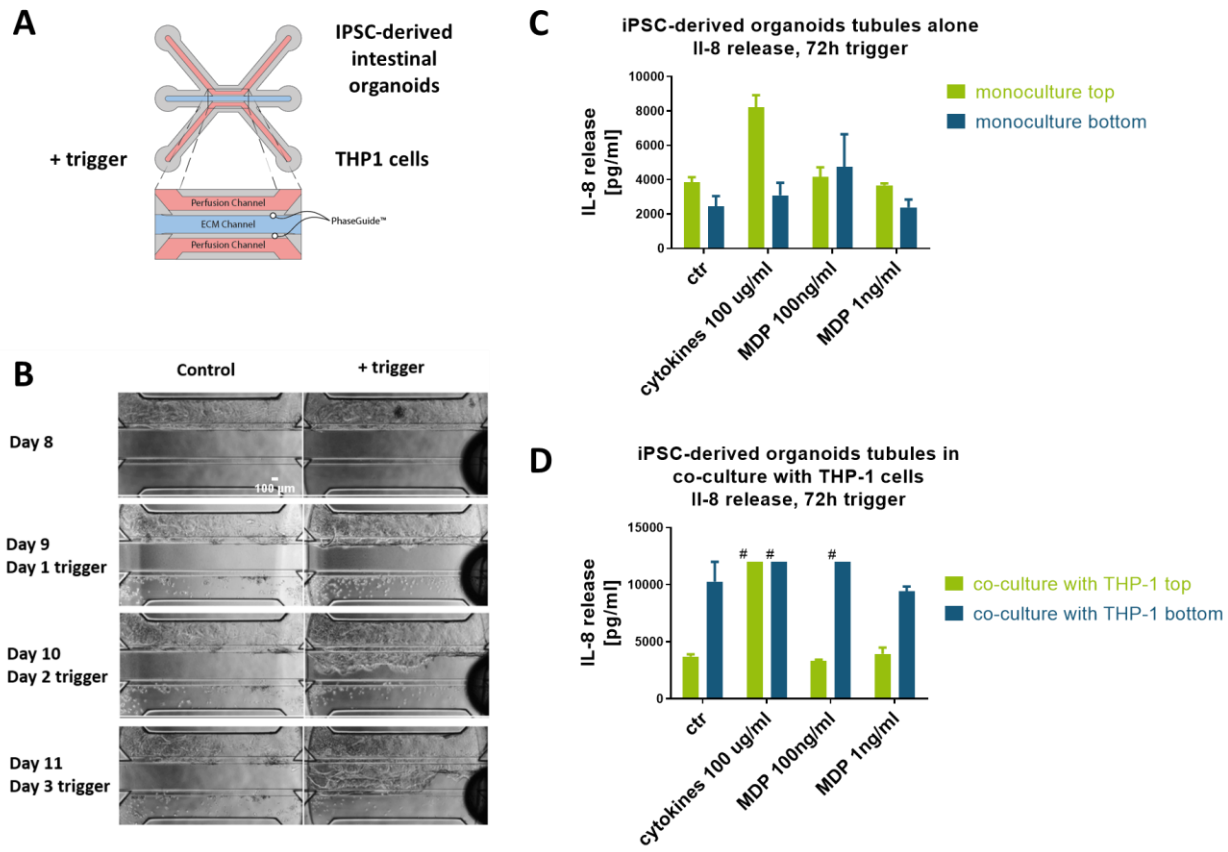

Figure 56. Improving the IBD model: addition of the immune cells.

iPSC-derived organoids were cultured as tubules in the top channel of the OrganoPlate® and differentiated THP-1 cells together with a trigger were added to the bottom channel at day 8 of culture. (A) experimental set-up; (B) morphological changes upon stimulation; Il-8 release upon stimulation in monoculture (C) and co-culture (D). Asterisks indicate that values were above the detection limit of the assay, N=1.

3.3.2.4. Discussion

3.3.2.4.1. Advantages and disadvantages of the iPSC-derived organoids

In this chapter, we used more physiologically relevant material to model gut on a chip. As the data gathered on Caco-2 cells showed, there was a need for a more sensitive tissue model to successfully recreate the inflamed phenotype in the gut. iPSC-derived gut organoids

proved to be easy to culture in our system and showed some overall good results. Traditionally, organoids are grown as closed 3D structures embedded in Matrigel droplets. Even though the 3D structure is very much appreciated and is one of the main advantages of the system, making it more representative of an organ, it is also a major issue when performing experiments. Firstly, a very interesting property of a gut organoid is the inside of the 3D structure (the apical side) as it is crucial for transport and drug absorption studies (Fatehullah, Tan and Barker, 2016). In such culture conditions, it is virtually impossible to access the apical side without using a microinjection needle. Such manipulations are very difficult to perform, require experienced user and are not suitable for high throughput experiments. Secondly, the presence of a thick layer of Martigel around the organoids disturbs penetration of the triggers added to the medium and limits access to the secreted factors. Considering practical aspects, it is also very challenging to perform imaging on such cultures and most often sectioning is required. This procedure is very time consuming and again requires expert technical skills.

To overcome those limitations, we cultured the organoids in previously presented OrganoPlate®. Thanks to this device, we were able to sustain the 3D structure of organoids by growing them in a form of tubules with an easy access to the apical side. TEER of those tubes was measured and the results indicated that fully leak tight barriers were established. The values were significantly lower than the ones of Caco-2 tubes. The gut model should form a leak tight barrier but when we compare it to the physiological conditions, iPSC-derived organoids seem to resemble the natural conditions more closely (Srinivasan *et al.*, 2015b). Permeability of the monolayer is increased in iPSC model; most likely due to the fact that it contains various cell types which are not as tightly connected one with another as in the monolayer formed exclusively by enterocytes. Similarly, co-culture of Caco-2 and goblet like HT-29 cells has much lower electrical resistance than a monoculture (Gijzen *et al.*, 2020).

The cells, even though not embedded in Matrigel, remained supported by ECM on the basolateral side but its thickness was not as substantial as in the droplet cultures. That allowed for the maintenance of a microenvironment similar to the basal membrane. Design of the chips permitted for sampling from both apical and basolateral side of the tubes. Importantly, in this set up we could examine each organoid structure separately because they were grown in individual chips, as compared to the culture of dozens of organoids in a single

Matrigel droplet. Other possibilities of culturing organoids presented in the literature cover culture as monolayer (Ettayebi *et al.*, 2016; Braverman and Yilmaz, 2018) or in suspension (Takahashi *et al.*, 2018). Those approaches eliminate some of the limitations but are not ideal. When culturing in a monolayer format, the 3D structure is disturbed and the differentiation of organoids is promoted. It could be seen as an advantage because some experiments should be performed on differentiated material with all the cell types represented. Growing the organoids in suspension allows for easier manipulation and the high throughput experiments can be performed if 384 well plates are used. However, the access to the apical side remains as an obstacle and the gradient of added factors and penetration to the inside of the organoids cannot be easily determined.

We have established that the culture of the organoids in the OrganoPlate® is beneficial as compared to the Matrigel droplets method. The next step was to determine how this model relates to the Caco-2 system. Therefore, we compared the expression levels of most relevant markers between previously used Caco-2 and both types of organoids (iPSC-derived and primary organoids). All three models showed good expression of villin and ezrin, suggesting that the brush border is fully formed. It has been confirmed that organoids show expression of markers characteristic to Paneth cells (lysozyme), goblet cells (mucin) and enteroendocrine cells (chromogranin). This is a huge advantage over Caco-2 system, as having the population of different cell types normally present in the gut makes the model more physiologically relevant. Presence of Paneth cells allows for modelling the bacterial infection. Mucins are extremely important in modelling the gut environment, they line the epithelium and influence the absorption of substances as well as form a protective barrier between the microbiome and gut tissue. It is important to point out that in our system the mucin producing cells were not abundant and we only tested for the expression levels of *MUC2* by qPCR and immunostaining. Caco-2 are known to lack the expression of mucins and co-cultures with HT-29 cells are well established either on the Transwell® systems or the OrganoPlate®. It would be reasonable to include another assay to detect the presence of a mucus layer, i.e. alcian blue direct staining that does not require fluorescence imaging or sampling of the medium for mucins detection by ELISA and compare the results to the goblet-like cell cultures (HT-29 cells). Since the organoids were cultured in the maintenance medium, the full differentiation was not possible. To develop the model further, we would advise on optimizing the medium

composition in such a way that it would not support the stem cell niche but rather push the cells towards differentiation. This could solve the issue with the lack of PGP efflux pump expression. It has not been detected in either Matrigel droplets or the OrganoPlate® cultures. Performance of an additional functional assay would be advised. PGP activity could be detected with fluorescence-based assay in which we provide Rhodamine to the apical side of the tube and measure fluorescence in the adjacent channel (basolateral side). This assay is well established in the Caco-2 model, which could serve as a positive control, as these cells are known to have highly active PGP transporter. Another cell type detected in our organoid cultures were enteroendocrine cells, which besides the role in nutrient sensing and digestion are signalling to the immune cells upon bacterial infections. Those cells may be important in the disorders like obesity and metabolic diseases (Beumer *et al.*, 2020). Having those present in the *in vitro* gut tubes would enable research on the mentioned diseases. Caco-2 cells on the contrary to our organoid model, are representative of the enterocyte population and can be relevant in studies on absorption and toxicity, even though the co-cultures with mucin producing goblet cells seem to be more beneficial. Having a tissue model composed of all the different cell types is much more versatile and would aid research ranging from toxicity to disease modelling.

Looking at the staining of iPSC-derived gut organoids, it is interesting that the cells positive for lysozyme are highly abundant. These are the markers specific for Paneth cells, which normally reside at the base of the crypt adjacent to the stem cells. Those cells are not as abundant in the intestine as the staining suggest. Our explanation for it is that since the gut organoids are derived from iPS cells, they do not constitute of individual differentiated cells but are rather a group of cells that represent mixed phenotype. Our claim is supported by the expression of *CDX2* (presented qPCR data and immunofluorescence data not shown). In that case, most of the cells were positive for *CDX2* (enterocyte marker) which means the cells would be positive for Paneth cells and enterocytes marker at the same time. It is also possible that the anti-lysozyme antibody dilution used in our experiments was too low and observed staining includes unspecific background signal.

After confirming that the organoids form tubes that express most of the essential gut markers, we performed an experiment in which we generated and then rescued the inflammation of the gut. The primary reason for exchanging the Caco-2 for anther cell type

was the low sensitivity of the model to the cytokines treatment. As expected, iPSC-derived gut organoids proved to be more sensitive to the treatment. They required lower dose of the trigger as the stimulation in the conditions previously used for Caco-2 cells led to cell death (data not shown). Our aim was to generate an IBD model on a chip that could be used in a high throughput drug screening. It was important that the model would be sensitive enough and that the assays used for validation of such response would allow for the detection in a reproducible manner. We focused mainly on IL-8 release, which concentration we measured in the medium. The samples were harvested separately from top (apical side) and bottom (basolateral side) channels and the volume of the culture medium in each channel was 100 µL. In our ELISA kit the minimum sample volume was 100 µL which means that we could not reduce the volume of the medium added to the culture in order to obtain a more concentrated sample to assess the release of IL-8 in response to the trigger. In the case of Caco-2 culture, the response was close to the detection limit (about four times lower than in organoids) thus detection was challenging. Organoid based model allowed us for more robust detection of the cytokine in the culture medium. Having established efficiently triggered model we were able to reverse the inflammation by addition of an anti-inflammatory drug. The rescue was very efficient, leading to the downregulation of IL-8 release to the control levels. This experiment showed a huge promise for the possible drug screen based on the pro-inflammatory response. In the line with those results, it can be concluded that the generated iPSC-derived organoid gut model possesses some advantages to the Caco-2 model. However, it should be noted that the model is derived from iPS cells and thus is not a direct representation of an adult human gut tissue.

IPSC-derived intestinal organoids are one of the sources of intestinal epithelial cells and generation of those organoids is costly and time consuming. In our study w used organoids that are commercially available therefore the generation time was not an issue. However, an alternative approach to perform a direct differentiation of iPSCs into intestinal tubules in the OrganoPlate® was published (Naumovska *et al.*, 2020). In the described protocol iPSCs undergo differentiation through definitive endoderm, hindgut and into the intestinal phenotype. Within a week cells form a barrier with apical-basal polarization. Expression of adult intestinal markers including *PGP* and *CYP3A4* was confirmed and when exposed to the cytokines treatment show the signs of inflammatory response. As shown in

this thesis and the published research, various cell sources can be used to establish gut on the chip models and the choice of the material should be motivated by future application and available resources.

3.3.3. Primary gut organoids: source of physiologically relevant material most faithfully reflecting the biology of the intestine

As mentioned in the introduction, another way to obtain organoids is to isolate relevant intestinal cells from the material taken while a biopsy. In order to expand such material, $LGR5^+$ cells need to be isolated. Those cells reside in the crypts, the basal part of the villi and give rise to any cell type present in the gut. These adult stem cells were first discovered by Hans Clevers lab and since then they are extensively used to study the biology of the gut outside of the human body (Sato *et al.*, 2011). This model is a perfect representation of an organ's biology of a single individual. Unlike the iPSC-derived organoids, the primary material reflects biology on structural, transcriptional and epigenetics level. It is an exact representation of the tissue from a particular patient. However, isolation and culture of these organoids is challenging. In the following section, some of the initial experiments on the primary gut organoids will be presented.

3.3.3.1. Sustaining stem cells in *in vitro* culture by recreating niche environment: production of WNT3A conditioned medium

After the biopsy from the patient is taken and the crypts are successfully isolated, they can be embedded in Matrigel droplets and cultured in order to expand fully grown organoids. Essential factor in culturing primary organoids is a good quality WNT3A conditioned medium. WNT signalling regulates tissue regeneration in vertebrates (Goessling W. *et al.*, 2009) and is indispensable in maintaining proliferation of $LGR5^+$ cells in organoids. In the gut, Paneth cells provide WNT together with NOTCH and EGF thus generating a suitable niche for the maintenance of adult stem cells in the intestinal crypts (Sato *et al.*, 2013). Given that, to be

able to work with primary colon organoids we first needed to produce WNT3A conditioned medium which is the basis of the culture medium. The quality of FBS is a very important factor in production of conditioned medium and therefore, number of FBS lots were tested initially. Conditioned medium is produced by L Wnt-3A murine fibroblast cell line. Samples of the medium were tested for WNT3A activity by incubation with reporter LSL cell line and assessment of WNT-dependent TCF/LEF luciferase reporter activity (Blitzer and Nusse, 2006). **Figure 57** shows successful generation of a conditioned medium that poses high WNT activity.

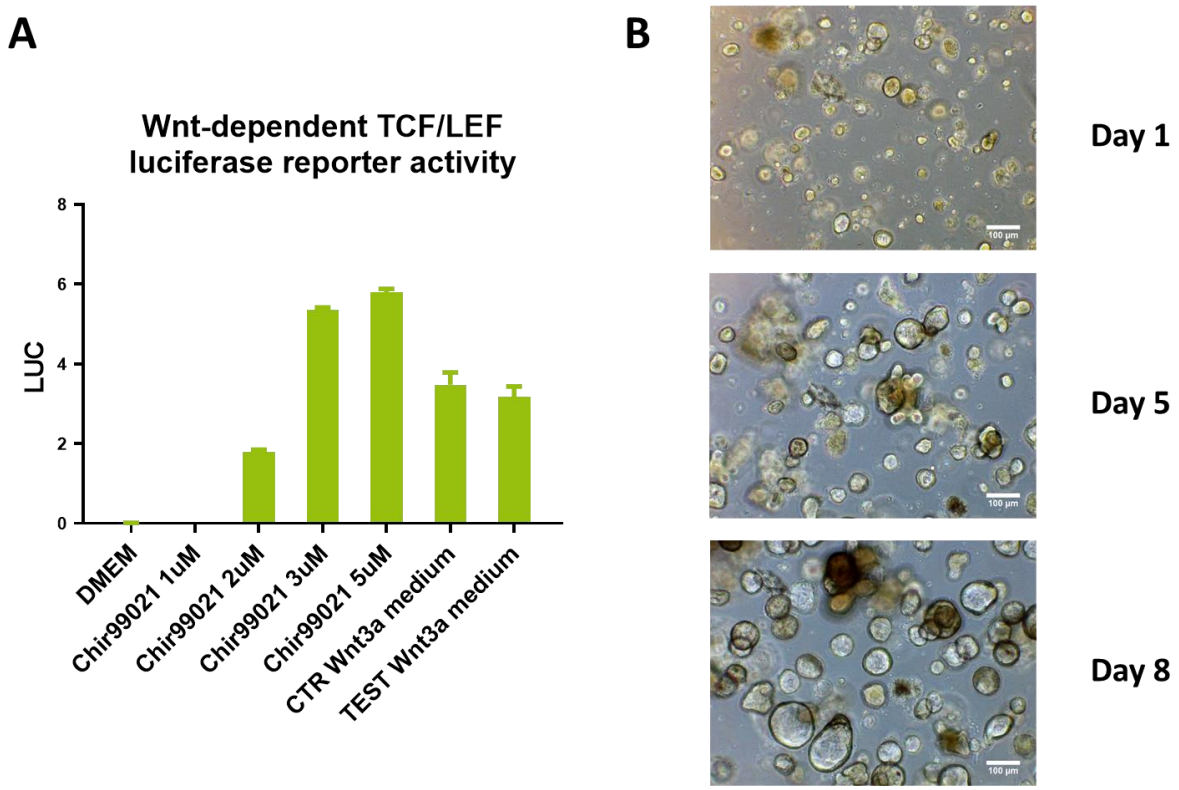

Figure 57. Assessment of Wnt-dependent TCF/LEF luciferase reporter activity in generated medium.

(A) Generated conditioned medium (TEST Wnt3a medium) was tested for Wnt3a activity in comparison to the control medium of known high Wnt3a activity (CTR Wnt3a medium), inhibitor of GSK-3 enzyme (known activator of Wnt signalling) and DMEM (negative control); (B) primary colon organoids were successfully cultured in the medium containing generated Wnt3a conditioned medium.

3.3.3.2. Changing organoids' architecture: establishment of tubular structures in the microfluidic device

Primary colon organoids were seeded in the top channel of the 3-lane OrganoPlate® as all the previously described models. Even though cultured in good quality medium, difficulties with cell attachment inside the channel were encountered. Efficiency of tubule formation was very low in comparison to the other cell types. This significantly limited the possibilities to perform experiments, as the number of available chips with fully developed tubes was usually low. However, those tubes that managed to be developed showed promising results. TEER measurement on day 13 of culture suggested that the tubes are leak-tight with the values around 40 Ω.cm^2 (**Figure 58**). Such values could seem low when compared to extremely leak tight barriers formed by Caco-2 tubes. However, our experience with many different cell types proves that tubes with values ranging from around 30 Ω.cm^2 appear to be impermeable for 4 kDa dextrans. Organoids stained positive for tight junction marker ZO-1 and showed developed brush border (ezrin and villin staining) as shown in **Figure 59**.

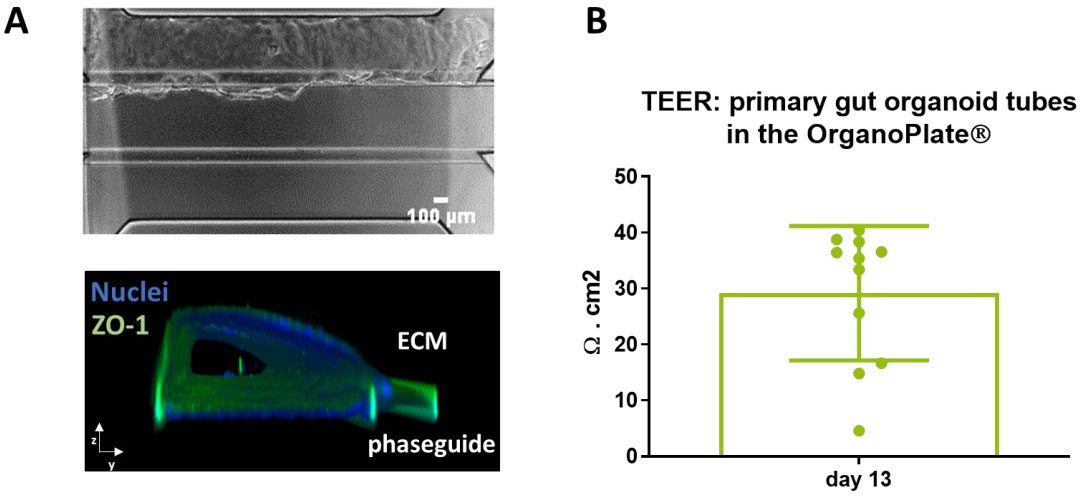

Figure 58. Primary colon organoids form tubules in the OrganoPlate®.

Morphology of the gut tube formed in the top channel of the OrganoPlate® shown in phase contrast image (top) and fluorescent staining depicting 3D reconstruction of the confocal z-stack with nuclei (DAPI in blue) and tight junction marker (ZO-1 in green); (B) Leak-tightness of the formed barrier represented with transepithelial electrical resistance measurement (TEER) of the tubes on day 13, N=1.

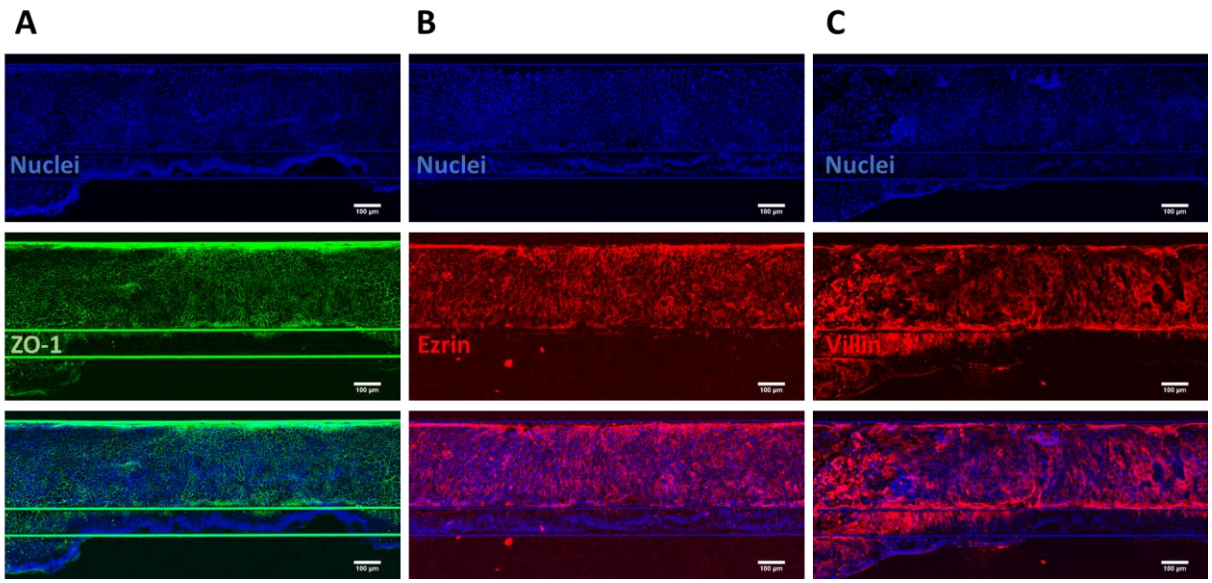

Figure 59. Expression of intestinal markers in primary colon organoids cultured as tubules in the OrganoPlate®.

Cells were cultured in form of tubules in a 3-lane OrganoPlate® and subject to immunostaining. Nuclei (DAPI in blue), intestinal markers: tight junctions (ZO-1 in green), brush border (ezrin and villin in red). Images represent top view of the top channel of the OrganoPlate®. PhaseGuide seen as a horizontal band at the bottom of each panel. Scale bars 100 µm.

3.3.3.2.1. Modelling IBD on a chip: inflamed phenotype of primary organoids-derived tubules

Even though the seeding protocol was not yet fully optimized due to the time constraints of the project, we attempted to induce inflammation in this model. We wanted to see if cytokines would induce pro-inflammatory response in these organoids and how the response would compare to Caco-2 and iPSC-derived organoids. Cells were very sensitive to cytokines treatment and released high amounts of IL-8. As seen in phase contrast image, 72 h incubation with the trigger led to death of most of the cells forming the tube. Since previously, we aimed to model NOD2-dependent IBD on a chip we tested if these organoids were responsive to MDP. Alike all the other gut models presented in this thesis, the IL-8 release upon MDP treatment was comparable to the control condition.

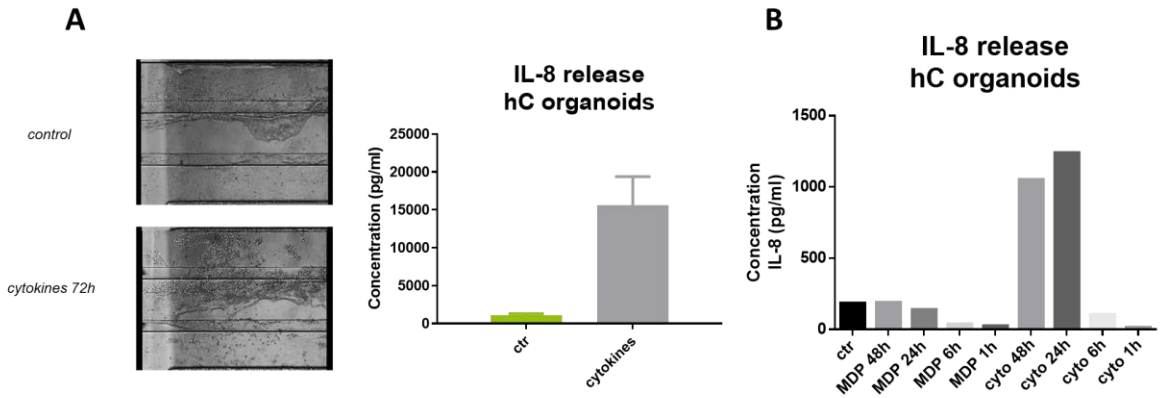

Figure 60. Induction of pro-inflammatory response on a chip.

(A) Primary organoid tubes were treated with cytokines for 72 h. Phase contrast images on the left panel, Il-8 release measured in the medium on the right panel; (B) Induction with MDP to model NOD2-depended IBD, cytokines treatment as a positive control. Graph represents concentration of Il-8 in the medium, N=1.

3.3.3.3. Discussion

The aim of this thesis was to generate human gut on a chip model that would be suitable for drug development research. In the previous sections, we presented the results on adenocarcinoma cell lines as well as iPSC-derived organoids. All the generated models had positive aspects and limitations. As the primary gut organoids are believed to be a huge promise in research, we aimed at generation of the most physiologically relevant gut model with the use of these cells. As shown in the results section, we were able to grow fully formed tubes that formed leak tight barriers and expressed some of the key markers (villin and ezrin for brush border, ZO-1 for tight junctions). Expression of other markers was tested by qPCR and was included in the graph together with iPSC-derived organoids as compared to Caco-2 model (**Figure 51**). Those expression levels are representative of the Matrigel droplet culture. Expression pattern is similar to the one of iPSC-derived organoids, except that it can be classified as less differentiated with higher *LGR5* levels (stem cells marker) and lower *CHGA* (enteroendocrine marker), *CDX2*, *MUC2*, *VIL1* (enterocytes markers). *PGP* levels are similarly low and as discussed in the previous section can be explained by the undifferentiated state of the cells. Primary organoids, alike the iPSC-derived ones were cultured in expansion

medium that was promoting the stem cell niche. Clearly, the medium composition needs to be modified in order to obtain differentiated cells, which in result would lead to upregulation of the mentioned gut markers specific to various cell types (Sato *et al.*, 2011).

Culture of primary organoids has its challenges. In order to obtain organoids, the crypts need to be isolated from biopsy material. It is necessary to arrange for transfer of such patient material and even though there are companies dealing with such requests, the process requires extensive administration work and is expensive. Having primary material in the lab, special precautions need to be taken because the tissues can be infected with HBV or other transmittable diseases. It is advised that dedicated space should be used for isolation and culture in order to limit the risk of contamination of other materials in the lab. Successful culture is laborious, donor dependent and microbial infections of the initial cultures can occur (intestine is lined with microbiota and to eliminate those from the culture antibiotics are used). The most limiting factor is the variability between donors. At the initial phase, multiple different donor samples should be collected and culture of organoids should be compared. The differences can occur not only in the growth in Matrigel droplets but also in the efficiency of attachment inside of the microfluidics channels.

In our experiments, we observed low attachment efficiency of the organoid epithelial cells in the OrganoPlate®. Different optimization steps were undertaken, including addition of Rock inhibitor to the medium (prevention of disassociation-induced apoptosis) and lengthening the static incubation at the initial seeding phase. We tested the model for the response to the pro-inflammatory triggers. In **Figure 60**, the differences between experiments in the amounts of IL-8 released in response to cytokines result from variability in cell number (in some of the chips taken for the experiment tubules were only partially formed). It could be concluded that the organoids react to the cytokines treatment but are insensitive to MDP. This was consistent with all the other gut models established. We were able to establish cytokine-induced IBD phenotype but modelling the disease in relation to NOD2 signalling was unsuccessful. This has been extensively discussed in **Chapter II** of this thesis. We hypothesise that even though the presence of the marker for Paneth cells was detected, the number of those cells had to be very low in each chip (this would be in line with physiological abundance). Those cells, when low in number could not produce the signal strong enough to be detectable in the assay. Additionally, the region of biopsy would be a determining factor

for the presence of Paneth cells as the distal region of the intestine does not contain this cell type. More in depth investigation should have been performed, for example immunofluorescence, detection of defensins production and the assessment of the increase of endocytosis.

Primary organoids indeed seem to be the best representation of a human gut tissue but the modification of culture conditions in order to favour differentiation process is necessary to generate a faithful model. In this thesis, only the initial experiments were performed and much more time and efforts should be devoted in the future. There is a huge promise in the studies involving gut organoids and our approach to culture them in the form of tubules adds benefit to the current state of the art. As discussed earlier in this chapter, transfer of the culture away from Matrigel droplets allows for easier and more thorough experimentation on this material. Generated model with more physiologically relevant growth conditions (3D structure, fluid flow, ECM layer mimicking basal membrane), will allow for more faithful representation of a human tissue therefore improving the current drug development process.

3.4. General conclusions and future considerations

The main aim of this research was to generate a novel organ on a chip model for Inflammatory Bowel Disease that would be suitable for high throughput drug screening. We described the development of different variants of the gut on a chip model, including (1) PDMS-based organ on chip model incorporating Caco-2 cell line; (2) OrganoPlate® with Caco-2 and DLD-1 monocultures; (3) OrganoPlate® with Caco-2/THP-1 and (4) Caco/Raji B co-cultures; (5) OrganoPlate® with iPSC-derived gut organoids in mono and (6) co-culture with THP-1 cells and (7) OrganoPlate® with primary gut organoids-derived tubular structures. In our approach we adopted a novel organ on a chip technology to generate versatile models that could be used in high throughput drug screenings. We discussed the advantages and limitations of each model, proving that the specific aspects of the research question need to be considered and there is no 'one fits all' model. Our initial idea for IBD modelling evolved around the impairment of NOD2 signalling as it is reported to be one of the susceptibility factors for Crohn's disease. As the data showed, finding an epithelial cell line that would show functional NOD2 signalling proved to be challenging. Contradictory to some of the published reports, in our experiments we did not observe the effects of the stimulation of Caco-2 cells with MDP and concluded that this cell line could not be used in IBD modelling based on NOD2 signalling. None of the other epithelial cell lines used in this study showed pronounced immune response to this stimulus. In our experiments only THP-1 monocyte cell line was reactive upon stimulation with the bacterial cell wall component. The expression of NOD2 in the gut epithelium has been reported for goblet cells (Ramanan *et al.*, 2014), enterocytes (Hisamatsu *et al.*, 2003), stem cells (Nigro *et al.*, 2014) and accompanying Paneth cells (Ogura *et al.*, 2003) with the highest levels observed in the latter two cell types. So far, the expression pattern has not been compared between small intestine and colon. Unfortunately the NOD2-based disease modelling remained unsuccessful in our hands and more efforts in examining the NOD2 signalling activity should be invested. Hematopoietic cells appear to be a better target than epithelium in this regard as we could clearly observe the NOD2 activity in the monocyte cell line. Similar approach with introducing genetic modifications in NOD2 gene could be applied and change of immune response to the stimulus should be pronounced.

In the following steps we focused on recreating the inflamed phenotype by exposing the gut tubules to the exogenous cytokines by either stimulating the cells with cytokines cocktail or adding the immune cells to the culture. We observed inflamed phenotype of the epithelium reflected in the drop in TEER values and upregulation of IL-8 release. Developed models differed in sensitivity to the trigger with Caco-2 being the least reactive. We have established the model with iPSC-derived organoids in which we demonstrated efficient reduction of the immune response with an anti-inflammatory drug TPCA-1. This data proved applicability of the model in the anti-inflammatory drug screen. Finally, we presented preliminary results on generation of the primary-derived gut organoid model which holds the promise of being the true representation of patient's biology on the chip. We conclude that organoids are the preferred model to be used in IBD modelling due to its high sensitivity and physiological relevance. However, the protocols need to be developed further in order to favour a more differentiated phenotype of the cells. Ideally, differentiated cultures would contain physiological numbers of each cell type present in the gut. To achieve that goal, most likely the modifications in the media composition would need to be applied. Furthermore, donor to donor variability should be taken into account and reproducibility of the data should be tested among a number of lines. In the future, the proper representation of the population should be included in the experiments in the interest to develop therapies with improved efficacy. As shown in this thesis, the versality of the design of the platform facilitates co-culturing of different cell types which in IBD modelling could be utilized by merging cultures of epithelium, immune component and fibroblasts. An ideal in vitro IBD model would incorporate all relevant cell types that are associated with the disease pathogenesis. Epithelium containing all intestinal cell types derived from human organoids, fibroblasts embedded in the extracellular matrix and immune cells isolated from patient blood. Since microbiome plays an important role in gut homeostasis addition of microbial components would bring the model to the most physiologically relevant level. Complexity of such model would allow for modelling complex cell-cell interactions and would serve as a tool to decipher mechanisms underlying intestinal inflammation. All things considered, such *in vitro* models would accelerate the drug development process by providing human-derived and physiologically relevant material to include at the early stage in the pipeline. In the current drug development process candidate drugs are tested in simple *in vitro* models that not always accurately represent human biology. Next, the promising compounds are tested in

animal models. Even though valuable, these models differ in many biological aspects from humans and in some cases fail to predict the efficacy of the drugs. Improvements in the initial stages of the research would greatly impact the success rate, lower the costs and reduce the time needed to release novel drugs on the market.

The ultimate goal of organ on chip technology would be to interconnect crucial organs to generate a human on a chip model. In the current state of the art, this has not yet been achieved at the satisfactory level, although many promising studies are being published (Wu et al., 2020). One of the approaches involves co-culturing gut and liver tissues (Midwoud, Merema and Groothuis, 2010). Orally administered drugs are the most common on the market and testing their metabolism and bioavailability in humans is of major interest. A challenge in human on a chip approach is the development of the universal culture media suitable for all the tissues in the system. This is especially difficult when dealing with primary material. Lastly, with increasing complexity of the systems delineation of the meaningful datapoints becomes challenging. Careful interpretation of the obtained data and design of the novel data analysis approaches are indispensable and are crucial for excluding artefactual information. Developments such as those presented in this thesis show that the organ on chip technology is a rapidly evolving field and will most likely change the way drug research is performed. The main findings described in this thesis show that it is possible to generate a perfusable 3D tissue culture model of the intestine that is suited for the use in high throughput screening. We believe that features like the lack of an artificial barrier in the system and a possibility of co-culturing various cell types within a single chip add value to the already available models. As shown in the final chapter, incorporation of the organoids in the system is feasible and shows an obvious direction for further research. Combining organoid cultures with the organ on chip technology advances the current state of the art in tissue and disease modelling giving a promise for significant developments in the drug discovery field.

3.5.Appendix

3.5.1. Generation of NOD2 KO cell lines

As the previous data have shown, it could be concluded that Caco-2 and DLD-1 cell lines do not express *NOD2* on high levels and therefore knocking out this gene would not produce any valuable phenotype. However, previously described experiments on *NOD2* expression were performed simultaneously with the ones presented in this section. Even though the endogenous expression was not as expected, it was interesting to investigate if any differences in response to immune trigger would be observed between wild type and knock-out cell lines. Furthermore, we planned on generating the cell lines bearing one of the most commonly occurring *NOD2* mutations, *1007fs*. In order to do it successfully we needed a *NOD2* knock-out cell line without any background expression of the protein. At the later stage we were planning to transfect it with a plasmid coding for a tagged *1007fsNOD2* version of the protein. Eventually, due to the restricted timeline of the project we did not proceed with those experiments and the below results contain the data on NOD2KO cell lines.

CRISPR/Cas9 technology was used to alter the genomes of gut epithelial cell lines. This versatile technique was first described by the lab of Jennifer Doudna (Martin Jinek *et al.*, 2012) and used to genetically modify eukaryotic cells shortly after (Cong *et al.*, 2013) (Mali *et al.*, 2013). **Figure 61** shows how the system introduces genome modifications. We have decided to generate a complete knock-out of *NOD2* gene and therefore relied on NHEJ repair pathway. In Crohn's patients, *NOD2* is expressed at the normal levels but contains mutations that inhibit its signalling function. The most predominant mutations are localized in the LLR region at the C-terminal side of NOD2 protein. This region is responsible for MDP sensing and if its function is disturbed, the signalling is not induced. Ideally, we would need to introduce those precise mutations in the gene coding region to faithfully recapitulate what occurs in patients. However, introduction of precise modifications is more challenging because NHEJ repair pathway is favoured in the eukaryotic cells. Additionally, Caco-2 cell line is tetraploid and it would be extremely difficult to generate homozygous clones with single nucleotide mutations. We hypothesize that complete knock-out of the protein would give the same non-

functional phenotype as the mutated version. The absence of the protein should result in disturbance of the signalling pathway alike the mutation leading to dysfunction in ligand sensing.

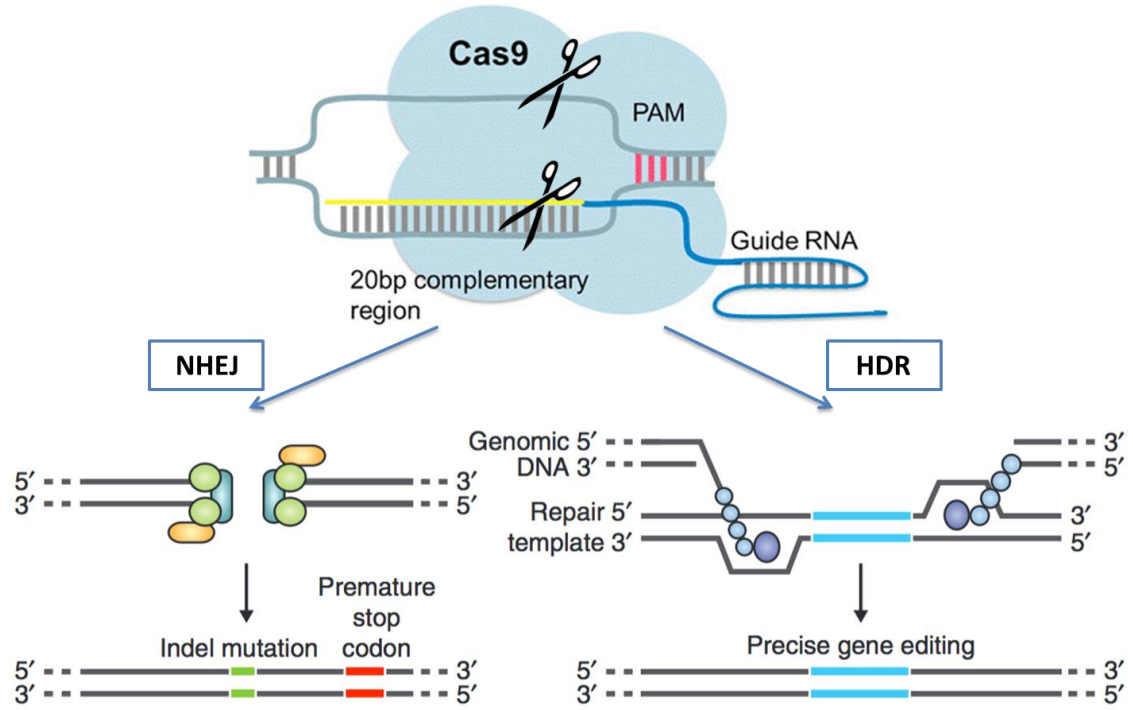

Adapted from Jinek et al., Science 2012 and Ran et al, Nature 2013

Figure 61. Type II CRISPR/Cas9 system and its use in genome engineering.

Cas9 nuclease is guided by sgRNA and cleaves double stranded DNA at the site adjacent to PAM motif. Naturally occurring double strand breaks repair promotes gene editing. The repair can occur with non-homologous end joining pathway (NHEJ) in which the DNA ends are re-joined by endogenous repair system. If performed with errors, this process can lead to formation of frameshift in a gene coding region and formation of a premature STOP codon. If an exogenous repair template is provided, homology directed repair (HDR) can be favoured and precise editing would be reinforced.

To generate a complete knock out of the protein, the sgRNAs were designed to target the very beginning of the coding sequence in exon 1 (see **Figure 62**). Cells were transfected with a vector containing Cas9 nuclease, sgRNA sequence and GFP to allow for selection. To validate the designed sgRNA sequences, T7 assay was performed. The efficiency of introducing mutations was first validated in a more suitable transfection host - HEK293 cells. After 24 h cells were harvested, GFP positive cells were collected and lysed. DNA extraction

and PCR of the target region was performed. It is important to be noted that the Cas9 nuclease is not 100% efficient and in addition to fully repaired sequences, it leads to formation of various in-del mutations. Therefore, the DNA isolated from transfected cells is heterogeneous. In T7 assay, PCR product is initially heated up to force formation of single stranded DNA fragments and as the reaction cools down the strands form random duplexes. T7 endonuclease, when added to the reaction mix, cleaves mismatched regions. The products are subject to gel electrophoresis and the efficiency of introduced mutations can be judged by the intensity of the cleaved bands. The higher the intensity of the smaller band, the higher percentage of cells that were successfully genetically modified. Both of the designed sgRNAs proved to be efficiently targeting the sequence. As shown in **Figure 62B**, sgRNA2 was more efficient. As soon as the guides were validated, the experiment in Caco-2 cell line was performed. It could be concluded that sgRNA2 transfected sample contained sufficient fraction of mutated cells. Due to the low number of cells sorted from sgRNA1 transfected population no conclusions could be drawn. Single cell sorted cells were expanded and once there was enough material, the genomic DNA was extracted and target region was PCR amplified. Three clones were investigated further by sequencing. As shown in the electropherograms, each of the clones was heterozygous. It was expected as Caco-2 is tetraploid and introduction of the same mutation in all alleles was highly unlikely.

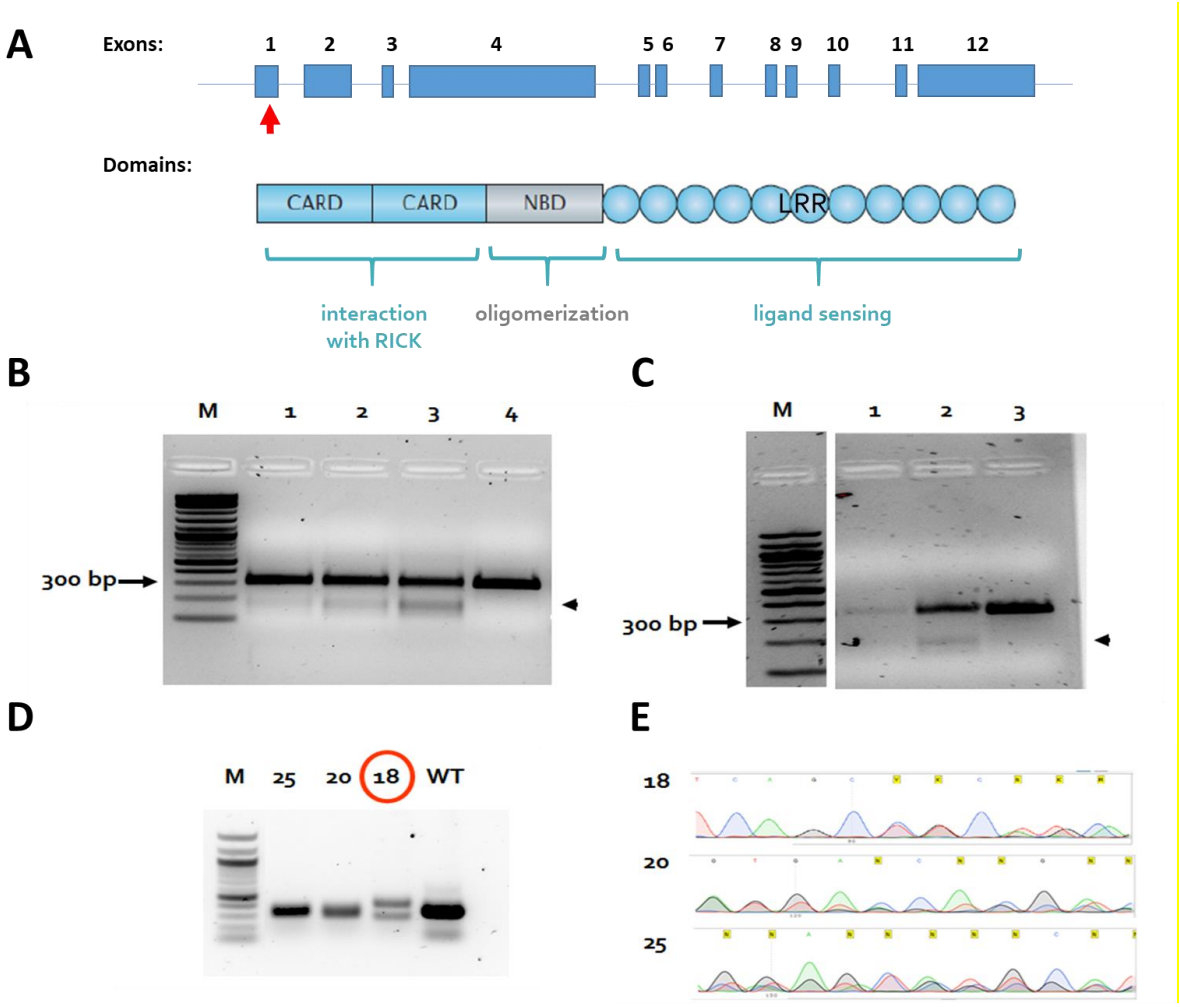

Figure 62. CRISPR experiment results for sgRNA1 and sgRNA2 targeting exon 1 in NOD2 gene.

(A) Schematics of NOD2 gene coding region on top with translation site marked with red arrow. On the bottom corresponding functional domains of NOD2 protein; (B) T7 Endonuclease I assay performed on HEK293 cells transfected with pX458 plasmid containing Cas9 and sgRNA targeting NOD2 gene. (M – marker; 1 – GFP+ cells sorted after transfection with sgRNA1; 2 - GFP+ cells sorted after transfection with sgRNA2; 3 - GFP+ cells sorted after transfection with sgRNA1 and sgRNA2; 4 – untransfected control). (C) T7 Endonuclease I assay performed on Caco-2 cells transfected with pX458 plasmid containing Cas9 and sgRNA targeting NOD2 gene. (M – marker; 1 – GFP+ cells sorted after transfection with sgRNA1; 2 - GFP+ cells sorted after transfection with sgRNA2; 3 – untransfected control). Result for sgRNA1 not clear due to the low number of cells obtained after FACS. (D) Amplification of target region – single clones. (M – marker; 25, 20, 18 – single clones; WT – wild type). (E) Fragments of electropherograms from gDNA sequencing (clone 18, 20 and 25).

It was possible to dissect each allele of the mutated clones by sub cloning the PCR product into TOPO vector. However, the more straightforward solution was to focus on the clone 18 that gave two PCR products of very distant sizes. Each of the bands was extracted

from the gel separately and sent for sequencing (**Figure 63**). The results suggested that there are two versions of the target region, none of which is the wild type version. The band of higher size contains insertion of about 70 nucleotides that led to formation of the premature stop codon (highlighted in blue on the electropherogram). When translated into protein sequence, it gives 34 aa long protein (only first 8 aa are the same as in the WT). The smaller band contains deletion of about 30 nt in the expected Cas9 cut site. This deletion led to the frameshift and formation of the premature stop codon (highlighted in blue on the electropherogram). When translated into protein sequence, it gives 10 aa long protein. In conclusion, clone 18 is a successful *NOD2* knock out.

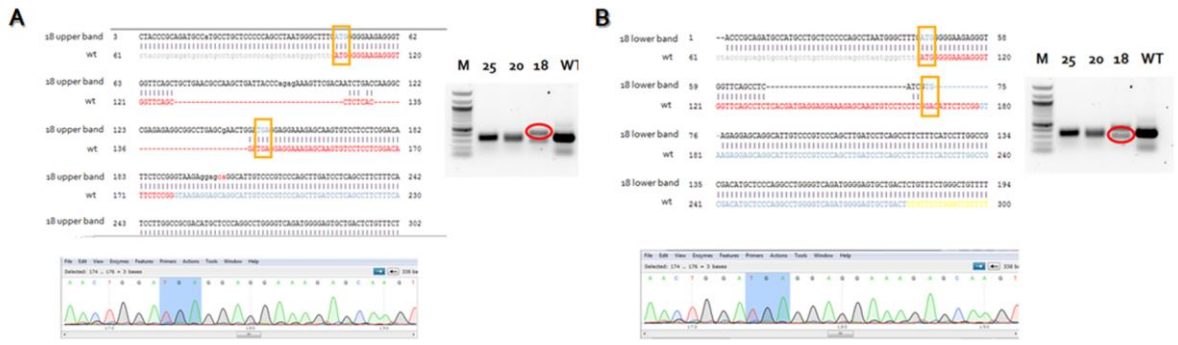

Figure 63. Analysis of sequencing data – clone 18, Caco-2.

(A) upper band on agarose gel: top line – upper band sequence; bottom line – wild type sequence; red font – exon 1; blue font – UTR sequence and intron 1; orange rectangles – ATG (start codon) and TGA (premature stop codon). Observed insertion of about 70 nt in the expected Cas9 cut site. This insertion led to formation of the premature stop codon (highlighted in blue on the electropherogram). (B) bottom band on agarose gel: top line – upper band sequence; bottom line – wild type sequence; red font – exon 1; blue font – UTR sequence and intron 1; orange rectangles – ATG (start codon) and TGA (premature stop codon). Observed deletion of about 30 nt in the expected Cas9 cut site. This deletion led to the frameshift and formation of the premature stop codon (highlighted in blue on the electropherogram).

Following the same approach, clone 3 was selected from the experiment in DLD-1 cell line. This knock out line contains frameshift that led to formation of a premature STOP codon. When translated into a protein sequence, it results in 11 aa long protein (**Figure 64**).

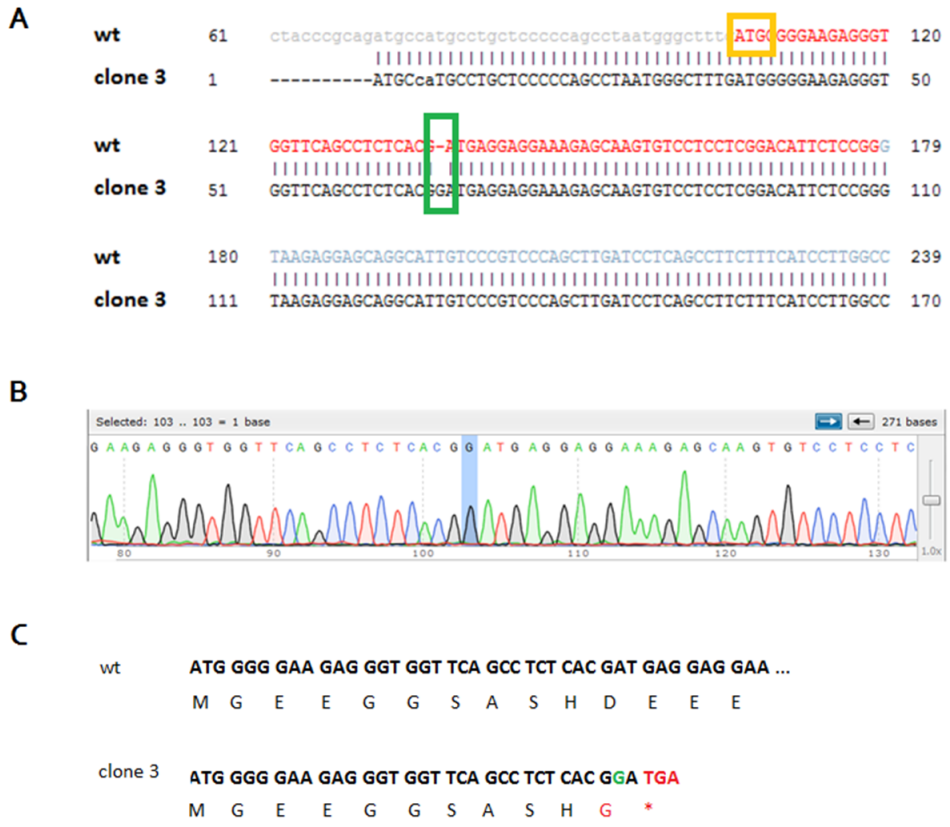

Figure 64. Analysis of sequencing data – clone 3, DLD-1.

(A) comparison between sequences: top line – wild type; bottom line – clone 3; red font – exon 1; blue font – UTR sequence and intron 1; orange rectangle – ATG (start codon); green rectangle – introduced mutation. (B) fragment of electropherogram – sequencing of target region, clone 3. (C) comparison between wild type and clone 3: top line – nucleotide sequence; bottom line – amino acid sequence; introduced mutation marked in green.

In order to validate the gene knock out, the absence of NOD2 protein had to be determined in the generated cell lines. Multiple commercially available anti-NOD2 antibodies were used and none of them confirmed the lack of NOD2 expression. See **Section 3.2.2.1. Characterization of the cell lines in relation to NOD2 signalling** for the attempts to validate the antibodies in WT cell lines. Since it appeared that NOD2 was possibly expressed in the knock out cell lines, available literature on NOD2 splicing was extensively researched. It has been shown that there is an alternative translation site in *NOD2* gene and it is located in exon 2 (Rosentiel *et al.*, 2007). Since in the previous experiments, exon 1 was targeted, the initial plan was revisited and new sgRNAs were designed. **Figure 65** shows in detail the translation

sites and the experiment outcome in Caco-2 and DLD-1 cell lines. Both, sgRNA3 and sgRNA4 produced some fraction of genetically modified cells. The introduction of mutations was less efficient in Caco-2 cell line due to the lower transfection efficiency (less GFP positive cells sorted) and tetraploidy (lower probability of successful targeting of multiple alleles in the same cell). As the result of the experiment, eight NOD2 knock out cell lines derived from DLD-1 and three Caco-2 NOD2 knock outs were isolated (**Figure 66**).

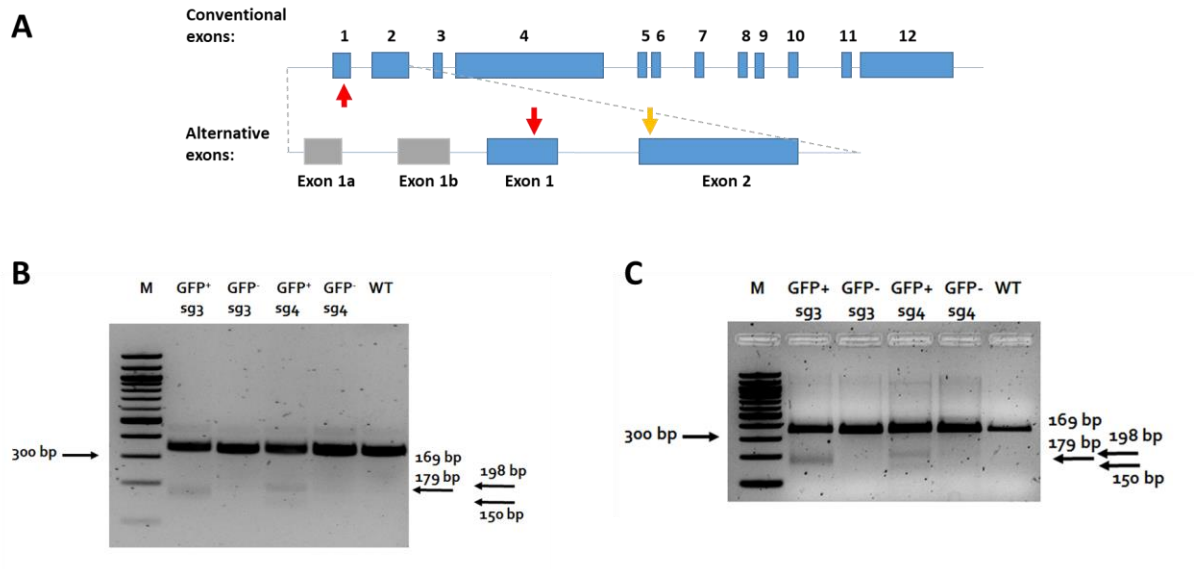

Figure 65. Efficiency of introducing mutations by Cas9, transfection with sgRNA3 and sgRNA4 targeting exon 2 in NOD2 gene.

(A) Schematics of NOD2 gene coding region. On top conventional 12 exons with primarily targeted start of translation (red arrow). Bottom panel represents alternative translation site (yellow arrow) targeted in this experiment; (B) T7 Endonuclease I assay performed on Caco-2 (A) and DLD-1 cells (C) transfected with pX458 plasmid containing Cas9 and sgRNA targeting exon 2 of NOD2 gene. (M – marker; 1 – GFP+ cells sorted after transfection with sgRNA3; 2 - GFP+ cells sorted after transfection with sgRNA4; 3 – untransfected control). Black arrows on the right indicate cleaved sites.

Figure 66. Genomic analysis of generated homozygous NOD2 knock-out clones in DLD-1 (A, B) and Caco-2 (C) cell lines.

Genomic analysis of clones derived from DLD-1 targeted with sgRNA3 (A) and sgRNA4 (B); clones derived from Caco-2 targeted with sgRNA4. In blue alternative translation site in exon 2; in grey target site with adjacent underlined PAM sequence; in red STOP codon; dashes indicate deletion site, insertions in green and substitutions in yellow. Numbers above the sequence represent CDS position in NG_007508.1 Genbank human NOD2.

This time again, the validation of the lack of NOD2 expression proved to be difficult. Multiple anti-NOD2 antibodies were tested in immunostaining, immunoblotting and FACS (**Figure 67**). None of the experiments produced convincing results. It appears that the commercially available antibodies fail to reliably detect NOD2 protein and the band detectable while immunoblotting seems to be unspecific. It is yet another confirmation of the results from **Figure 35** and **Figure 36** (validation of anti-NOD2 antibodies) where the anti-NOD2 siRNAs failed to decrease the intensity of those bands.

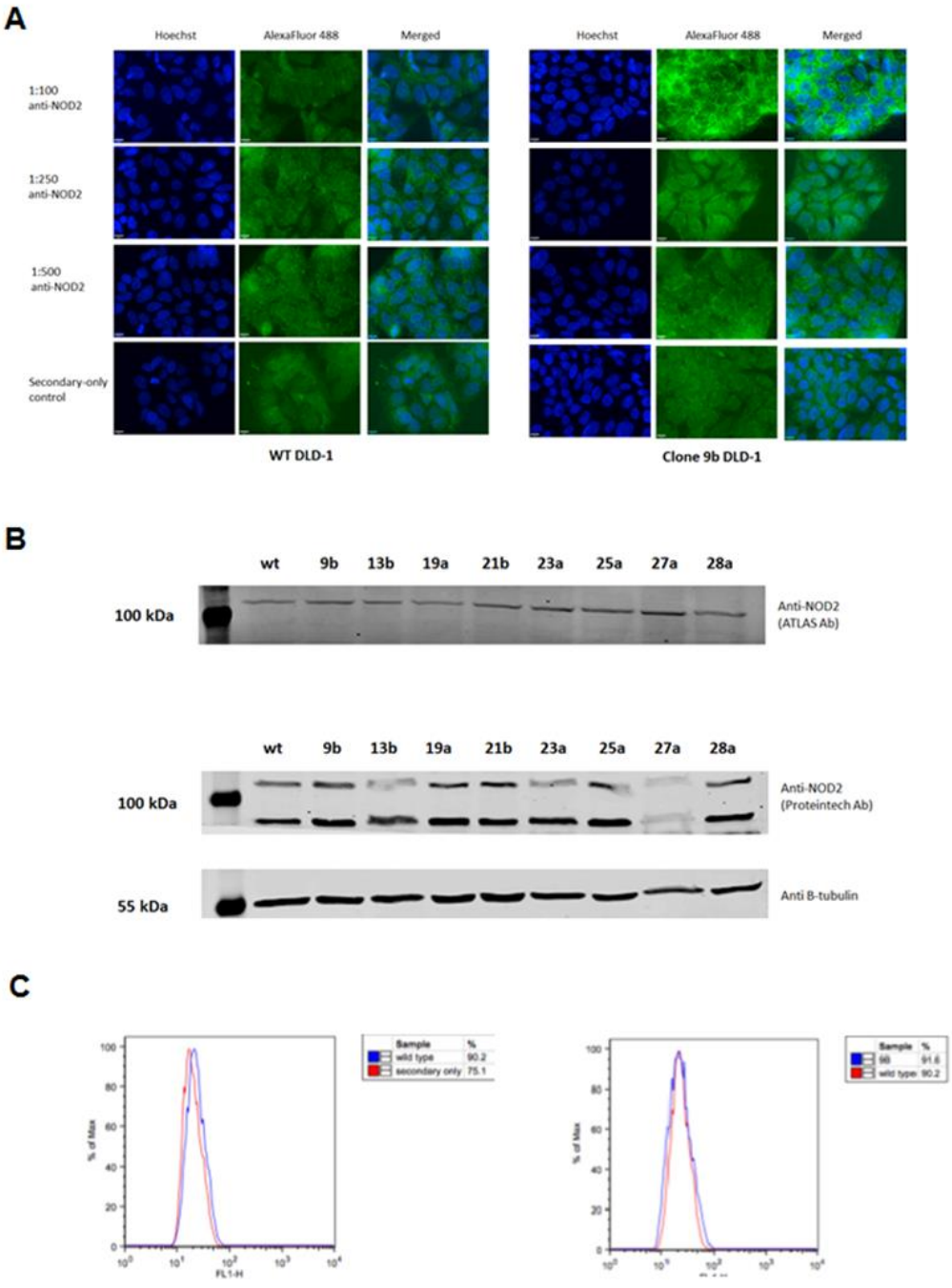

Figure 67. NOD2 expression in derived DLD-1 clones.

(A) Representative microscopy images of anti-NOD2 staining in wild type cells and knock-out DLD-1. Left panel wild type cells, right panel clone 9b. Various anti-NOD2 (Atlas Antibodies) dilutions were checked ranging from 1:500 to 1:100. Hoechst for nuclei staining. Scale bar 11µm. (B) Western blot analysis of homozygous mutants, deletions ranging from 2 to 31nt; upper panel primary anti-NOD2 antibody from Atlas Antibodies; middle panel primary anti-NOD2 antibody from Proteintech; lower panel loading control. (C) Intracellular anti-NOD2 staining of wild type and knock-out DLD-1 cells analyzed by flow cytometry. Left panel anti-NOD2 staining (NovusBio (1:100), AlexaFluor 488 (1:500)) of fixed wild type cells in comparison with control (secondary only); right panel comparison of staining in wild type and knock-out cells (clone 9b).

Since the detection of NOD2 at the protein level was not successful, we decided to confirm the lack of the expression on the RNA level. In order to do that we isolated RNA from the WT and three of DLD-1 clones and synthesized cDNA which was used as a template for PCR amplification of the target region. The product was sent for sequencing and the presence of mutations at RNA level was confirmed (**Figure 68**). Assuming that non-sense mediated decay pathway (NMD) is properly functioning in Caco-2 and DLD-1 cell lines it could be concluded that the generated knock out cell lines do not express NOD2. NMD is a well-known eukaryotic mRNA surveillance pathway that eliminates defective mRNA prior to release from the nucleus. This process occurs when STOP codon is misplaced due to the improper splicing or gene editing (Alberts, B., Johnson, A., Lewis, J., Raff, M., Roberts, K., & Walter, 2002).

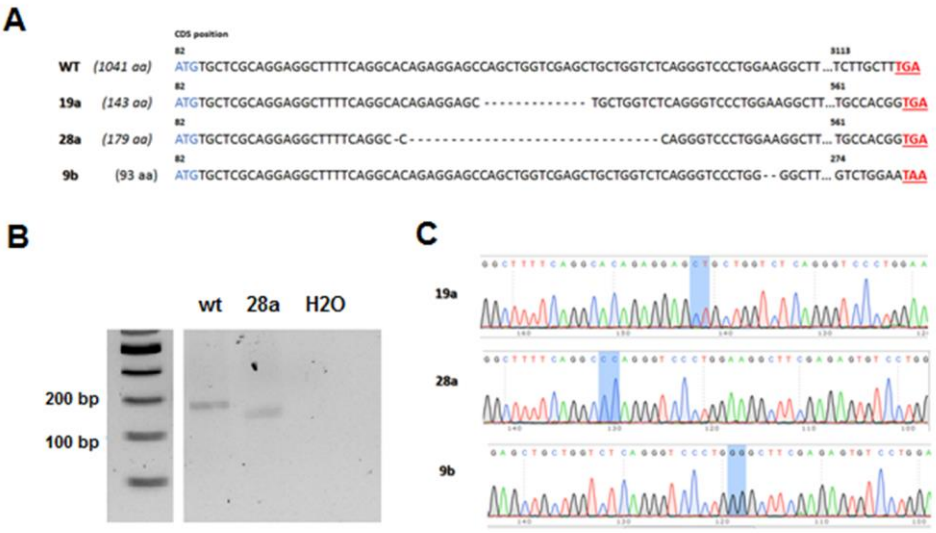

Figure 68. Detection of introduced mutations at RNA level.

(A) Analysis of cDNA sequencing data in comparison to wild type sequence of NOD2 (NG_007508.1 Genbank human) in blue alternative translation site in exon 2; in red STOP codon; dashes indicate deletion site. Numbers above the sequence represent CDS position in NG_007508.1 Genbank human NOD2. (B) Electrophoresis of RT-PCR product. Samples run on 2% agarose gel. DLD-1 wt, 28a knock-out clone (deletion of 31 bp), no template control. (C) Fragments of chromatograms with highlighted mutations' sites.

3.5.2. Modelling IBD on a chip based on deficiency in NOD2 signalling: incorporation of the NOD2KO cell lines into the microfluidic device

The following step in generation of Crohn's disease model on a chip was to incorporate the derived NOD2 KO cell lines into the OrganoPlate®. Standard seeding protocol was followed and KO cell lines were compared to the WT parental lines. Tube formation was assessed by phase contrast imaging. Barrier integrity was tested by Barrier Integrity Assay and TEER. Cells were cultured for an extended period of time and the tubes remained stable for at least 11 days. Both WT cell lines and NOD2 KO clones tubes had similar morphology and were leak tight (**Figure 69**).

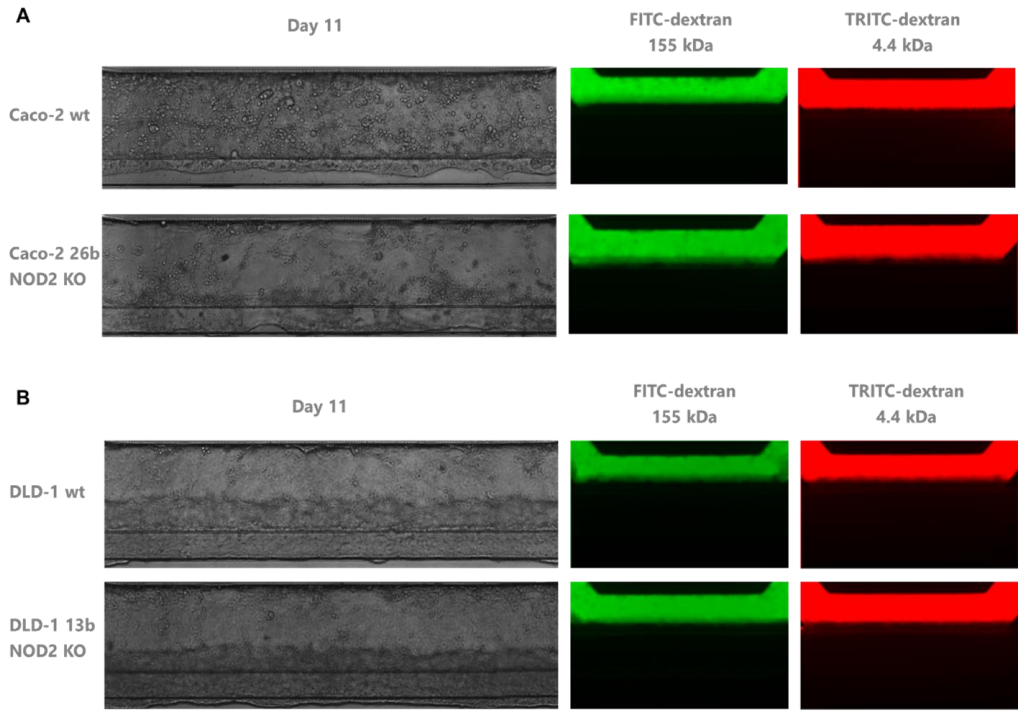

Figure 69. Tube formation by NOD2 KO cell lines.

Derived cell lines form leak tight tubes that are stable for at least 11 days of culture. Phase contrast images on the left, Barrier Integrity Assay on the right panel. (A) Caco-2; (B) DLD-1.

3.5.3. Modelling IBD on a chip based on deficiency in NOD2 signalling: introduction of the pro-inflammatory trigger and its effect on barrier integrity and release of IL-8

The ultimate goal of this project was to generate Crohn's disease on a chip that would be suitable for high throughput drug screening. Our aim was to have a NOD2 deficient cell line incorporated in an organ on a chip device that would show IBD phenotype and respond to the anti-inflammatory treatment. As shown in the previous sections, it was challenging to observe activation of NOD2 signalling pathway in the wild type Caco-2 and DLD-1 cell lines (**Section 3.2.2.1.2. Functional analysis of NOD2 signalling**). Nevertheless, NOD2 KO cell lines were derived and incorporated into the OrganoPlate®. Even though we did not manage to induce parental cell lines with MDP (ligand specific to NOD2), we observed some differences in NOD2KO clones phenotype in response to the cytokines treatment which served as a positive control for induced inflammation. The trigger was composed of the cytokines commonly found at the inflamed sites of the intestine in IBD patients, namely TNFα, IFNγ and IL-1β. The cytokines were added in high concentrations (100 µg/mL) and it was expected that the cells would show decreased viability in extended time of the treatment. After seven days of the treatment, wild type cells begun to round up and detach from the microfluidics channel, clearly showing necrotic phenotype. Interestingly, we observed that NOD2 KO cell lines remained resistant to this treatment (**Figure 70**). This was the case for both, Caco-2 and DLD-1 derived cell lines.

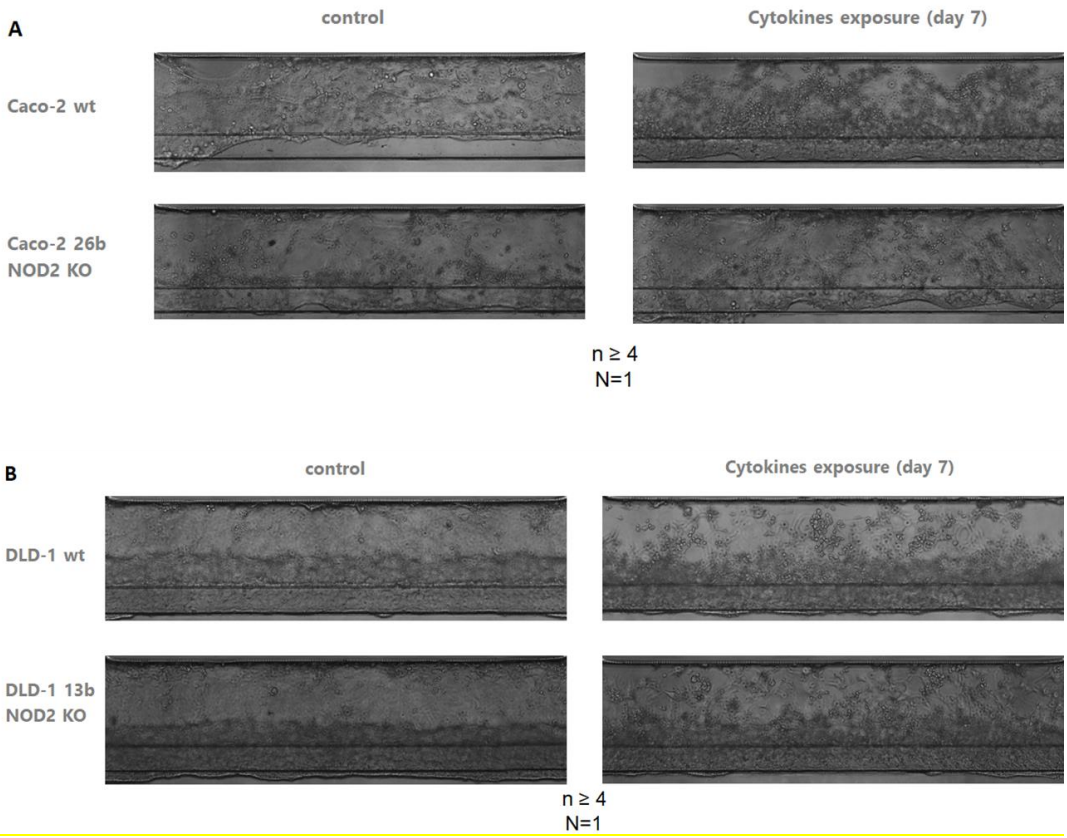

Figure 70. Changes in morphology upon cytokine exposure.

(A) Caco-2 WT vs. KO, (B) DLD-1 WT vs. KO. Wild type cells are sensitive to the cytokine exposure and die upon treatment. KO cells seem to be resistant to the treatment, especially Caco-2 NOD2 KO (morphology of the tube not changed on day 7 of treatment).

To investigate this phenomenon further we assessed the barrier integrity of the tubes upon cytokines treatment (**Figure 71**). If the cells were suffering due to the treatment, we would expect a drop in the TEER values because with cells detaching from the microfluidics channel, holes in the tubes would form and this would allow for the flow of current to the lower channel, resulting in lower electrical resistance. Three Caco-2 NOD2 KO clones were included in the experiment. Surprisingly, each clone had different electrical resistance before the start of the treatment, with clone 5b being the least leak tight. We did not observe those differences in BIA assay and it was previously concluded that all of the derived clones were forming leak tight barriers in the OrganoPlate®. This experiment shows that TEER measurement is a more sensitive method and is able to pick up slight differences in barrier integrity otherwise not noticeable in a fluorescence-based permeability assay. As expected,

the TEER values of WT tubes treated with cytokines dropped significantly and similarly did the values for the clone 17b. However, the barriers formed by the clones 5b and 26b remained stable even after 72 h of cytokines exposure. All three NOD2 KO cell lines were derived from separate single clones. To confirm the presence of NOD2 mutations, samples were collected from two different passage numbers while these experiments were performed and sequencing analysis showed that all the clones still had the same mutation as at the moment of characterization.

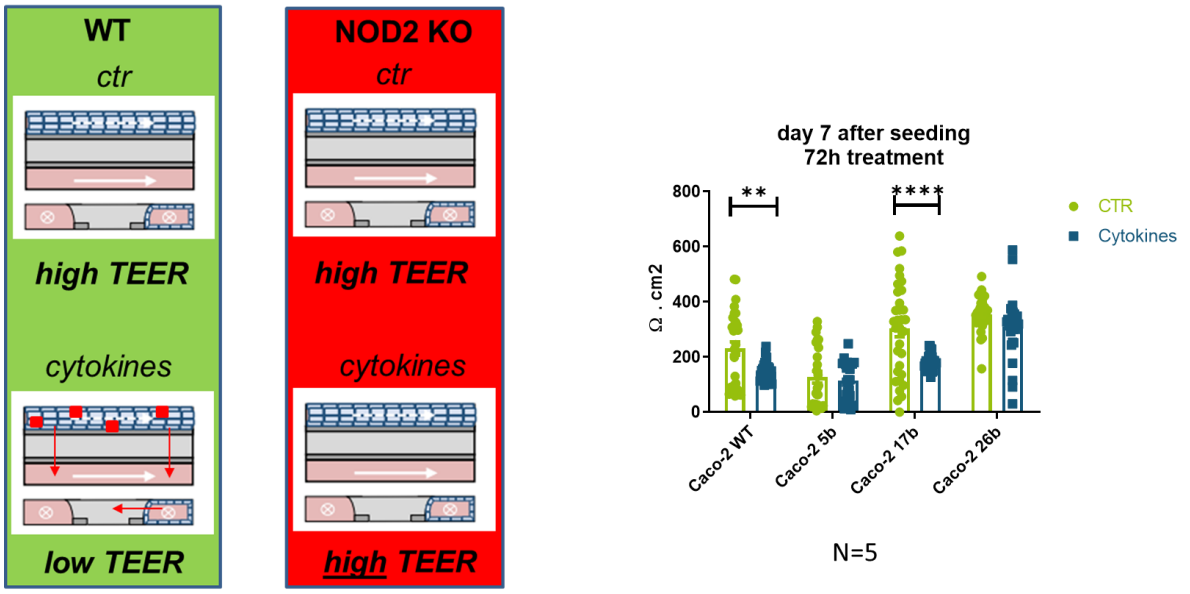

Figure 71. Barrier integrity in NOD2 mutants.

Left panel shows the schematic of the culture in the 3-lane OrganoPlate®, WT in green and NOD2 KO in red. The graph on the right is the summary of TEER data from 5 independent experiments, in which cells were treated with cytokines for 72h. Clones 5b, 17b and 26b are all Caco-2 NOD2 KO cell lines. The red bar shows data of clone 26b that shows the most striking phenotype. Mean with 95% CI, Two-way ANOVA ** p=0,0049, **** p<0,0001.

To examine further the reaction to the cytokines trigger, we investigated the expression of a pro-inflammatory cytokine IL-8 by those cells. Expression levels were measured by qPCR and concentration of IL-8 released into the medium was measured in ELISA experiments (**Figure 72**). Wild type tubes alike clone 5b and 17b showed upregulated IL-8 at

mRNA level upon trigger. Clone 26b did not show elevated IL-8 release when treated with cytokines. In the ELISA experiment we included medium collected from THP-1 culture. This monocyte cell line is known to efficiently respond to the pro-inflammatory trigger and was expected to serve as a positive control in this set up. Concentration of IL-8 in the medium was very high in the chips with the WT and 17b tubes. Slightly lower amounts of IL-8 were found in the chips containing 5b clone tubes. Consistently with the previous results, clone 26b did not show elevated IL-8 release in the triggered condition.

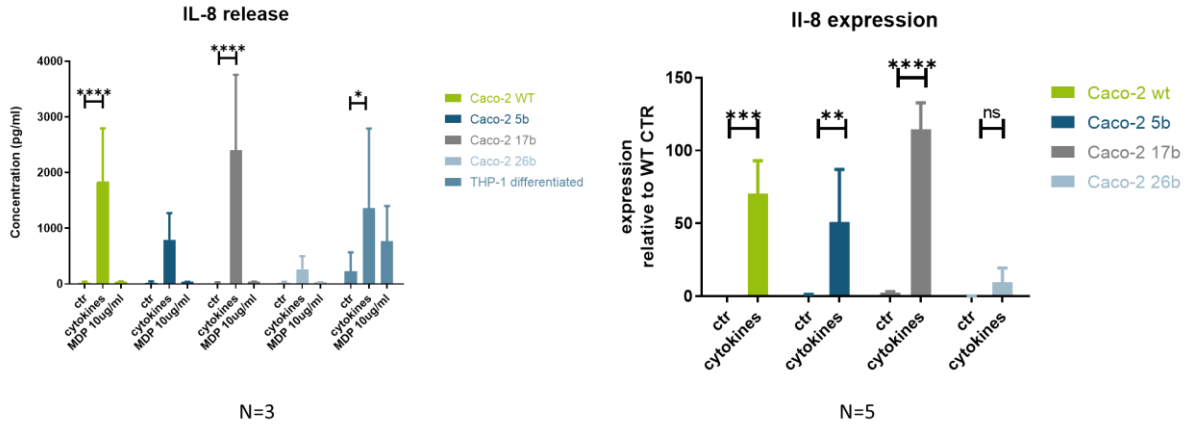

Figure 72. Pro-inflammatory response of WT and NOD2 KO clones.

Relative Il-8 expression measured by qPCR (left panel) and Il-8 release to the culture medium (right panel). Clones 5b, 17b and 26b are all NOD2 KO cell lines. In green positive control – THP-1. Mean with 95% CI, Two-way ANOVA, ** p=0,0077, *** p=0,0004, ****p<0,0001.

3.5.4. Discussion

3.5.4.1. Controversial phenotype of NOD2KO cell lines

As described in the section **3.2.2.1. Characterization of the cell lines in relation to NOD2 signalling**, detection of NOD2 in Caco-2 and DLD-1 cell lines proved to be challenging. Therefore confirmation of the lack of NOD2 expression in generated knock-out cell lines was not complete. We were able to show that the introduced mutations were present at the RNA level but the detection on the protein level did not show reliable data. Additional lack of inducibility of the wild type cell lines with MDP turned this model into not particularly useful.

In the end it was not possible to study NOD2 signalling in either of the cell lines used in the project, thus we proceeded with the alternative plan described earlier in this thesis. However, during our experiments we noticed an interesting phenomena, namely the lack of sensitivity of the knock out cell lines to the cytokines treatment. This striking phenotype was observed in two clones only which suggests presence of off-target mutations in those clones. In order to conclude that the observed effect was due to the introduced mutations in NOD2 gene, in depth analysis of the potential off-target effects of CRISPR/Cas9 would need to be performed. Interestingly, three Caco-2 NOD2KO clones differed significantly in the ability to form barriers, with clones 17b and 26b showing high TEER values and clone 5b lower TEER values than the WT. This heterogeneity suggests that some additional mutations might have been introduced. Caco-2 is a carcinoma cell line and might spontaneously mutate during long term culture. While deriving the cell line, cells were sorted as single cells and expanded further. This process might have facilitated introduction of random mutations. Sequencing of the targeted region confirmed presence of initially detected mutations but other genomic regions were not checked, therefore we cannot confirm that the genetic background of the generated lines was identical to the parental WT cell line. Assumption that the observed insensitivity to the cytokines treatment was directly related to the absence of NOD2 would not be credible. Nonetheless, NOD2 remains an interesting target to be investigated in the future research and more attention should be paid to the characterisation of the chosen model with regard to the NOD2 signalling.

3.5.4.2. Modelling IBD *in vitro* based on NOD2 signalling

IBD is a very complex condition and its pathogenesis cannot be narrowed down to an individual mechanism or a dysfunction in a single signalling pathway. More than 40 genetic loci have been described as susceptibility factors associated with either Crohn's disease or Ulcerative colitis, of which substantial number of genes is common to both conditions. This implies that genetics reflects the susceptibility but environment determines the phenotypic representation of the disease (Barrett *et al.*, 2008; Budarf *et al.*, 2009). NOD2 indisputably is the genetic factor with the highest heritability to Crohn's disease and phenotypic manifestation of its variants can be clearly distinguished as (1) downregulation of NFκB

signalling pathway activation, (2) loss of regulatory response to TLR2 stimulation, (3) lack of sufficient IL-10 regulatory response, (4) downregulation of defensins expression (Fritz *et al.*, 2010). However, its mode of action has not been fully understood yet. Interestingly, Nod2$^{-/-}$ mice do not spontaneously develop Crohn's disease. It is suggested that the lack of Nod2 expression leads to downregulation of α-defensins expression by Paneth cells, which in turn contributes to the change in control of microbiota in the intestine (Kobayashi *et al.*, 2005). It has also been reported that proximity of microbiota leads to upregulation of Nod2 expression (Petnicki-Ocwieja *et al.*, 2009) but the contribution of commensal flora to the development of the disease is still controversial. Only some IBD patients have significantly altered microbiota composition as compared to the healthy individuals and it is unknown whether host genetics contributes to those changes (Frank *et al.*, 2007). Since it is equally probable for both Crohn's and Ulcerative colitis patients to have the altered commensal flora composition, it cannot be confirmed that NOD2 is the causing factor of this phenomena (NOD2 is the susceptibility factor for Crohn's disease only). The same study points out that the patients with altered microbiota composition show a decrease in total number of bacteria in their intestine which is contradictory to the studies on Nod2$^{-/-}$ mice which have higher load of commensal flora as well as to the hypothesis of downregulation of defensins production in Crohn's patients. The complexity of the matter increases with the fact that the inflammation process regardless of the initial cause leads to significant changes in microbiota composition (Lupp *et al.*, 2007).

Additionally, there are other genetic factors that influence Paneth cells' biology. *ATG16L1* and *IRGM* have been reported as autophagy-related susceptibility genes to Crohn's disease (The Welcome Trust Consortium, 2007; Hampe *et al.*, 2007). Mice with mutations in *ATG16L1* show change in Paneth cells' granules and differential expression of inflammatory genes (Cadwell *et al.*, 2008). Dysregulation in resolving endoplasmic reticulum stress has been suggested to be another mechanism involved in IBD pathogenesis (Kaser and Blumberg, 2009). Mutations in *XBP1* gene (component of unfolded protein response in ER stress response) leads to dysfunction of Paneth cells and to a lesser degree goblet cells which leads to the development of spontaneous inflammation (Kaser *et al.*, 2008).

In conclusion, the interplay between host and intestinal microbiota is key to the pathogenesis of IBD. Despite many reports published in the topic we are still far from

understanding the mechanisms involved in reoccurring intestinal inflammation in IBD patients. It is certain that various biological pathways contribute to the development of the disease and generation of a simplified *in vitro* model remains a challenge.

Bibliography

Abbott, D. W. *et al.* (2004) 'The Crohn's Disease Protein, NOD2, Requires RIP2 in Order to Induce Ubiquitinylation of a Novel Site on NEMO', *Current Biology*, 14(24), pp. 2217–2227. doi: 10.1016/j.

Adolph, T. E. *et al.* (2013) 'Paneth cells as a site of origin for intestinal inflammation', *Nature*, 503(7475), pp. 272–276. doi: 10.1038/nature12599.

Alberts, B., Johnson, A., Lewis, J., Raff, M., Roberts, K., & Walter, P. (2002) *Molecular Biology of the Cell*. New York: Garland Science.

Aldhous, M. C. *et al.* (2001) 'Characterization of conditions for the primary culture of human small intestinal epithelial cells', *Clin Exp Immunol*, 125, pp. 32–40.

Antunes, F. *et al.* (2013) 'Models to Predict Intestinal Absorption of Therapeutic Peptides and Proteins', *Current Drug Metabolism*, 14(1), pp. 4–20.

Araujo, F. *et al.* (2015) 'In vitro M-like cells genesis through a tissue-engineered triple-culture intestinal model', *Journal of biomedical materials research*, (4), pp. 782–788. doi: 10.1002/jbm.b.33508.

Artursson, P. and Karlsson, J. (1991) 'Correlation between oral drug absorption in humans and apparent drug permeability coefficients in human intestinal epithelial (Caco-2) cells', *Biochemical and Biophysical Research Communications*, 175(3), pp. 880–885. Available at: http://www.sciencedirect.com/science/article/pii/0006291X9191647U.

Baas, A. F. *et al.* (2004) 'Complete polarization of single intestinal epithelial cells upon activation of LKB1 by STRAD', *Cell*, 116(3), pp. 457–466. doi: 10.1016/S0092-8674(04)00114-X.

Balzola, F. *et al.* (2012) 'Ustekinumab induction and maintenance therapy in refractory Crohn's disease: Commentary', *Inflammatory Bowel Disease Monitor*, 13(2), p. 69. doi: 10.1056/NEJMoa1203572.

Bamias, G. *et al.* (2012) 'New insights into the dichotomous role of innate cytokines in gut homeostasis and inflammation', *Cytokine*. Elsevier Ltd, 59(3), pp. 451–459. doi: 10.1016/j.cyto.2012.06.014.

Barnich, N. *et al.* (2005) 'Membrane recruitment of NOD2 in intestinal epithelial cells is essential for nuclear factor-KB activation in muramyl dipeptide recognition', *Journal of Cell Biology*, 170(1), pp. 21–26. doi: 10.1083/jcb.200502153.

Barrett, J. C. *et al.* (2008) 'Genome-wide association defines more than 30 distinct susceptibility loci for Crohn ' s disease', *Nature Genetics*, 40(8), pp. 955–962. doi: 10.1038/ng.175.

Basson, M. D. and Di, C. (1996) 'Amplitude-Dependent Modulation of Brush Border Enzymes and Proliferation by Cyclic Strain in Human Intestinal Caco-2 Monolayers', *Journal of Cellular Physiology*, 168, pp. 476–488.

Beaurivage, C. *et al.* (2019) 'Development of a gut-on-a-chip model for high throughput disease modeling and drug discovery', *International Journal of Molecular Sciences*, 20(22). doi: 10.3390/ijms20225661.

Beloqui, A. *et al.* (2017) 'A human intestinal M-cell-like model for investigating particle, antigen and microorganism translocation', *Nature Protocols*, 12(7), pp. 1387–1399. doi: 10.1038/nprot.2017.041.

Benam, K. H. *et al.* (2016) 'Small airway-on-a-chip enables analysis of human lung inflammation and drug responses in vitro', *Nature Methods*, 13(2), pp. 151–157. doi: 10.1038/nmeth.3697.

Berg, K. C. G. *et al.* (2017) 'Multi-omics of 34 colorectal cancer cell lines - a resource for biomedical studies', *Molecular Cancer*. Molecular Cancer, 16(116), pp. 1–16. doi: 10.1186/s12943-017-0691-y.

Beumer, J. *et al.* (2020) 'High-Resolution mRNA and Secretome Atlas of High-Resolution mRNA and Secretome Atlas of Human Enteroendocrine Cells', *Cell*, 181, pp. 1291–1306. doi: 10.1016/j.cell.2020.04.036.

Blitzer, J. T. and Nusse, R. (2006) 'A critical role for endocytosis in Wnt signaling', *BMC Cell Biology*, 7, pp. 1–10. doi: 10.1186/1471-2121-7-28.

Le Bourhis, L. *et al.* (2009) 'Role of Nod1 in mucosal dendritic cells during Salmonella pathogenicity island 1-independent Salmonella enterica serovar typhimurium infection', *Infection and Immunity*, 77(10), pp. 4480–4486. doi: 10.1128/IAI.00519-09.

Boyle, J. P., Parkhouse, R. and Monie, T. P. (2014) 'Insights into the molecular basis of the nod2 signalling pathway', *Open Biology*, 4(12). doi: 10.1098/rsob.140178.

Braverman, J. and Yilmaz, H. (2018) 'From 3D Organoids back to 2D Enteroids', *Developmental Cell*, pp. 533–534. doi: 10.1016/j.devcel.2018.02.016.

Budarf, M. L. *et al.* (2009) 'GWA studies : rewriting the story of IBD', *Trends in Genetics*, 25(3), pp. 137–146. doi: 10.1016/j.tig.2009.01.001.

Cadwell, K. *et al.* (2008) 'A key role for autophagy and the autophagy gene Atg16l1 in mouse and human intestinal Paneth cells', *Nature*, 456(November), pp. 259–264. doi: 10.1038/nature07416.

Chamaillard, M. *et al.* (2003) 'Gene-environment interaction modulated by allelic heterogeneity in inflammatory diseases', *Proceedings of the National Academy of Sciences*, 100(6), pp. 3455–3460. doi: 10.1073/pnas.0530276100.

Chapman, C. G. and Pekow, J. (2015) 'The emerging role of miRNAs in inflammatory bowel disease: A review', *Therapeutic Advances in Gastroenterology*, 8(1), pp. 4–22. doi: 10.1177/1756283X14547360.

Chelakkot, C., Ghim, J. and Ryu, S. H. (2018) 'Mechanisms regulating intestinal barrier integrity and its pathological implications', *Experimental and Molecular Medicine*. Springer US, 50(8). doi: 10.1038/s12276-018-0126-x.

Chen, Y. *et al.* (2015) 'Robust bioengineered 3D functional human intestinal epithelium', *Nature Publishing Group*. Nature Publishing Group, pp. 1–11. doi: 10.1038/srep13708.

Cheng, K. C., Li, C. and Uss, A. S. (2008) 'Prediction of oral drug absorption in humans - From cultured cell lines

and experimental animals', *Expert Opinion on Drug Metabolism and Toxicology*, 4(5), pp. 581–590. doi: 10.1517/17425255.4.5.581.

Cho, J. H. and Brant, S. R. (2011) 'Recent Insights Into the Genetics of Inflammatory Bowel Disease', *Gastroenterology*. Elsevier Inc., 140(6), pp. 1704-1712.e2. doi: 10.1053/j.gastro.2011.02.046.

Cong, L. *et al.* (2013) 'Cong, L., Ran, F. A., Cox, D., Lin, S., Barretto, R., Habib, N., … Zhang, F. (2013). Multiplex Genome Engineering Using CRISPR/Cas Systems. Science (New York, N.Y.)', *Science (New York, N.Y.)*, 339(6121), pp. 819–823. doi: 10.1126/science.1231143.Multiplex.

Consortium, T. W. T. C. C. (2007) 'Genome-wide association study of 14,000 cases of seven common diseases and 3,000 shared controls', *Nature*, 447(June). doi: 10.1038/nature05911.

Cooney, R. *et al.* (2010) 'NOD2 stimulation induces autophagy in dendritic cells influencing bacterial handling and antigen presentation', *Nature Medicine*. Nature Publishing Group, 16(1). doi: 10.1038/nm.2069.

Cosnes, J. *et al.* (2011) 'Epidemiology and natural history of inflammatory bowel diseases', *Gastroenterology*. Elsevier Inc., 140(6), pp. 1785-1794.e4. doi: 10.1053/j.gastro.2011.01.055.

Costa, J. and Ahluwalia, A. (2019) 'Advances and Current Challenges in Intestinal in vitro Model Engineering ':, *Frontiers in Bioengineering and Biotechnology*, 7(June), pp. 1–14. doi: 10.3389/fbioe.2019.00144.

Cui, J. *et al.* (2012) 'NLRP4 negatively regulates type I interferon signaling by targeting the kinase TBK1 for degradation via the ubiquitin ligase DTX4', *Nature Immunology*, 13, pp. 387–95.

Danese, S. (2012) 'New therapies for inflammatory bowel disease: From the bench to the bedside', *Gut*, 61(6), pp. 918–932. doi: 10.1136/gutjnl-2011-300904.

Dave, M. *et al.* (2015) 'Immunology of Inflammatory Bowel Disease and Molecular Targets for Biologics', *Gastroenterol Clin North Am.*, 43(3), pp. 405–424. doi: 10.1016/j.gtc.2014.05.003.Immunology.

Davies, P. F. (1995) 'Flow-Mediated Endothelial Mechanotransduction', *Physiol Rev*, 75(3), pp. 519–560.

Diegelmann, J. *et al.* (2013) 'Intestinal DMBT1 expression is modulated by Crohn's disease-associated IL23R variants and by a DMBT1 variant which influences binding of the transcription factors CREB1 and ATF-2', *PLoS ONE*, 8(11), pp. 1–16. doi: 10.1371/journal.pone.0077773.

Dige, A. *et al.* (2016) 'Reduced numbers of mucosal DR macrophages and increased numbers of CD103 dendritic cells during anti-TNF- α treatment in patients with Crohn ' s disease', *Scandinavian Journal of Gastroenterology*, 5521. doi: 10.3109/00365521.2015.1134649.

Ding, N. S., Hart, A. and Cruz, P. De (2015) 'Alimentary Pharmacology and Therapeutics Systematic review : predicting and optimising response to anti-TNF therapy in Crohn ' s disease – algorithm for practical management', *Alimentary Pharmacology and Therapeutics*, (October). doi: 10.1111/apt.13445.

Dosh, R. H. *et al.* (2019) 'Long-term in vitro 3D hydrogel co-culture model of inflammatory bowel disease',

Scientific Reports, 9(1), pp. 1–15. doi: 10.1038/s41598-019-38524-8.

Duerr, R. H. *et al.* (2006) 'A Genome-Wide Association Study Identifies IL23R as an Inflammatory Bowel Disease Gene', *Science*, 314(December), pp. 1461–1464.

Van Dussen, K. L. *et al.* (2015) 'Development of an enhanced human gastrointestinal epithelial culture system to facilitate patient-based assays', *Gut*, 64(6), pp. 911–920. doi: 10.1136/gutjnl-2013-306651.

Eckmann, L., Kagnoff, M. F. and Fierer, J. (1993) 'Epithelial cells secrete the chemokine interleukin-8 in response to bacterial entry', *Infection and Immunity*, 61(11), pp. 4569–4574. doi: 10.1128/iai.61.11.4569-4574.1993.

Economou, M. *et al.* (2004) 'Differential effects of NOD2 variants on Crohn's disease risk and phenotype in diverse populations: A metaanalysis', *American Journal of Gastroenterology*, 99(12), pp. 2393–2404. doi: 10.1111/j.1572-0241.2004.40304.x.

Ettayebi, K. *et al.* (2016) 'Replication of human noroviruses in stem cell–derived human enteroids', *Science*, 353(6306), pp. 1387–1394.

Farin, H. F. *et al.* (2014) 'Paneth cell extrusion and release of antimicrobial products is directly controlled by immune cell-derived IFN-γ', *Journal of Experimental Medicine*, 211(7), pp. 1393–1405. doi: 10.1084/jem.20130753.

Fatehullah, A., Tan, S. H. and Barker, N. (2016) 'Organoids as an in vitro model of human development and disease', *Nature Publishing Group*. Nature Publishing Group, 18(3). doi: 10.1038/ncb3312.

Ferrand, A. *et al.* (2019) 'NOD2 Expression in Intestinal Epithelial Cells Protects Toward the Development of Inflammation and Associated Carcinogenesis', *Cmgh*. Elsevier Inc, 7(2), pp. 357–369. doi: 10.1016/j.jcmgh.2018.10.009.

Fogh, J., Wright, W. C. and Loveless, J. D. (1977) 'Absence of HeLa cell contamination in 169 cell lines derived from human tumors', *Journal of the National Cancer Institute*, 58(2), pp. 209–214. doi: 10.1093/jnci/58.2.209.

Fowler, S. *et al.* (2020) 'Microphysiological systems for ADME-related applications: Current status and recommendations for system development and characterization', *Lab on a Chip*. Royal Society of Chemistry, 20(3), pp. 446–467. doi: 10.1039/c9lc00857h.

Frank, D. N. *et al.* (2007) 'Molecular-phylogenetic characterization of microbial community imbalances in human inflammatory bowel diseases', *Proceedings of the National Academy of Sciences*, 104(34), pp. 13780–13785.

Fritz, T. *et al.* (2010) 'Controversy Over NOD2, Inflammation, and Defensins', *Inflammatory bowel diseases*, 16(11), pp. 1996–1998. doi: 10.1002/ibd.21213.Controversy.

Frolkis, A. D. *et al.* (2013) 'Risk of surgery for inflammatory bowel diseases has decreased over time: A

systematic review and meta-analysis of population-based studies', *Gastroenterology*. Elsevier, Inc, 145(5), pp. 996–1006. doi: 10.1053/j.gastro.2013.07.041.

Fujiwara, M. *et al.* (2015) 'Desmocollin-2 alone forms functional desmosomal plaques, with the plaque formation requiring the juxtamembrane region and plakophilins', *Journal of Biochemistry*, 158(4), pp. 339–353. doi: 10.1093/jb/mvv048.

Fuss, I. J. *et al.* (2004) 'Nonclassical CD1d-restricted NK T cells that produce IL-13 characterize an atypical Th2 response in ulcerative colitis', *J Clin Invest*, 113(10), pp. 1490–7.

Geddes, K. *et al.* (2010) 'Nod1 and Nod2 regulation of inflammation in the Salmonella colitis model', *Infection and Immunity*, 78(12), pp. 5107–5115. doi: 10.1128/IAI.00759-10.

Gijzen, L. *et al.* (2020) 'An Intestine-on-a-Chip Model of Plug-and- Play Modularity to Study Inflammatory Processes'. doi: 10.1177/2472630320924999.

Girardin, S. E., Boneca, I. G., Carneiro, L. A. M., *et al.* (2003) 'Nod1 Detects a Unique Muropeptide from Gram-Negative Bacterial Peptidoglycan', *Science*, 300(5625), pp. 1584–1587.

Girardin, S. E., Boneca, I. G., Viala, J., *et al.* (2003) 'Nod2 is a general sensor of peptidoglycan through muramyl dipeptide (MDP) detection', *Journal of Biological Chemistry*, 278(11), pp. 8869–8872. doi: 10.1074/jbc.C200651200.

Giusti, S. *et al.* (2014) 'A novel dual-flow bioreactor simulates increased fluorescein permeability in epithelial tissue barriers', *Biotechnology Journal*, 9(9), pp. 1175–1184. doi: 10.1002/biot.201400004.

Goessling W. *et al.* (2009) 'Genetic interaction of PGE2 and Wnt signaling regulates developmental specification of stem cells and regeneration Wolfram', *Cell*, 136(6), pp. 1136–1147. doi: 10.1016/j.cell.2009.01.015.Genetic.

Gretchen J., M., Shulerb L., M. and Glahnc P., R. (2009) 'Characterization of Caco-2 and HT29-MTX cocultures in an in vitro digestion/cell culture model used to predict iron bioavailability', *Journal of Nutricional Biochemistry*, 20(7), pp. 494–502.

Gribar, S. C. *et al.* (2008) 'No longer an innocent bystander: Epithelial toll-like receptor signaling in the development of mucosal inflammation', *Molecular Medicine*, 14(9–10), pp. 645–659. doi: 10.2119/2008-00035.Gribar.

Grimes, C. L. *et al.* (2012) 'The innate immune protein Nod2 binds directly to MDP, a bacterial cell wall fragment', *Journal of the American Chemical Society*, 134(33), pp. 13535–13537. doi: 10.1021/ja303883c.

Gullberg, E. *et al.* (2000) 'Expression of Specific Markers and Particle Transport in a New Human Intestinal M-Cell Model', 813, pp. 808–813. doi: 10.1006/bbrc.2000.4038.

Haeussler, M. *et al.* (2016) 'Evaluation of off-target and on-target scoring algorithms and integration into the

guide RNA selection tool CRISPOR', *Genome Biology*. Genome Biology, 17(1), pp. 1–12. doi: 10.1186/s13059-016-1012-2.

Hagemann, N. *et al.* (2013) 'The serologically defined colon cancer antigen-3 interacts with the protein tyrosine phosphatase PTPN13 and is involved in the regulation of cytokinesis', *Oncogene*, 32(39), pp. 4602–4613. doi: 10.1038/onc.2012.485.

Hampe, J. *et al.* (2007) 'A genome-wide association scan of nonsynonymous SNPs identifies a susceptibility variant for Crohn disease in ATG16L1', *Nature Genetics*, 39(2), pp. 207–211. doi: 10.1038/ng1954.

van der Helm, M. W. *et al.* (2019) 'Non-invasive sensing of transepithelial barrier function and tissue differentiation in organs-on-chips using impedance spectroscopy', *Lab on a Chip*. Royal Society of Chemistry, 19(3), pp. 452–463. doi: 10.1039/c8lc00129d.

Hidalgo, I. J., Raub, T. J. and Borchardt, R. T. (1989) 'Characterization of the Human Colon Carcinoma Cell Line (Caco-2) as a Model System for Intestinal Epithelial Permeability', *Gastroenterology*. American Gastroenterological Association, 96(2), pp. 736–749. doi: 10.1016/S0016-5085(89)80072-1.

Hisamatsu, T. *et al.* (2003) 'CARD15/NOD2 functions as an antibacterial factor in human intestinal epithelial cells', *Gastroenterology*, 124(4), pp. 993–1000. doi: 10.1053/gast.2003.50153.

Ho, F. and Khalil, H. (2015) 'Crohn's disease: A clinical update', *Therapeutic Advances in Gastroenterology*, 8(6), pp. 352–359. doi: 10.1177/1756283X15592585.

Hoffmann, J. C. *et al.* (2003) 'Animal models of inflammatory bowel disease: An overview', *Pathobiology*, 70(3), pp. 121–130. doi: 10.1159/000068143.

Hovhannisyan, Z. *et al.* (2011) 'Characterization of interleukin-17-producing regulatory T cells in inflamed intestinal mucosa from patients with inflammatory bowel diseases', *Gastroenterology*. Elsevier Inc., 140(3), pp. 957–965. doi: 10.1053/j.gastro.2010.12.002.

Hugot, J. P. *et al.* (2001) 'Association of NOD2 leucine-rich repeat variants with susceptibility to Crohn's disease', *Nature*, 411(6837), pp. 599–603. doi: 10.1038/35079107.

Iborra, M. *et al.* (2012) 'MicroRNAs in autoimmunity and inflammatory bowel disease: Crucial regulators in immune response', *Autoimmunity Reviews*. Elsevier B.V., 11(5), pp. 305–314. doi: 10.1016/j.autrev.2010.07.002.

Ikeuchi, T. *et al.* (2013) 'A vitamin D3 analog augmented interleukin-8 production by human monocytic cells in response to various microbe-related synthetic ligands, especially NOD2 agonistic muramyldipeptide', *International Immunopharmacology*. Elsevier B.V., 15(1), pp. 15–22. doi: 10.1016/j.intimp.2012.10.027.

Imura, Y. *et al.* (2009) 'A Microfluidic System to Evaluate Intestinal Absorption', *Analytical Sciences*, 25(December), pp. 1403–1407.

Imura, Y., Sato, K. and Yoshimura, E. (2010) 'Micro Total Bioassay System for Ingested Substances : Assessment of Intestinal Absorption , Hepatic Metabolism , and Bioactivity', 82(24), pp. 9983–9988. doi: 10.1021/ac100806x.

Janeway, C. A. *et al.* (2001) *The Immune System in Health and Disease.* Garland Science.

JL, F. *et al.* (2016) *Derivation of Intestinal Organoids from Human Induced Pluripotent Stem Cells for Use as an Infection System*.

Jong Hwan Sung, Jiajie Yu, Dan Luo, Michael L. Shuler, J. C. M. (2011) 'Microscale 3-D hydrogel scaffold for biomimetic gastrointestinal (GI) tract model', *Lab on Chip*, 11, pp. 389–392. doi: 10.1039/c0lc00273a.

Joseph B.Kirsner (1961) 'Experimental "Colitis" With Particular Reference to Hypersensitivity Reactions in the Colon', *Gastroenterology*, 40(2), pp. 307–312.

Jostins, L. *et al.* (2012) 'Host-microbe interactions have shaped the genetic architecture of inflammatory bowel disease', *Nature*. Nature Publishing Group, 491(7422), pp. 119–124. doi: 10.1038/nature11582.

Kalla, R. *et al.* (2015) 'MicroRNAs: New players in IBD', *Gut*, 64(3), pp. 504–517. doi: 10.1136/gutjnl-2014-307891.

Kamada, N. *et al.* (2008) 'Unique CD14 intestinal macrophages contribute to the pathogenesis of ...', *J Clin Invest*, (June).

Kämpfer, A. A. M. *et al.* (2017) 'Development of an in vitro co-culture model to mimic the human intestine in healthy and diseased state', *Toxicology in Vitro*. Elsevier, 45(May), pp. 31–43. doi: 10.1016/j.tiv.2017.08.011.

Kasendra, M. *et al.* (2020) 'Duodenum Intestine-Chip for preclinical drug assessment in a human relevant model', 450, pp. 1–23.

Kaser, A. *et al.* (2008) 'XBP1 Links ER Stress to Intestinal Inflammation and Confers Genetic Risk for Human Inflammatory Bowel Disease', *Cell*, 134, pp. 743–756. doi: 10.1016/j.cell.2008.07.021.

Kaser, A. and Blumberg, R. S. (2009) 'Endoplasmic reticulum stress in the intestinal epithelium and inflammatory bowel disease', *Seminars in Immunology*, 21, pp. 156–163.

Kerneis, S. *et al.* (1997) 'Conversion by Peyer ' s Patch Lymphocytes of Human Enterocytes into M Cells that Transport Bacteria', *Science*, 277(August).

Kernéis, S. *et al.* (1997) 'Conversion by Peyer ' s Patch Lymphocytes of Human Enterocytes into M Cells that Transport Bacteria Conversion by Peyer ' s Patch Lymphocytes of Human Enterocytes into M Cells that Transport Bacteria', *Science*, 949(277), p. 949. doi: 10.1126/science.277.5328.949.

Kim, H. J. *et al.* (2012) 'Human gut-on-a-chip inhabited by microbial flora that experiences intestinal peristalsis-like motions and flow', *Lab on a Chip*, pp. 2165–2174. doi: 10.1039/c2lc40074j.

Kim, H. J. and Ingber, D. E. (2013) 'Gut-on-a-Chip microenvironment induces human intestinal cells to undergo villus differentiation', *Integrative Biology (United Kingdom)*, 5(9), pp. 1130–1140. doi: 10.1039/c3ib40126j.

Kim, Y. K., Shin, J. S. and Nahm, M. H. (2016) 'NOD-like receptors in infection, immunity, and diseases', *Yonsei Medical Journal*, 57(1), pp. 5–14. doi: 10.3349/ymj.2016.57.1.5.

Kimura, H. *et al.* (2008) 'An integrated microfluidic system for long-term perfusion culture and on-line monitoring of intestinal tissue models', pp. 741–746. doi: 10.1039/b717091b.

Kobayashi, K. S. *et al.* (2005) 'Nod2-Dependent Regulation of Innate and Adaptive Immunity in the Intestinal Tract', *Science*, 307(February), pp. 731–735.

Krieg, A. *et al.* (2009) 'XIAP mediates NOD signaling via interaction with RIP2', *Proceedings of the National Academy of Sciences of the United States of America*, 106(34), pp. 14524–14529. doi: 10.1073/pnas.0907131106.

Kues, W. A. *et al.* (2000) 'Cell Cycle Synchronization of Porcine Fetal Fibroblasts : Effects of Serum Deprivation and Reversible Cell Cycle Inhibitors 1', *Biology of Reproduction*, 419(62), pp. 412–419.

Kufer, T. A. *et al.* (2006) 'Role for erbin in bacterial activation of Nod2', *Infection and Immunity*, 74(6), pp. 3115–3124. doi: 10.1128/IAI.00035-06.

Kufer, T. A. and Sansonetti, P. J. (2011) 'NLR functions beyond pathogen recognition', *Nature Immunology*. Nature Publishing Group, 12(2), pp. 121–128. doi: 10.1038/ni.1985.

Kühn, R. *et al.* (1993) 'Interleukin-10-deficient mice develop chronic enterocolitis', *Cell*, 75(2), pp. 263–274. doi: 10.1016/0092-8674(93)80068-P.

Lahar, N. *et al.* (2011) 'Intestinal Subepithelial Myofibroblasts Support in vitro and in vivo Growth of Human Small Intestinal Epithelium', 6(11), pp. 1–9. doi: 10.1371/journal.pone.0026898.

de Lau, W. *et al.* (2012) 'Peyer's Patch M Cells Derived from Lgr5+ Stem Cells Require SpiB and Are Induced by RankL in Cultured "Miniguts"', *Molecular and Cellular Biology*, 32(18), pp. 3639–3647. doi: 10.1128/MCB.00434-12.

Lee, K. H. *et al.* (2012) 'Proteasomal degradation of Nod2 protein mediates tolerance to bacterial cell wall components', *Journal of Biological Chemistry*, 287(47), pp. 39800–39811. doi: 10.1074/jbc.M112.410027.

Leonard, F., Collnot, E. M. and Lehr, C. M. (2010) 'A three-dimensional coculture of enterocytes, monocytes and dendritic cells to model inflamed intestinal mucosa in vitro', *Molecular Pharmaceutics*, 7(6), pp. 2103–2119. doi: 10.1021/mp1000795.

Lesage, S. *et al.* (2002) 'CARD15/NOD2 mutational analysis and genotype-phenotype correlation in 612 patients with inflammatory bowel disease', *American Journal of Human Genetics*, 70(4), pp. 845–857. doi: 10.1086/339432.

Leung, C. H. *et al.* (2009) 'Butyrate mediates nucleotide-binding and oligomerisation domain (NOD) 2-dependent mucosal immune responses against peptidoglycan', *European Journal of Immunology*, 39(12), pp. 3529–3537. doi: 10.1002/eji.200939454.

Li, J. *et al.* (2004) 'Regulation of IL-8 and IL-1β expression in Crohn's disease associated NOD2/CARD15 mutations', *Human Molecular Genetics*, 13(16), pp. 1715–1725. doi: 10.1093/hmg/ddh182.

Li, N. *et al.* (2013) 'Development of an improved three-dimensional in vitro intestinal mucosa model for drug absorption evaluation', *Tissue Engineering - Part C: Methods*, 19(9), pp. 708–719. doi: 10.1089/ten.tec.2012.0463.

Linnankoski, J. *et al.* (2010) 'Paracellular porosity and pore size of the human intestinal epithelium in tissue and cell culture models', *Journal of Pharmaceutical Sciences*, 99(4), pp. 2166–2175. doi: 10.1002/jps.21961.

Lipinski, S. *et al.* (2012) 'RNAi screening identifies mediators of NOD2 signaling: Implications for spatial specificity of MDP recognition', *Proceedings of the National Academy of Sciences of the United States of America*, 109(52), pp. 21426–21431. doi: 10.1073/pnas.1209673109.

Liu, B. *et al.* (2013) 'Irgm1-deficient mice exhibit paneth cell abnormalities and increased susceptibility to acute intestinal inflammation', *American Journal of Physiology - Gastrointestinal and Liver Physiology*, 305(8), pp. 573–584. doi: 10.1152/ajpgi.00071.2013.

Loddo, I. and Romano, C. (2015) 'Inflammatory bowel disease: Genetics, epigenetics, and pathogenesis', *Frontiers in Immunology*, 6(NOV), pp. 6–11. doi: 10.3389/fimmu.2015.00551.

Lodes, M. J. *et al.* (2004) 'Bacterial flagellin is a dominant antigen in Crohn disease', *Journal of Clinical Investigation*, 113(9), pp. 1296–1306. doi: 10.1172/JCI200420295.

Lupp, C. *et al.* (2007) 'Article Host-Mediated Inflammation Disrupts the Intestinal Microbiota and Promotes the Overgrowth of Enterobacteriaceae', *Cell Host and Microbe*, (August), pp. 119–129. doi: 10.1016/j.chom.2007.06.010.

Mabbott, N. A. *et al.* (2013) 'Microfold (M) cells : important immunosurveillance posts in the intestinal epithelium', *Mucosal Immunology*. Nature Publishing Group, 6(4). doi: 10.1038/mi.2013.30.

Maekawa, T., Kufer, T. A. and Schulze-Lefert, P. (2011) 'NLR functions in plant and animal immune systems: So far and yet so close', *Nature Immunology*, 12(9), pp. 818–826. doi: 10.1038/ni.2083.

Magalhaes, J. G. *et al.* (2011) 'Essential role of Rip2 in the modulation of innate and adaptive immunity triggered by Nod1 and Nod2 ligands', *European Journal of Immunology*, 41(5), pp. 1445–1455. doi: 10.1002/eji.201040827.

Mali, P. *et al.* (2013) 'RNA-guided human genome engineering via Cas9', *Science*, 339(6121), pp. 823–826. doi: 10.1126/science.1232033.

Mannon, P. J. *et al.* (2004) 'Anti–Interleukin-12 Antibody for Active Crohn's Disease', *New England Journal of Medicine*, 351(20), pp. 2069–2079. doi: 10.1056/nejmoa033402.

Marks, D. J. B. *et al.* (2006) 'Defective acute inflammation in Crohn's disease: a clinical investigation', *Lancet*, 367(9511), pp. 668–78.

Martin Jinek *et al.* (2012) 'A Programmable Dual-RNA–Guided DNA Endonuclease in Adaptive Bacterial Immunity', *Science*, 337(6096), pp. 816–821. doi: 10.1126/science.1138140.

McDonald, C. *et al.* (2005) 'A role for Erbin in the regulation of Nod2-dependent NF-κB signaling', *Journal of Biological Chemistry*, 280(48), pp. 40301–40309. doi: 10.1074/jbc.M508538200.

McGough, I. J. *et al.* (2014) 'Identification of molecular heterogeneity in SNX27-retromermediated endosome-to-plasma-membrane recycling', *Journal of Cell Science*, 127(22), pp. 4940–4953. doi: 10.1242/jcs.156299.

McKay, D. M. and Perdure, M. H. (1993) 'Intestinal epithelial function: the case for immunophysiological regulation. Implications for disease', *Dig Dis Sci*, 38(9), pp. 1735–49.

McKay, D. M., Philpott, D. J. and Perdue, M. H. (1997) 'In vitro models in inflammatory bowel disease research - A critical review', *Alimentary Pharmacology and Therapeutics, Supplement*, 11(3), pp. 70–80. doi: 10.1111/j.1365-2036.1997.tb00811.x.

Di Meglio, P. *et al.* (2011) 'The IL23R R381Q gene variant protects against immune-mediated diseases by impairing IL-23-induced Th17 effector response in humans', *PLoS ONE*, 6(2), pp. 1–10. doi: 10.1371/journal.pone.0017160.

Misaka, S., Müller, F. and Fromm, M. F. (2013) 'Clinical relevance of drug efflux pumps in the gut', *Current Opinion in Pharmacology*, 13(6), pp. 847–852. doi: 10.1016/j.coph.2013.08.010.

Mo, J. *et al.* (2012) 'Pathogen sensing by nucleotide-binding oligomerization domain-containing protein 2 (NOD2) is mediated by direct binding to muramyl dipeptide and ATP', *Journal of Biological Chemistry*, 287(27), pp. 23057–23067. doi: 10.1074/jbc.M112.344283.

Molodecky, N. A. *et al.* (2012) 'Increasing incidence and prevalence of the inflammatory bowel diseases with time, based on systematic review', *Gastroenterology*. Elsevier Inc., 142(1), pp. 46-54.e42. doi: 10.1053/j.gastro.2011.10.001.

Moss, A. C. and Farrell, R. J. (2006) 'Infliximab for induction and maintenance therapy for ulcerative colitis', *Gastroenterology*, 131(5), pp. 1649–1651. doi: 10.1053/j.gastro.2006.09.039.

Mowat, A. M. (2018) 'To respond or not to respond — a personal perspective of intestinal tolerance', *Nature Reviews Immunology*. Springer US. doi: 10.1038/s41577-018-0002-x.

Mowat, A. M. and Agace, W. W. (2014) 'Regional specialization within the intestinal immune system', *Nature Reviews Immunology*, 14(10), pp. 667–685. doi: 10.1038/nri3738.

Na, Y. R. *et al.* (2019) 'Macrophages in intestinal inflammation and resolution : a potential therapeutic target in IBD', *Nature Reviews Gastroenterology & Hepatology*. Springer US, 16. doi: 10.1038/s41575-019-0172-4.

Naumovska, E. *et al.* (2020) 'Direct On-Chip Differentiation of Intestinal Tubules from Induced Pluripotent Stem Cells', *International Journal of Molecular Sciences*.

Neurath, M. F. (2007) 'IL-23 : a master regulator in Crohn disease', *Nature Medicine*, 13(1), pp. 26–28.

Neurath, M. F. (2017) 'Current and emerging therapeutic targets for IBD', *Nature Reviews Gastroenterology and Hepatology*, 14(5), pp. 269–278. doi: 10.1038/nrgastro.2016.208.

Nigro, G. *et al.* (2014) 'The cytosolic bacterial peptidoglycan sensor Nod2 affords stem cell protection and links microbes to gut epithelial regeneration', *Cell Host and Microbe*. Elsevier Inc., 15(6), pp. 792–798. doi: 10.1016/j.chom.2014.05.003.

Nikolaev, M. *et al.* (2020) 'Homeostatic mini-intestines through scaffold-guided organoid morphogenesis', *Nature*. Springer US, in Press(June 2018). doi: 10.1038/s41586-020-2724-8.

Noel, G. *et al.* (2017) 'A primary human macrophage-enteroid co-culture model to investigate mucosal gut physiology and host-pathogen interactions', *Scientific Reports*. Nature Publishing Group, 7(September 2016), pp. 1–14. doi: 10.1038/srep45270.

Ogino, T. *et al.* (2013) 'Increased Th17-Inducing Activity of CD14+ CD163low Myeloid Cells in Intestinal Lamina Propria of Patients With Crohn's Disease', *Gastroenterology*. Elsevier, Inc, 145(6), pp. 1380-1391.e1. doi: 10.1053/j.gastro.2013.08.049.

Ogura, Y. *et al.* (2001) 'A frameshift mutation in NOD2 associated with susceptibility to Crohn's disease', *Nature*, 411(6837), pp. 603–606. doi: 10.1038/35079114.

Ogura, Y. *et al.* (2003) 'Expression of NOD2 in Paneth cells: A possible link to Crohn's ileitis', *Gut*, 52(11), pp. 1591–1597. doi: 10.1136/gut.52.11.1591.

Pariente, B. *et al.* (2011) 'Activation of the receptor NKG2D leads to production of Th17 cytokines in CD4+ T cells of patients with crohn's disease', *Gastroenterology*. Elsevier Inc., 141(1), pp. 217-226.e2. doi: 10.1053/j.gastro.2011.03.061.

Petnicki-Ocwieja, T. *et al.* (2009) 'Nod2 is required for the regulation of commensal microbiota in the intestine', *Proceedings of the National Academy of Sciences*, 106(37), pp. 15813–15818.

Philpott, D. J. *et al.* (2014) 'NOD proteins: Regulators of inflammation in health and disease', *Nature Reviews Immunology*, 14(1), pp. 9–23. doi: 10.1038/nri3565.

Philpott, D. J. and Girardin, S. E. (2010) 'Nod-like receptors: Sentinels at host membranes', *Current Opinion in Immunology*. Elsevier Ltd, 22(4), pp. 428–434. doi: 10.1016/j.coi.2010.04.010.

Plichta, D. R. *et al.* (2019) 'Therapeutic Opportunities in Inflammatory Bowel Disease: Mechanistic Dissection of

Host-Microbiome Relationships', *Cell*. Elsevier Inc., 178(5), pp. 1041–1056. doi: 10.1016/j.cell.2019.07.045.

Podolsky, D. K. (2002) 'The current future understanding of inflammatory bowel disease', *Bailliere's Best Practice and Research in Clinical Gastroenterology*, 16(6), pp. 933–943. doi: 10.1053/bega.2002.0354.

Pontier, C. *et al.* (2001) 'HT29-MTX and Caco-2/TC7 Monolayers as Predictive Models for Human Intestinal Absorption: Role of the Mucus Layer', *Journal of Pharmaceutical Sciences*, 90(10), pp. 1608–06019.

Powrie, F. *et al.* (1994) 'Inhibition of Th1 responses prevents inflammatory bowel disease in scid mice reconstituted with CD45RBhi CD4+ T cells', *Immunity*, 1(7), pp. 553–62.

Pugazhendhi, S. *et al.* (2013) 'NOD2 gene mutations associate weakly with ulcerative colitis but not with Crohn's disease in Indian patients with inflammatory bowel disease', *Gene*. Elsevier B.V., 512(2), pp. 309–313. doi: 10.1016/j.gene.2012.10.015.

Qi, Z. *et al.* (2017) 'BMP restricts stemness of intestinal Lgr5þ stem cells by directly suppressing their signature genes BMP restricts stemness of intestinal Lgr5þ stem cells by directly suppressing their signature genes', *Nature Communications*. Nature Publishing Group. doi: 10.1038/ncomms13824.

Rajili, M. and Vos, W. M. De (2014) 'The first 1000 cultured species of the human gastrointestinal microbiota', *FEMS Microbiology Reviews*, 38, pp. 996–1047. doi: 10.1111/1574-6976.12075.

Ramanan, D. *et al.* (2014) 'Bacterial sensor Nod2 prevents inflammation of the small intestine by restricting the expansion of the commensal bacteroides vulgatus', *Immunity*. Elsevier Inc., 41(2), pp. 311–324. doi: 10.1016/j.immuni.2014.06.015.

Rieder, F. and Fiocchi, C. (2009) 'Intestinal fibrosis in IBD — a dynamic , multifactorial process', *Nature*, 6(April), pp. 228–236. doi: 10.1038/nrgastro.2009.31.

Roda, G. *et al.* (2016) 'Loss of Response to Anti-TNFs: Definition, Epidemiology, and Management', *Clinical and Translational Gastroenterology*, 7(November 2015), pp. 1–5. doi: 10.1038/ctg.2015.63.

Rodansky, E. S. *et al.* (2018) 'Intestinal organoids: A model of intestinal fibrosis for evaluating anti-fibrotic drugs', *Exp Mol Pathol*, 98(3), pp. 346–351. doi: 10.1016/j.yexmp.2015.03.033.Intestinal.

Ronaldson-Bouchard, K. and Vunjak-Novakovic, G. (2018) 'Organs-on-a-Chip : A Fast Track for Engineered Human Tissues in Drug Development', *Stem Cell*. Elsevier Inc., 22(3), pp. 310–324. doi: 10.1016/j.stem.2018.02.011.

Rosenstiel, P. *et al.* (2003) 'TNF-α and IFN-γ regulate the expression of the NOD2 (CARD15) gene in human intestinal epithelial cells', *Gastroenterology*, 124(4), pp. 1001–1009. doi: 10.1053/gast.2003.50157.

Rosentiel, P. *et al.* (2007) 'Functional characterization of two novel 5' untranslated exons reveals a complex regulation of NOD2 protein expression', *BMC Genomics*, 8, pp. 1–9. doi: 10.1186/1471-2164-8-472.

Rouch, J. D. *et al.* (2016) 'Development of functional microfold (M) cells from intestinal stem cells in primary

human enteroids', *PLoS ONE*, 11(1). doi: 10.1371/journal.pone.0148216.

Sabbah, A. *et al.* (2009) 'Activation of innate immune antiviral response by NOD2', *Nature Immunology*, 10(10), pp. 1073–1080. doi: 10.1038/ni.1782.Activation.

Sadlack, B. *et al.* (1993) 'Ulcerative colitis-like disease in mice with a disrupted interleukin-2 gene', *Cell*, 75(2), pp. 253–261. doi: 10.1016/0092-8674(93)80067-O.

Samak, G. *et al.* (2014) 'Cyclic stretch disrupts apical junctional complexes in Caco-2 cell monolayers by a JNK-2- , c-Src- , and MLCK-dependent mechanism', *Am J Physiol Gastrointest Liver Physiol*, 306, pp. 947–958. doi: 10.1152/ajpgi.00396.2013.

Sato, T. *et al.* (2009) 'Single Lgr5 stem cells build crypt – villus structures in vitro without a mesenchymal niche', *Nature*. Nature Publishing Group, 459(May), pp. 262–266. doi: 10.1038/nature07935.

Sato, T. *et al.* (2011) 'Long-term expansion of epithelial organoids from human colon, adenoma, adenocarcinoma, and Barrett's epithelium', *Gastroenterology*. Elsevier Inc., 141(5), pp. 1762–1772. doi: 10.1053/j.gastro.2011.07.050.

Sato, T. *et al.* (2013) 'Paneth cells constitute the niche for Lgr5 stem cells in intestinal crypts', 469(7330), pp. 415–418. doi: 10.1038/nature09637.Paneth.

Sato, T. and Clevers, H. (2015) 'SnapShot: Growing Organoids from Stem Cells', *Cell*, 161(7), pp. 1700-1700.e1. doi: 10.1016/j.cell.2015.06.028.

Satsu, H. *et al.* (2006) 'Induction by activated macrophage-like THP-1 cells of apoptotic and necrotic cell death in intestinal epithelial Caco-2 monolayers via tumor necrosis factor-alpha', *Experimental Cell Research*, 312(19), pp. 3909–3919. doi: 10.1016/j.yexcr.2006.08.018.

Schreiber, S. *et al.* (2005) 'Genetics of Crohn disease, an archetypal inflammatory barrier disease', *Nature Reviews Genetics*, 6(5), pp. 376–388. doi: 10.1016/j.proeng.2013.11.041.

Seiderer, J. *et al.* (2006) 'Homozygosity for the CARD15 frameshift mutation 1007fs is predictive of early onset of Crohn's disease with ileal stenosis, entero-enteral fistulas, and frequent need for surgical intervention with high risk of re-stenosis', *Scandinavian Journal of Gastroenterology*, 41(12), pp. 1421–1432. doi: 10.1080/00365520600703900.

Sidiq, T. *et al.* (2016) 'Nod2: A critical regulator of ileal microbiota and Crohn's disease', *Frontiers in Immunology*, 7(SEP), pp. 18–20. doi: 10.3389/fimmu.2016.00367.

Smith, P. D., Ochsenbauer-jambor, C. and Smythies, L. E. (2005) 'Intestinal macrophages : unique effector cells of the innate immune system', *Immunological Reviews*, 206, pp. 149–159.

De Souza, H. S. P. and Fiocchi, C. (2016) 'Immunopathogenesis of IBD: Current state of the art', *Nature Reviews Gastroenterology and Hepatology*. Nature Publishing Group, 13(1), pp. 13–27. doi: 10.1038/nrgastro.2015.186.

Spence, J. R. *et al.* (2011) 'Directed differentiation of human pluripotent stem cells into intestinal tissue in vitro.', *Nature*. Nature Publishing Group, 470(7332), pp. 105–9. doi: 10.1038/nature09691.

Srinivasan, B. *et al.* (2015a) 'TEER Measurement Techniques for In Vitro Barrier Model Systems', *Journal of Laboratory Automation*, 20(2), pp. 107–126. doi: 10.1177/2211068214561025.

Srinivasan, B. *et al.* (2015b) 'TEER Measurement Techniques for In Vitro Barrier Model Systems', *Journal of Laboratory Automation*, 20(2), pp. 107–126. doi: 10.1177/2211068214561025.

Steidl, C. *et al.* (2011) 'MHC class II transactivator CIITA is a recurrent gene fusion partner in lymphoid cancers', *Nature*, 17(471), pp. 377–81.

Steinbach, E. C. and Plevy, S. E. (2014) 'The Role of Macrophages and Dendritic Cells in the Initiation of In fl ammation in IBD', *Inflammatory bowel diseases*, 20(1), pp. 166–175. doi: 10.1097/MIB.0b013e3182a69dca.

Sternini, C., Anselmi, L. and Rozengurt, E. (2008) 'Enteroendocrine cells: A site of "taste" in gastrointestinal chemosensing', *Current Opinion in Endocrinology, Diabetes and Obesity*, 15(1), pp. 73–78. doi: 10.1097/MED.0b013e3282f43a73.

Takahashi, K. and Yamanaka, S. (2006) 'Induction of Pluripotent Stem Cells from Mouse Embryonic and Adult Fibroblast Cultures by Defined Factors', *Cell*, 126(4), pp. 663–676. doi: 10.1016/j.cell.2006.07.024.

Takahashi, Y. *et al.* (2018) 'A Refined Culture System for Human Induced Pluripotent Stem Cell-Derived Intestinal Epithelial Organoids', *Stem Cell Reports*. ElsevierCompany., 10(1), pp. 314–328. doi: 10.1016/j.stemcr.2017.11.004.

Takenaka, T. *et al.* (2014) 'Human Small Intestinal Epithelial Cells Differentiated from Adult Intestinal Stem Cells as a Novel System for Predicting Oral Drug Absorption in Humans', *Drug Metabolism and Disposition*, 42(11), pp. 1947–1954.

Tan, G., Zeng, B. and Zhi, F. C. (2015) 'Regulation of human enteric α-defensins by NOD2 in the Paneth cell lineage', *European Journal of Cell Biology*. Elsevier GmbH., 94(1), pp. 60–66. doi: 10.1016/j.ejcb.2014.10.007.

Tanabe, T. *et al.* (2004) 'Regulatory regions and critical residues of NOD2 involved in muramyl dipeptide recognition', *EMBO Journal*, 23(7), pp. 1587–1597. doi: 10.1038/sj.emboj.7600175.

TARGAN, S. R. *et al.* (1997) 'A SHORT-TERM STUDY OF CHIMERIC MONOCLONAL ANTIBODY cA2 TO TUMOR NECROSIS FACTOR a FOR CROHN'S DISEASE', *The New England Journal of Medicine*, pp. 1029–1035.

Theobald, J. *et al.* (2018) 'Liver-Kidney-on-Chip To Study Toxicity of Drug Metabolites'. doi: 10.1021/acsbiomaterials.7b00417.

Thiébaut, R. *et al.* (2016) 'Characterization and genetic analyses of new genes coding for NOD2 interacting proteins', *PLoS ONE*, 11(11), pp. 1–24. doi: 10.1371/journal.pone.0165420.

Tibbe, M. P. *et al.* (2018) 'Microfluidic Gel Patterning Method by Use of a Temporary Membrane for Organ-On-

Chip Applications', 1700200, pp. 1–6. doi: 10.1002/admt.201700200.

Travassos, L. H. *et al.* (2010) 'Nod1 and Nod2 direct autophagy by recruiting ATG16L1 to the plasma membrane at the site of bacterial entry', *Nature Immunology*. Nature Publishing Group, 11(1), pp. 55–62. doi: 10.1038/ni.1823.

Trietsch, S. J. *et al.* (2017) 'Membrane-free culture and real-time barrier integrity assessment of perfused intestinal epithelium tubes', *Nature Communications*. Springer US, 8(1), pp. 1–7. doi: 10.1038/s41467-017-00259-3.

Ude, V. C. *et al.* (2019) 'Using 3D gastrointestinal tract in vitro models with microfold cells and mucus secreting ability to assess the hazard of copper oxide nanomaterials', *Journal of Nanobiotechnology*. BioMed Central, pp. 1–20. doi: 10.1186/s12951-019-0503-1.

Vandussen, K. L. *et al.* (2015) 'that Define Subtypes of Crohn ' s Disease', 146(1), pp. 200–209. doi: 10.1053/j.gastro.2013.09.048.Genetic.

Vavricka, S. R. *et al.* (2015) 'Extraintestinal manifestations of inflammatory bowel disease', *Inflammatory Bowel Diseases*, 21(8), pp. 1982–1992. doi: 10.1097/MIB.0000000000000392.

Verhoeckx, K. *et al.* (2015) *The Impact of Food Bioactives on Health*, *The Impact of Food Bioactives on Health*. doi: 10.1007/978-3-319-16104-4.

Voss, E. *et al.* (2006) 'NOD2/CARD15 mediates induction of the antimicrobial peptide human beta-defensin-2', *Journal of Biological Chemistry*, 281(4), pp. 2005–2011. doi: 10.1074/jbc.M511044200.

Vulto, P. *et al.* (2011) 'Phaseguides: A paradigm shift in microfluidic priming and emptying', *Lab on a Chip*, 11(9), pp. 1596–1602. doi: 10.1039/c0lc00643b.

Wahl, S. M. *et al.* (1987) 'Transforming growth factor type β induces monocyte chemotaxis and growth factor production', *Proceedings of the National Academy of Sciences of the United States of America*, 84(16), pp. 5788–5792. doi: 10.1073/pnas.84.16.5788.

Watanabe, F. *et al.* (2004) 'Development of the method for evaluating protective effect of food factors on THP-1-induced damage to human intestinal Caco-2 monolayers', *BioFactors*, 21(1–4), pp. 145–147. doi: 10.1002/biof.552210129.

Wehkamp, J. *et al.* (2005) 'Reduced Paneth cell α-defensins in ileal Crohn's disease', *Proceedings of the National Academy of Sciences of the United States of America*, 102(50), pp. 18129–18134. doi: 10.1073/pnas.0505256102.

West, N. R. *et al.* (2017) 'Oncostatin M drives intestinal inflammation and predicts response to tumor necrosis factor–neutralizing therapy in patients with inflammatory bowel disease', *Nature Medicine*. Nature Publishing Group, 23(5), pp. 579–589. doi: 10.1038/nm.4307.

WMS, R. and RL, B. (1959) *The principles of humane experimental technique*. Universities Federation for Animal Welfare.

Yamazaki, K. *et al.* (2002) 'Absence of mutation in the NOD2/CARD15 gene among 483 Japanese patients with Crohn's disease', *Journal of Human Genetics*, 47(9), pp. 469–472. doi: 10.1007/s100380200067.

Yi, B. *et al.* (2017) 'Three-dimensional in vitro Gut Model on a Villi-shaped Collagen Scaffold', 11, pp. 219–231. doi: 10.1007/s13206-017-1307-8.

Yu, J. *et al.* (2012) 'In Vitro 3D Human Small Intestinal Villous Model for Drug Permeability Determination', *Biotechnology and Bioengineering*, 109(9), pp. 2173–2178. doi: 10.1002/bit.24518.

Zhong, Y., Kinio, A. and Saleh, M. (2013) 'Functions of NOD-Like Receptors in Human Diseases', *Frontiers in Immunology*, 4(October), pp. 1–18. doi: 10.3389/fimmu.2013.00333.